Stromal loss of JUNB promotes distant metastasis

Dissertation

Faculty of Biosciences
Ruperto Carola University Heidelberg

Juliane Wutschka
2019

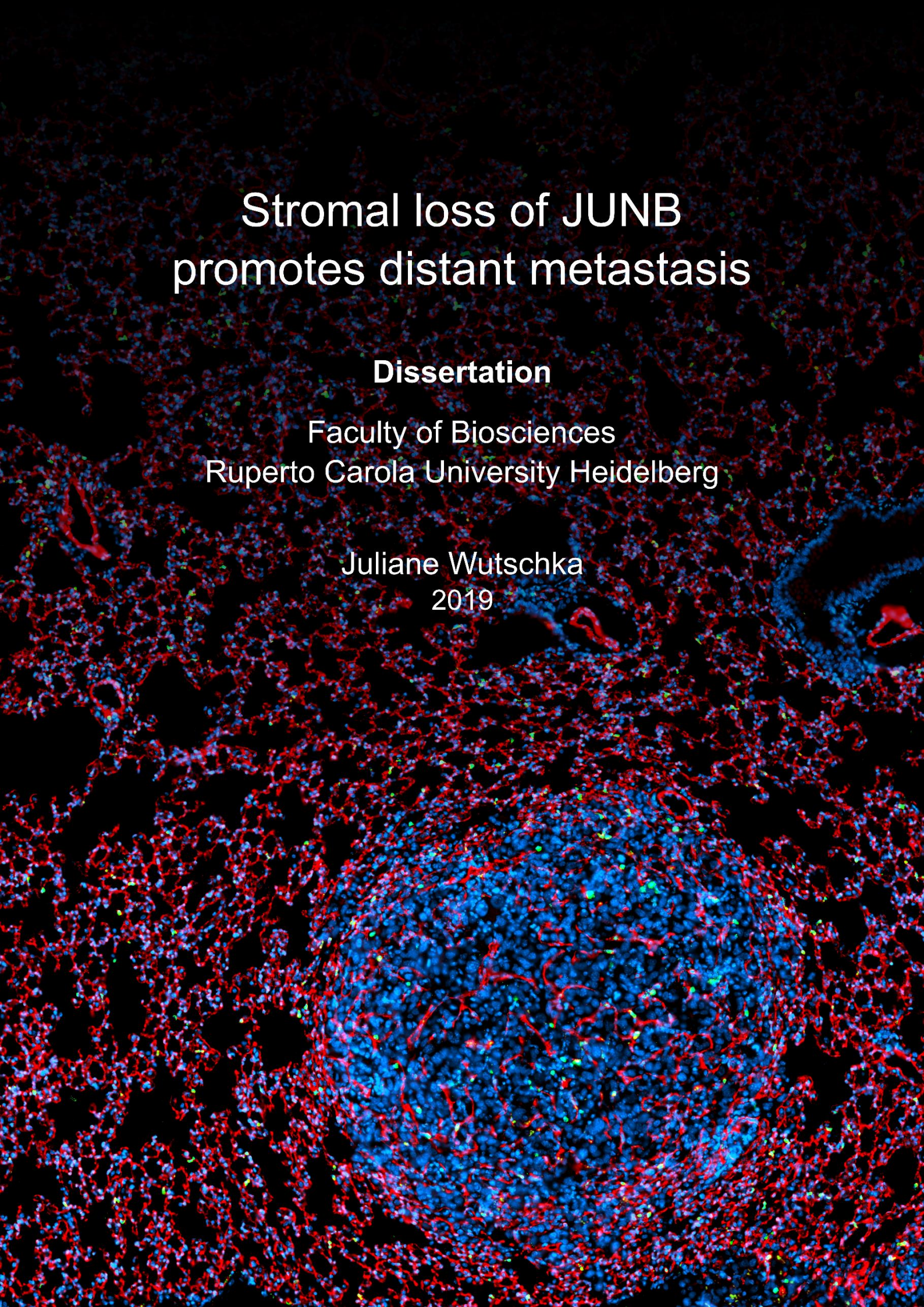

Dissertation

submitted to the

Combined Faculty of Natural Sciences and Mathematics

of the Ruperto Carola University Heidelberg, Germany

for the degree of

Doctor of Natural Sciences

Presented by

Juliane Wutschka, M.Sc.

born in: Grimma, Germany

Oral examination: 13th May, 2019

Stromal loss of JUNB promotes distant metastasis

Referees: Prof. Dr. Peter Angel

Prof. Dr. Jonathan Sleeman

SUMMARY

The AP-1 family member JUNB is a context dependent transcriptional regulator implicated in essential cellular processes, such as proliferation, differentiation and inflammation. JUNB has furthermore been described to function both as tumor suppressor and as oncogene, largely dependent on the tumor entity. JUNB loss of function is predominantly observed in leukemia, for example in chronic myeloid leukemia as well as acute myeloid leukemia. In contrast, JUNB is frequently overexpressed in solid tumors, such as breast and colon cancer, but also in a multitude of lymphomas. Functionally, JUNB has been associated with invasion and metastasis. Yet, the majority of data linking JUNB to disease progression have been obtained either in *in vitro* experiments or are based on correlational studies. All studies assessing the contribution of JUNB to metastasis have focused on JUNB expression in the tumor cells themselves. JUNB is, however, an essential regulator in a vast plethora of cells of the tumor microenvironment. Such being the case, JUNB is crucial for the development and homeostasis of the blood vascular system and has also been implicated in the formation of the lymphatic system. Moreover, JUNB controls the differentiation of T helper cells and is required for the activation of macrophages. Thus, the aim of this dissertation was to elucidate the functional consequences of JUNB loss in the stroma on metastasis *in vivo* in mice. For this purpose, elaborate spontaneous metastasis assays involving primary tumor resections were performed using conditional *Junb* knockout mice and syngeneic cell lines.

In line with previous findings of the group, primary tumor growth was unaffected by stromal deletion of *Junb*. Strikingly though, stromal JUNB loss facilitated distant metastasis to the lungs in a breast cancer model developing spontaneous metastasis. Yet, tumor cell extravasation and metastatic colonization were not influenced by *Junb* ablation, implying that JUNB controls the initial steps of the metastatic cascade. In order to mechanistically decipher the contribution of stromal JUNB to metastasis, various cellular compartments were analyzed for JUNB-dependent changes. Despite its essential role in vascular biology, no defects in the blood and lymphatic vascular system could be determined in *Junb* knockout mice. Similarly, fibroblast density was unaltered upon ablation of stromal *Junb*. Remarkably, a prominent accumulation of immune cells, in particular of neutrophils, was found upon JUNB loss in primary breast tumors and even more strikingly in pre-metastatic lungs. Concomitantly, neutrophil recruiting factors, such as *Tnfα* and *Il-1β*, were upregulated upon JUNB loss. Bone marrow transplantation experiments further pointed towards neutrophil recruitment being mediated by deletion of *Junb* in the stroma rather than a neutrophil-intrinsic mechanism. In an attempt to directly link neutrophil accumulation to enhanced metastasis, neutrophils were ablated pharmacologically using an anti-LY6G antibody. Yet, depletion efficiency was too low to establish direct functional proof. The experiment did, however, clearly confirm the initial data that JUNB loss in the stroma promotes breast cancer metastasis. In conclusion, the data of this dissertation provide the first functional evidence that deletion of stromal *Junb* indeed facilitates metastatic spread possibly by the formation of a pre-metastatic niche. Since JUNB is a target of Mitogen-activated protein kinase (MAPK) signaling, these findings are especially important with regard to the development of novel targeted approaches for cancer therapy. Unless cancer cells can be targeted specifically, strategies resulting in JUNB loss in the microenvironment should be avoided.

ZUSAMMENFASSUNG

JUNB, Mitglied der AP-1 Transkriptionsfaktor-Familie, ist ein kontextabhängiger transkriptionaler Regulator, der eine wichtige Rolle in diversen zellulären Prozessen, wie Proliferation, Differenzierung and Inflammation spielt. Abhängig von der Krebsart, kann JUNB als Tumorsuppressor oder als Onkogen agieren. Der Verlust von JUNB wird hauptsächlich in Leukämie, wie z.B. in chronischer myeloischer und akuter myeloischer Leukämie, beobachtet. Im Gegensatz dazu findet man JUNB in soliden Krebsarten, z.B. in der Brust oder im Darm, aber auch in Lymphomen, häufig überexprimiert. Funktionelle Studien haben JUNB zwar mit Invasion and Metastasierung in Verbindung gebracht, dennoch basiert der Großteil dieser Daten auf *in vitro* Experimenten bzw. stellt lediglich eine Korrelation von JUNB zum schnellen Fortschreiten des Krebses her. So haben alle Studien, welche den Zusammenhang von JUNB und Metastasierung untersucht haben, den Fokus auf JUNB in den Tumorzellen selbst gelegt. JUNB stellt jedoch einen essentiellen Regulator in einer Vielzahl von Zellen aus der Tumor-Mikroumgebung dar. So wurde JUNB eine essentielle Rolle in der Entwicklung und Homöostase des Blutgefäßsystems aber auch eine Beteiligung an der Ausbildung des lymphatischen Systems zugeschrieben. Des Weiteren reguliert JUNB die Differenzierung von T Helfer Zellen und wird für zur Aktivierung von Makrophagen benötigt. Das Ziel dieser Dissertation war es daher, die Rolle von JUNB in der Metastasierung *in vivo* in der Maus zu untersuchen. Zu diesem Zweck wurden aufwendige spontane Metastasierungsmodelle nach chirurgischer Entfernung des Primärtumors mit konditionalen *Junb* Knockout Mäusen und syngenen Zelllinien angewendet.

In Übereinstimmung mit früheren Ergebnissen der Arbeitsgruppe war das Wachstum des Primärtumors unabhängig von stromalem JUNB. Bemerkenswerterweise förderte die Deletion von *Junb* im Stroma aber die Metastasierung in der Lunge in einem Brustkrebsmodell, welches spontan metastasiert. Tumorzellextravasation und metastatische Kolonisierung waren nicht vom *Junb* Verlust beeinflusst. Dies deutet darauf hin, dass JUNB möglicherweise die initialen Schritte der metastatischen Kaskade kontrolliert. Um den Beitrag von stromalem JUNB zur Regulation der Metastasierung aufzuklären, wurden im Anschluss verschiedene Zelltypen hinsichtlich JUNB-abhängiger Veränderungen untersucht. Trotz essentieller Funktionen von JUNB in der Vaskulatur konnten nach *Junb* Deletion keine Defekte des Blut- bzw. Lymphgefäßsystems festgestellt werden. Ebenso war die Dichte von Fibroblasten unverändert. Interessanterweise waren jedoch Immunzellen, insbesondere Neutrophile, im primären Brusttumor aber noch auffälliger in prä-metastatischen Lungen von *Junb* Knockout Mäusen akkumuliert. Gleichzeitig waren Neutrophil-rekrutierende Faktoren, wie *Tnfα* und *Il-1*β hochreguliert. Experimente mit Knochenmarkstransplantationen deuteten außerdem an, dass diese Infiltration von Neutrophilen durch den Verlust von *Junb* im Stroma vermittelt wird, nicht aber durch einen Neutrophil-intrinsischen Effekt. Um die Akkumulation von Neutrophilen direkt mit der erhöhten Metastasierung in Verbindung zu setzen, wurden Neutrophile anschließend mit Hilfe eines gegen LY6G gerichteten Antikörpers pharmakologisch depletiert. Da die Effizienz dieser Neutrophil Depletion jedoch zu gering war, konnte keine direkte Assoziation hergestellt werden. Das Depletionsexperiment bestätigte allerdings eindeutig die initialen Ergebnisse, dass der Verlust von JUNB im Stroma die Metastasierung von Brustkrebs begünstigt. Schlussfolgernd stellen die Daten aus dieser Dissertation den ersten direkten und funktionellen Beweis dar, dass die Deletion von stromalem *Junb* die Metastasierung begünstigt. Vermutlich wird dieser Effekt durch die Ausbildung einer prä-metastatischen Nische vermittelt. Da JUNB ein nachgeschaltetes Ziel des Mitogen-aktivierten Proteinkinase

(MAPK) Signalwegs ist, sind diese Ergebnisse mit Hinblick auf die Neuentwicklung zielgerichteter Therapieansätze zur Behandlung von Krebs besonders wichtig. Sofern Tumorzellen nicht spezifisch attackiert werden können, sind zielgerichtete Therapien, die einen JUNB Verlust in der Tumormikroumgebung nach sich ziehen, unbedingt zu vermeiden.

TABLE OF CONTENTS

LIST OF FIGURES

LIST OF TABLES

LIST OF EQUATIONS

ABBREVIATIONS

7AAD	7-Aminoactinomycin D
ABC	Avidin-biotin complex
ACK	Ammonium Chloride Potassium
Adgre1	Adhesion G protein-coupled receptor E1
AJCC	American Joint Committee on Cancer
AP-1	Activating protein 1
B2m	Beta-2-microglobulin
BMDC	Bone marrow-derived cells
BMT	Bone marrow transplantation
bp	Base pair
BSA	Bovine serum albumin
CAF	Cancer-associated fibroblast
CAM	Cellular adhesion molecule
CCL	C-C Motif Chemokine Ligand
CCR	C-C chemokine receptor
CD	Cluster of differentiation
cDNA	Complementary DNA
CO_2	Carbon dioxide
Cre	Cre recombinase
CRE	cAMP Responsive Elements
CRISPR	Clustered Regularly Interspaced Short Palindromic Repeats
CSF-1	Colony-stimulating factor 1
C_T	Cycle of threshold
CTC	Circulating tumor cell
CTR	Control
CXCL	C-X-C chemokine ligand
CXCR	C-X-C chemokine receptor
d	day(s)
DAB	3,3'-diaminobenzidine
DMEM	Dulbecco's Modified Eagles Medium
DMSO	Dimethyl sulfoxide
DNA	Deoxyribonucleic acid
DNase	Deoxyribonuclease
dNTP	Deoxynucleotide triphosphate
DPBS	Dulbecco's Phosphate buffered saline
DTC	Disseminated tumor cell
DTT	Dithiothreitol
ECM	Extracellular matrix
EDTA	Ethylenediaminetetraacetic acid
EGF	Epidermal growth factor
EMT	Epithelial to mesenchymal transition
EtOH	Ethanol
FACS	Fluorescence-activated cell sorting
FBS	Fetal Bovine Serum
FITC	Fluorescein isothiocyanate

for	Forward primer
FOXP3	Forkhead box P3
FSC	Forward scatter
g	Gravity
G	Gauge
GEMM	Genetically engineered mouse model
GFP	Green fluorescent protein
GOI	Gene of interest
h	hour
H_2O	water
H2O2	Hydrogen peroxide
HE	Hematoxylin and eosin
HEPES	4-(2-hydroxyethyl)-1-piperazineethanesulfonic acid buffer
HER2	Human epidermal growth factor receptor 2
HEV	High endothelial venule
HRP	Horse radish peroxidase
IgG	Immunoglobulin
IHC	Immunohistochemistry
IL	Interleukin
ILC	Invasive lobular carcinoma
i.p.	Intraperitoneal
Itgam	Integrin alpha M
i.v.	intravenous
kDa	Kilodalton
Ki67	Kiel 67
Klrb1c	Killer cell lectin-like receptor subfamily b member 1c
KO	Knockout
LL/2-Luc	Lewis Lung Carcinoma (Luciferase-tagged)
M	Molar
MHC	Major histocompatibility complex
MIC	Metastasis initiating cell
MMPs	Matrix metalloproteinases
mTOR	Mammalian target of rapamycin
ND	Not defined
NST	Invasive carcinoma of no special type
PBS	Phosphate buffered saline
PCR	Polymerase chain reaction
PDPN	Podoplanin
PDGF	Platelet-derived growth factor
PFA	Paraformaldehyde
pH	potential of hydrogen
PI	Propidium Iodide
PI3K	Phosphoinositide 3-kinase
Ppia	Cyclophilin A
Ptprc	Protein tyrosine phosphatase, receptor type C
qRT-PCR	Quantitative real-time PCR
REF	Reference gene
rev	Reverse primer
RIPA	Radioimmunoprecipitation assay buffer

RNA	Ribonucleic acid
RPMI	Roswell Park Memorial Institute medium
RT	Room temperature
s.c.	Subcutaneous
SD	Standard deviation
SSC	Side scatter
TNBC	Triple negative breast cancers
TPA	12-O-Tetradecanoylphorbol-13-acetate
TRE	TPA response elements
VEGF-A	Vascular endothelial growth factor A
Vol%	Volume percent
WT	Wildtype

1 INTRODUCTION

1. INTRODUCTION

1.1. Metastasis

In 2018, about 17 million people were diagnosed with cancer around the world and this disease resulted in 9.6 million cases in mortality [1, 2]. Horrifyingly, this means that cancer is responsible for 1 out of 6 deaths globally making it the second leading cause of death [2]. The majority of people do not die due to primary tumor formation, though, but from metastasis. Metastasis, the spread of tumor cells from the primary tumor to a distant organ site, is a very inefficient process with estimates of less than 0.02% of disseminated tumor cells (DTCs) being able to successfully establish a distant lesion [3]. Despite this inefficiency, metastasis remains clinically most relevant urging the need to better investigate this deadly disease mechanistically. With the help of new elaborate preclinical models formerly unaddressed steps in the metastatic cascade can be explored in order to reveal novel drug targets or therapeutic windows.

1.1.1. The metastatic cascade

Initially, the primary tumor is confined and restricted from spread by the surrounding microenvironment and extracellular matrix (Figure 1-1). Upon progression, cancer cells acquire the capability of detaching from the primary tumor mass and of invading into the surrounding tissue either as individual cells or collectively as a cluster [4, 5]. Depending on the microenvironment, individual cells migrate either in an elongated or rounded manner [4, 6]. Invasion is facilitated by degradation of extracellular matrix (ECM) which is achieved by overexpression of matrix metalloproteinases (MMPs) in tumor cells [7-9]. Besides degradation also further alterations to the ECM, such as thickening or linearization of collagen fibers, can promote cancer cell invasion by acting as tracks for cancer cells [10].

After invasion into the stroma, further dissemination of cancer cells can occur via the hematogenous or lymphatic route. Tumor cells are directed towards blood endothelial or lymphatic vessels by chemotactic signals. It has been shown that tumor cells can migrate towards gradients of epidermal growth factor (EGF) [11] or colony-stimulating factor 1 (CSF-1) expressed by endothelial cells or macrophages in immediate vicinity [12]. Tumor cell entering into the lymphatic system was long believed to be by chance due to the fenestrated morphology and absence of pericytes around the initial lymphatics which render them highly permeable [13]. Lymphatic endothelial cells do, however, just as blood endothelial cells, constitutively express chemokines. Of special note are thereby the CCR7 ligands CCL19 and CCL21 [14]. They typically mediate lymphocyte migration into the lymph nodes but have also been found to guide CCR7-expressing tumor cells to lymphatic vessels [14, 15].

Upon contact with a blood vessel, cancer cells invade directly through the vessel wall by a process called transendothelial migration and enter the circulation. These circulating tumor cells (CTCs) are extremely rare with estimates of only one CTC in 1 billion normal blood cells even in patients with metastatic tumors [16]. In the bloodstream, CTCs are exposed to a foreign and hostile microenvironment. To withstand hemodynamic forces and shear stress CTCs show a surprising plasticity in terms of stiffness and shape of plasma membrane and nuclear envelope, most probably also aiding their traverse of constraining capillary beds [17].

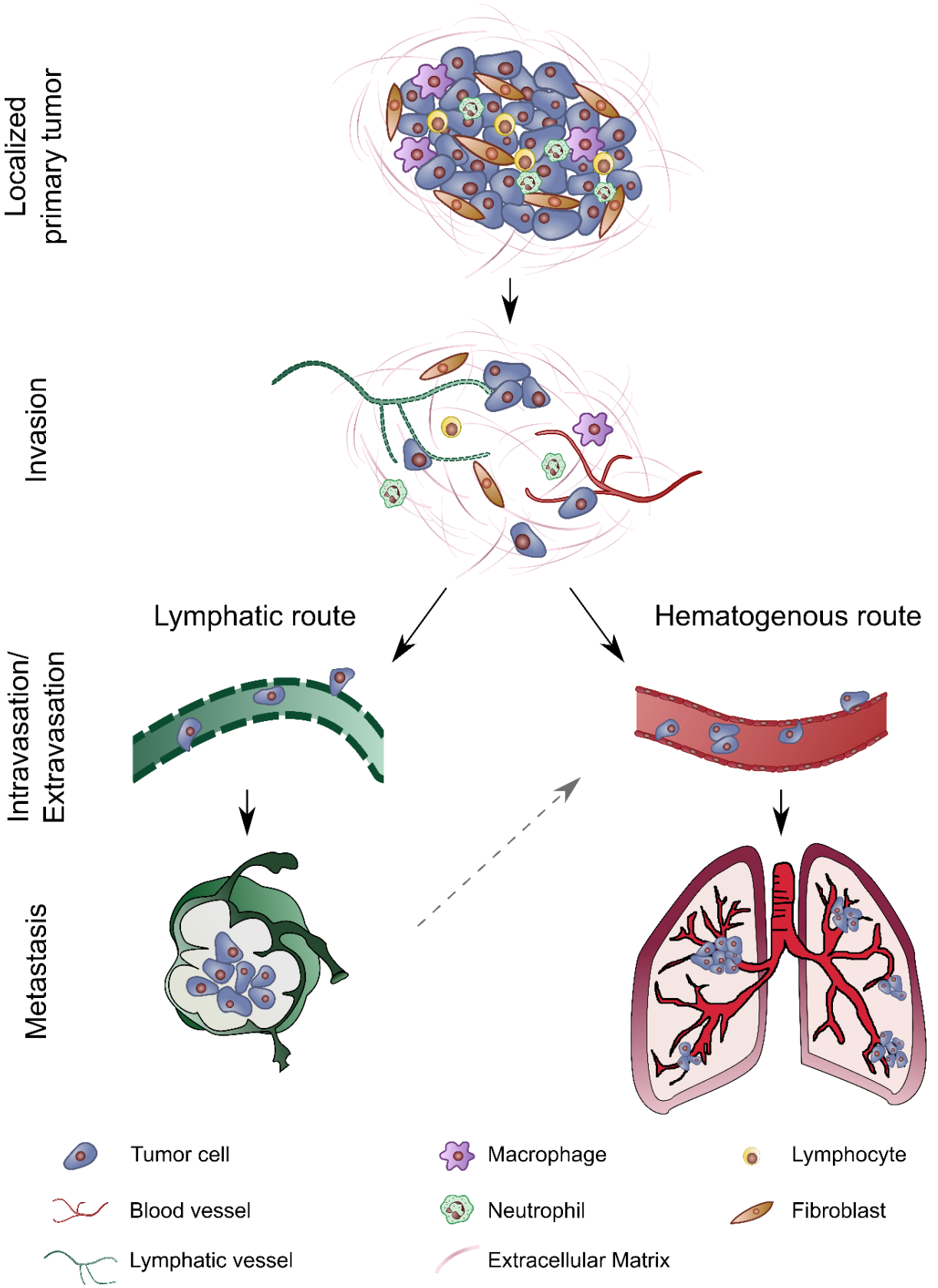

Figure 1-1: Schematic representation of the metastatic cascade.

A portion of cancer cells acquires invasive properties, escapes from the locally confined primary tumor and invades the tumor microenvironment. Upon contact with blood or lymphatic vessels, cancer cells intravasate and are distributed to a distant organ via the hematogenous or the lymphatic route. At a distant site, cancer cells extravasate, invade the local surrounding and eventually grow out to form metastases.

To survive in circulation, CTCs furthermore have to become resistant to anoikis, a form of cell death initiated upon loss of attachment to neighboring cells or the ECM [18]. It has been shown that this resistance can be conferred by inducing epithelial to mesenchymal transition [19], by signals from co-travelling stromal cells [20] or by Wnt signaling [21]. Survival can also be facilitated if CTCs travel in clusters and therefore retain their intercellular contacts [22]. Traversing through the bloodstream in clusters may have an additional benefit: protecting from assault by immune cells [23, 24]. CTCs furthermore interact with platelets and use them as a "shield" to escape from lysis by NK cells [25]. Nevertheless, also individual CTCs have a plethora of mechanisms to evade the immune system, such as downregulation of major histocompatibility complex (MHC) class I to hide from cytotoxic T-cells [26] or upregulation of cytokeratins to interfere with the recognition of MHC class I by the T cell receptor complex [27]. CTCs have furthermore been demonstrated to express PD-L1 (Programmed death-ligand 1) resulting in T cell inhibition [28, 29], or CD47 providing an anti-phagocytic signal to myeloid cells [30, 31].

Extravasation, the egress of CTCs out of the circulation, has long been believed to occur when CTCs are mechanically retained in the first capillary bed they encounter due to size limitations [32]. It is now evident though, that extravasation is much more complex but the exact mechanisms are still unclear. Cancer extravasation does, however, resemble leukocyte diapedesis under inflammatory conditions leading to the hypothesis that cancer cells may rely on similar mechanisms when exiting the vasculature [33]. The exact initial step leading to cancer cell arrest in the vasculature is still under debate as both passive trapping in small capillaries [34-36] and active adhesion to the endothelium in larger vessels have been observed [36-38]. The reports that cancer cells preferentially adhere to certain tissue-specific endothelia [37, 39, 40] does, however, point towards a more regulated mechanism than mere entrapment. Before firm arrest, leukocytes interact with the endothelium via selectins and start "rolling" along the vessel wall. Whether cancer cell "rolling" is crucial for attachment is controversial but it has been observed and reported to involve selectins [41-44]. In order to establish a stable interaction with the endothelium, cancer cells express different integrins, such as $\alpha_4\beta_1$ [45-47] or $\alpha_v\beta_3$ [48], or CD44 [49] to bind to various cell adhesion molecules (CAMs) on the endothelial surface thereby stimulating transendothelial migration.

Even after successful extravasation, cancer cells are confronted with new challenges at the distant organ site, whereby the majority of cells fail to establish macroscopic tumors. These cells predominantly enter a state of dormancy or are eliminated from the tissue altogether [50]. The persistence of dormant cells may also explain why recurrences can be observed so long after primary tumor removal or therapy [51]. When the cell has productively engaged with the surrounding matrix and stromal compartment, it can ultimately proliferate and colonize the distant organ site forming micrometastasis and eventually overt macroscopic metastasis [52].

1.1.2. Factors influencing metastasis – "seed versus soil"

The origin of metastasis initiating cells (MICs) has been highly disputed since Stephen Paget's theory of "seed and soil" in 1889 [53]. Therein, he proposes that metastatic spread is not purely directed by blood flow, which had been the prevalent concept at that time [54], but that the microenvironment of the metastasis-receiving organ ("soil") is of pivotal importance and has to be susceptible for "seeding" [53]. The proclamation of James Ewing in 1922 that metastatic patterns can be solely explained by blood flow has further fueled the discussion [55]. These opposing publications have led to two different schools of thought advocating to focus on either

intrinsic properties of the tumor cells (“seed”) or on changes in the microenvironment of the recipient organ (“soil”) when investigating metastasis.

1.1.2.1. Tumor-intrinsic properties facilitating metastasis

Several mechanisms have been proposed with regard to tumor-intrinsic properties being required for the cell’s capability to initiate metastasis. Cues for the development of these MICs can either reside within the tumor cell itself or are produced by the microenvironment. MICs have been suggested to arise by (I) epithelial to mesenchymal transition (EMT) [56], (II) by accumulation of mutations in tissue-resident stem cells [57], (III) by selection for driver mutations during tumor progression [58] or (IV) by epigenetic regulation [59, 60]. Undergoing EMT, tumor cells lose their epithelial characteristics, such as cell polarity and adherens junctions [56]. Concomitantly, cells express mesenchymal markers, such as fibronectin, vimentin and N-cadherin, and obtain a more spindle-shaped morphology [56]. Besides EMT, it has also been reasoned that tissue stem cells could give rise to MICs due to an accumulation of mutations [57]. Having stem cell characteristics is, however, not a sure indication for metastasis, therefore this theory does not explain the origin of MICs in all tumor types [57]. Furthermore, Reiter and colleagues identified that different metastases within individual patients shared the same driver mutations suggesting a selection for driver mutations of metastasis during tumor progression [58]. Over the past years, it has, however, become increasingly clear that metastasis cannot be explained only by the presence of genetic mutations. Analysis of mutational load revealed an unexpectedly high variation within cancer types [61]. Thereby, melanoma, the most rapidly metastasizing skin cancer [62], showed the highest mutational frequency [61], confirming the notion that genetic alteration is facilitating metastatic spread. Contrarily, rhabdoid tumors [63] as well as medulloblastoma [64] metastasize at high frequency despite their generally low somatic mutational burden [61]. Aberrant DNA methylation patterns, such as hypermethylation in tumor suppressor genes [65] and, albeit less studied, hypomethylation of oncogenes [66, 67], have already been associated with tumor onset and progression. Whether epigenetic regulation also specifically influences metastatic dissemination was non-evidenced, though, until distinct changes in methylation patterns in key metastatic genes were found. DNA methylation-induced silencing of E-cadherin was thereby associated with reduced overall survival and increased metastasis [59] and was correlated with enhanced cell motility [60]. Overall, it seems, however, very probable, that all these suggested factors do not contribute to the formation of MICs individually but rather act in a complex interplay, which is potentially further dependent on the tumor entity or environmental factors.

1.1.2.2. Changes in the microenvironment influencing metastasis – the pre-metastatic niche

According to the alternative school of thought, investigations were focused on changes in the target organs of metastasis (“soil”). Multiple reports stated that the target organs are not just passive hosts but are actively modulated by the primary tumor in order to be more permissive for metastatic colonization [68]. The microenvironment of the target organ is remodeled even prior to arrival of any tumor cell leading to the concept of the formation of the “pre-metastatic niche” [68-70]. The pre-metastatic niche is actively prepared by tumor-derived factors and extracellular vesicles and involves induction of angiogenesis, remodeling of the ECM, metabolic reprogramming and attraction of immune cells [71].

One of the earliest events in shaping the pre-metastatic niche is the induction of vascular permeability by the secretion of vascular endothelial growth factor A (VEGF-A) thereby promoting influx of immune cells and extravasation of CTCs [70, 72]. Later on, VEGF-A is required for angiogenesis at the metastatic site [73], thus, enabling macrometastatic outgrowth [74, 75]. Apart from the blood vasculature also the lymphatic system is impacted by tumor-secreted factors, such as VEGF-A/C/D [69, 76] and hepatocyte growth factor (HGF) [77]. Multiple reports have linked lymphangiogenesis and lymph node lymphangiogenesis to sentinel lymph node metastasis but also to distant metastasis [76, 78-80]. This may at least partially be mediated by increasing lymph flow thereby enhancing the chances for tumor cells to disseminate but also propagating the distribution of tumor-secreted factors [81]. Besides vascular changes also the remodeling of ECM components is important for metastatic colonization. Remodeling can be induced by tumor-secreted factors, both enzymatic and non-enzymatic, such as MMPs, and by reprogramming local fibroblasts to, for example, produce fibronectin [69]. In addition, the ECM, especially collagen, can be modified by lysyl oxidase (LOX), an enzyme that is secreted by tumor cells upon hypoxia and catalyzes crosslinking of collagens and elastins [82, 83]. Supporting the notion that ECM components are important for metastatic colonization, Aguago et al. implanted scaffolds into tumor-bearing mice and showed enhanced colonization if these scaffolds had been coated with collagen IV or fibronectin [84]. Changes in vasculature and ECM in the pre-metastatic niche have been described extensively whereas the contribution of metabolic changes is just at the onset of being explored. Disseminated tumor cells face multiple challenges when arriving at the metastatic site: structural and cellular components differ but also the availability of nutrients, requiring a certain plasticity of the cancer cell. Metabolic reprogramming, thus, supports the tumor cells in their new environment [85]. As one example, the microRNA miR-122, derived from tumor exosomes, promoted metastasis by locally suppressing glucose uptake [86]. Besides these effects on local components of the future metastatic sites, tumor-derived factors also stimulate recruitment of bone-marrow derived cells and immune cells. In a pioneering study, Kaplan et al. demonstrated the attraction of VEGFR1+ bone marrow-derived cells (BMDC) to pre-metastatic lungs thereby enhancing local permeability and facilitating extravasation and colonization [69]. Several groups showed the recruitment of myeloid cells, such as macrophages [87, 88], monocytes [88, 89] and neutrophils [88, 90, 91] to pre-metastatic lungs, thus, fostering metastasis. Several investigations have, however, also found suppression of metastatic dissemination as a consequence of immune cell accumulation in the pre-metastatic niche. So, did the infiltration of neutrophils inhibit seeding in a murine breast cancer model [92]. These contradictory results as well as the fact that not only tumor-secreted factors but also factors deposited by the surrounding stroma can impact the-pre-metastatic niche, have made the subject extremely complex. For an overview, further important mediators are listed in Table 1-1.

Table 1-1: Mediators of the pre-metastatic niche.

Factor	Induced change in pre-metastatic niche	Reference
VEGF-A	VEGFR1+ BMDC recruitment to pre-metastatic lung, enhancing local permeability, promoting metastasis	[69]
Placental growth factor (PLGF)	VEGFR1+ BMDC recruitment to pre-metastatic lung, upregulation of fibronectin in resident fibroblasts, promoting metastasis	[69]
Macrophage migration inhibitory factor (MIF)	Secretion of TGFβ and fibronectin, recruitment of F4/80+ macrophages and Gr1+ myeloid cells	[88]
TGFβ, Tumor necrosis factor α (TNFα), VEGF-A	Induction of S100A8/S100A9, recruitment of Mac+ myeloid cells	[93]
S100A8/S100A9	Recruitment of Mac1+ myeloid cells, enhanced migrational activity of cancer cells; induction of serum amyloid A (SAA) 3, increase in metastasis	[89, 93]
VEGFR1 signaling (through VEGF-A and PLGF)	MMP9 induction in resident macrophages and endothelial cells, increase in metastasis	[87]
Granulocyte colony stimulating factor (G-CSF)	mobilization of Ly6G+Ly6C+ granulocytes and 7/4+ neutrophils, increase in metastasis	[91, 94]
Granulocyte colony stimulating factor (G-CSF)	Increased neutrophil infiltration and expression of Bv8, S100A8, S100A9 and MMP9, enhanced metastasis	[95]
Granulocyte colony stimulating factor (G-CSF)	Neutrophil infiltration and arachidonate 5-lipoxygenase (Alox5) expression, promoting metastasis	[96]
Tissue inhibitor of metalloproteinases (TIMP-1)	Increase in stromal derived factor 1 (SDF1) levels, increase in susceptibility of liver metastasis	[90]
Osteopontin	Recruitment of BMDCs and promotion of colonization and outgrowth	[97]
Interleukin-11, Osteopontin, CXCR4, MMP1, TGFβ	Angiogenesis and osteolysis, increase in bone metastasis	[98]
SDF1	Direction of CXCR4+ tumor cells to target organs	[99]
MMPs	ECM degradation and remodeling, vascular remodeling	[69, 72, 100, 101]
miR-122	Metabolic reprogramming, promotes metastasis	[86]
LOX	Enhanced invasion	[82]

1.1.3. Organ tropism of metastasis

As already established above, metastatic spread is not random, but is in fact influenced by tumor-intrinsic factors as well as signals coming from the microenvironment. Originally, it was,

however, thought that metastatic patterns are solely determined by the anatomic location of the primary tumor and dissemination thereafter occurs passively by flow of blood and lymph fluid [55]. This would mean that DTCs preferentially home to the organ whose microcapillary bed they encounter first. This is indeed observed in prostate cancer, which preferentially metastasizes to one organ, namely bone, in particular pelvis and spine [40, 102, 103]. The fact that in colorectal cancer sequential organ metastasis via liver to lung is observed [104, 105] and that in breast and prostate cancer actually percentagewise more bone metastases are detected than can be exclusively deduced from flow characteristics indicates that more factors than pure entrapment impact the distribution of metastasis [106]. As already stated in section 1.1.1 (The metastatic cascade), organ-specific endothelia can influence tumor spread. Vascular beds can consist of continuous non-fenestrated endothelium, like in skin or lung, continuous fenestrated endothelium, such as in endocrine glands, or discontinuous sinusoidal endothelium, for example in the liver, spleen and bone marrow [107]. It may therefore seem logical that extravasation is facilitated when the vasculature is lined by a permeable discontinuous endothelium rather than a tightly sealed blood brain barrier, but this does not explain why different tumor types have different preferences. In addition to a distinct endothelial morphology, also the expression of adhesion molecules may play a role why certain organs are more affected than others. In line with the observed preferential bone metastasis, prostate cancer cells adhered more efficiently to endothelial cells derived from bone marrow than lung [104, 108]. These favored interactions of tumor cells to the endothelium were mediated by several differentially expressed adhesion molecules, such as various integrins [109], E-selectin [110, 111], L-selectin [112] and ICAM-1 [113]. Distinct integrins have, for example, been shown to direct cancer cells to respective organs by establishing a favorable pre-metastatic niche. Packaging of $\alpha_6\beta_4$ integrin into tumor-shedded exosomes guided cancer cells to the lung, whereas integrin $\alpha_v\beta_5$ targeted them towards the liver [114].

It is thereby conceivable that metastatic patterns are not exclusively influenced by either flow, favorable endothelial adhesion or a permissive pre-metastatic niche but most likely all actions combined. As recently highlighted in a publication by Follain et al. melanoma and breast cancer metastasis are determined by particular flow patterns but also by active remodeling of the endothelial cells at the target site [115]. As a summary, observed organ tropisms are listed for various cancer types in Table 1-2.

Table 1-2: Organ tropism of metastasis.

Cancer type	Metastasis	Reference
Lung cancer	Brain, bone, adrenal glands, lymph nodes, lung	[102, 106, 116]
Breast cancer	Lymph node, lung, bone, liver, brain	[102, 106, 117]
Prostate cancer	Bone, lymph node	[40, 102]
Colorectal cancer	Liver, lung, lymph nodes	[104, 105]
Melanoma	Lymph nodes, skin, brain, lung, small intestine	[102, 118]
Pancreatic cancer	Liver, lymph nodes, peritoneum, liver	[102]

1.2. Breast cancer and breast cancer metastasis

1.2.1. Molecular subtypes of breast cancer – determinants of metastasis

Investigations of metastasis frequently make use of models of breast cancer due to the broad availability of patient material and preclinical models. Breast cancer is the most frequent cancer in women and responsible for 15% of cancer-related deaths in women [2]. Accumulating evidence did, however, show that breast cancer is not a single disease but rather consists of several distinct pathological entities arising in the breast. It has furthermore become increasingly clear that these pathological entities exhibit profoundly different biological characteristics as well as prognosis and also differ in their response towards therapy. It is therefore crucial to accurately group these breast cancers into different subtypes in order to apply the optimal treatment regimen. According to histological examination, breast cancer is divided into invasive carcinoma of no special type (NST, formerly invasive ductal carcinoma (IDC)) and invasive lobular carcinoma (ILC) [119]. Yet, more important for treatment decisions and prediction of prognosis is the classification according to molecular characteristics [120]. Assessment of hormone receptor status, as examined by immunohistochemistry, and clinicopathological features such as tumor size, stage and nodal involvement, were used to categorize breast cancer in the conventional classification system. With the availability of microarrays and gene expression profiling this conventional classification has been further refined and discovered biomarkers have been incorporated into the system. Based on gene expression analysis, at least 4 distinct subtypes have been proposed for breast cancer: Luminal A, Luminal B, HER2-overexpression and basal breast cancer [121-123]. A majority of triple negative breast cancers (TNBC) fall into the category of basal breast cancers [124]. Due to the limited availability of gene expression analyses to physicians, the classical immunohistochemical markers, such as progesterone receptor (PR), estrogen receptor (ER) and human epidermal growth factor receptor 2 (HER2) in addition to the determination of the proliferative index as measured by Ki67 staining, have been adopted to the refined subtypes [123]. Several research groups have identified different gene signatures for molecular classification of breast cancer leading to inconsistencies in the number of subtypes and proposed further subdivision [122, 125, 126]. Moreover, classical immunohistochemical marker expression could not be adequately assigned to all proposed subtypes. In an attempt to resolve confusion, the American Joint Committee on Cancer (AJCC) has revised the existing classification system in its 8th edition in 2018 and added prognostic stage groups [121]. Given the topicality, most published studies to date have, however, relied on existing breast cancer classifications, which are therefore also used herein and are summarized for clarity in the table below (Table 1-3).

Table 1-3: Classification of breast cancer subtypes.

Breast cancer subtype	IHC markers	Preferential metastatic sites	Reference
Luminal A	ER+ and/or PR+; HER2-; Ki67-	Bone,	[127, 128]
Luminal B	ER+ and/or PR+; HER2+/-; Ki67-	Bone	[127, 128]
HER2-overexpression	ER-; PR-; HER2+, Ki67+	Bone, brain, liver	[127, 128]
Basal	ER-; PR-; HER2-, basal markers+ (Keratins); Ki67+	Lung, lymph node	[127-131]

As already established in section 1.1.3 (Organ tropism of metastasis), breast cancer preferentially metastasizes to the bone, followed by liver, brain, lymph nodes and lung [132]. These routes of metastasis have been commonly studied and the monitoring of lymph nodes for diagnosis and tumor staging has entered clinical routine. Accumulating evidence shows that individual subtypes do not only determine clinical outcome and prognosis but also have differential patterns of metastasis. In a large comparative study, ILCs were found to predominantly metastasize to peritoneum, gastrointestinal tract and ovaries [133]. In contrast, in patients with IDC, metastases to lung/pleura, distant lymph nodes and brain were more common [133]. A recent epidemiological study concluded that all breast cancers are susceptible to bone metastases but other target organs presented with subtype-specific preferences [128]. HER2-overexpressing tumors were more likely to develop brain and liver metastasis compared to the luminal subtypes whereas basal breast cancers tended to have lung and lymph node metastasis [128, 131].

1.2.2. Breast cancer subtypes – implications in therapy

Despite generally declining numbers in breast cancer deaths over the last decades, mortality continues to be high especially for advanced stages [134]. But even if women present with early-stage disease at diagnosis, almost 30% will eventually develop distant metastasis indicating that the effectiveness of current breast cancer therapies is still insufficient [135]. The standard of care for breast cancer currently involves chemotherapy, radiation, surgery, hormonal therapy as well as immunotherapy but also more targeted approaches relying on monoclonal antibodies and small molecule inhibitors [136]. The primary choice of therapy and survival thereby depend on tumor stage at diagnosis, age and level of fitness, but also on the molecular subtype of breast cancer [137]. A population-based analysis of data extracted from the Ontario Cancer Registry concluded that patients with Luminal A breast cancer have the greatest survival whereas patients with TNBC do worst [138]. It is quite similar with therapeutic options: patients with hormone-receptor positive (HR+) subtypes can benefit from multiple targeted therapies whereas options for TNBC patients are still limited to date. For hormone receptor-positive breast cancer the mainstay of therapy is endocrine therapy downregulating hormone levels or blocking hormone-induced signalling. These therapeutics generally include selective estrogen receptor modulators (SERMs), selective estrogen receptor downregulators (SERDs) and aromatase inhibitors (AIs) which are usually administered sequentially [139, 140] but also combination therapy has been suggested [141]. HER2-targeting therapies are the standard regimen of care for HER2-overexpression breast cancers. First line of treatment

thereby consists of neoadjuvant therapy with chemotherapy and/or HER2-targeting therapy followed by surgery, persistent anti-HER2 therapy and radiotherapy [139, 140]. As already mentioned, TNBC is the most aggressive breast cancer subtype and prognosis is generally poor. This might at least partially be due to the limited treatment options as molecular targets are yet to be defined. Chemotherapy usually involving taxanes, anthracycline or platinum-based drugs partially in combination with anti-angiogenic therapy (anti-VEGF, bevacizumab) is the only FDA-approved treatment option so far [140, 142]. Due to the non-satisfactory results of this treatment regimen, several new strategies are currently in clinical testing. The discovery of a subtype of TNBC with *BRCA1/2* mutations is the first promising step towards a targeted therapy suggesting the use of Poly(ADP-ribose) Polymerase Inhibitors (PARP) in combination with existing chemotherapy [143].

Despite initial response to treatment, breast cancer patients often develop resistance, so that novel strategies are being exploited and new small molecule inhibitors have been developed. An approach successfully tested in the treatment of various solid tumors is immunotherapy, for example with PD-1 [144-146] and PD-L1 [147], which is currently tested on patients with TNBC [148]. Very promising results were also obtained with Cyclin Dependent Kinase 4 and 6 Inhibitors for the treatment of hormone receptor positive breast cancer, but also inhibitors targeting Histone Deacetylase have entered clinical testing [140]. Moreover, targeting of signal transduction pathways and transcription factors is being explored. For the PI3K/AKT as well as mTOR pathway small molecule inhibitors have already been approved or are tested in clinical trials [140, 149]. Further potential targets identified in preclinical models include retinoid receptors, as their ligand retinoid acid was shown to interfere with breast cancer growth and invasiveness, and the transcription factor AP-1, which is able to induce cell transformation. Aberrant AP-1 activation results in sustained survival and enhanced motility [150]. Blocking of AP-1 inhibited proliferation and consequently growth of breast cancer *in vitro* [151, 152] and *in vivo* [153]. Approaches to target AP-1 include RNA interference [154], transcription factor decoys [154] and small molecule inhibitors [150, 155], which have partially advanced to clinical trials [155].

Despite recent advances in breast cancer therapy, therapy resistance and late recurrence remain major challenges. The use of systemic chemotherapy as first line treatment for TNBC or as a “last option” in advanced stages furthermore poses a detrimental deterioration of quality of life for breast cancer patients. This urges the need for the identification of novel therapeutic targets but also the exploration and implementation of anti-metastatic therapies.

1.3. JUNB/AP-1 – a context-dependent transcriptional regulator

1.3.1. Structure, function, physiology and pathophysiology

Activating Protein-1 (AP-1) is a family of transcription factors implicated in physiological as well as pathological conditions, such as proliferation [156-159], differentiation [156, 157] and inflammation [156, 157, 160, 161]. AP-1 members are comprised of homo- or heterodimers predominantly formed by JUN (JUNB, c-JUN, JUND) and FOS proteins (FOSB, FOS, FRA-1, FRA-2). In addition, also the Activating Transcription factor (ATF) proteins (ATF2, LRF1/ATF3, B-ATF, JDP1 and JDP2) can be components of AP-1. Members of the JUN family can assemble into homo- and heterodimers whereas FOS proteins need a JUN partner for DNA binding. Depending on the exact dimer composition, DNA binding occurs at so called TPA

responsive elements (TRE) with a consensus motif 5′-TGA(C/G)TCA-3′ or cyclic AMP responsive elements (CRE) (5′-TGACGTCA-3′) [162] but binding has also been demonstrated to sites deviating from the optimal sequence [162-164]. Structurally, DNA binding is mediated by the evolutionary conserved bZIP domain which can be further subdivided into two distinct parts: the basic region mediating DNA binding and the leucine-zipper required for dimerization of the two AP-1 members [165, 166] (Figure 1-2).

AP-1 members are considered immediate early gene products which are rapidly induced upon extracellular stimulation by growth factors [167, 168], cytokines [169], stress signals [170], carcinogens [171] or tumor promoters such as 12-O-Tetradecanoylphorbol-13-acetate (TPA) [168, 172, 173]. Due to its vast involvement in a multitude of signaling pathways, AP-1 activity must be tightly controlled. Regulation is achieved at the level of gene expression of AP-1 subunits, mRNA stability or posttranslationally for example by phosphorylation [165]. Gene expression of AP-1 targets is furthermore controlled by cooperative recruitment of additional transcription factors and coactivators to promoter regions. In this context, it has been shown that AP-1 can interact with CBP/p300 [174, 175], Smad proteins [176], NFAT [177] and Ets [178].

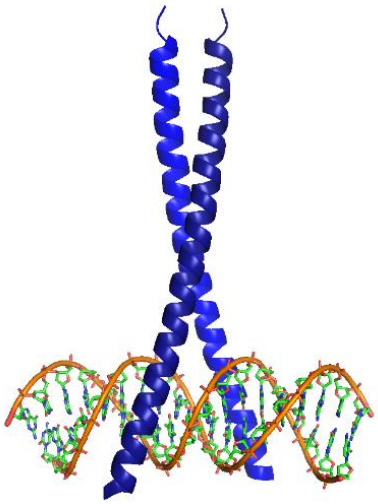

Figure 1-2: Structure of the AP-1 dimer bound to DNA.

The bZIP domain of the v- Jun homodimer in complex with DNA. Structure visualized with PyMOL based on PDB entry 2H7H.

Gene knockout studies have established that the individual AP-1 members cannot compensate each other in some cases but are also partially redundant in others. With this approach it has been established that JUN [179, 180], JUNB [181], FRA-1 [182] and FRA-2 [183] are indispensable for embryonic development as mutants failed to survive until adulthood. Embryonic lethality of JUN-null mice could, however, be rescued by re-expression of JUNB thereby restoring liver and cardiac defects [184]. Tissue-specific deletion strategies further confirmed the notion that individual AP-1 members had distinct functions. JUN was shown to be important for liver and heart development [185], eye lid closure [186] and skin homeostasis [186, 187] as well as liver regeneration [188] whereas JUNB was found to be essential for placentation [181], neovascularization [181] and angiogenesis [189] as well as T helper cell differentiation [190, 191]. Genetic ablation of FOS revealed its strong necessity in bone development [192] and physiology of the central nervous system [193]. At the cellular level,

AP-1 members have been implicated in proliferation, differentiation and survival, where they can exert both stimulatory as well as inhibitory functions [165]. As best exemplified in proliferation, AP-1 is able to both promote and inhibit cellular growths by regulating gene expression of components of the cell cycle control system, such as cyclin A [159], cyclin D1 [194], cyclin E [195], $p16^{INK}$ [196], $p21^{Cip1}$ [184] and p53 [184].

1.3.2. AP-1 in oncology

Originally, JUN [197, 198] and FOS [199] had been identified as cellular homologues of the retroviral v-Jun and v-Fos which act as oncoproteins inducing aberrations in cell cycle control. This hinted the notion that AP-1 could not only have functions in physiology but also be involved in pathophysiology and neoplastic transformation. Early studies demonstrated that overexpression of AP-1 components could lead to cell immortalization and tumor formation as FOS-expressing transgenic mice ultimately developed bone tumors [200-202]. FOS was furthermore shown to be essential for the progression of skin tumors in a TPA-induced skin cancer model [203]. For JUN proteins, the picture was a little more complex. Despite initial reports showing that epidermal expression of a dominant negative JUN mutant lead to a substantial reduction in papilloma induction in a two-step skin carcinogenesis mouse model [204], deletion of JUN in keratinocytes could not confirm JUN to be absolutely required for skin tumourigenesis [186]. In a model of liver cancer, requirement of JUN was restricted to early stages whereas in later stages no effect of JUN deletion on tumor progression was found [205]. These studies highlight that the involvement of individual AP-1 members in oncogenesis is highly dependent on tumor type, stage and differentiation status.

1.3.3. JUNB in cancer and metastasis

In contrast to JUN, JUNB has traditionally been considered a tumor suppressor. Original publications attributed JUNB anti-tumoral activity due to the observed antagonistic effect on JUN-mediated growth and transformation [202, 206]. This notion is furthermore supported by the fact that *JUNB* is downregulated in the hematopoietic stem cell compartment of patients with acute myeloid leukemia [207] (Figure 1-3). Similarly, the *JUNB* promoter is silenced by hypermethylation and expression is consequently lost in patients suffering from chronic myeloid leukemia [208]. Moreover, inactivation of *Junb* in the myeloid compartment led to a transplantable myeloproliferative disease eventually progressing to blast crisis resembling human chronic myeloid leukemia [209]. In line with these findings, JUNB levels have been found to be lower in breast [210, 211] and prostate cancer [212, 213] compared to the surrounding normal tissue. Contrary results have, however, also been published, underscoring that the picture might be less clear than originally thought. Although ectopic expression of *Junb* did not result in an overt phenotype in mice [214], JUNB overexpression has been observed in a multitude of human cancers. It has been especially well studied in various lymphomas, such as Hodgkin's lymphoma [215], anaplastic large cell lymphoma [216] and CD30+ diffuse large B-cell lymphoma [217] but has also been found in a wide variety of other cancers, for example in the colon [218], ovaries [219], breast [210], von Hippel-Lindau-deficient clear-cell renal-cell carcinoma (ccRCC) [220] and murine fibrosarcoma [221].

Although levels of JUNB have been found to be deregulated in a multitude of cancer types, functional consequences have not been fully elucidated to date. In a screen of BRAF(V600E)-mutated cell lines of malignant melanoma, JUNB emerged to confer resistance to Raf inhibitors

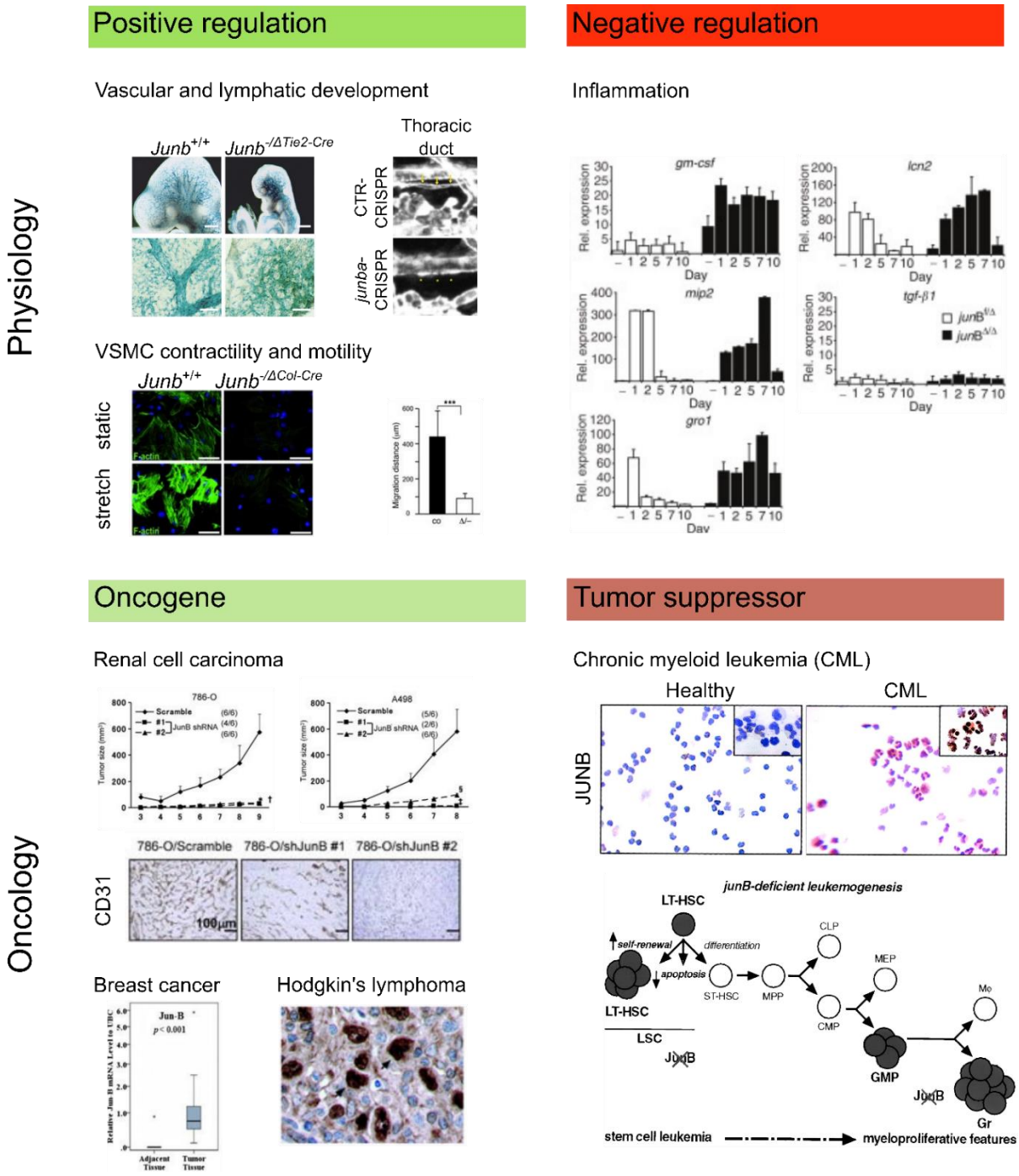

Figure 1-3: Functions of JUNB in physiology and oncology.

JUNB positively regulates vascular as well as lymphatic development [227], vascular homeostasis [228] and vascular smooth muscle cell (VSMC) contractility and motility [229]. JUNB exerts a negative impact on gene expression, especially on inflammatory cytokines [230]. Moreover, JUNB also has a dual role in tumorigenesis. It can function as an oncogene, for example in renal cell carcinoma [220], breast cancer [210] and Hodgkin's lymphoma [215]. In leukemia, such as chronic myeloid leukemia [208, 231], JUNB acts as tumor suppressor.

[222]. In correlational studies, JUNB has been associated with oncogenesis and metastasis but findings have been partially contradictory. On one hand, JUNB levels were found significantly upregulated in specimens of prostate [213] and breast cancer [210, 211] compared to the surrounding normal tissue but on the other hand *JUNB* levels were negatively correlated to tumor stage [210]. In an earlier functional study, ectopic expression of JUNB led

to cell transformation in mild fibromatosis cells [221]. In line with the context-dependent expression patterns, the association of JUNB with invasiveness also seems to depend on the type of cancer. In ccRCC cell lines, diminished *JUNB* expression by short hairpin-mediated knockdown suppressed their invasiveness *in vitro* and resulted in slower tumor growth and reduced angiogenesis *in vivo* when xenotransplanted into nude mice [220]. Likewise, reduction of JUNB levels by siRNA-mediated knockdown decreased the potential of breast cancer cells to invade into a collagen matrix upon TGFβ stimulation [223]. Indicating a similar association of JUNB with invasive features, *Junb* levels were induced in mammary cells upon TGFβ-induced EMT [224] as well as in IL6-driven invasion in uveal melanoma cells [225]. In contrast, mice were more prone to invasive cancer development when JUNB had been ablated in the prostate epithelium [213]. This enhanced progression was most likely the result of increased proliferation and reduced senescence due to attenuated levels of $p16^{Ink4a}$ and $p21^{Cip1}$ [213]. Functional studies connecting JUNB to metastasis are limited so far. By genomic analyses Hyakusoku et al. initially identified JUNB as a key regulator of metastasis in head and neck squamous cell carcinoma (HNSCC) [226]. The authors showed that genetic deletion of *JUNB* by CRISPR-Cas9 in metastatic HNSCC cell lines limited metastasis to the lungs of nude mice in an experimental metastasis assay. Furthermore, cell invasion was reduced as shown in a matrigel invasion assay. All these studies have, however, largely focussed on JUNB expression in the tumor cells thereby neglecting a potential impact of the surrounding stroma. A previous investigation focussing on the contribution of stromal JUNB to primary tumor growth and tumor angiogenesis reported no differences between *Junb* knockout and control mice, though [232]. JUNB has, however, been shown to be essential in the blood [228, 229] and lymphatic vascular system [227], which are important players in the dissemination of metastatic cells. Moreover, JUNB was published to regulate T helper cell polarization [190, 191] and macrophage activation [233]. Whether these functions of stromal JUNB play a role in tumor progression and metastatic spread has, however, not been addressed so far.

Taken together, these reports exemplify that JUNB is a highly context-dependent transcriptional regulator and its involvement in cancer and metastatic dissemination is by far not fully understood. Depending on the tissue, cell type and tumor stage JUNB has different roles both promoting as well as inhibiting tumor progression.

1.4. Objective

Assessment of primary tumor invasion and metastatic spread are clinically most relevant but mechanistically still insufficiently understood. Already several years ago, AP-1 transcription factors have been shown to be decisive components in the regulation of essential cellular processes, such as proliferation, differentiation and apoptosis. Imbalances in expression levels have been linked to pathophysiology and cellular transformation. The AP-1 member JUNB has thereby been shown to exert a dual role: it can act both as a tumor suppressor and as an oncogene, largely depending on the tumor type and stage. JUNB levels have been found deregulated in multiple cancer entities and JUNB has furthermore been linked to invasion and metastasis. To date, these links to invasion and metastasis are, however, largely based on *in vitro* experiments assessing matrix invasion in trans-well systems or on experimental metastasis assays *in vivo*. Consequently, these assays ignore the complexity of the metastatic cascade and the importance of the surrounding native environment. Existing human studies are predominantly correlational and have even yielded partially contradictory results. Furthermore most investigations have exclusively examined JUNB expression in tumor cells

or focussed on gene expression analyses of the bulk of the tumor or metastatic tissue thereby neglecting the potential contribution of stromal JUNB. Direct functional evidence assessing the influence of stromal JUNB on metastasis is, thus, still missing.

Consequently, I aimed to investigate the functional consequences of JUNB loss in the stroma on metastasis following an *in vivo* approach in mice.

(I) For this purpose, elaborate spontaneous metastasis models involving primary tumor excision were performed *in vivo*, thereby comparing metastatic burden in mice with conditional *Junb* deletion in the stroma to adequate controls.

(II) Furthermore, various components of the microenvironment, such as tumor angiogenesis, lymphangiogenesis and immune cell infiltration were examined in primary tumors and in pre-metastatic lungs to gain a more mechanistic insight on the role of JUNB in metastasis.

2 MATERIALS

2. MATERIALS

2.1. Antibodies and compounds

2.1.1. Primary antibodies

Table 2-1: Primary antibodies used for immunohistochemistry and immunofluorescence

Antigen	Clone	Host species	Dilution	Antigen retrieval	Company/catalogue number
CD31	polyclonal	rabbit	1:200	TE pH 9	Abcam # ab28364
Lyve-1	ALY7	rat	1:100	TE pH 9	affymetrix #14-0443
Podoplanin	8.1.1.	Syrian hamster	1:500	Citric buffer pH 6	Hybridoma Bank
mCherry	polyclonal	rabbit	1:300	Proteinase K	Abcam #ab167453
CD45	30-F11	rat	1:100	Citric buffer pH 6	Novus #NB100-77417
CD11b	EPR1344	rabbit	1:2000	Citric buffer pH 6; EDTA pH 8	Abcam #ab133357
CD3	CD3-12	rat	1:100/1:200	EDTA pH 8; TE pH 9	Bio-Rad #MCA1477T
Foxp3	FJK-16s	rat	1:100	EDTA, pH 8	ebioscience #14-5773-80
Ly6B.2	7/4	rat	1:300	TE pH 9	Abcam #ab53457
F4/80	CI:A3-1	rat	1:100	Proteinase K	Genetex #GTX26640
CD8	EPR20305	rabbit	1:2000	TE pH 9	Abcam #ab209775

Table 2-2: Primary antibodies used for flow cytometry

Antigen	Clone	Dilution	Company/catalogue number
CD16/CD32	93	1:100	ebioscience # 14-0161-82
CD45.1	A20	1:200	Invitrogen #48-0453-82
CD45.2	104	1:500	Biolegend #109814
CD11B	M1/70	1:200	Biolegend #101261
LY6G	1A8	1:500	BD #551460
LY6C	HK1.4	1:200	Biolegend #128035
GR-1	RB6-8C5	1:200	Biolegend #108405
CCR2	475301	1:50	R&D #FAB5538P-025

Table 2-3: Primary antibodies for *in vivo* use

Antibody	Clone	Company/catalogue number	LOT number
*InVivo*Plus anti-mouse Ly6G	1A8	BioXCell #BP0075-1	626717M2B
*InVivo*Plus rat IgG2a, κ isotype control anti-trinitrophenol	2A3	BioXCell #BP0089	686318F1B

2.1.2. Secondary antibodies

Table 2-4: Secondary antibodies used for immunohistochemistry and immunofluorescence

Antigen	Host species	Dilution	Conjugation	Company/catalogue number
Rabbit IgG	Goat	1:500	biotin	Vector Laboratories #BA-1000
Rat IgG	Goat	1:500	biotin	Vector Laboratories #BA-9400
Syrian Hamster IgG	Goat	1:500	biotin	Jackson ImmunoResearch #107-065-142
Rabbit IgG	Donkey	1:250	Alexa 647	Invitrogen #A31573
Rabbit IgG	Goat	1:250	Alexa 546	Invitrogen #A11010
Rat IgG	Goat	1:250	Alexa 647	Invitrogen #A21247
Rat IgG	Goat	1:250	Alexa 546	Invitrogen #A11081

2.1.3. Reagents used for immunofluorescence and flow cytometry

Table 2-5: Compounds used for immunofluorescence

Compound	Dilution	Company/Catalogue number
Streptavidin-Cy3	1:500	Biolegend #405215
Hoechst 33342	1:1000	chemodex #CDX-B0030

Table 2-6: Viability dyes used for flow cytometry

Dye	Dilution	Company/catalogue number
Propidium Iodide (PI)	1 µL/test	Biolegend #421301
7-Aminoactinomycin D (7AAD)	2 µL/test	Biolegend #420404

2.2. Biomolecular reagents and enzymes

2x *Power* SYBR™ Green Master Mix	Applied Biosystems, UK
10% Normal Goat Serum	Thermo Scientific, USA
Normal Goat Serum	Vector Laboratories, USA
Oligo $(dT)_{18}$ primers	Thermo Scientific
Phosphatase Inhibitor Cocktail II	Sigma, Steinheim
Protease Inhibitor Cocktail	Sigma, Steinheim
Proteinase K	Sigma, Steinheim
Random Hexamer primers	Fermentas, USA
RevertAid Reverse Transcriptase	Thermo Scientific, USA
RiboLock RNase Inhibitor	Thermo Scientific, USA

2.3. Buffers and solutions

Buffer	Composition
ACK erythrocyte lysis buffer (pH 7.2-7.4)	150 mM NH_4Cl 10 mM $KHCO_3$ 0.1 mM EDTA
Blocking buffer for immunofluorescent staining	5% goat serum 5% Normal Goat Serum Blocking Solution (10%)
Blocking buffer for immunohistochemistry	10% goat serum/PBS
Citrate buffer (pH 6) for antigen retrieval	1.8 mM citric acid 8.2 mM sodium citrate
EDTA buffer (pH 8) for antigen retrieval	1 mM EDTA
Extraction buffer for DNA isolation (pH 12.0)	10 mM Tris-HCl, pH 8.0 0.1 M NACl 1 mM EDTA 1% SDS
FACS buffer	1% BSA/PBS
PBS, 10x (pH 7.2)	1.5 M NaCl 27 mM KCl 82 mM Na_2HPO_4 x 2 H_2O 17 mM NaH_2PO_4 x H_2O
TE buffer (pH 9) for antigen retrieval	10 mM Tris-HCl 1 mM EDTA

2.4. Cell lines, cell culture conditions and reagents

Table 2-7: Cell lines

Name	Species	Tissue	Origin
B16F10	mouse	Melanoma	R. Offringa, Heidelberg
EO771.LMB	mouse	Mammary Carcinoma	R. Anderson, Melbourne
Lewis Lung Carcinoma (LL/2-Luc M38)	mouse	Lung Carcinoma	Caliper Life Sciences

Table 2-8: Cell culture conditions

Cell line	Culture conditions	Medium	Additives	Company/catalogue number
B16F10	37°C, 5% CO_2	RPMI 1640, GlutaMAX		
			10% FBS	Sigma #F7524
EO771.LMB	37°C, 5% CO_2	DMEM		
			10% FBS	Sigma #F7524
			1% L-glutamine	Sigma #G7513
			20 mM HEPES	
Lewis Lung Carcinoma	37°C, 8% CO_2	DMEM		
			10% FBS	Sigma #F7524
			1% L-glutamine	Sigma #G7513

Table 2-9: Cell culture reagents

Reagent	Company/catalogue number
Accutase	Sigma #A6964
Dulbecco's Phosphate Buffered Saline (DPBS)	PAN Biotech #P04-36500
Trypan Blue	Fluka, Neu-Ulm

2.5. Chemicals and reagents

Ammonium acetate (NH_4OAc)	Roth, Karlsruhe
Ammonium chloride (NH_4Cl)	Merck, Darmstadt
Bovine serum albumin (BSA)	PAA, Austria
Bradford MX™	Expedeon, UK
Calcium chloride	Merck, Darmstadt
Citric acid	AppliChem, Darmstadt
Chloroform	Sigma-Aldrich, Steinheim
Desoxynucleotide triphosphates	Fermentas, Lithuania
Dimethylsulfoxide (DMSO)	Biomol, Hamburg
Disodium phosphate (Na_2HPO_4)	Fluka, Seelze
Dithiothreitol (DTT)	Gerbu, Heidelberg
Eosin B	Morphisto, Frankfurt am Main
Ethanol	VWR, France
Ethylenediamine-tetraacetate (EDTA)	Roth, Karlsruhe
Eukitt®	O. Kindler, Bobingen
FITC-dextran 70 kDa	Invitrogen, USA
Fluorescent Mounting Medium	Dako/Agilent, USA
Hematoxylin	Morphisto, Frankfurt am Main
HEPES	Gerbu, Heidelberg
Hydrogen peroxide (H_2O_2)	AppliChem, Darmstadt
Isopropanol (2-propanol)	Fisher Chemical, UK
Ketamine hydrochloride (Ketavet100)	Zoetis, USA
Methanol	Fisher Chemical, UK
Nuklease-free water	Qiagen, Hilden
Paraformaldehyde (PFA)	Roth, Karlsruhe
Potassium chloride (KCl)	Roth, Karlsruhe
Potassium bicarbonate ($KHCO_3$)	Merck, Darmstadt
Pre-diluted Protein Assay Standards (BSA)	Thermo Scientific, USA
Sodium chloride	Fisher Scientific, UK
Sodium citrate tribasic dihydrate	Fluka, Buchs
Sodium dihydrogen phosphate (NaH_2PO_4)	Neolab, Heidelberg
Sodium dodecyl sulfate (SDS)	Fluka, Buchs
Sodium hydroxide	Sigma-Aldrich, Steinheim
Tris hydrochloride (Tris HCl)	Roth, Karlsruhe
Triton-X-100	AppliChem, Darmstadt
Xylazin hydrochloride (Rompun®)	Bayer, Leverkusen
Xylene	VWR, France

2.6. Commercially available Kits

DAB Peroxidase Substrate kit	Vector Laboratories, USA
MiRNeasy® Mini kit	Qiagen, Hilden
VECTASTAIN® Elite® ABC HRP Kit	Vector Laboratories, USA
Venor®GeM Classic Kit	Minerva biolabs®, Berlin

2.7. Consumables

BD Micro-Fine™+ U-100 Insuline syringes	Becton Dickinson, USA
Cell culture plates	Sigma, USA
Cell strainer (70 µm)	Corning, USA
Cellulose Swabs Beesana®	Beese Medical, Barsbuttel
Conical centrifuge tubes 15 mL	Corning, USA
Conical centrifuge tubes 50 mL	Corning, USA
Cover slips	Th. Geyer, Renningen
CryoTube™ vials	Thermo Fisher, Denmark
EDTA-coated tubes Microvette® 100 K3E	Sarstedt, Nümbrecht
ELISA plates 96-well clear	Sarstedt, Nümbrecht
Embedding cassette Histosette	Simport, The Netherlands
Embedding cassette Mega Cassette	Sakura, USA
Feather disposable scalpel	Feather, Japan
Filter pipette tips (10 µL/20 µL/200 µL)	Kisker, Steinfurt
Filter pipette tips (1000 µL)	Nerbe Plus, Winsen
Foam biopsy pads Surgipath®	Leica, The Netherlands
Hypodermin needles	Chirana T. Injecta, Slovac republic
ImmEdge Pen™	Vector Laboratories, USA
MicroAmp® fast optical 96-well reaction plate	Applied Biosystems, USA
MicroAmp® optical adhesive covers	Applied Biosystems, Singapore
Microplate 96 well clear bottom, black	Greiner Bio-One, Frickenhausen
Object slides Superfrost® Plus	Thermo Scientific, USA
Parafilm PM996	Bemis, USA
Pasteur capillary pipettes	WU, Mainz
PCR reaction tubes	Nerbe Plus, Winsen
Petri dishes (35 mm, 60 mm)	Greiner Bio-One, Frickenhausen
Pipette tips (10 µL/20 µL/200 µL/1000 µL)	Steinbrenner, Wiesenbach
Povidone Iodine Braunol®	B. Braun Melsungen AG, Melsungen
Reaction tubes (1.5 mL)	Sarstedt, Nümbrecht
Reaction tubes (2 mL)	Eppendorf, Hamburg
Reaction tubes (2 mL, amber)	VWR, USA
Reaction tubes (5 mL)	Sarstedt, Nümbrecht
Serological pipet (2.5 mL/5 mL/10 mL/25 mL)	Corning, USA
Round bottom tubes	Greiner Bio-One, Austria
Sugi® Eyespear pointed tips	Kettenbach, Eschenburg
Suture Ethilon (4-0/5-0)	Ethicon, UK
Syringes 1 mL Injekt®-F	B. Braun Melsungen AG, Melsungen

Syringes Terumo® 10 mL	Terumo®, Japan
Tissue embedding medium Histo-Comp®	Vogel, Fernwald

2.8. Equipment

Animal Trimmer Aesculap® Isis	Braun, Suhl
Axio Scan.Z1 Slidescanner	Zeiss, Oberkochen
Bacterial incubator Kelvitron®t	Heraeus Instruments, Hanau
BD FACSCanto™ II	Becton Dickinson, Heidelberg
Bioruptor	Diagenode, Belgium
Cauterizer	Fine Sciene Tools, Heidelberg
Cauterizer Tips	Fine Sciene Tools, Heidelberg
Cell incubator Heraeus HERA cell 240	Heraeus Instruments, Hanau
Cell incubator	Binder, Tuttlingen
Centrifuge Biofuge 13	Thermo Scientific, Osterode am Harz
Centrifuge Heraeus Megafuge 16	Thermo Scientific, Osterode am Harz
Centrifuge Heraeus Pico 17	Thermo Scientific, Osterode am Harz
Centrifuge Variofuge 3.0R	Heraeus Sepatech, Osterode am Harz
Cooling centrifuge 5403, 5415R	Eppendorf, Hamburg
Digital caliper	RS Pro, Mörfelden-Walldorf
Embedding machine Tissue-Tek TEC	Sakura, USA
Fine scale XS205 DualRange	Mettler Toledo, Gießen
Gooseneck lamp KL1500	Schott, Mainz
Heating mat Bosotherm 2000	Bosch+Sohn, Jungingen
Hemavet 950FS	Drew Scientific, USA
Isoflurane gas vaporizer Vapor 19.3	Dräger, Lübeck
Magnetic stirrer/heat plate Ika® RH basic 2	IKA, Staufen
Magnetic stirrer/heat plate Variomag Monotherm	H+P Labortechnik, München
Mikroplate reader Clariostar	BMG Labtech, Ortenberg
Mikroscope Leica DMLB	Leica, Bensheim
Mikroscope Nikon Ti Eclipse	Nikon, Düsseldorf
Microscope Olympus TH4-200	Olympus, Japan
Microtome SM2010 R	Leica, Bensheim
Microtome Hn40	Reichert-Jung/Leica, Bensheim
NanoDrop UV-VIS ND-1000 Spectrophotometer	PeqLab, Erlangen
pH meter 765 Calimatic	Knick, Berlin
Pipettes (Pipetman)	Gilson, USA
Pipettes (Eppendorf Research)	Eppendorf, Hamburg
Pipettor Pipetboy acu	Integra Biosciences, Switzerland
Red light lamp LF-15E	Zoo Med Laboratories, USA
Scale KERN® 440-47N	Kern & Sohn, Balingen
Silicon mat	René Remie Surgical Skill Centre, The Netherlands
Shaker SD5D	CAT Laboratories, Staufen
Slide Staining Tray	Pyramid Innovation, UK
StepOnePlus Real-time PCR system	Applied Biosystems, UK

Sterile GARD Hood VBM600	Baker Company Inc., USA
Surgical hooks	René Remie Surgical Skill Centre, The Netherlands
Surgical tools	Fine Science Tools, Heidelberg
Thermocycler PTC-200	MJ Research, USA
Thermocycler MJ Mini	Bio-Rad Laboratories, Munich
Thermomixer 5437	Eppendorf, Hamburg
Water bath	GFL, Burgwedel
Vortex	Bender&Hobein/IKA, Staufen
Vacuum Infiltration Processor	Sakura, Heidelberg
Z2 Coulter Particle Count and Size Analyzer	Beckman Coulter, USA

2.9. Mice

Table 2-10: Mouse lines

Mouse line	Description	Company/origin
C57BL/6NCrl	Wildtype	Charles River
C57BL/6NRj	Wildtype	Janvier
B6.SJL-PtprcaLy5.1	Expression of *Ptprca*	DKFZ
Col1α2-Cre B6.Tg(Col1α2-Cre)23Angl	Expression of Cre recombinase in multiple cell types derived from mesenchyme	P. Angel, DKFZ [234]
Junb$^{>/>}$ B6.*Junb*^{tm3Wag}/N	Floxed *Junb* allele	M Schorpp-Kistner, DKFZ
CMV-Cre B6.TgN(CMV-Cre)1Cgn	Ubiquitous expression of Cre Recombinase	P. Angel, DKFZ, Originally from K. Rajewski, Cologne, [235]
Junb $^{\Delta \text{ CMV Cre/+}}$ B6.*Junb*$^{tm3.1Angl}$/+	Obtained by crossbreeding CMV-Cre and *Junb* $^{>/+}$	M Schorpp-Kistner, DKFZ
Junb $^{\Delta \text{ CMV-Cre/+, Col1α2-Cre}}$	Obtained by crossbreeding *Junb*$^{\Delta \text{ CMV-Cre/+}}$ and Col1α2-Cre	M Schorpp-Kistner, DKFZ
Junb $^{\Delta \text{ CMV-Cre/}\Delta \text{ Col1α2-Cre}}$	Obtained by crossbreeding *Junb*$^{\Delta \text{ CMV-Cre/+, Col1α2-Cre}}$ and *Junb* $^{>/>}$	M Schorpp-Kistner, DKFZ
Junb $^{+/+, \text{ Col1α2-Cre}}$	Obtained by crossbreeding Col1α2-Cre and *Junb* $^{+/+}$	M Schorpp-Kistner, DKFZ

2.10. Oligonucleotides

Table 2-11: Oligonucleotide primers for qRT-PCR

Gene	Forward/ reverse	Sequence	Effi-ciency	Fragment size	Refe-rence
Adgre1	for rev	GTGCCATCATTGCGGGATTC AAGAGCATCACTGCCTCCAC	2.02	79 bp	
B2m	for rev	CTCGGTGACCCTGGTCTTTC TTGAGGGGTTTTCTGGATAGCA	1.90	70 bp	
Ccl2	for rev	CGGCTGGAGCATCCACGTGTT TAGCAGCAGGTGAGTGGGGC	2.02	63 bp	[236]
Ccl5	for rev	CCTCACCATATGGCTCGGACACC GCGCGAGGGAGAGGTAGGCA	2.07	57 bp	[236]
Cd163	for rev	GTGCTGGATCTCCTGGTTGTA GGAGCGTTAGTGACAGCAGA	1.87	97 bp	
Cd3ε	for rev	CAGGACGATGCCGAGAACATT GAGGGCACGTCAACTCTACA	1.95	70 bp	
Cd8α	for rev	GAATCTGCGTGGCCCTTCTG ACTAGCGGCCTGGGACATTT	2.01	94 bp	
Csf3	for rev	GCAGGCTCTATCGGGTATTTCC GCAACATCCAGCTGAAGCAA	1.80	66 bp	[237]
Cxcl1	for rev	CCGAAGTCATAGCCACACTCAA GCAGTCTGTCTTCTTTCTCCGTTAC	1.85	128 bp	[238]
Cxcl2	for rev	AGACAGAAGTCATAGCCACTCTCAAG CCTCCTTTCCAGGTCAGTTAGC	1.94	126 bp	[238]
Cxcl5	for rev	TGCCCTACGGTGGAAGTCAT AGCTTTCTTTTTGTCACTGCCC	1.92	120 bp	
Cxcl12	for rev	TGCATCAGTGACGGTAAACCA CACAGTTTGGAGTGTTGAGGAT	1.96	118 bp	[239]
Foxp3	for rev	GACCCCCTTTCACCTATGCC GGCGAACATGCGAGTAAACC	1.94	107 bp	
Fap	for rev	ACGCTGTGCAGTGAGAATCAG GACAGTTTTCAGCCATGTCTTCATT	1.96	70 bp	
Il-1α	for rev	GAGAAGACCAGCCCGTGTTG TGGATAAGCAGCTGATGTGAAGTAG	2.10	131 bp	J. Leibold
Il-1β	for rev	TTCAGGCAGGCAGTATCACTC CGGAGCCTGTAGTGCAGTTG	1.99	195 bp	J. Leibold
Itgam	for rev	CATCCCCCTGCAAGTACCTC GGGGGACAGTAGAAACAGCC	1.92	74 bp	
Klrb1c	for rev	AGTGTCTTAGTGCGAGTCTTAGT CCAGTCTTGTGGGCACTCTA	1.92	120 bp	
Ly6c	for rev	GCAGTGCTACGAGTGCTATGG ACTGACGGGTCTTTAGTTTCCTT	1.90	140 bp	[240]

Gene	Forward/ reverse	Sequence	Effi-ciency	Fragment size	Refe-rence
Ly6g	for rev	TTGTATTGGGGTCCCACCTG CCAGAGCAACGCAAAATCCA	1.91	77 bp	[241]
mCherry	for rev	GACCACCTACAAGGCCAAGAAG AGGTGATGTCCAACTTGATGTTGA	1.93	74 bp	[242]
Ppia	for rev	AATTCATGTGCCAGGGTGGTG TGCCTTCTTTCACCTTCCCAA	1.84	231 bp	
Prptc	for rev	GAGGTGTCTGATGGTGCAAG TGTATTCCACTAAAGCCTGATGAA	1.99	65 bp	[243]
S100a8	for rev	TCCTTGCGATGGTGATAAAA GGCCAGAAGCTCTGCTACTC	1.96	73 bp	[244]
S100a9	for rev	CACCCTGAGCAAGAAGGAAT TGTCATTTATGAGGGCTTCATTT	1.99	95 bp	[244]
Spp1	for rev	GACAACAACGGAAAGGGCAG ATCACATCCGACTGATCGGC	2.05	116 bp	
Tnfα	for rev	GTAGCCCACGTCGTAGCAAA TTGAGATCCATGCCGTTGGC	1.89	95 bp	
Vimentin	for rev	AGCTGCTAACTACCAGGACACTATTG CGAAGGTGACGAGCCATCTC	1.90	81 bp	[242]

2.11. Software

BD FACSDiva™ Software	Becton Dickinson Biosciences, Heidelberg
EndNote v.X7	Adept Scientific GmbH, Frankfurt
FlowJo V10	Tree Star, Inc., Ashland, USA
GraphPad Prism 7.05	GraphPad Software, Inc., La Jolla, USA
Image J	National Institutes of Health, USA
Inkscape 0.92.3	Inkscape Project, USA
NIS Elements AR 4.13.04	Nikon, Darmstadt
Office 2013	Microsoft, USA
Primer-BLAST, https://www.ncbi.nlm.nih.gov/tools/primer-blast/	National Institutes of Health, USA
StepOne Software v2.3	Life Technologies, Darmstadt
ZEN2.3 (blue edition)	Zeiss, Oberkochen

3 METHODS

3. METHODS

3.1. Molecular biology methods

3.1.1. RNA isolation with on-column DNase-digestion

Tissue samples stored in QIAzol® lysis reagent (Qiagen) were thawed on ice and disrupted mechanically with an ULTRA-TURRAX® T25 (IKA® Labortechnik). Tissue homogenates were subsequently transferred to fresh reaction tubes and RNA was isolated using the miRNeasy® Mini Kit (Qiagen) according to manufacturer's instructions. On-column DNase digestion was performed with the RNase-Free DNase Set (Qiagen) following manufacturer's recommendations. RNA was finally eluted in 50 µL RNase-free H_2O and stored at -80°C until further use.

3.1.2. DNA isolation for quantification of metastatic burden

For quantification of metastatic burden via Quantitative real time PCR (qRT-PCR) on the mCherry reporter, genomic DNA was prepared from the same samples previously processed for RNA isolation as described above. The protocol for simultaneous extraction of RNA and DNA using Ambion's ToTALLY RNA™ RNA Isolation Kit (Thermo Fisher) was adapted for use with the miRNeasy® Mini Kit (Qiagen). Following phase separation with chloroform and removal of the aqueous phase, the organic phase including the interphase remain. An equal volume of DNA extraction buffer adjusted to pH 12.0 is added and vigorously shaken for 1 min. After the phases were allowed to separate for 10 min on ice and centrifuged at 12000 g for 20 min at 4°C, the aqueous phase was recovered without contamination of any interphase. Subsequent to addition of 1/15 volume of 7.5 M NH_4OAc and 2 volumes of ice-cold 100% ethanol, samples were inverted once and DNA was allowed to precipitate at -20°C O/N. DNA was pelleted by centrifugation at 12000 g at 4°C for 30 min and the supernatant discarded without detaching the pellet from the vessel wall. Impurities were removed by washing the pellet in 70% ethanol. To ensure the pellet stayed attached to the wall of the tube, the centrifugation step was repeated as stated above. Remaining ethanol was allowed to evaporate at RT and DNA resuspended in 25 µL DNase-free H_2O. DNA was solved by incubation at 37°C for 2-3 h under shaking and eventually vortexing. DNA was stored at -20°C until qRT-PCR.

3.1.3. Determination of DNA and RNA yield and quality

To determine the yield and to detect remaining contaminations, RNA and DNA obtained after isolation described in sections 3.1.1 (RNA isolation with on-column DNase-digestion) and 3.1.2 (DNA isolation for quantification of metastatic burden), were measured by the NanoDrop Spectrophotometer UV-VIS ND-1000 (PeqLab Biotechnology). A 260/280 ratio of absorption of approximately 1.8 or 2.0 was considered pure for DNA or RNA, respectively, and indicated neglectable contamination with proteins or phenolic substances. The 230/260 ratio was used as an additional indicator. Values between 2.0 to 2.2 were generally regarded as good quality.

3.1.4. Reverse transcription

Double stranded cDNA was synthesized from a total of 2 µg isolated RNA. RNA was diluted to 200 ng/µL in H_2O, mixed with 0.25 µL Oligo $(dT)_{18}$ primer (100 µM, Thermo Scientific) as well as 0.25 µL Random Hexamer Primer (100 µM, Fermentas) and heated to 65°C for 5 min to assure that RNA is fully single-stranded. After this denaturation step, a reaction mixture of 4 µL 5x Reaction buffer (Thermo Scientific) supplemented with 0.5 µL dNTPs (25 mM, Fermentas), 0.5 µL RiboLock RNase Inhibitor (40 U/µl, Thermo Scientific) and 1 µL RevertAid Reverse Transcriptase (200 U/µL, Thermo Scientific) was added and reverse transcription performed according to the program below (Table 3-1). Assuming optimal efficiency of the reaction, cDNA is obtained at a concentration of 100 ng/µL. cDNA was stored at -20°C until use.

Table 3-1: Program for reverse transcription

Step	Temperature	Time
Reverse transcription	42°C	1 h
Termination	72°C	10 min
Cooling	10°C	forever

3.1.5. Quantitative real time PCR

Relative target gene expression was determined by quantitative real-time PCR (qRT-PCR) using the StepOnePlus Real-Time PCR system (Applied Biosystems). The reaction was performed in duplicates in 96-well plates in a total reaction volume of 12.5 µL (Table 3-2). Respective forward and reverse primers specific for the target genes are listed in Table 2-11. Quantitative real-time PCR was performed according to the following two-step protocol (Table 3-3).

Table 3-2: Composition of master mix for quantitative real-time PCR

Reagent	Volume
cDNA (1 ng/µL)	2.5 µL
2x *Power* SYBR™ Green Master Mix	6.25 µL
Forward primer (50 µM)	0.075 µL
Reverse primer (50 µM)	0.075 µL
H_2O	3.6 µL

Table 3-3: Program of quantitative real-time PCR

Stage	Temperature	Time	
Holding	95°C	10 min	
Cycling	95°C	15 s	40 cycles
	60°C	1 min	
Melt Curve	95°C	15 s	
	60°C	1 min	
	+0.3°C (up to 95°C)	15 s	

Expression of the gene of interest (GOI) was analysed using StepOne™ software v2.3 (Life Technologies) and calculated following the $\Delta\Delta C_T$ method. Thereby, the cycle of threshold (C_T) determined for the GOI is set relative to the C_T measured for the reference gene (REF). Additionally, the efficiency of the used primer is taken into account. The formula used for calculation is given below (Equation 3-1).

Equation 3-1: Calculation of relative gene expression.

$$Relative\ expression = \frac{Efficiency\ (GOI)^{\Delta C_T(control\ (GOI) - sample(GOI))}}{Efficiency\ (REF)^{\Delta C_T(control\ (REF) - sample(REF))}}$$

3.1.6. Validation of primers used for qRT-PCR

Specific primers used in qRT-PCR were designed using PrimerBLAST (National Institutes of Health; https://www.ncbi.nlm.nih.gov/tools/primer-blast/). Primers were optimized for a melting temperature of 60°C and a GC content of 40-60%. Primer efficiency was analyzed in a qRT-PCR reaction using a 1:3 dilution series of cDNA from the EO771.LMB tumor bulk and pre-metastatic lung. cDNA input ranged from 100 ng to 0.14 ng per reaction mixture. Primer efficiency was calculated according to the formula below (Equation 3-2), efficiencies between 1.8 and 2.1 were considered suitable. Only primers which showed an appropriate efficiency and specificity as assessed by analysis of the melting curve were used for the experiment.

Equation 3-2: Calculation of primer efficiency.

$$Efficiency\ E = 10^{-\frac{1}{x}}$$

x - slope of linear regression of C_T versus log(cDNA)

3.2. Protein biochemistry methods

3.2.1. Whole cell extracts for permeability assay

Snap-frozen pieces of primary Lewis Lung tumors or lungs were transferred into a reaction tube which had been cooled in liquid nitrogen. Tissue was subsequently ground using a tissue

grinder. Tissue was lysed by adding 50 µL RIPA buffer per 10 mg of tissue. Prior to use, RIPA buffer was supplemented with protease and phosphatase inhibitor cocktail (1:100, Sigma) and 1 mM Dithiothreitol (DTT). After incubation for 15 min on ice, samples were quickly (<30 s) sonicated to shear DNA without overheating the sample. To further aid fractionation, samples were subjected to three subsequent freeze thaw cycles. Quick snap freezing in liquid nitrogen is thereby followed by thawing in a 37°C heating block. Caution was exercised to not fully thaw the samples on the heating block but rather vortex until fully liquid in order to prevent denaturation of proteins. The supernatant was eventually cleared from remaining debris by centrifugation at 16000 g at 4°C for 30 min. Supernatant was stored in the dark at -80°C until determination of protein concentration and subsequent fluorescent measurement.

3.2.2. Determination of protein concentration

Protein content of obtained whole cell extracts was determined by Bradford assay. Isolated lysates were diluted 1:10 in RIPA buffer with supplements as stated above. A Pierce™ Bovine Serum Albumin Standard Pre-Diluted Set with BSA dilutions ranging from 125 µg/mL to 2000 µg/mL was used to generate a standard curve for calculation of protein concentrations. RIPA buffer was used as blank. Of each standard and diluted sample 2.5 µL were prepared in duplicates in clear 96-well flat bottom plates and 150 µL Bradford MX™ (expedeon) were added. Absorption was measured at a wavelength of 595 nm in a microplate reader (BMG Labtech).

3.2.3. Fluorescence measurement of permeability

Vessel permeability was determined by quantifying the fluorescent intensity of the extravasated FITC-dextran in the isolated whole cell protein extracts. As fluorescent intensity is influenced by the presence of peptide bonds, the protein concentration of all samples was adjusted to 18.2 µg/mL with RIPA buffer. Whole cell extracts isolated from lungs of mice which had not been injected with FITC-dextran were treated accordingly and served as diluent for the fluorescent standard. This fluorescent standard was prepared by diluting FITC-dextran in serial dilutions from 12.5 µg/mL to 0.19 µg/mL. For fluorescence measurement, 55 µL of each sample were transferred in duplicates to a black 96-well flat bottom plate with clear bottom. Fluorescence of FITC-dextran was measured with excitation at 494 nm and emission at 521 nm after adjustment of gain in a microplate reader (BMG Biotech). Absolute fluorescence intensity/µg protein was calculated from the linear regression generated from the fluorescence standard.

3.3. Cell culture

3.3.1. Cultivation of cell lines

Melanoma cell line B16F10 was cultivated in RPMI 1640 medium supplemented with GlutaMAX™ (Gibco) and 10% FBS (Sigma). Lewis Lung Carcinoma cell line was grown in DMEM (Sigma) supplemented with 10%FBS (Sigma) and 1% L-Glutamine (Sigma). Metastatic breast cancer cell line EO771.LMB was cultivated according to Johnstone et al., 2015 [242]. In short, the cell line was kept in DMEM (Sigma) with addition of 10% FBS (Sigma), 1% L-Glutamine (Sigma) and 20 mM HEPES (Gerbu). Medium was renewed every 2-3 days

and cells were passaged when 80-90% confluency was reached. For passaging, cells were washed once with DPBS and subsequently detached in accutase. To determine the cell number, a single cell suspension was obtained by carefully resuspending the cells in respective medium and carefully pipetting up and down. Thereafter, cells were automatically counted using the cell counter (Z2 Coulter Particle Count and Size Analyzer; Beckman Coulter, USA).

3.3.2. Contamination test for cell cultures

Cell lines were regularly tested for mycoplasma contaminations using the Venor®GeM Classic Kit (Minerva biolabs®, Berlin). Cell culture supernatant which had been on the cells for at least 48 h was used and processed according to manufacturer's instructions. All cell lines were tested to be mycoplasma-free.

To exclude further contaminations, 1-5 Mio cells were harvested and pelleted by centrifugation. The pellet was resuspended in 100 µL DPBS and lysed by placing the sample on 95°C for 15 min. The clear lysate gained after centrifugation at 10000 g for 5 min was transferred to a new 1.5 mL safe-lock tube and sent in to Multiplexion (Heidelberg) for analysis. All tested samples were free of contamination with Squirrel Monkey Retrovirus, Epstein-Barr virus and mycoplasma and also no cross-contamination of cells from a different origin than mouse was detected.

3.4. Animal experiments

3.4.1. Housing

C57BL/6N mice were purchased from Charles River or Janvier. *Junb*$^{+/+,\ Col1\alpha2\text{-}Cre}$, *Junb*$^{\Delta/>,\ Col1\alpha2\text{-}Cre}$ and C57BL/6-Ly5.1 mice were bred in the Center for Preclinical Research of the DKFZ. For the experiments, mice were transferred to experimental barriers of the DKFZ and housed under specific-pathogen free conditions in individually ventilated cages. A temperature of 21°C, humidity of 50-60% and light cycles of 12 h were maintained. Food and water were available *ad libitum*. Genotyping and housing of mice was done as previously described [229].

All procedures performed on animals were approved by the local government authorities (Regierungspräsidium Karlsruhe, AZ G-206/13, G-26/16 and G-93/18) and were conducted according to the German Animal Welfare Act.

3.4.2. Spontaneous metastasis assay

A single cell suspension was prepared and counted as described above. Cells were diluted and stored on ice till injection (Table 3-4).

Table 3-4: Preparation of cell suspensions for injection *in vivo*

Cell line	Number of cells/injection volume	Diluent
B16F10	1 Mio cells/100 µL	DPBS
EO771.LMB	100000 cells/20 µL	Culture medium
LL/2-Luc	1 Mio cells/100 µL	DPBS

6-8 weeks old female mice were anesthetized with isoflurane (O_2 Flow 2l/min, 1,5-2 Vol% isoflurane), placed on a heating mat to maintain 37°C body temperature and eyes were covered with eye ointment to prevent them from dehydration. Mice were shaved around the injection site: 4th mammary fat pad left (EO771.LMB) or the right flank (B16F10 and LL2/-Luc). The single cell suspension was subsequently filled into 1 mL syringes (Dispomed) and 100 µL were injected s.c. with a 27G needle (B16F10 and LL/-Luc). For the EO771.LMB breast cancer model, cells were injected into the 4th mammary fat pad using a 500 µL insulin syringe (BD) with 30G needle. Formation of a bulge at the injection site indicated the proper application of the cell suspension. Mice were kept warm on heating mats until recovered from anesthesia.

Primary tumor growth was subsequently measured 3 times a week using a digital caliper. Primary tumor volume was calculated according to the formula below (Equation 3-3).

Equation 3-3: Calculation of primary tumor volume.

$$V = \frac{1}{2} \times l \times w^2$$

l - length

w - width

The primary tumor was surgically removed once it had reached a size of approximately 500 mm^3. For preoperative analgesia mice were injected with 2 mg/kg of bodyweight Metacam® (Meloxicam, Boehringer Ingelheim) s.c. 30 min prior to operation. Mice were anesthetized with isoflurane as described above. After an initial incision into the skin at the base of the tumor, the skin and surrounding tissue was carefully detached using scissors and forceps. Blood vessels were atrophied using a Cauterizer (Fine Science Tools). If the tumor had invaded the overlaying skin, it was removed in order to prevent primary tumor regrowth. Immediately after excision, mice were thoroughly controlled for persisting bleedings and wounds closed using sterile suture thereafter. Mice were maintained on heating mats until recovered from anesthesia and observed for motoric defects. Excised primary tumors were collected for further analysis either in 4% paraformaldehyde (PFA) in DPBS for histological examination or in QIAzol® lysis reagent (Qiagen) for subsequent RNA isolation.

24 and 48 h after the operation mice were treated with 2 mg/kg bodyweight Meloxicam s.c. for postoperative analgesia. Afterwards, mice were controlled 2-3 times a week for general well-being, wound healing and potential primary tumor regrowth or lymph node metastases.

Three weeks after primary tumor removal, mice were sacrificed by cervical dislocation and perfused with DPBS through the left ventricle. Organs were dissected and processed either for RNA isolation or histological analysis as described below.

3.4.3. Analysis of tumor-induced changes in lungs and lymph nodes

Mice were injected with tumor cells and grown as described above. When the primary tumor had reached a size of approximately 500 mm^3, the experiment was terminated and mice euthanized. Primary tumors as well as lungs, inguinal and axillary lymph nodes were excised and examined for tumor-induced changes by gene expression analysis and histology. For analysis of blood vessel permeability, mice were i.v. injected with 100 µL per 20 g bodyweight FITC-dextrane in DPBS (70 kDa, Invitrogen) 30 min before euthanasia. 15 min after the injection, mice were anesthetized with 100 mg/kg bodyweight Ketaset (Ketamin hydrochloride, Zoetis) and 15 mg/kg bodyweight Rompun® (Xylazin hydrochloride, Bayer). Animals were placed on warm heating mats to maintain body temperature and eyes were covered with eye ointment. Additional 15 min later, mice were sacrificed by cardiac puncture and perfused with DPBS through the left ventricle to remove non-extravasated FITC-dextrane from the circulation. Lungs and tumors were immediately snap-frozen in liquid nitrogen and stored at -80°C until analysis.

3.4.4. Experimental metastasis assay

Single cell suspensions of tumor cells were prepared as described above. 6-8 weeks old female *Junb*$^{+/+,\ Col1\alpha2\text{-}Cre}$ or *Junb*$^{\Delta/>,\ Col1\alpha2\text{-}Cre}$ mice were exposed to an infrared lamp to induce hyperemia. Mice were subsequently placed in a rodent restrainer and 500000 cells in 200 µL DPBS were injected into the tail vein using a 30G needle. Animals were sacrificed when reaching termination criteria (19 days after injection) by cervical dislocation and lungs were used as described below for either DNA and RNA isolation or histology.

3.4.5. Bone marrow transplantations

Total bone marrow of 6-8 weeks old female C57BL/6-Ly5.1 (*Junb*$^{+/+}$/CD45.1 isoform), C57BL/6N (*Junb*$^{+/+}$/CD45.2 isoform) or *Junb*$^{\Delta/>,\ Col1\alpha2\text{-}Cre}$ (CD45.2 isoform) mice was isolated from tibiae, femurs and ilia. Total white blood cells were counted automatically (Hemavet 950FS, Drew Scientific) and diluted in DPBS. Bone marrow suspension was placed on ice and directly used for injection without delay.

Eight weeks old female C57BL/6-Ly5.1 (*Junb*$^{+/+}$) or *Junb*$^{\Delta/>,\ Col1\alpha2\text{-}Cre}$ mice were lethally irradiated using a fractionated dose of 2x450 cGy 2 hours apart. After additional 2 hours, mice were reconstituted by i.v. injection of 3 million bone marrow cells in 200 µL DPBS as already described. To compensate for the increased risk of infections 90 mg/kg bodyweight per day Sulfamethoxazol and Trimethoprim were administered via the drinking water for 21 days. Reconstitution efficiency was assessed 4 weeks after bone marrow transplantation by flow cytometric analysis of whole blood. Blood was taken by puncture of the tail vein with a 25G needle after exposing the mice to an infrared lamp and collected in EDTA-coated tubes Sarstedt, Nümbrecht). When the reconstitution efficiency exceeded 80%, the spontaneous metastasis assay was subsequently started on day 32 after bone marrow transplantation (details in section 3.4.2 Spontaneous metastasis assay).

3.4.6. Neutrophil depletion *in vivo*

For neutrophil depletion *in vivo,* a spontaneous metastasis assay using the breast cancer cell line EO771.LMB was performed with 6-8 weeks old female *Junb*$^{+/+,\ Col1\alpha2\text{-}Cre}$ or *Junb*$^{\Delta/>,\ Col1\alpha2\text{-}Cre}$

mice as described in the previous section. Neutrophils were depleted by administration of Ly6G blocking antibody (clone 1A8, BioXCell). These experimental mice were thereby compared to a control group of mice injected with a matching rat IgG2a, κ isotype control (clone 2A3, BioXCell). When the primary tumor was palpable, initial 400 µg in 200 µL DPBS of depleting antibody or isotype control were administered i.p. and followed by injections of 100 µg in 100 µL DPBS 3 times per week (in total 6 injections). The success of neutrophil depletion was confirmed by flow cytometric analysis. For that reason, whole blood was drawn from the tail vein once a week for 3 consecutive weeks starting after the first antibody injection as previously described. For validation of neutrophil depletion in pre-metastatic lungs, mice were treated with depleting antibody or isotype control as above and sacrificed when the primary tumor had reached a volume of roughly 500mm^3.

3.4.7. Sacrifice mice and sample processing

At the respective end point or when termination criteria were reached, mice were euthanized by cervical dislocation unless stated otherwise. Whole blood was drawn by cardiac puncture using syringes and needles pretreated with 0.5M EDTA. Blood was transferred to EDTA-coated collection tubes and processed within a few hours. Mice were then perfused with DPBS through the left ventricle and organs dissected for further analysis. For subsequent gene expression studies or DNA isolation, tissue was placed in QIAzol® lysis reagent and immediately snap-frozen in liquid nitrogen. Samples were stored at -80°C until RNA isolation. For histological examination, tissue was fixed in 4% PFA in DPBS at 4°C for approximately 24h and ultimately embedded in paraffin.

3.5. Flow cytometry

3.5.1. Preparation of blood

Blood was drawn from mice as described above. For flow cytometric analysis (FACS), approximately 45 µL whole blood were transferred to a fresh tube and placed on ice. Erythrocytes were lysed by incubating whole blood with ACK lysis buffer for 2 min on ice. Lysis was stopped by addition of an equal volume of FACS buffer. Supernatant was decanted after centrifugation at 4°C. Erythrocyte lysis was repeated until the remaining cell pellet was white.

3.5.2. Staining and analysis by flow cytometry

In order to block non-specific binding of immunoglobulin to Fc receptors, the white cell pellet obtained after erythrocyte lysis was resuspended in 50 µL anti-mouse CD16/CD32 antibody in FACS buffer at appropriate dilution (Table 2-2). After 5-10 min incubation on ice, cells were stained with 50 µL of 2x concentrated antibody cocktail (Table 2-2) for 20 min in the dark. Thereafter, cells were washed in 900 µL FACS buffer and resuspended to a final volume of 300 µL in FACS buffer. To remove any remaining cell clumps, cells were flushed through a 70 µm strainer shortly before analysis. Dead cells were identified by addition of either 0.16 µg/mL Propidium Iodide (PI) or 0.33 µg/mL 7AAD depending on the FACS panel. At least 10000 events were recorded for analysis at the BD FACS Canto II.

3.6. Histology

3.6.1. Tissue fixation and processing for paraffin-embedding

Immediately after euthanasia of mice as described above, organs were dissected and placed in 4% PFA/DPBS at 4°C for approximately 24 h. Tissues were transferred into tissue cassettes to 70% ethanol and stored at 4°C under mild shaking until subsequent processing for paraffin embedding. Sample processing for paraffin embedding was performed fully automated in the Vacuum Infiltration Processor (Sakura) according to the program given below. For paraffin embedding, plastic tissue cassettes were removed and tissue placed into metal molds which were filled with liquid paraffin. Paraffin was cooled down by placing molds on a 4°C cooling plate and blocks separated from molds when paraffin was completely solidified. Paraffin blocks were stored at RT until sectioning.

Table 3-5: Tissue processing prior to paraffin embedding

Step	Temperature	Time	Cycles
70% EtOH	35°C	60 min	1
80% EtOH	35°C	90 min	1
90% EtOH	35°C	90 min	2
96% EtOH	35°C	90 min	2
100% Isopropanol	35°C	90 min	2
Xylene	40°C	120 min	2
Paraffin	58°C	120 min	4

3.6.2. Sectioning of paraffin blocks

Serial sections of 6 µm were cut by Angelika Kritschke or Bettina Kast using the sliding microtome SM2010 R (Leica) or Hn40 (Reichert-Jung). After sections had been smoothened in a 40°C water bath, sections were transferred to SuperFrost slides and dried at 42°C O/N. Sections were stored dry at RT until staining.

3.6.3. Hematoxylin and eosin staining

Tissue sections were stained for hematoxylin and eosin essentially as stated in the table below (Table 3-6). Paraffin was removed by immersing the sections in xylene in two subsequent steps. Deparaffinization was followed by rehydration of the tissue in an ethanol dilution series with decreasing concentration. After incubation in distilled H_2O for 2 min, sections were stained with hematoxylin for 1-3 min depending on the desired intensity. Prior to counterstaining with eosin for 1 min, sections were blued by washing in tap water for 10 min. Excess eosin was removed by quickly rinsing the slides in distilled H_2O before differentiation by dipping the slides into 80% ethanol. Tissue was dehydrated in a series of increasing alcohol concentration and eventually mounted in xylene-based mounting medium (Eukitt).

Table 3-6: Protocol for hematoxylin and eosin staining

Step	Substance	Time	Step
1	Xylene 1	10 min	Deparaffinization
2	Xylene 2	2 min	
3	96 % ethanol	2 min	Rehydration
4	80% ethanol	2 min	
5	70% ethanol	2 min	
6	60 % ethanol	2 min	
9	H_2O dest.	2 min	
10	Hematoxylin	1-3 min	Staining
13	Tap water	10 min	
15	0.1 % eosin	1 min	
16	H_2O dest.	rinse shortly	
17	80% ethanol	dip a few times	Dehydration
20	96% ethanol	dip a few times	
21	96% ethanol	1 min	
22	100% isopropanol	1 min	
25	Xylene 4	5 min	
26	Xylene 5	5 min	
27	Xylene-based mounting medium (Eukitt)		Mounting

3.6.4. Immunohistochemistry staining

Prior to immunohistochemial staining, tissue sections were deparaffinized and dehydrated as stated for hematoxylin and eosin staining above. In the final step of rehydration, PBS was used instead of distilled H_2O. Depending on the primary antibody used (Table 2-1), antigen retrieval was performed according to Table 3-7.

Table 3-7: Methods of antigen retrieval

Antigen retrieval	Composition	Treatment
Heat-mediated	10 mM citrate buffer pH 6.0	95°C, 15 min
Heat-mediated	1 mM EDTA pH 8.0	95°C, 15 min
Heat-mediated	10 mM Tris, 1 mM EDTA pH 9.0	100°C, 25 min
Enzymatic	Proteinase K 20 µg/mL in TE buffer pH 8.0	37°C, 15 min

After antigen retrieval, slides were washed in PBS for 5 min. To block endogenous peroxidase, slides were immersed in 3% H_2O_2 in Methanol for 10 min at RT. In the case of CD45 staining, this step of peroxidase blocking was performed after secondary antibody incubation, as the epitope was sensitive to peroxidase treatment. Prior to incubation with 10% goat serum in PBS (Vector Laboratories) for 30 min at RT, slides were rinsed in PBS for 5 min and tissue sections encircled with ImmEdge Pen™ (Vector Laboratories). Sections were stained with primary

antibodies appropriately diluted in 10% goat serum in PBS (Table 2-1). One tissue section of each slide was left in 10% goat serum without primary antibody and served as staining control. After O/N incubation at 4°C, primary antibody was removed and slides washed 3x for 15 min in PBS. All sections including staining controls were incubated with biotinylated secondary antibodies of the appropriate species at a dilution of 1:500 in 10% goat serum in PBS for 1 h at RT. In parallel, a solution containing avidin and horse radish peroxidase (VECTASTAIN® Elite® ABC HRP Kit, Vector Laboratories) was prepared 30 min before use. Subsequent to secondary antibody incubation, another washing step of 3x 15 min in PBS was conducted and sections incubated with ABC reagent for 30 min at RT. After a final washing step in PBS, staining was developed with DAB reagent (DAB Peroxidase Substrate kit, Vector Laboratories). When a brown signal of desired intensity was visible under the microscope, the colorimetric reaction was stopped by transferring the slides into tap water. The sections were counterstained by quickly dipping into hematoxylin for <10s and subsequently bluing for 10 min under running tap water. Tissue sections were dehydrated and mounted as described above.

3.6.5. Immunofluorescence staining

After incubation with primary antibody followed by washing in PBS (section 3.6.4), tissue sections were incubated with fluorescently-labelled secondary antibodies for 2 h at RT (Table 2-4: Secondary antibodies used for immunohistochemistry and immunofluorescence). To remove unwanted background, slides were purged in 0.3% Triton-X in PBS for 15 min followed by two further washing steps in PBS. To visualize nuclei, sections were counterstained with Hoechst 33342, washed and eventually mounted in fluorescent mounting medium (Dako).

3.6.6. Image acquisition and analysis

Images were acquired using Nikon Eclipse Ti (Nikon) or Axio Scan.Z1 (Zeiss). For presentation, raw images were processed and adjusted for brightness, contrast and gamma using the Zen Blue software (Zeiss) or Image J. Unedited images were quantified utilizing macros for Image J written by Barbara Costa or myself together with Damir Krunic.

3.7. Statistical analysis

Non-normally distributed data of three groups (wildtype, control and knockout mice), such as fold changes obtained from gene expression analyses or proportions obtained from quantifications of histology or flow cytometry, were statistically analyzed using the non-parametric Kruskal-Wallis test. To determine the specific sample pair responsible for statistical significance, p-values were corrected by multiple comparisons with Dunn's multiple comparisons test. In the experimental metastasis assay, the metastatic burden of the two groups (control and knockout mice), which was determined by qRT-PCR or histology, was evaluated by Mann-Whitney test. Data following a normal distribution such as number of metastatic nodules, vessel area or number of lymphatic vessels, were compared by unpaired t-test or One-way ANOVA depending on the number of groups. For three or more groups Dunnett's multiple comparison test was used to correct p-values. Data were analyzed and visualized using GraphPad Prism 7.05 (Graphpad Software, Inc.). Annette Kopp-Schneider was consulted for statistical advice in the evaluation of flow cytometric data, Tim Holland-Letz

aided the analysis of metastatic burden and determination of group sizes for the animal licenses.

4 RESULTS

4. RESULTS

4.1. Selection of metastasis model

The AP-1 transcription factor JUNB has been implicated in a multitude of physiological as well as pathological conditions. As alluded to in section 1.3.3 (JUNB in cancer and metastasis), JUNB can act both as a tumor suppressor and as an oncogene in tumor cells but also has diverse functions in the stroma. Most prominently, JUNB plays a role in vascular development and homeostasis [181, 189, 228, 229], but it has also been described as an important player in lymphatic biology [227, 245], macrophage activation [233] and T cell differentiation [190] as well as polarization [191]. Moreover, JUNB has been found essential in the release of inflammatory cytokines from fibroblasts [246] and dendritic cells upon activation [247]. Studies assessing the contribution of JUNB derived from the microenvironment to tumorigenesis *in vivo* have, however, been limited so far [232]. For this purpose, mice with stromal deletion of *Junb* were required. In order to circumvent embryonic lethality of mice with global *Junb* loss, a conditional breeding strategy was applied. Therefore, mice with floxed *Junb* alleles were crossed with mice hemizygous for *Junb* and expressing Cre recombinase under the control of the *Col1α2* promoter (Figure 4-1 A). The resulting $Junb^{\Delta/\Delta,\ Col1\alpha2\text{-}Cre}$ mice display a loss of *Junb* in a wide array of mesenchymal-derived cells, such as fibroblasts, endothelial cells and smooth muscle cells but also in a multitude of immune cells and were therefore found appropriate to investigate the influence of stromal JUNB on tumor progression and metastasis [234].

In order to study metastatic spread, the selection of the appropriate model is of uttermost importance. As the complex metastatic cascade and the interplay with different components of the tumor microenvironment can hardly be mimicked *in vitro*, the contribution of stromal JUNB to metastasis is best assessed *in vivo*. For this purpose, different metastasis models with varying complexity are available.

The simplest approach is the experimental metastasis model where tumor cells are directly introduced into the circulation for example by tail vein or intra-cardiac injection. As this model is very straight forward and yields results rapidly within a few weeks, it is widely used to screen for factors impacting metastasis [248]. Albeit being very suitable to study extravasation and metastatic colonization, this assay has also multiple limitations. In the experimental model, there are typically large numbers of tumor cells injected into the blood stream, which is not at all resembling the actual clinical situation where CTCs are extremely rare. Even more importantly, the assay completely neglects the first steps of the metastatic cascade, such as tumor invasion and intravasation [248], making it unsuitable as a primary model for this project. The investigation of *de novo* tumor formation and progression including every step in the metastatic cascade is possible with the use of genetically engineered mouse models (GEMM). GEMMs model the scenario in humans more closely and can also display tumor heterogeneity but can have the disadvantage of rather long latencies and poor penetrance of metastatic disease [248, 249]. The requirement to obtain the appropriate genetic background (GEMM strain with conditional stromal deletion of *Junb*) overcomplicate the elaborate breeding schemes of *Junb*-deleted mice and were therefore considered to be technically too challenging for this project.

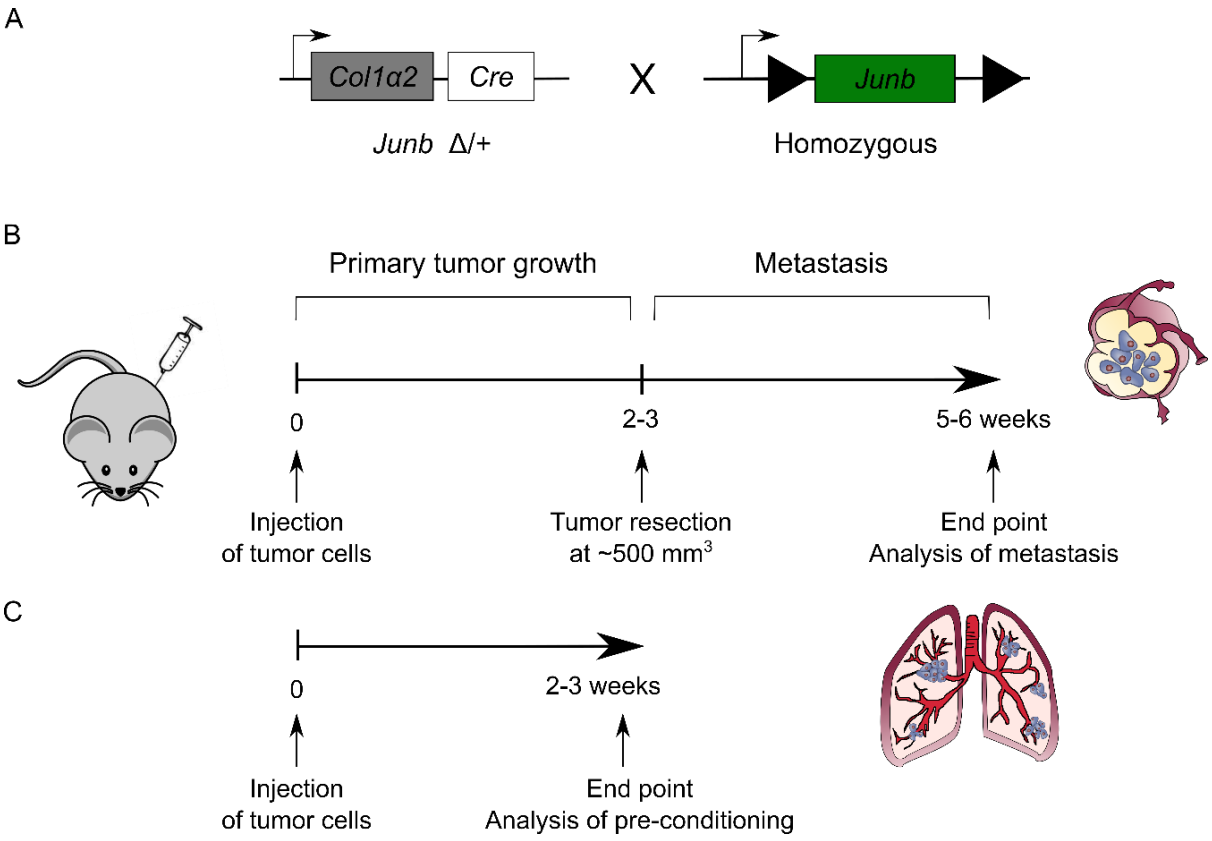

Figure 4-1: Schematic representation of the mouse model used in this dissertation.

(A) Depiction of the genetic mouse model in this study. General experimental setup for the spontaneous metastasis assay (B) and for the investigation of lung and lymph node pre-conditioning (C).

The third option are tumor transplantation models with spontaneous metastasis. Cancer cell lines are thereby implanted ectopically or orthotopically, depending on the model, and usually form a primary tumor within a few weeks [250]. With the selection of syngeneic cell lines, this assay allows the use of immunocompetent mice thereby enabling the investigation of the complex crosstalk of the tumor cells with the surrounding stroma.

Originally, primary tumors had been allowed to grow until distant metastasis was observed resulting in enormous primary tumors and, therefore, in a rather artificial scenario. To resemble the human situation more closely, whereby the primary therapy involves surgical removal of the primary tumors often before detection of macroscopic metastasis, primary tumor resections were established for this project. This primary tumor resection furthermore makes it possible to observe the mice over a prolonged period of time. Termination criteria due to overly large primary tumors are avoided, thus, facilitating metastatic outgrowth. For this project, the contribution of JUNB expressed in the microenvironment to metastasis was therefore assessed using a spontaneous metastasis model including primary tumor resection (Figure 4-1 B). In an alternative setting, the experiment was terminated at the time point of primary tumor removal in order to examine changes in lungs and lymph nodes pre-conditioned by tumor-derived factors (Figure 4-1 C). With this investigation of pre-metastatic organs, the role of JUNB in metastasis was elucidated more mechanistically.

As the mice with conditional deletion of *Junb* in the stroma ($Junb^{\Delta/\Delta,\ Col1\alpha2\text{-}Cre}$) are congenic C57BL/6, the availability of cell lines previously reported to be metastatic in the resection model

were limited. In order to be able to study both hematogenous and lymphatic metastasis, three cell lines derived from cancer entities known to spread via the blood and lymphatic system were selected: the B16F10 melanoma model, the LL/2 Lewis Lung Model and the EO771.LMB breast cancer model. The B16F10 cell line is a highly metastatic variant of the B16 melanoma. It has been widely used in the experimental metastasis assay after tail vein injection and was reported to result in robust metastasis to the lungs [251-253]. B16F10 cells had also been described to yield spontaneous metastasis after subcutaneous implantation into the back [254, 255], ear [256] or tail of mice [257]. Implantation into the tail resulted in metastasis to lung and lymph node. Yet, no substantial primary tumor growth was observed [257], so that this model does not accurately mimic the human situation. In order to give rise to metastasis upon subcutaneous injection into the back or ear of mice, primary tumors were allowed to reach large sizes [254-256]. Such a setting is again not in line with the clinical situation. For this project, a resection model of B16F10 melanoma had to be established, which is in detail described in the following section (Section 4.2.1). The Lewis Lung cell line was originally derived from a spontaneously arising lung tumor and has since then been widely used in the study of primary tumor formation and metastasis [258]. The EO771.LMB breast cancer model is a newly available metastatic cell line generated by repeated *in vivo* passaging and shown to metastasize to the lungs [242]. For both the Lewis Lung model [259] and the EO771.LMB breast cancer model [242], there were published protocols available describing spontaneous metastasis after primary tumor excision, which I adopted for this project and further optimized the experimental setup.

4.2. Functional role of stromal JUNB in metastasis

4.2.1. Stromal deletion of *Junb* does not influence primary tumor growth but promotes metastasis

In order to assess the dynamic crosstalk between tumor cells and the surrounding environment, a spontaneous metastasis model with the use of three syngeneic cell lines was chosen for this project: B16F10 melanoma, Lewis Lung carcinoma (LL/2-Luc) and EO771.LMB breast cancer. The spontaneous metastasis assay can in principle be performed in two ways: either the tumor is excised after a pre-determined time or at a certain tumor volume. Consequently, I first needed to establish and optimize all these models. In order to determine the growth kinetics of the individual cancer cell lines *in vivo* and to define the ideal time point of tumor resection, *Junb* $^{\Delta/\Delta\ Col1\alpha2\text{-}Cre}$ mice (thereafter called Knockout: KO) and the respective controls (*Junb* $^{+/+,\ Col1\alpha2\text{-}Cre}$, Controls: CTR as well as C57BL/6N Wildtype: WT) were inoculated with the different cell lines and primary tumor formation was monitored (Figure 4-2). B16F10 and LL/2-Luc were implanted subcutaneously into the flanks of mice, whereas EO771.LMB cells were introduced orthotopically into the 4th mammary fat pad. Irrespective of the investigated model, primary tumor growth was similar in all genotypes. All three models displayed quick primary tumor development and reached exponential growth within 2-3 weeks. B16F10 cells grew most rapidly with tumor volumes reaching 500 mm^3 after approximately 14 days (Figure 4-2 A). LL/2-Luc cells displayed a slightly slower primary tumor growth reaching 500 mm^3 on average on day 15 (Figure 4-2 B). EO771.LMB cells showed a delayed tumor onset compared to B16F10 and LL/2-Luc but grew quickly afterwards (Figure 4-2 C). Tumor volumes of roughly 500 mm^3 were measured around day 17-20 independent of the genotype. Due to the rather high variations between the individual mice, I decided to perform

the tumor resections according to primary tumor volume rather than time and defined the time point of resection as soon as a volume of 500 mm^3 was reached for all models. This size was chosen as it allowed maximal primary tumor growth and consequently maximal time for tumor cells to disseminate without rendering the tumor inoperable. At bigger volumes, tumors became highly necrotic and had coopted huge blood vessels in order to sustain their enormous need of energy and oxygen. These vessels were extremely challenging to close during the surgery. Furthermore, tumors then had partially become invasive by growing attached to the peritoneal wall. This would have hindered complete removal of the primary tumor and would have let to primary tumor regrowth, consequently resulting in the exclusion of the respective mouse from further analysis.

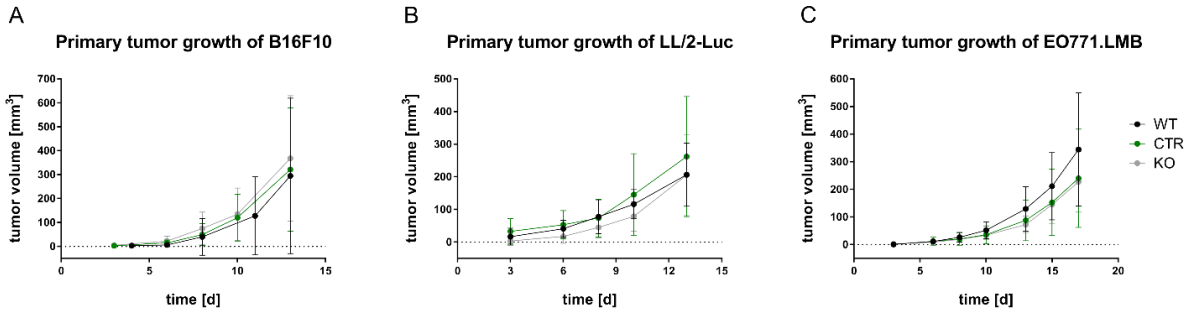

Figure 4-2: Primary tumor growth of B16F10 melanoma, Lewis Lung carcinoma and EO771.LMB breast cancer is independent of stromal JUNB.

Primary tumor growth was not different in B16F10 melanoma (A), Lewis Lung Carcinoma (B) and EO771.LMB (C) in mice with stromal *Junb* deletion (KO) compared to respective controls (CTR and WT).

For the spontaneous metastasis assay, tumor cells were injected as described above and primary tumors were allowed to grow until they reached a size of approximately 500 mm^3. Thereafter, tumors were surgically removed, wounds closed and mice were allowed to recover. After 21 days, mice were euthanized and organs were dissected for further examination of metastatic burden. Mice were sacrificed prematurely if termination criteria were met, such as overly weight loss, primary tumor regrowth or formation of macroscopic lymph node metastases exceeding allowed dimensions. These mice were excluded from analysis of metastatic burden.

The B16F10 cell line had predominantly been used in the experimental but not in the spontaneous metastasis model involving primary tumor resections [251-257]. As part of establishing this spontaneous model, surgical removal of the primary tumor was performed at a size of approximately 500 mm^3 for reasons stated above. The time point of 21 days between surgery and analysis of lung metastasis was chosen for several reasons. (I) B16F10 cells form visible nodules in the lung in the experimental model already after a few days [252]. Assuming much fewer circulating tumor cells in the spontaneous model, cells were given more time to establish clearly visible macroscopic lesions. (II) In other established metastasis models, the time between resection and analysis is typically 14-21 days, for example in the 4T1 breast cancer [260-262] or Lewis Lung carcinoma [263-265]. As B16F10 cells displayed similar growth characteristics *in vivo* as 4T1 and LL/2-Luc, 21 days were found suitable. Following this experimental setup, virtually no tumors were observed when macroscopically examining the lungs at the end point. This first impression was confirmed by histological assessment by

hematoxylin and eosin (HE) staining (Figure 4-3 A). In both CTR and KO mice, lung metastasis was found extremely inefficient, so that no conclusion could be drawn.

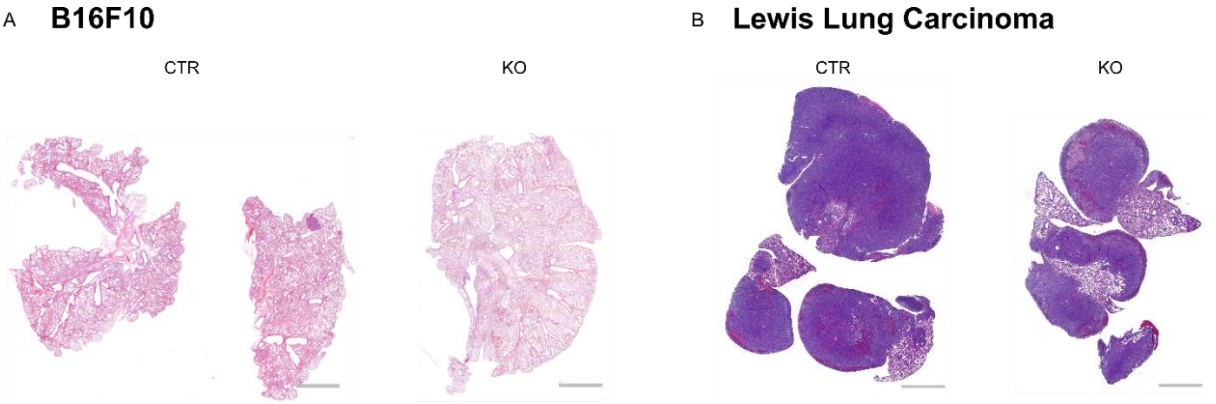

Figure 4-3: Lung metastasis after the spontaneous metastasis assay with B16F10 and LL/2-Luc cells.

(A) Very inefficient lung metastasis was determined for B16F10 cells by hematoxylin and eosin staining, so that the impact of stromal *Junb* deletion on metastasis could not be assessed. Severe metastatic burden was detected in the LL/2-Luc model after staining with hematoxylin and eosin (B) but no difference was observed between the different genotypes. Scale bar 2 mm.

In contrast to the B16 model, the Lewis Lung carcinoma model had been widely used in the resection model und was reported to result in strong lung metastasis [264-267]. The experimental setup was essentially as described for the B16F10 model. Primary tumors were established by subcutaneous injection of tumor cells into the flanks of mice, grown until a size of 500 mm^3 and resected thereafter. Macroscopic examination of the lungs 21 days after primary tumor removal revealed severe lung metastasis in all three genotypes. This first impression was subsequently supported by histological assessment. Hematoxylin and eosin staining confirmed that in this model no influence of stromal *Junb* deletion on distant metastasis could be detected (Figure 4-3 B). Lung metastasis was so strong in this experimental setup, with some mice almost reaching termination criteria at end point, that the effect of JUNB may have been masked by the rapid proliferation and outgrowth of the tumor cells in the lung.

In order to further investigate the impact of *Junb* on metastasis and to potentially confirm or disprove the findings with the LL/2-Luc cell line, the metastasis model using EO771.LMB cells stably transduced with an mCherry reporter was used. The experimental setup was adopted from the original publication but was essentially the same as already performed for B16F10 and LL/2-Luc [242]. In contrast to the previous cell lines, EO771.LMB cells were injected orthotopically into the mammary fat pad and tumors were allowed to grow until a volume of roughly 500 mm^3 had been reached. Analysis of metastatic burden in the lungs was performed 21 days after resection. Upon macroscopic investigation, several surface nodules were obvious in KO mice whereas hardly any metastases were observed in neither CTR nor WT. For more in-depth analyses a dual approach was followed: one part of the lung was examined for metastatic burden by quantification of the *mCherry* reporter on genomic DNA level by qRT-PCR, whereas the other part was subjected to histological analysis by HE staining and immunohistochemistry for mCherry. In agreement with the macroscopic observations, both approaches confirmed a significantly enhanced metastatic burden in KO mice compared to WT and CTR (Figure 4-4).

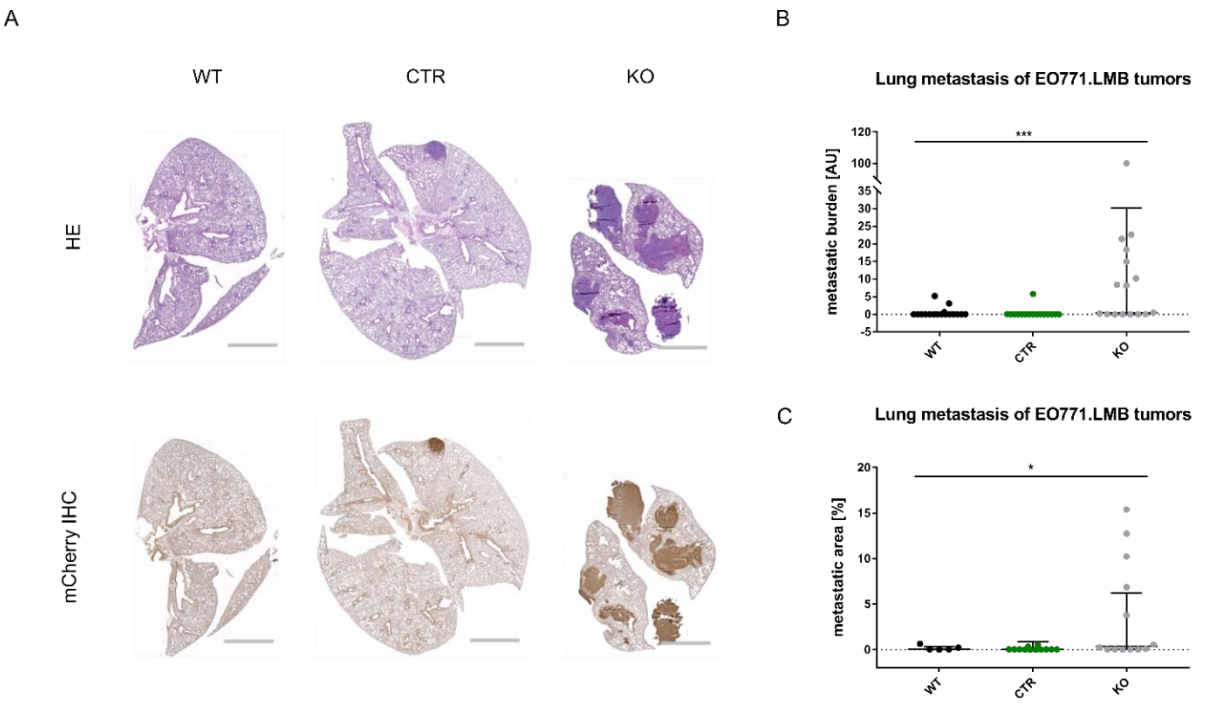

Figure 4-4: Role of stromal *Junb* in metastasis as assessed in the spontaneous metastasis assay.

Loss of stromal *Junb* promotes lung metastasis in the EO771.LMB model as shown by quantification of the *mCherry* reporter on genomic DNA levels by qRT-PCR (B), HE staining and immunohistochemistry of the mCherry reporter (A). Quantification of the mCherry reporter by immunohistochemistry is displayed in (C). Scale bar 2 mm. Data are geometric mean + gemoetric SD (B+C). Significance assessed by Kruskal-Wallis test with P<0.05 as the limit of significance. *P≤0.05, ***P<0.001

In summary, stromal loss of JUNB indeed promotes distant metastasis to the lungs in a murine model of breast cancer. As no clear conclusions could be drawn from the experiments with B16F10 cells and as no difference was observed in the LL/2-Luc model, the following experiments were focused predominantly on the EO771.LMB breast cancer model. Yet, for answering some questions, the B16F10 and LL/2-Luc models were also used for complementation.

4.2.2. Stromal loss of *Junb* does not influence extravasation and metastatic colonization

After *Junb* was found to play an important role in spontaneous metastasis, I next investigated in which step of the metastatic cascade JUNB may be involved. For this purpose, an experimental metastasis assay was performed. EO771.LMB cells stably expressing mCherry were injected into the tail vein of *Junb* KO and CTR mice and lung metastasis was examined 19 days later when end point criteria were reached. Macroscopically, no difference in metastasis was noticed. For quantification of metastasis, the same dual approach as described in the previous section (4.2.1) was followed. Although there was a trend towards less metastasis in *Junb* KO mice compared to CTR animals, with regard to both numbers of metastatic foci as well as metastatic area, statistical significance was not reached (Figure 4-5 B, C+D). These findings indicate that *Junb* does not facilitate extravasation and colonization in the EO771.LMB model (Figure 4-5).

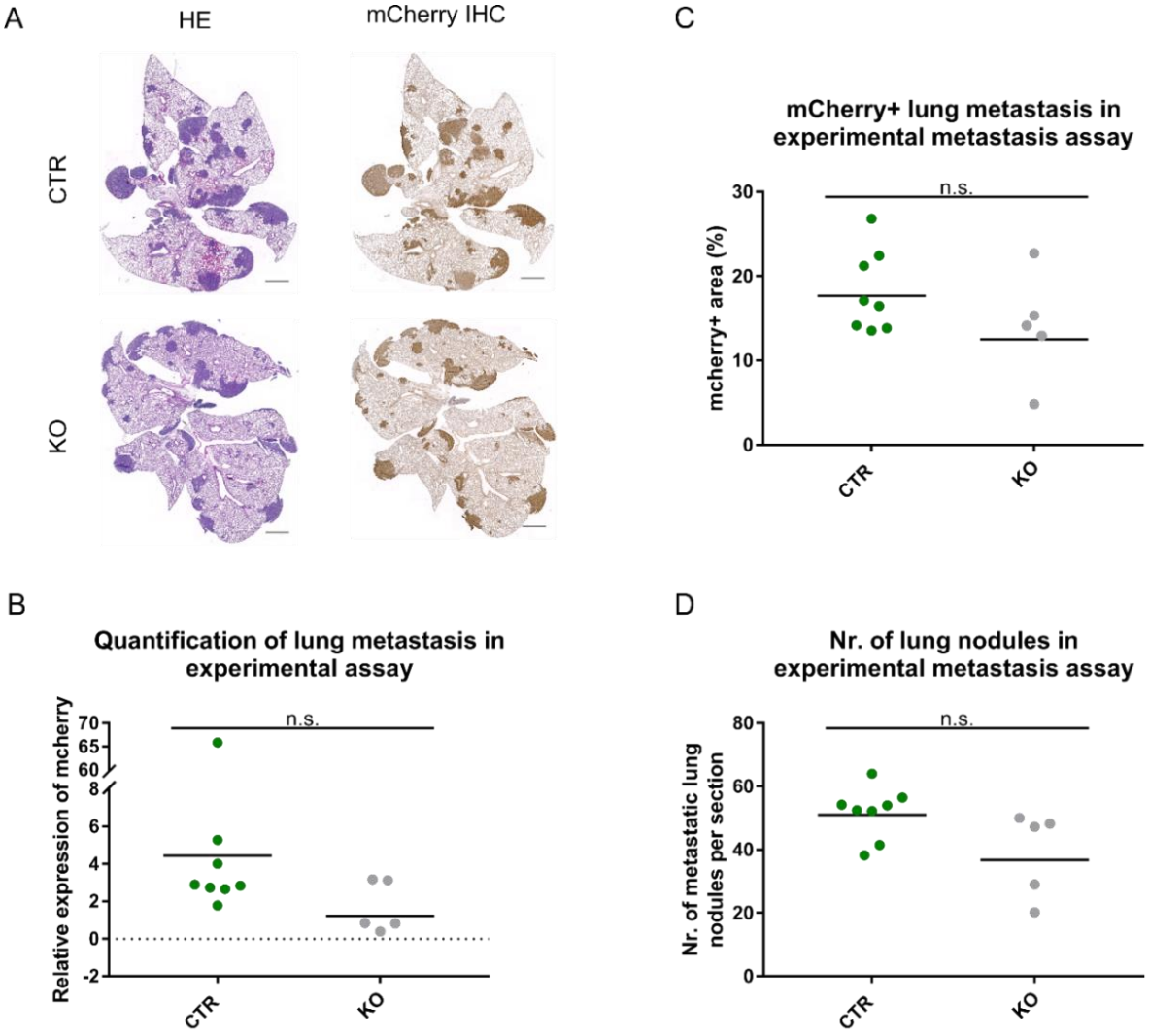

Figure 4-5: Experimental metastasis assay with EO771.LMB breast cancer cells.

Deletion of *Junb* does not influence metastatic colonization as shown by histological examination of metastatic lungs by HE and immunohistochemistry (IHC) for mCherry (A). Quantification of metastatic area by immunohistochemistry (B) and number of metastatic nodules (D) is shown. Metastatic burden was assessed in parallel by measuring the presence of the *mCherry* reporter on genomic DNA by qRT-PCR (C).Scale bar in (A) 2 mm. Geometric mean shown in (A+B), arithmetic mean in (D). Significance assessed by Mann-Whitney test (B+C) or by unpaired t-test (D) with $P<0.05$ as the limit of significance. *$P \leq 0.05$.

4.3. Alterations in cellular compartments upon stromal JUNB loss

After it had been established in above experiments, that stroma-derived JUNB indeed influences metastatic spread, the aim was now to further decipher which microenvironmental compartment was influenced by which mechanism. For this purpose, the spontaneous metastasis assay was terminated at the time point of surgical removal, when the primary tumor had reached a size of 500 mm^3 (Figure 4-1 C). Primary tumors, lungs and lymph nodes were dissected and distinct cellular components were analyzed by histology and qRT-PCR for changes in gene expression.

4.3.1. Tumor associated vascular density and function are JUNB-independent

Global *Junb* knockout mice are embryonic lethal due to defects in placentation and neovascularization [181]. Furthermore, JUNB was reported to regulate angiogenesis as well as tumor angiogenesis [189], vascular contractility [229] and lymphatic development [227] thereby establishing *Junb* as an essential regulator of the vascular system. Therefore, it seemed obvious to investigate whether vascular defects were also the underlying cause of the metastatic phenotype of *Junb.*

For this reason, primary tumors were examined by immunofluorescent staining regarding blood vascular and lymphatic density. Quantification of blood vessel area by staining for the endothelial marker CD31 did not reveal a difference in *Junb* KO mice compared to CTR and WT, neither in the EO771.LMB nor the B16F10 model (Figure 4-6 A, B+C). In EO771.LMB primary tumors, lymphatic vessels, as identified by LYVE-1 staining, were not evenly distributed throughout the tumor but predominantly located at the tumor periphery (Figure 4-6 D). Thus, the number of lymphatic vessels was counted rather than LYVE-1+ area quantified. *Junb* deletion did neither influence the number of all lymphatic vessels nor the number of peritumoral lymphatics in particular, in EO771.LMB primary tumors (Figure 4-6 D, E+F). In B16F10 tumors, hardly any lymphatics could be detected.

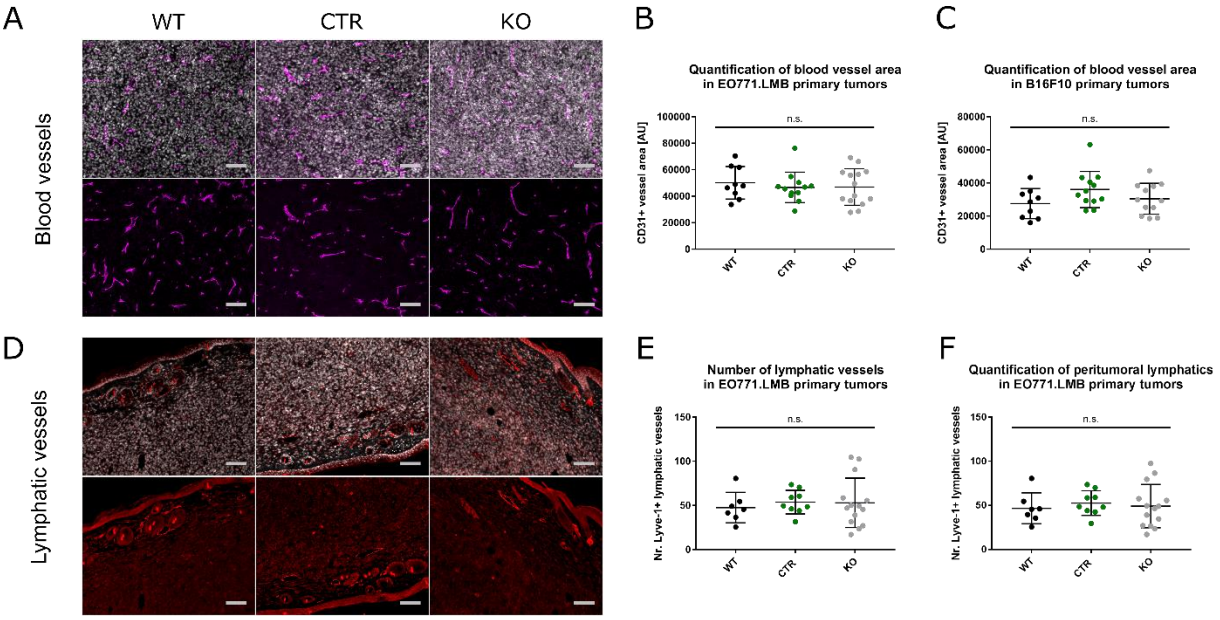

Figure 4-6: Stromal loss of *Junb* does not affect vascular density in primary tumors of EO771.LMB or B16F10.

Blood and lymphatic vasculature in EO771.LMB primary tumors were assessed by CD31 (magenta, A) and LYVE-1 (red, D) immunofluorescent staining, respectively. No difference was found between the genotypes. The upper panels show the overlay with nuclear Hoechst staining (grey), the lower panels show only the respective marker. Of each tumor 5-6 fields were analyzed. Scale bar 100 µm. For quantification of blood vascular density, area covered by CD31 was assessed and shown for primary tumors of EO771.LMB (B) and B16F10 (C). Lymphatic density was examined in EO771.LMB tumors by counting all LYVE-1+ vessels (E) or by counting only peritumoral LYVE-1+ vessels located at the edges of the tumor (F). Quantifications are shown as mean±SD. Significance assessed by Kruskal-Wallis test (CD31 area) or One-way ANOVA (Nr. of of LYVE-1+ vessels) with $P<0.05$ as the limit of significance. *$P \leq 0.05$.

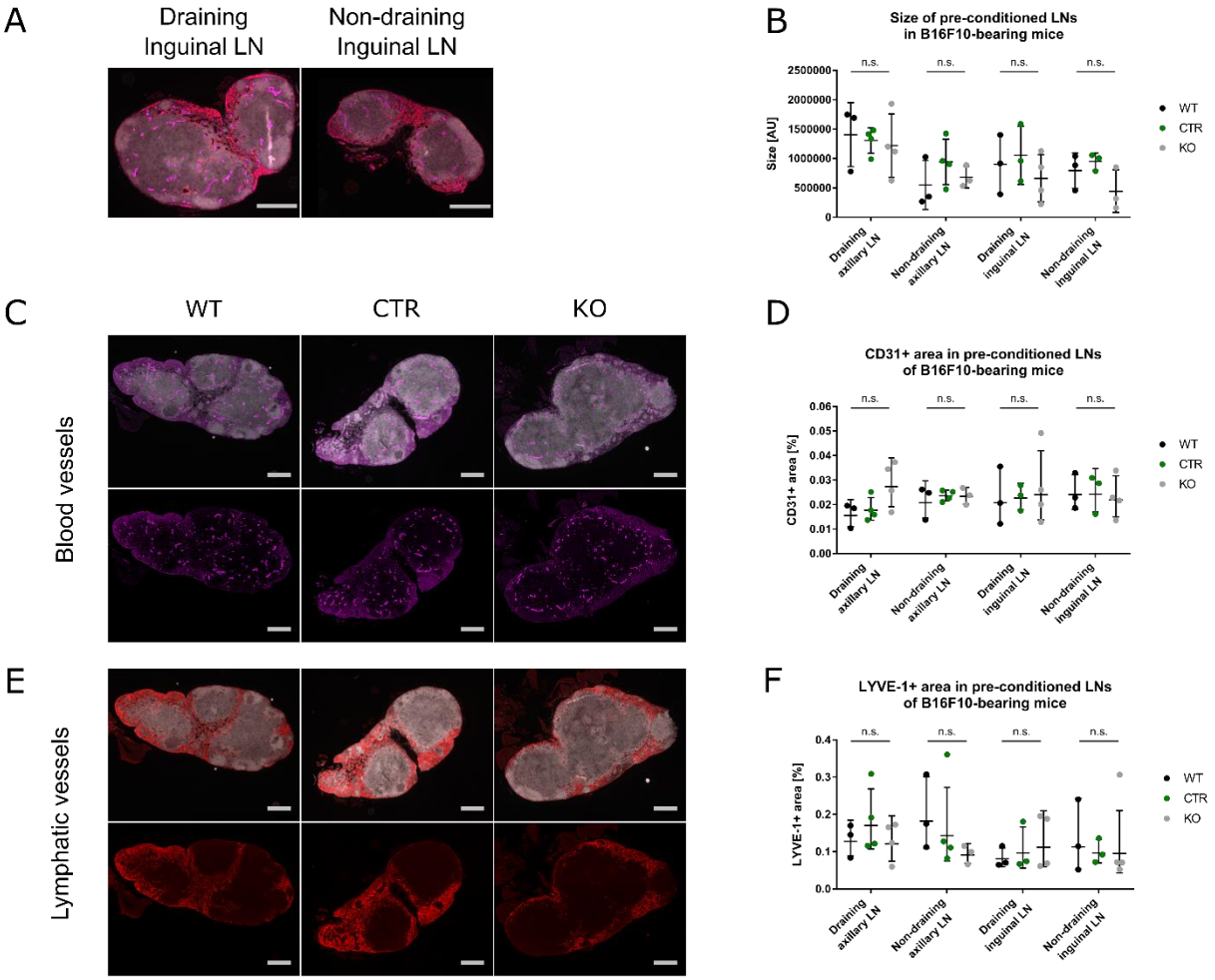

Figure 4-7: Stromal loss of *Junb* does not influence vascular changes in pre-conditioned lymph nodes in the B16F10 model.

Tumor-draining lymph nodes (LN) were generally bigger than their non-draining counterparts as assessed by immunofluorescent staining of CD31 (magenta), LYVE-1 (red) and Hoechst (grey) but this change was independent of *Junb* deletion (B). Representative pictures of an inguinal LN pair from a WT mouse is shown in (A). Ablation of *Junb* does not influence blood vessel density (D) and lymphatic vessel density (F) in pre-conditioned LNs. The CD31+ or LYVE-1+ area of two mid-sections of complete LNs was quantified and averaged (D+F). Representative images are shown for draining axillary LNs (C+E). The upper panels show the overlay with nuclear Hoechst staining (grey), the lower panels show only the respective marker. Scale bar 250 µm. Mean+SD shown in (B), geometric mean with geometric SD shown in (D+F). Significance assessed by Kruskal-Wallis test (D+F) or One-way ANOVA (B) with $P<0.05$ as the limit of significance. *$P \leq 0.05$.

As it had been published that changes in vascular density could not only be observed in primary tumors but also in organs that had been exposed to tumor-derived factors [268, 269], I next investigated whether JUNB had any impact on lymph node vasculature. As tumor-draining lymph nodes seemed enlarged compared to non-draining counterparts and this difference was more obvious in the B16F10 model rather than the EO771.LMB model, I decided to study the lymph node pre-conditioning in the B16F10 model. Due to the site of implantation, B16F10 tumors predominantly drain to the inguinal and axillary lymph nodes. In order to estimate the variability between individual mice and to see whether tumor-derived factors had an impact at all, not only lymph nodes on the same site of the tumor (draining) but also the respective contra-lateral ones (non-draining) were dissected. The first macroscopic impression that draining lymph nodes are bigger in size than their counterparts was confirmed

by more thorough histological analysis (Figure 4-7 A). These size differences were observed in nearly all mice but were independent of *Junb,* and indicate that tumor-draining lymph nodes were indeed pre-conditioned by tumor-secreted factors (Figure 4-7 B). Lymph nodes possess specialized blood endothelial vessels called high endothelial venules (HEVs) which permit the egress of lymphocytes out of the circulation into the lymph node cortex [269]. These HEVs can undergo morphological changes and express the endothelial marker CD31 [269, 270]. CD31 was, thus, used to specifically label HEVs in lymph nodes of *Junb* KO mice as well as of respective controls. No difference was found in CD31+ area between the different genotypes, though (Figure 4-7 C+D). Similarly, lymphatic vascular density was investigated by LYVE-1 immunofluorescent staining. No consistent regulation by JUNB was detected but variations in lymphatic area among the individual mice were also rather high (Figure 4-7 E+F).

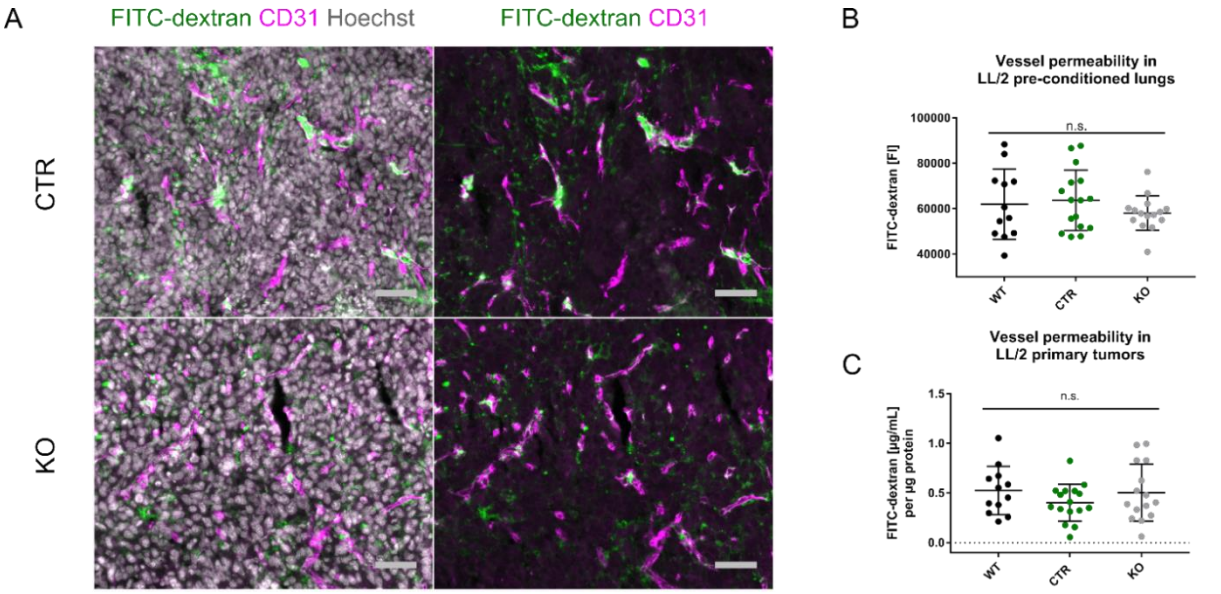

Figure 4-8: Vascular permeability as assessed by tail vein injection of FITC-labelled dextran is not altered upon *Junb* loss.

(A) Representative pictures of primary LL/2-Luc tumors stained with the endothelial marker CD31 (magenta) and nuclear counterstaining with Hoechst (grey) show remains of FITC-dextran (green) inside the circulation but also extravasated into the tissue. Scale bar 50 µm. Quantifications of permeability by fluorescent measurement of tissue supernatant of LL/-2-Luc pre-conditioned lungs (B) and primary tumors (C). Data are presented as mean with SD. Significance assessed by One-way ANOVA with $P<0.05$ as the limit of significance. *$P \leq 0.05$.

Vascular and lymphatic density in primary tumors but also in pre-conditioned lymph nodes were apparently not affected by JUNB loss in the stroma. More important for metastatic spread is, however, the functionality of these vessels. As alluded to in the introduction in section 1.1.1 (The metastatic cascade), more permeable vessels facilitate intravasation but also extravasation and consequently promote metastatic spread. In order to test whether JUNB might regulate vascular permeability, the LL/2-Luc model was investigated closer because this model shows the highest metastatic burden which may be due to a higher vascular permeability. Primary Lewis Lung carcinoma cells were injected into *Junb* KO mice and respective controls and a tumor was allowed to form. When the primary tumor had reached a size of 500 mm^3, vascular permeability was assessed by i.v. injection of a fluorescently-labelled dextran. This dextran remains within the circulation and extravasates only at sites of

enhanced permeability and endothelial damage. Subsequent perfusion of the mice with DPBS removed the remaining non-extravasated dextran from the circulation. By immunofluorescent staining of the endothelium, sites of vascular leakage can later be localized. In a parallel approach, remaining dextran in the tissue can be quantified by fluorescent measurement of the supernatant obtained after mincing the tissue. Following this protocol, sites of vascular permeability could be visualized by immunofluorescent staining of LL/2-Luc primary tumors in both CTR and KO mice and did not seem to be affected upon ablation of *Junb* (Figure 4-8 A). This notion was supported by fluorescent measurement of the remaining dextran, as fluorescence intensity was not different neither in LL/2-Luc primary tumors nor in pre-conditioned lungs (Figure 4-8 B+C).

In summary, no difference upon *Junb* KO was determined in vascular and lymphatic density neither in primary tumors nor in pre-conditioned organs, such as lymph nodes. In addition, vascular permeability was found to be not altered. In conclusion, these findings are in line with a previous study of our lab, showing that stroma-derived JUNB seems to be dispensable for tumor angiogenesis independently of the tumor model used [232]. In addition, my data also indicate, that despite its decisive role in vascular development and physiology, lymphangiogenesis and vascular integrity as far as was assessed in this study are also not affected by stromal JUNB loss. Thus, the observed phenotype in metastasis does not seem to be a consequence of vascular defects.

4.3.2. Stromal JUNB does not alter fibroblast abundance

The tumor microenvironment is formed by a multitude of stromal cell types. The predominant portion is thereby made up of fibroblasts, also called cancer-associated fibroblasts (CAFs). Fibroblasts do not only provide essential structural components by producing various components of the ECM but also influence tumorigenesis by secretion of cytokines and growth factors. *Junb* was shown to influence fibroblast proliferation as well as transformation induced by Src or Ras which was furthermore shown to also impact tumor growth [196]. Thus, I next investigated whether fibroblast content was affected by stromal *Junb* deletion. Assessment of fibroblasts is, however, complicated by the lack of specific markers which are abundantly and specifically expressed by all fibroblasts. Rather, different markers are utilized to identify distinct subpopulations of fibroblasts. Furthermore, many fibroblast markers can also be expressed by tumor cells. Thus, I assessed several published markers, such as *Fap* (Fibroblast activation protein), *Fsp1* (Fibroblast specific protein 1/S100A4) and *Vim* (Vimentin) for their gene expression in EO771.LMB breast cancer cells [271, 272]. In contrast to *Fsp1* and *Vim*, only *Fap* showed low expression in the tumor cells. Hence, I continued to examine gene expression for *Fap* in EO771.LMB tumors grown in WT, CTR or *Junb* KO mice. *Fap* expression level was found to be independent of JUNB, though (Figure 4-9 A). In order to confirm this finding on protein level and to be able to assess fibroblast morphology or localization, immunohistochemical stainings were performed. As immunohistochemistry for FAP did, however, not produce a convincing staining pattern, alternative markers had to be tested. CAFs were also reported to be positive for alpha smooth muscle actin (αSMA) [273]. Nevertheless, staining for αSMA did only reveal positive cells around larger vessels indicating that these cells are rather smooth muscle cells than CAFs. Recently, also the use of Podoplanin (PDPN) as fibroblast marker has been more widely observed [274-276]. Staining of tumor sections, revealed a distinct staining pattern characteristic for fibroblasts and absent in tumor cells confirming its suitability for this project (Figure 4-9 C). Quantification of PDPN+ area as an indicator for fibroblast content, was, however, found unaffected by loss of JUNB (Figure 4-9 B).

Besides numbers, also morphology or distribution in the tumor were unaltered between the genotypes (Figure 4-9 C). The majority of cells expressing PDPN displayed the typical spindle-like shape resembling mesenchymal cells, but also a few more roundish cells were observed. PDPN+ cells were predominantly located lining the tumor-stroma interphase, in close proximity to larger vessels and in necrotic areas but could generally also be found rather evenly distributed throughout the tissue.

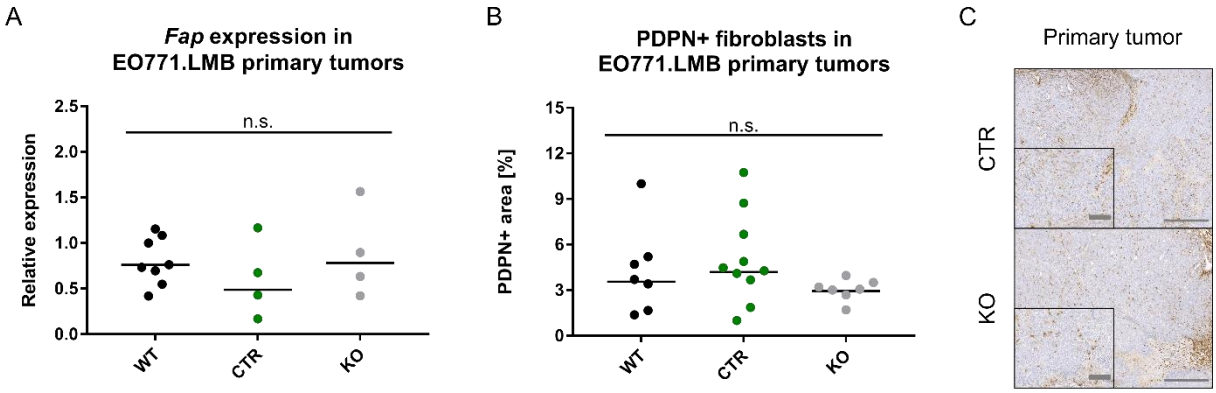

Figure 4-9: JUNB does not play a role in fibroblast abundance, morphology or distribution in EO771.LMB primary tumors.

Fibroblast content as quantified by *Fap* expression on RNA level (A) and by immunohistochemistry for PDPN on protein level (B) did not result in differences between WT, CTR and KO mice. Immunohistochemistry did furthermore not show an impact on cell morphology or localization within the tumor (C). PDPN+ area was quantified using whole sections of primary tumors. PDPN+ lymphatic vessels were excluded from the analysis as long as they could unambiguously be identified by morphology. Scale bar in (C) 200 µm, magnification is shown in the insert: scale bar 50 µm. Significance assessed by Kruskal-Wallis test with $P<0.05$ as the limit of significance. *$P \leq 0.05$.

In summary, the presence of fibroblasts in EO771.LMB primary tumors was not influenced by *Junb* genotype. Likewise, also morphology and distribution were similar.

4.3.3. Stromal ablation of *Junb* influences immune cell infiltration into primary tumors and pre-metastatic lungs

Besides endothelial cells and fibroblasts, immune cell infiltrates constitute a major component of the tumor stroma. JUNB had been implicated in the activation and differentiation of various immune cells. Consequently, I proceeded with the investigation of number, localization and composition of the immune cell infiltrate in *Junb* KO and respective control animals using the pan-immune cell marker CD45.

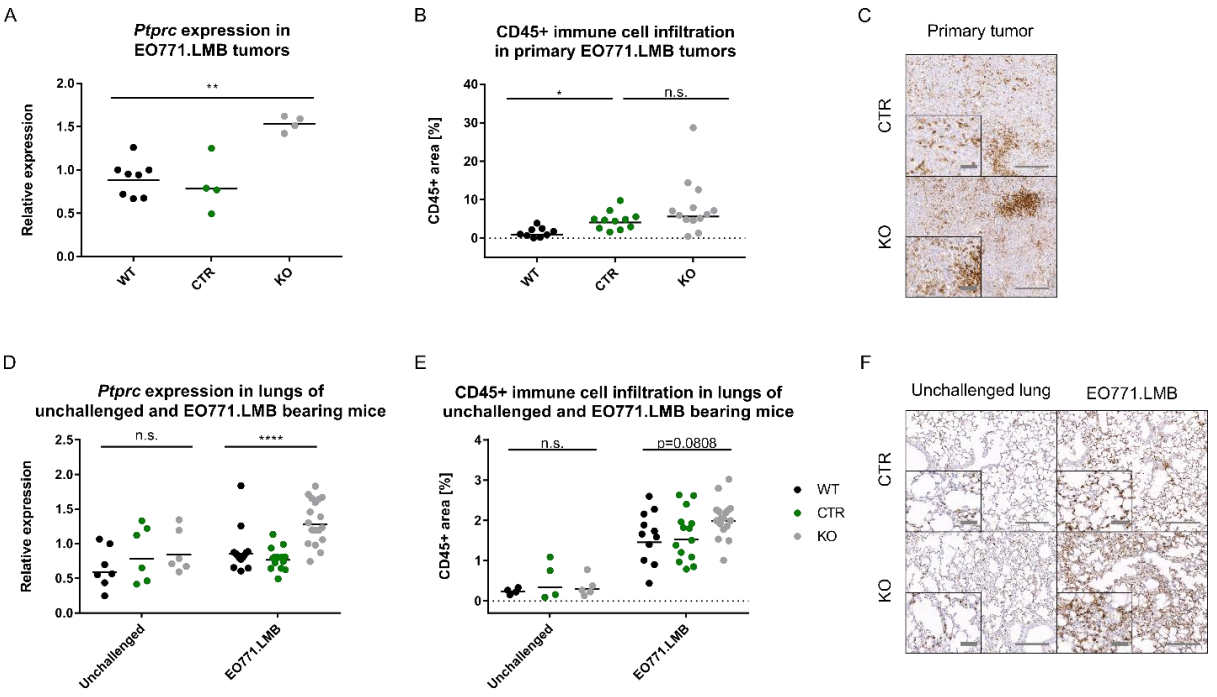

Figure 4-10: JUNB impacts CD45+ immune cell infiltration in EO771.LMB primary tumors and pre-metastatic lungs.

Ptprc is upregulated on RNA level in tumors (A) and pre-metastatic lungs but not in unchallenged lungs (D). An increased accumulation of CD45+ immune cells as determined by immunohistochemistry for CD45 is not visible in primary tumors (B, C) and lungs of unchallenged mice (E, F) but in lungs of EO771.LMB tumor-bearing animals (E, F). CD45+ area was quantified using whole sections of primary tumors or lungs. In primary tumors, CD45+ cells were accumulating especially at the tumor periphery and within necrotic areas (C). In the lungs, CD45+ cells were evenly distributed in the tissue (F). Scale bar 200 µm, insert shows magnification with scale bar 50 µm. Significance assessed by Kruskal-Wallis test (Dunnett's multiple comparison test shown in B) with $P<0.05$ as the limit of significance. *$P\leq0.05$; **$P<0.01$; ***$P<0.001$, ****$P<0.0001$.

First, I focused on gene expression analysis addressing the bulk of the EO771.LMB primary tumor and of pre-metastatic lungs. Absence of tumor cells in these lungs had been confirmed by the lack of *mCherry* expression on DNA level and the missing positive signal in immunohistochemistry for mCherry. Hence, expression of *protein tyrosine phosphatase, receptor type C (Ptprc)*, coding for CD45, was measured by qRT-PCR in EO771.LMB primary tumor samples obtained from *Junb* KO or respective control mice. *Ptprc* was found to be significantly increased by 1.7-fold in KO tumors compared to CTR and WT (Figure 4-10 A). Similarly, *Ptprc* expression was found to be significantly enhanced by a factor of 1.5 in pre-metastatic lungs of *Junb* KO animals (Figure 4-10 D). To exclude a potential influence of JUNB on the basal level of immune cell infiltration, lungs of unchallenged mice, such as age matched animals which had not been injected with tumor cells, were also analyzed for *Ptprc* expression. Expression in these mice was independent of JUNB indicating that the observed phenotype can be specifically attributed to tumor-bearing mice (Figure 4-10 D). Increased gene expression can be the result of multiple factors: increased expression of *Ptprc* on individual cells, enhanced number of immune cells or a different composition of the immune cell infiltrate as different kinds of immune cells express CD45 at varying levels. Thus, in order to determine whether enhanced *Ptprc* transcript levels in KO mice can be translated into an accumulation of CD45+ immune cells in KO mice or is a mere result of increased expression on individual cells, EO771.LMB primary tumors and pre-metastatic lungs were immunohistochemically

stained for CD45. Analysis of EO771.LMB primary tumors revealed that immune cells could be predominantly detected at the tumor periphery and within large necrotic areas, yet being unchanged in *Junb* KO mice (Figure 4-10 C). The overall number of CD45+ cells, as estimated by CD45+ area, was not consistently affected by JUNB loss indicating that differences observed in gene expression are likely the result of enhanced expression in individual cells or are simply too small to be visible on protein level (Figure 4-10 B+C). In unchallenged mice, the number of CD45+ immune cells in lungs was not different in KO mice compared to the controls, which is in agreement with the data obtained on RNA level (Figure 4-10 E+F). However, as soon as the mice did bear a tumor, accumulation of CD45+ cells was vastly increased in all genotypes but even more enhanced in lungs of mice with stromal *Junb* loss (Figure 4-10 E+F). Although this increase did not reach statistical significance, it is consistent with the RNA data. In general, the differences in CD45 expression between KO mice and controls both on RNA and protein level do not even reach a factor of two indicating that immune cell infiltration is not massively altered or that not all types of immune cells are influenced by JUNB loss in the same way. By gross examination of immunohistochemical staining for CD45, no obvious changes in cell composition could be spotted, although it seemed that immune cell infiltrates into necrotic areas of the primary tumors were slightly denser in KO mice compared to CTR (Figure 4-10 C). This did, however, not translate into a generally enhanced infiltration of CD45+ cells into primary KO tumors. It is therefore essential to further profile different immune cell subtypes in more detail and to define the immune cells preferentially localizing to necrotic areas.

These data provide a first hint, that JUNB may indeed promote immune cell infiltration potentially providing a mechanistic basis for the observed metastatic phenotype. The fact that this phenotype is more pronounced in pre-metastatic lungs than in the primary tumor, further implies that JUNB may be important in the pre-conditioning of a future metastatic site.

In order to clarify whether immune cell infiltration is generally enhanced or whether certain subtypes are specifically influenced, further immune cell markers which define certain subsets more specifically, were investigated. The same dual approach as for CD45 was followed: a rough estimation was obtained by gene expression analysis which was subsequently supported by histological assessment. In an initial step towards characterization of the pivotal cell type, it was assessed whether rather cells of the innate or the adaptive immune system are altered.

4.3.3.1. Deletion of Junb *in the microenvironment enhances accumulation of innate immune cells in pre-metastatic lungs*

The innate immune system is the first line of defense against internal and external danger signals, such as invading pathogens, and provides a rapid albeit non-specific immune response. Cells of the innate immune system are, however, not only essential in the reaction against pathogens such as viruses and bacteria but have also been implicated in cancer progression and metastasis. Innate immune cells comprise NK cells, macrophages, monocytes, dendritic cells and polymorphonuclear cells (PMN), such as neutrophils, eosinophils and basophils [277, 278]. As all these cell types in the mouse consistently express CD11b, I next focused on CD11b+ cells.

4.3.3.1.1. CD11b+ cells

Similarly, as for *Ptprc*, *integrin alpha M* (*Itgam)*, the gene which is encoding CD11b, is upregulated in EO771.LMB primary tumors derived from *Junb* KO mice compared to controls (Figure 4-11 A). In line with this, *Itgam* upregulation is also visible in KO lungs of EO771.LMB-bearing mice but not in unchallenged animals (Figure 4-11 D). Besides similar patterns of expression, CD11b+ cells, visualized by immunohistochemistry for CD11b, are also predominantly localized to the tumor periphery and necrotic areas (Figure 4-11 C). Just as seen with CD45, CD11b+ immune cell infiltration is independent of JUNB in EO771.LMB primary tumors and unchallenged lungs. In contrast, in pre-metastatic lungs from *Junb* KO animals, significantly more CD11b+ myeloid cells were detected (Figure 4-11 B, C, E+F). Of note is thereby, that, as opposed to *Ptprc*, the observed change in *Itgam* expression is more than 2-fold between KO and CTR or WT (Figure 4-11 D). This finding, in addition to corresponding spatial patterns, indicates, that the observed phenotype of enhanced CD45+ immune cell infiltration is likely due to an increase in CD11+ myeloid cells.

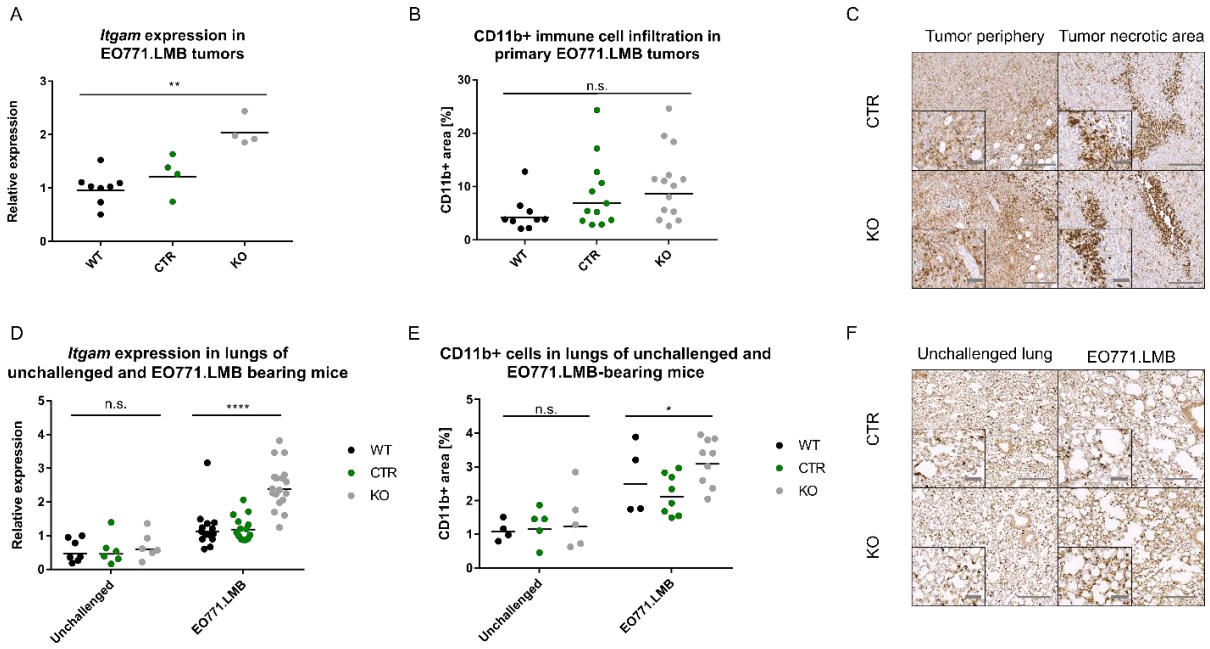

Figure 4-11: JUNB influences accumulation of CD11b+ myeloid cells in EO771.LMB primary tumors and pre-metastatic lungs.

Itgam expression is higher on RNA level in tumors (A) and pre-metastatic lungs (D) derived from KO animals but not in unchallenged lungs (D). An enhanced infiltration of CD11b+ immune cells in KO mice, as determined by immunohistochemistry for CD11b, is not visible in primary tumors (B, C) and lungs of unchallenged mice (E, F) but in lungs of EO771.LMB tumor-bearing animals (E, F). Quantification of CD11b+ area was performed on whole sections of primary tumors or lungs. In primary tumors, CD11b+ cells were present especially at the periphery of the tumor and within necrotic areas (C), in the lungs CD11b+ cells were evenly distributed throughout the tissue (F). Scale bar 200 µm, inset shows magnification with scale bar 50 µm. Significance assessed by Kruskal-Wallis test with P<0.05 as the limit of significance. *P≤0.05; **P<0.01; ***P<0.001, ****P<0.0001.

4.3.3.1.2. Macrophages

One prominent cell type of the myeloid lineage are macrophages. The association between macrophages and tumorigenesis has been described elaborately coining the term “Tumor-associated macrophages” (TAMs). Multiple reports have come to the conclusion that TAMs can have both tumor-suppressive and tumor-promoting functions, leading to the concept of an M1 versus M2 phenotype, respectively [279]. Over time, it has, however, become increasingly clear, that the impact of macrophages on tumor cells cannot clearly be differentiated into M1 versus M2 but is much more complex. One potential explanation for these observed phenotypical differences is based on the feature that macrophages can already be present in the tissue as tissue-resident macrophages or differentiate from monocytes which are recruited to inflammatory sites. Depending on the differentiation status, localization and signals from the microenvironment, these cells have different functions in homeostasis and inflammation as well as in regard to inflammatory cytokine secretion [280].

Upon examination of the localization of CD45+ as well as CD11b+ immune cells, it was apparent that these cells preferentially localized either to necrotic areas or along the tumor periphery, close to the tumor-stroma interphase. As macrophages appear to line up around the tumor border or accumulate in necrotic areas, it seemed reasonable to investigate cells of the monocyte/macrophage lineage.

The F4/80 molecule has originally been described as being solely expressed by murine macrophages. Since then it has also been found to be expressed by other immune cell types and it was shown that F4/80 expression is not uniformly throughout the different macrophage subsets [281]. Yet, F4/80 remains the pan-macrophage marker predominantly used in order to identify macrophages irrespective of whether they are tissue-resident or monocyte-derived. Therefore, F4/80 was also used in this study, in order to clarify whether F4/80+ macrophages, or macrophages expressing *adhesion G protein-coupled receptor E1 (Adgre1)* on RNA level, compose the predominant myeloid cell type present in high numbers in pre-metastatic lungs of *Junb* KO animals. In line with previous experiments, gene expression was analyzed in EO771.LMB primary tumors and lungs isolated from unchallenged or EO771.LMB tumor-bearing mice. No statistical difference was detected for *Adgre1* expression in primary tumors and unchallenged mice, whereas a slight but significant increase was noticed in pre-metastatic lungs of KO mice (Figure 4-12 A+B). It should be noted, that *Adgre1* expression in pre-metastatic lungs was generally at a similar level as in lungs of unchallenged mice, indicating that it was not specifically induced in the tumor setting. Furthermore, immunohistochemistry for F4/80 confirmed on protein level, that macrophage infiltration into primary tumors was independent of JUNB (Figure 4-12 C+D). Moreover, F4/80+ cells were predominantly localized around the tumor periphery but not so much in necrotic areas of EO771.LMB tumors. This provides a further indication that macrophages are not the cell population primarily altered in JUNB-deficient mice because both CD45+ and CD11b+ cells were accumulated not only at the tumor border but also in necrotic areas. To further support this notion, I measured gene expression of *Cd163* in primary tumors and lungs. CD163 had been described as an alternative pan-macrophage marker and had been proposed by some authors to be M2-specific [282, 283]. This does, however, remain controversial, as M2-specificity has been disproved by others [284]. Alike *Adgre1*, *Cd163* was slightly, albeit non-significantly, increased in primary tumors from KO mice but no regulation was obvious neither in unchallenged nor in pre-metastatic lungs (Figure 4-12 E+F). Macrophages therefore do not seem to be the predominant immune cell type being accumulated in the lungs of tumor-bearing animals upon JUNB loss.

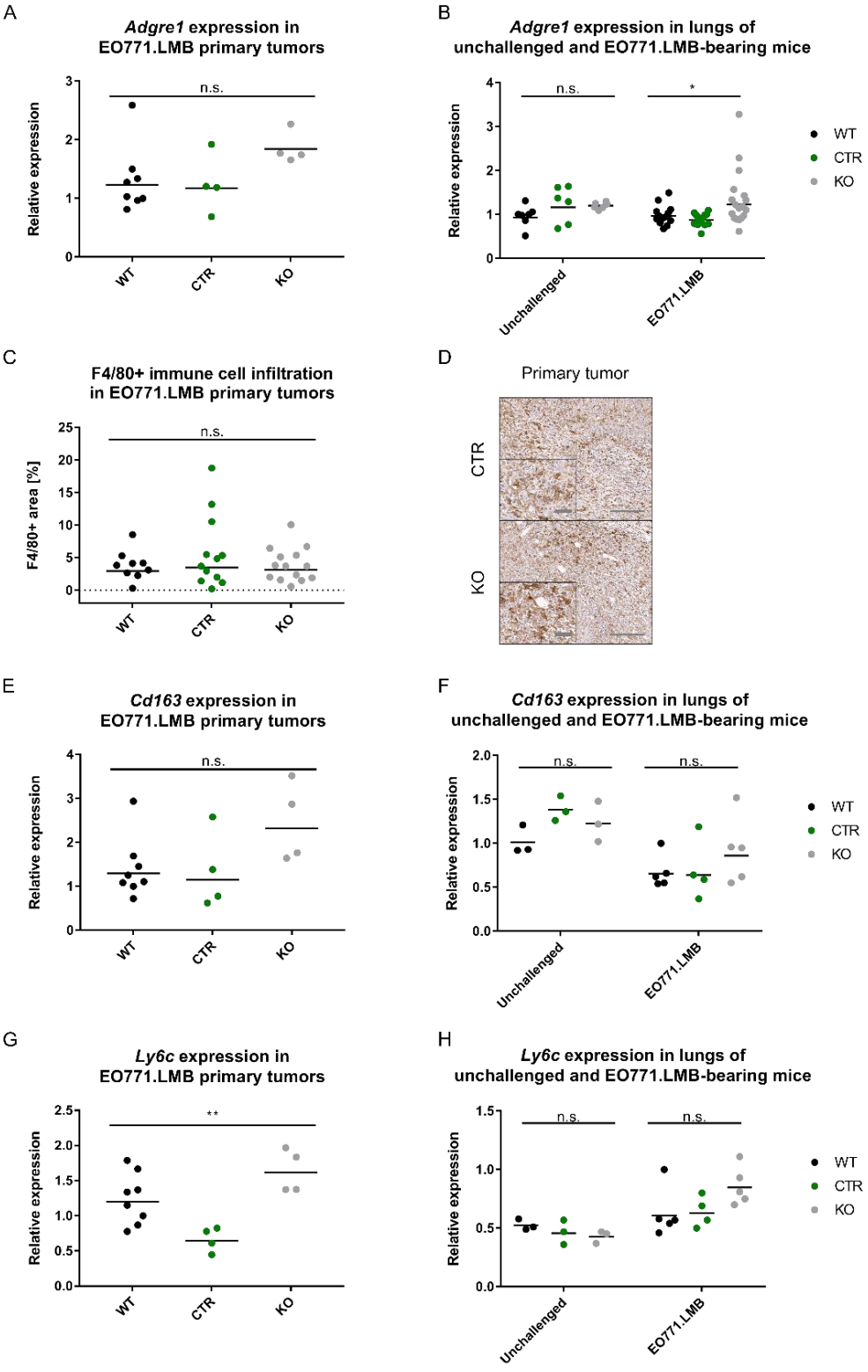

Figure 4-12: Deletion of stromal *Junb* does not affect macrophage abundance in EO771.LMB primary tumors and only mildly influences macrophage count in pre-metastatic lungs.

In primary tumors, markers of the monocyte and macrophage lineage are not consistently regulated by JUNB on RNA level: *Adgre1* (A), *Cd163* (E) and *Ly6c* (G). Similarly, in unchallenged as well as pre-metastatic lungs: *Cd163* (F) and *Ly6c* (H) are not consistently upregulated in *Junb* KO mice. A significant increase was found in *Adgre1* expression in pre-metastatic lungs from KO animals (B). That JUNB has no effect on F4/80+ macrophages in primary tumors was confirmed by immunohistochemical staining of F4/80 (C+D). Quantification of F4/80+ area was performed on whole sections of primary tumors. Scale bar 200 µm, inset shows magnification with scale bar 50 µm. Significance assessed by Kruskal-Wallis test with $P<0.05$ as the limit of significance. *$P\leq0.05$, **$P<0.01$.

Nevertheless, in order to exclude the possibility, that not terminally-differentiated macrophages but monocytes are increased, gene expression analysis was conducted for *Ly6c* [280]. *Ly6c* expression was significantly different between the genotypes in primary EO771.LMB tumors (Figure 4-12 G), albeit variations among individuals were rather high. An increase was also visible in *Junb* KO pre-metastatic lungs but did not reach significance (Figure 4-12 H). Since in primary tumors *Adgre1* and *Ly6c* expression was inconsistent and in pre-metastatic lungs the fold change difference between the genotypes was not as substantial as for *Itgam*, I concluded that the increased CD11b+ immune cell infiltration was not due to cells of the macrophage/monocyte lineage.

4.3.3.1.3. NK cells

NK cells are another essential cell type of the innate immune response and can kill target cells without the necessity of prior priming. NK cells are important in the control of early-disease cancer and ablation of NK cells has been demonstrated to fuel tumor progression and metastasis [285, 286]. Despite this clear anti-tumoral function, NK cells have also been found accumulated in breast and colorectal cancer and have been correlated to tumor progression [287, 288]. NK cells are furthermore positive for CD11b, and, thus, could be the cell type previously observed in high numbers in tumor-bearing KO animals. Consequently, I identified NK cells by gene expression analysis of *killer cell lectin-like receptor subfamily b member 1c (Klrb1c)*, which is coding for the pan-NK cell marker NK1.1. *Klrb1c* was significantly upregulated in EO771.LMB primary tumors isolated from *Junb* KO mice but expression was comparable in unchallenged as well as pre-metastatic lungs (Figure 4-13 A+B). As the primary difference in CD11b+ immune cell infiltration had been seen in pre-metastatic lungs rather than primary tumors, NK cells are most likely not the predominant cell type being affected upon JUNB loss.

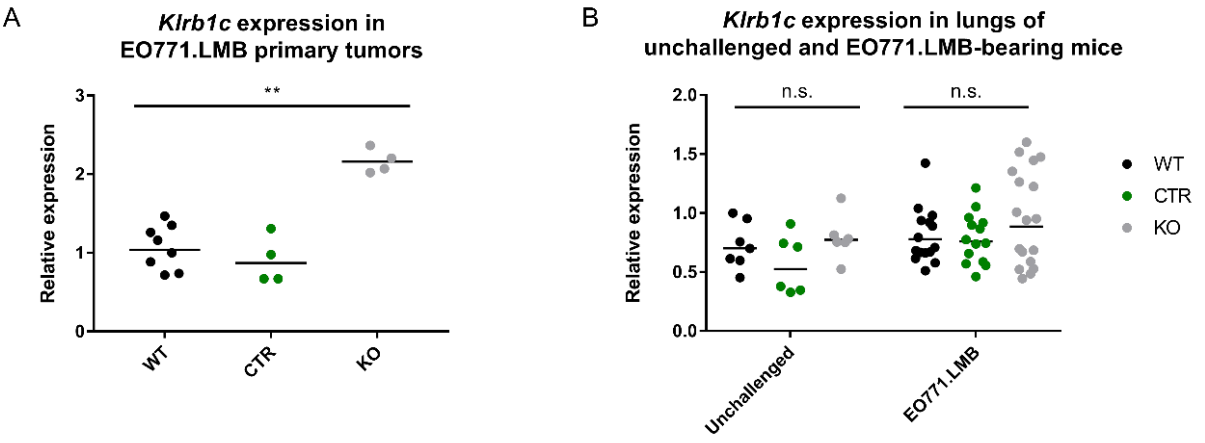

Figure 4-13: Presence of NK cells is different in EO771.LMB primary tumors and lungs with stromal *Junb* ablation.

JUNB loss does promote NK cell infiltration into primary tumors (A) but does not affect NK cell accumulation in unchallenged lungs or lungs from tumor-bearing mice (B) as determined by gene expression analysis for *Klrb1c*. Significance assessed by Kruskal-Wallis test with $P<0.05$ as the limit of significance. **$P<0.01$.

4.3.3.1.4. Polymorphonuclear cells (PMNs)

Despite the analysis of all these different innate immune cells, the identity of the cell type occupying the necrotic areas in primary EO771.LMB tumors and seemingly accumulated more in tumors derived from KO mice remained to be clarified. Closer examination of immunohistochemical sections stained for CD45 (Figure 4-10 C) and CD11b (Figure 4-11 C) revealed that especially very small leukocytes had invaded into these necrotic areas arguing for small lymphocytes or PMNs. PMNs, also called granulocytes, make up a substantial proportion of leukocytes in peripheral blood of mice. Neutrophils are the most prominent subtype with 20-30% of total white blood cells [289]. Neutrophils are formed in the bone marrow and are, due to their very short life span of only a few hours, constantly released into the circulation. Upon inflammation, neutrophils are the first immune cell type to arrive at sites of injury, typically within minutes [290]. Besides their role in resolving infections, neutrophils have also been implicated in tumorigenesis where they have been associated with both tumor-promoting [91, 96] and suppressive properties [92]. Irrespective of whether pro- or anti-tumorigenic, neutrophils were reported to accumulate in tumor pre-conditioned organs before arrival of tumor cells [91, 92, 96].

In order to clarify whether neutrophils also accumulated in tumors and pre-metastatic lungs of the EO771.LMB model, I examined these tissues by gene expression analysis for *Ly6g* and stained paraffin sections with anti-neutrophil antibody 7/4, which has been demonstrated to recognize LY6B.2 [291]. On RNA level, *Ly6g* was statistically significantly upregulated in EO771.LMB primary tumors from KO mice by approximately 2.5-fold (Figure 4-14 A). In line with this finding, increased accumulation of LY6B.2+ neutrophils could also be confirmed on protein level by immunohistochemistry (Figure 4-14 B+C). In agreement with data obtained with CD45 and CD11b, Ly6B.2+ cells localized preferentially to necrotic areas within the tumor core (Figure 4-14 C). That these cells also exhibited a roundish morphology and were of similar size as CD45+ or CD11b+ cells in necrotic areas, further indicated that the previously observed small leukocytes could indeed be neutrophils. Analysis of pre-metastatic lungs yielded an even more convincing picture: *Ly6g* was upregulated approximately 6-fold in lungs isolated from tumor-bearing KO mice, while being only slightly induced in non-tumor-bearing KO animals (Figure 4-14 D). The same was true for the protein level. Already qualitative assessment of immunohistochemical stainings for LY6B.2 showed an enhanced neutrophil infiltration into the pre-metastatic KO lungs, which was further substantiated by quantitative analysis (Figure 4-14 E+F). In the lungs of tumor-bearing KO mice, 3.7 times more Ly6B.2+ cells had accumulated compared to WT and CTR, whereas no increase in accumulation was visible in unchallenged mice. Also, *S100a8* and *S100a9*, which are abundantly expressed in the cytosol of neutrophils, were strongly upregulated 5-fold and 4-fold, respectively (Figure 4-14 J+K), further supporting the notion, that neutrophils are indeed the cell type accumulated upon JUNB loss. Moreover, the expression pattern of *S100a8* and *S100a9* also corresponded with *Ly6g* in unchallenged mice further indicating that *S100a8* and *S100a9* may indeed be derived from neutrophils in this setting.

At last, I investigated whether this accumulation of neutrophils to pre-metastatic lungs was specific for the EO771.LMB model or was a more common phenomenon observed upon *Junb* ablation in the stroma. In fact, *Ly6g* was found to be even higher expressed in pre-metastatic lungs of the LL/2-Luc model when compared to the EO771.LMB model (Figure 4-14 G). In the B16F10 model, neutrophil infiltration into the pre-metastatic lungs was similar to the EO771.LMB model as quantified by immunohistochemistry for Ly6B.2 (Figure 4-14 H+I).

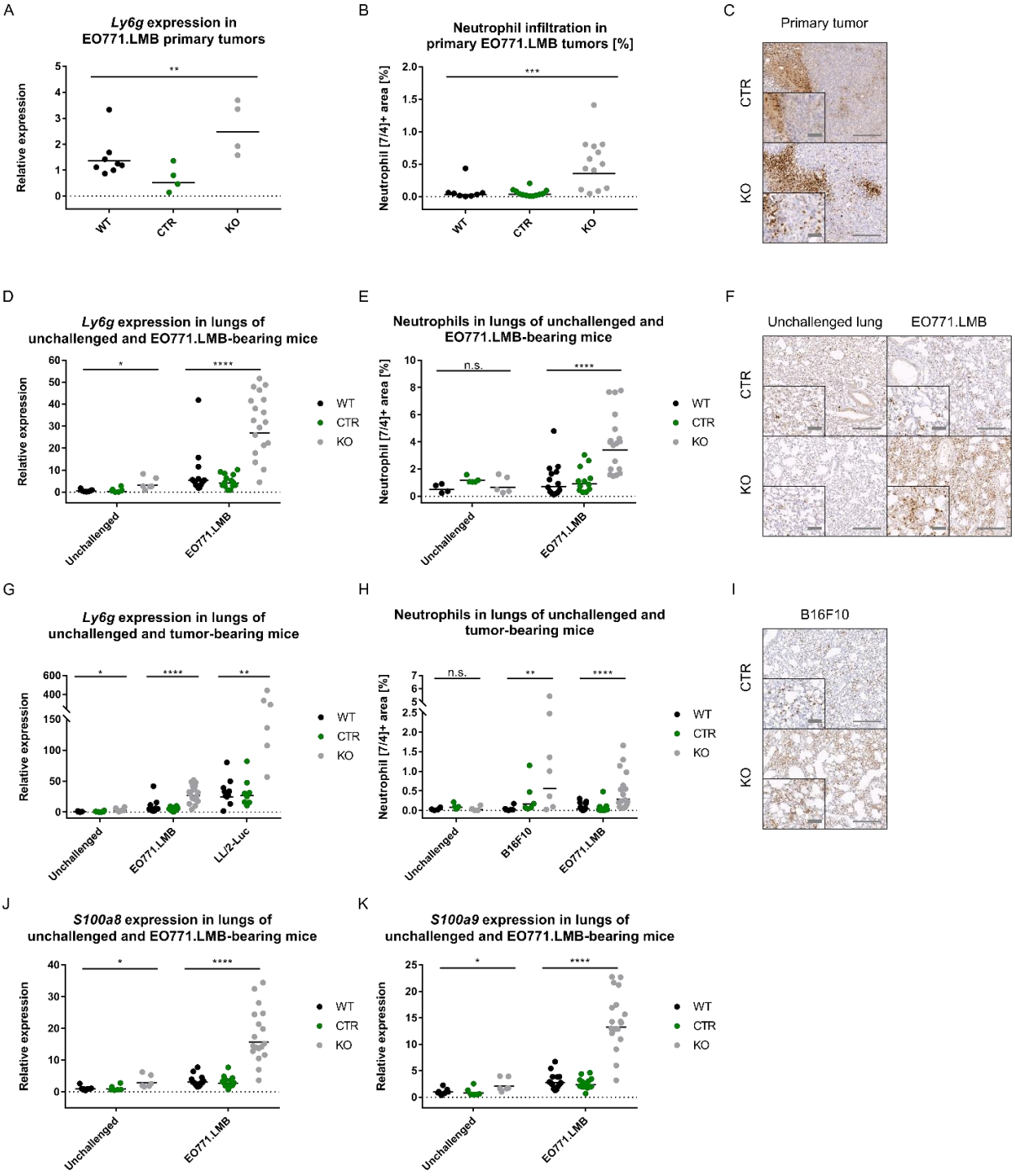

Figure 4-14: *Junb* deletion leads to neutrophil accumulation in primary tumors and pre-metastatic lungs in the EO771.LMB, B16F10 and LL/2-Luc model.

In the EO771.LMB model, enhanced neutrophil infiltration in KO mice was detected by gene expression analysis of *Ly6g* in primary tumors (A) and pre-metastatic lungs (D). This was confirmed by immunohistochemistry using the neutrophil marker 7/4 in EO771.LMB primary tumors (B+C) and in pre-metastatic but not in unchallenged lungs (E+F). Enhanced neutrophil recruitment to pre-metastatic lungs was also observed by gene expression analysis in the LL/2-Luc model (G) and by immunohistochemistry in the B16F10 melanoma model (H+I). In line with increased *Ly6g* expression, *S100a8* (J) and *S100a9* (K) were also upregulated in lungs of EO771.LMB tumor bearing KO animals. Quantification of Ly6B.2+ area was performed on whole sections of primary tumors or lungs. Scale bar in overview 200 µm, insert shows a magnification, scale bar 50 µm. Significance assessed by Kruskal-Wallis test with P<0.05 as the limit of significance. *P<0.05; **P<0.01; ***P<0.001, ****P<0.0001.

Overall, this high upregulation of *Ly6g* and Ly6B.2 in primary tumors and pre-metastatic lungs of KO mice together with the staining patterns of LY6B.2 resembling both CD45 and CD11b led to the conclusion that neutrophils are the predominant cell type recruited to these tissues. In summary, significantly more neutrophils did accumulate in the lungs of mice lacking *Junb* in the stroma compared to *Junb*$^{+/+}$ mice.

4.3.3.2. Deletion of JUNB in the stroma does not impact recruitment of adaptive immune cells

The significantly enhanced infiltration of neutrophils into primary tumors as well as into pre-metastatic lungs of mice with stromal JUNB loss does, however, not exclude that JUNB may also have an impact on cells of the adaptive immune system. The adaptive immune response is the second arm of immunity, which copes with infections that could not be resolved entirely by innate immune cells. The adaptive immunity is only initiated upon contact with innate immune cells, such as dendritic cells, functioning as antigen-presenting cells. This initial contact results in the activation of T lymphocytes and subsequent differentiation of B lymphocytes into antibody-producing plasma cells. The interaction with the innate immune system is crucial during infections, but also in tumorigenesis, innate immune cells engage with components of the adaptive immune system in multiple ways. In particular, neutrophils have been shown to influence cytotoxic T cells and regulatory T cells thereby either promoting or inhibiting tumor progression [91]. Consequently, I analyzed primary EO771.LMB tumors and pre-metastatic lungs for T cell infiltration in order to determine whether JUNB and JUNB-mediated neutrophil accumulation may have an impact on the recruitment.

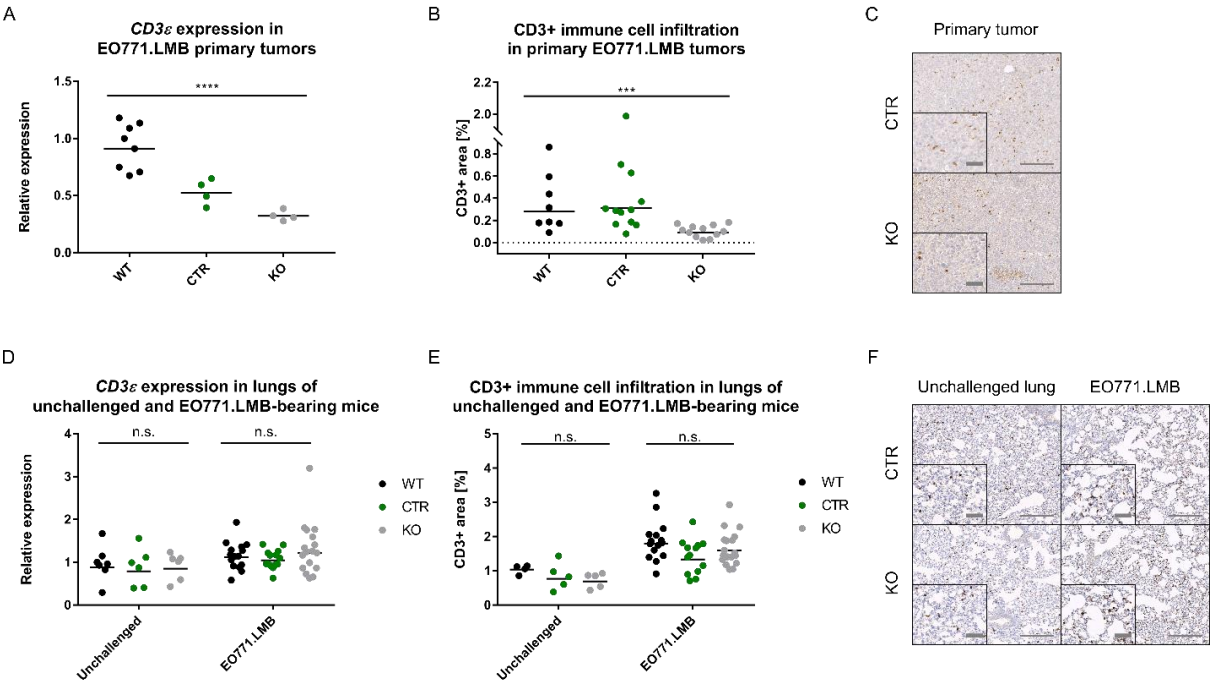

Figure 4-15: CD3+ T cell infiltration in the primary EO771.LMB tumor but not into pre-metastatic lungs is negatively influenced by JUNB ablation.

CD3 expression was markedly reduced in tumors from KO mice as analyzed by gene expression analysis for *CD3ε* (A) or immunohistochemistry for CD3 (B+C). In pre-metastatic and unchallenged lungs, no difference was observed neither on RNA (D) nor protein level (E+F). Quantification of immunohistochemistry was performed on whole lung or tumor sections. Representative images are shown in (C) for tumors and (F) for lungs. Scale bar 200 µm in larger image, inserted magnifications have a scale bar of 50 µm. Significance assessed by Kruskal-Wallis test with P<0.05 as the limit of significance. *P<0.05; **P<0.01; ***P<0.001, ****P<0.0001.

To gain a first insight, CD3+ T cells were examined. By gene expression analysis for *CD3ε*, a significantly reduced expression was detected in EO771.LMB primary tumors from KO mice (Figure 4-15 A). As expression was, however, also markedly different between WT and CTR mice, no clear conclusion could be drawn yet. Nevertheless, expression of CD3 varies considerably between T cell subtypes. In order to clarify, whether total numbers of T cells could be affected rather than the composition of the T cell infiltrate, immunohistochemistry for CD3 was performed. Quantification revealed, that CD3+ T cell infiltration, approximated by determining CD3+ areas, was in fact similar between WT and CTR mice but significantly lower in KO mice (Figure 4-15 B+C). In contrast, examination of unchallenged and pre-metastatic lungs did not reveal changes in CD3+ T cell contents, neither by expression analyses nor by immunohistochemical staining (Figure 4-15 D, E+F). This led me to conclude, that JUNB does not influence CD3+ T cell recruitment to the lungs but may have an adverse impact on infiltration into the primary tumor in the EO771.LMB model.

In order to assess whether T cells are generally impeded from migrating into the primary tumors in *Junb* KO mice, or whether some class of T cells is preferentially hindered, I proceeded with the analysis of T cell subtypes. Regulatory T cells (Tregs) as well as CD8+ T cells are thereby the most prominent subtype in the context of cancer.

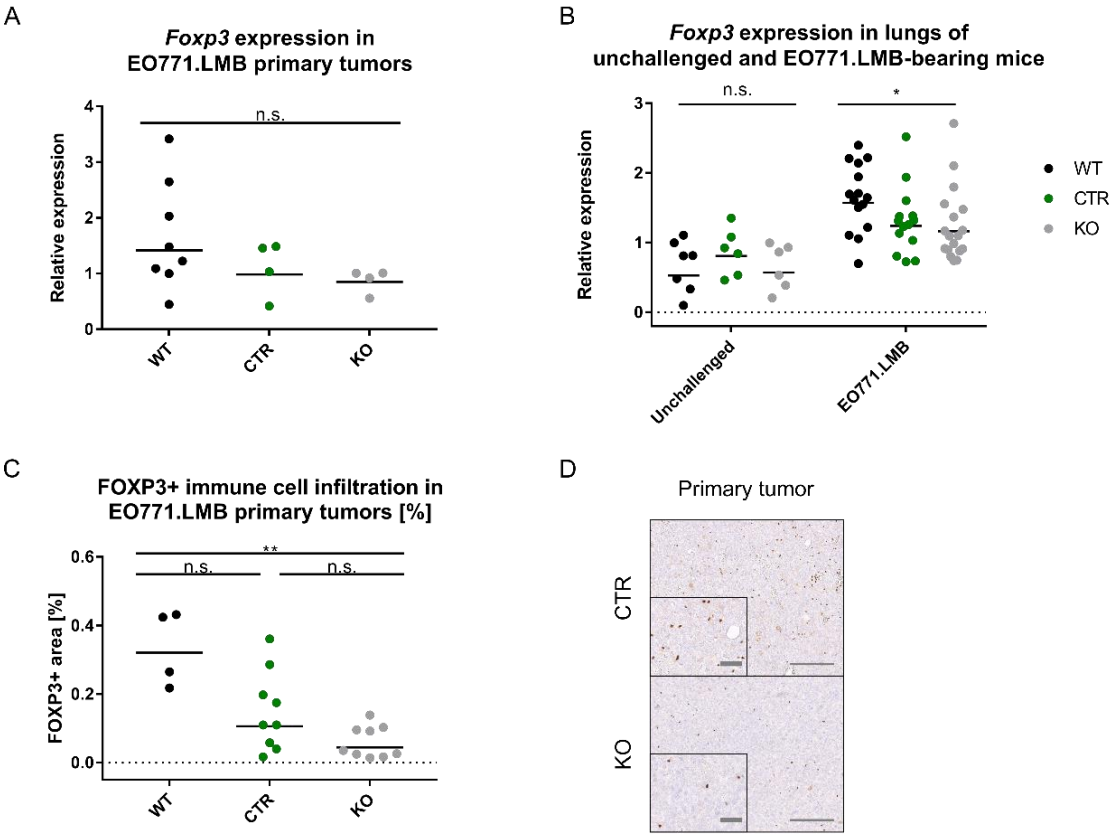

Figure 4-16: FOXP3+ regulatory T cells accumulate in EO771.LMB primary tumors and lungs independently of JUNB.

Infiltration of Tregs was quantified by qRT-PCR on RNA level for *Foxp3* in EO771.LMB primary tumors (A) and unchallenged as well as pre-metastatic lungs (B). Accumulation of Tregs was further assessed on protein level by immunohistochemistry for FOXP3 (D); quantification of immunohistochemistry in (C). No consistent regulation of Tregs was observed in any of these settings. For quantifications, whole sections of primary tumors were used, representative images are shown in (D) with scale bar 200 µm. Magnifications are presented as insets with scale bar 50 µm. Significance assessed by Kruskal-Wallis test (with Dunnett's multiple comparison test in C) with $P<0.05$ as the limit of significance.*$P<0.05$; **$P<0.01$.

Treg differentiation and function critically depends on the expression of the transcription factor FOXP3. As FOXP3 is claimed to be specifically expressed by Tregs [292, 293], this marker was utilized to assess the presence of Tregs in primary tumors and pre-conditioned lungs. Gene expression analysis of *Foxp3* revealed a similar trend as detected for *CD3ε* with tumors derived from KO mice exhibiting the lowest expression but also substantial differences between WT and CTR mice were detected (Figure 4-16 A). This inconsistency was confirmed by immunohistochemical analysis of FOXP3+ cells. Thereby, no clear JUNB-dependency could be observed (Figure 4-16 C+D). Similar expression patterns were also detected in pre-metastatic lungs (Figure 4-16 B). *Foxp3* expression was at a comparable level between CTR and KO mice but significantly higher in WT animals. High variations in unchallenged lungs furthered the impression, that FOXP3+ Tregs were not regulated in a JUNB-dependent manner in this model.

Apart from Tregs, also cytotoxic T cells are essential cellular components of the adaptive immune response which in addition have crucial functions during tumor progression. Besides NK cells, cytotoxic T cells are the main players in recognition and subsequent eradication of transformed cells. Cytotoxic T cells are, thus, an immensely important pillar in anti-tumor immunity.

As stromal *Junb* ablation did result in an overt metastatic phenotype in mice, I was wondering whether not only neutrophils were contributing to this effect but also cytotoxic T cells may be excluded from the tumor mass or suppressed in their function. Cytotoxic T cells are generally defined as being CD8+ T cells. Consequently, the abundance of cytotoxic T cells was evaluated by gene expression analysis of *CD8α.* In primary EO771.LMB tumors, expression of *CD8α* was significantly altered depending on the genotype (Figure 4-17 A). Yet, levels of *CD8α* were considerably higher in tumors derived from WT mice but more similar between CTR and KO mice. This discrepancy between WT and CTR mice could be the result of *CD8α* expression by other cell types, such as NK cells. In order to assure that only CD8+ T cells are evaluated, CD8 was co-stained together with the pan-T cell marker CD3 on histological sections. In line with previous immunohistochemical stainings, the paucity of CD3+ cells was apparent in tumors from KO mice, but no obvious difference was detected in the number of CD8+ T cells (Figure 4-17 D). For quantification, a macro for ImageJ was utilized enabling automated analysis. In this macro, the co-localization of CD3 and Hoechst identified CD3+ cells in a previously selected area. If CD3+ cells were additionally positive for CD8, they were regarded as CD8+ T cells. Quantification of the immunofluorescent images confirmed the initial impression that the number of CD8+ T cells in EO771.LMB tumors was not influenced by *Junb* KO in the stroma (Figure 4-17 C). Similar to primary tumors, no changes in CD8+ cell infiltration were observed by gene expression analysis for *CD8α* neither in unchallenged lungs nor in those isolated from tumor-bearing mice (Figure 4-17 B). In agreement with these data, the number of CD8+ T cells was also not affected by *Junb* loss in pre-metastatic lungs when assessed by immunofluorescence for CD3 and CD8 as described above (Figure 4-17 E+F). Overall, these findings imply that JUNB does not control the numbers of CD8+ T cells infiltrating primary tumors or accumulating in pre-metastatic lungs.

In conclusion, I could not detect any overt JUNB-dependent changes in the recruitment of adaptive immune cells to EO771.LMB primary tumors or lungs isolated from tumor-bearing mice. Although a significant decrease in the number of CD3+ T cells was observed in primary tumors, this difference could not be explained unambiguously by changes in regulatory or cytotoxic T cells. Variations among the genotypes were rather high, especially for FOXP3+ cells, so that no clear correlation with JUNB loss could be determined.

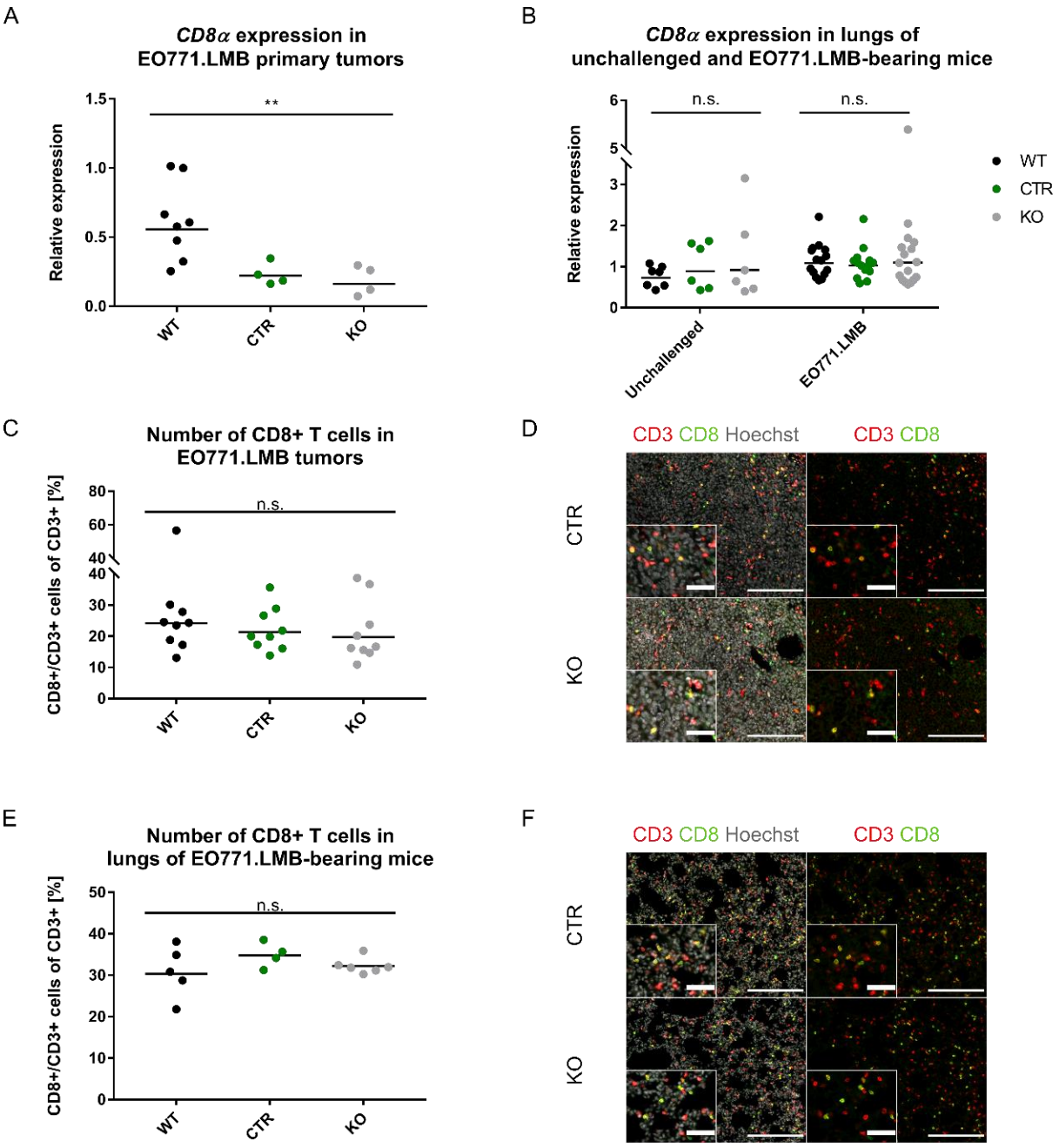

Figure 4-17: Infiltration of cytotoxic T cells is not affected by JUNB loss.

Infiltration of CD8+ cells was determined by gene expression analysis for *CD8α* in EO771.LMB primary tumors (A) and unchallenged as well as pre-metastatic lungs (B). No consistent JUNB-dependent regulation was detected. This was further confirmed by quantification of CD3 and CD8 double positive cells by immunofluorescence in EO771.LMB primary tumors (C) and pre-metastatic lungs (E). Quantification was performed in an automated manner using a macro for ImageJ on randomly selected T-cell rich fields of the tumor or lung. At least 150 CD3+ cells were analyzed for each tumor and at least 300 CD3+ cells for each lung. Representative pictures of T cell-rich areas stained for CD3 and CD8 in the tumor (D) and in the lung (F) are shown. CD3+ T cells are labelled in red, CD8+ cells are marked in green, nuclear staining by Hoechst in gray. CD3 and CD8 double positive cells appear yellow. Left panel shows the overlay with nuclear Hoechst staining, the right panel shows co-localization of CD3 and CD8 in some cells. Scale bar 200 µm, a blow up is displayed in the inset, scale bar 50 µm. **P<0.01. Significance assessed by Kruskal-Wallis test with P<0.05 as the limit of significance. **P<0.01.

In summary, assessment of immune cell infiltration clearly showed an upregulation of CD45+ and CD11b+ myeloid cells in EO771.LMB primary tumors but even more strikingly in pre-

metastatic lungs isolated from *Junb* KO mice. More in depth analyses of cellular components of the adaptive and innate immune system identified neutrophils as being the predominant cells affected by loss of JUNB, based on cell size and morphology as well as specific marker expression of *Ly6g* and LY6B.2. This observation provides first evidence, that JUNB may affect distant metastasis by controlling neutrophil recruitment to pre-metastatic organs.

4.4. Mechanistic assessment of JUNB-dependent neutrophil recruitment

After investigations of various cellular components of the tumor microenvironment had led to the conclusion, that predominantly neutrophil recruitment was enhanced upon stromal JUNB loss, several questions still remained. Was the effect of JUNB on neutrophil infiltration direct or was it indirectly conveyed by another cell type? Was it mediated by a factor secreted by the tumor microenvironment or the tumor itself? Which cell type upregulated potential neutrophil attracting chemokines or cytokines? In order to shed some light on these open questions, neutrophil recruitment was analyzed in more detail. Furthermore, *in vivo* experiments were performed to differentiate whether the metastatic phenotype was due to JUNB loss in the stroma or in the hematopoietic system. Finally, it was addressed whether neutrophils were directly responsible for enhanced metastasis in *Junb* KO mice.

4.4.1. Neutrophil-recruiting factors are regulated in a JUNB-dependent manner in EO771.LMB primary tumors and pre-metastatic lungs

The neutrophil pool in the circulation has to be constantly replenished due to the short life span of only a few hours in mice [294]. Neutrophil production and recruitment are therefore tightly controlled. Abnormalities in one of the regulating mechanisms can lead to either deficiencies, manifesting as recurrent infections, or excess leading to severe inflammation and associated tissue damage [295]. Neutrophils are produced in the bone marrow cavity from granulocyte-macrophage progenitors (GMP). After maturation, neutrophils are retained within the bone marrow via CXCR4-CXCL12 (SDF1) chemokine signaling. Release of mature neutrophils into the circulation is subsequently regulated by CXCR2 signaling, predominantly mediated by granulocyte-colony-stimulating factor (G-CSF). Upon inflammatory stimuli, G-CSF can be augmented potentiating the egress from the bone marrow partly also by reducing CXCL12 expression by bone marrow stromal cells [296-298]. Further cytokines, such as tumor necrosis factor alpha (TNFα) [294], Interleukin-8 (IL-8) [294], Interleukin-1 alpha (IL-1α) [299] and Interleukin-1 beta (IL-1β) [300-302] have also been reported to promote neutrophil mobilization. In the circulation, neutrophils subsequently react to chemotactic signals, such as chemokine (C-X-C motif) ligand 1 (CXCL1, KC), CXCL2 (MIP-2) and CXCL5 (LIX), which are the murine orthologues of human IL-8, promoting the recruitment into peripheral tissues [303]. Besides these classical chemokines, also further factors have been reported to stimulate neutrophil recruitment, namely: CCL2 (monocyte chemoattractant protein 1, MCP-1) [304], CCL5 (Regulated upon Activation, Normal T cell Expressed, and Secreted; RANTES) [305], Osteopontin [306] and Lipocalin 2 [307].

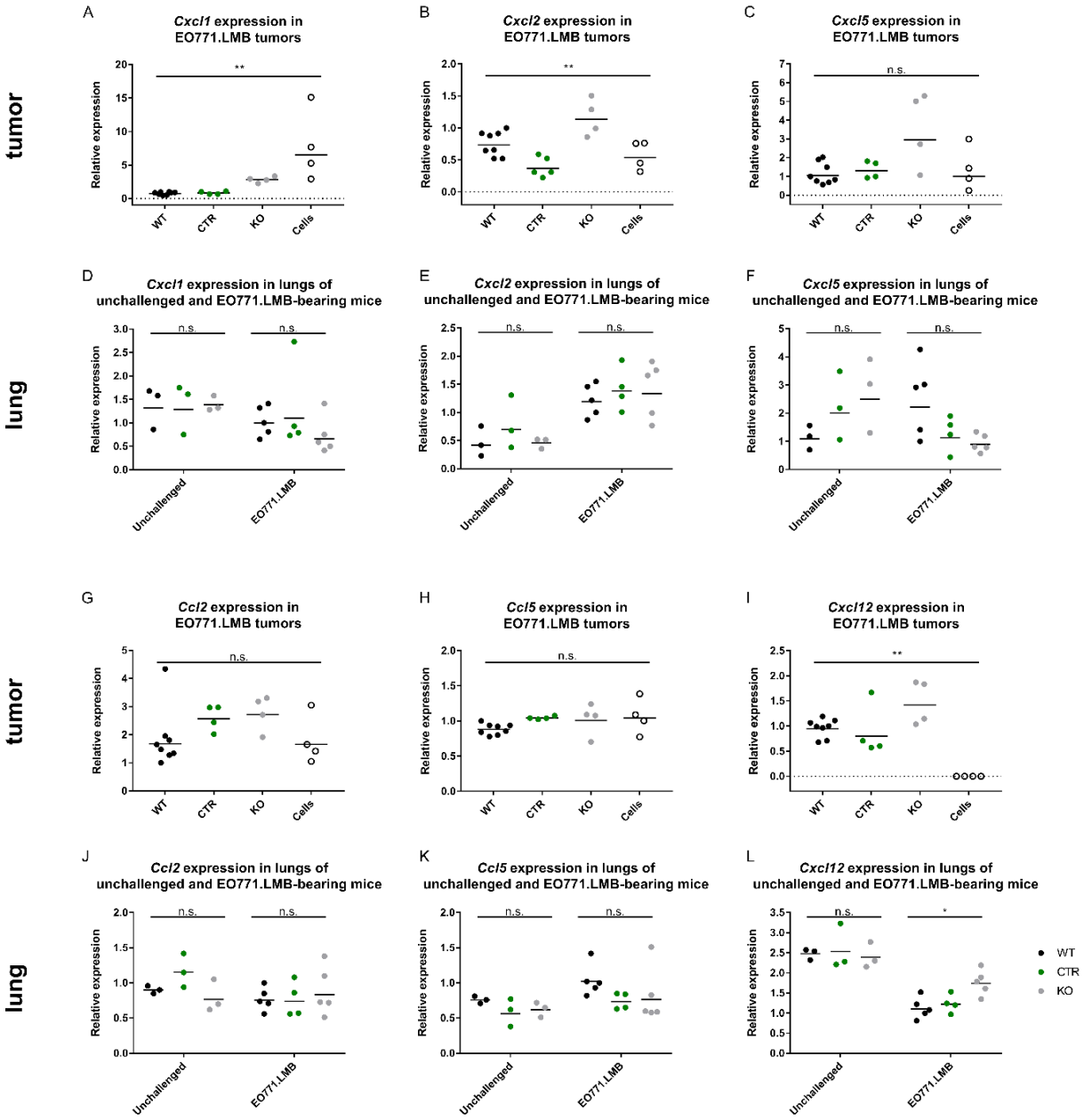

Figure 4-18: Loss of stromal *Junb* impacts neutrophil-attracting chemokines.

Expression levels were determined by qRT-PCT of bulk tumors derived from mice with or without JUNB in the stroma, as well as in EO771.LMB cells *in vitro*: *Cxcl1* (A), *Cxcl2* (B), *Cxcl5* (C), *Ccl2* (G), *Ccl5* (H) and *Cxcl12* (I). In parallel, these factors were also investigated in lungs isolated from unchallenged or tumor-bearing mice (D-F, J-L). Data are represented as geometric mean. Significance was assessed by Kruskal-Wallis test with $P<0.05$ as the limit of significance. *$P\leq0.05$ and **$P<0.01$.

In order to determine whether JUNB regulates neutrophil infiltration by influencing gene expression of these key neutrophil recruiting factors, existing material of tumors and lungs was analyzed by qRT-PCR. In addition to the analysis of bulk tumors derived from *Junb* KO or respective control animals, also pure EO771.LMB cells isolated *in vitro* were assessed. This was necessary in order to differentiate between factors derived from the tumor cells themselves and the tumor microenvironment. In a first set of factors, neutrophil chemotactic factors were studied. All these chemokines, *Cxcl1, Cxcl2, Cxcl5, Ccl2* and *Ccl5*, except for *Cxcl12* were expressed by EO771.LMB cells, indicating that *Cxcl12* is solely expressed by

cells of the tumor microenvironment (Figure 4-18 A-C, G-I). In contrast to all other factors, *Cxcl1* was expressed 2.3 times higher EO771.LMB cells than in the tumor bulk, implying that tumor cells may be its predominant source. No JUNB-dependent regulation was observed for *Ccl2* and *Ccl5,* where expression levels were similar or inconsistent between the genotypes (Figure 4-18 G+H). For *Cxcl1, Cxcl2* and *Cxcl5* a higher expression was detected in tumors derived from KO mice compared to controls but this did not reach significance for *Cxcl5* (Figure 4-18 A-C). For *Cxcl2,* not only KO mice but also WT mice showed elevated expression compared to CTR animals (Figure 4-18 B). In unchallenged or pre-metastatic lungs, no significant changes were observed for any chemokine except for *Cxcl12* implying that these factors may not play a decisive role in JUNB-dependent neutrophil recruitment to the lungs (Figure 4-18 D-F, J-L). *Cxcl12* was the only chemokine which showed differential expression upon JUNB loss which was only observed in pre-metastatic but not in unchallenged lungs (Figure 4-18 L). Consistently with the required downregulation of *Cxcl12* for mobilization of neutrophils from the bone marrow, *Cxcl12* levels were decreased in pre-metastatic compared to unchallenged lungs. Contrary to the increased accumulation of neutrophils in pre-metastatic lungs of KO mice, *Cxcl12* was, however, 40% higher expressed in KO than in CTR and WT. Apart from *Cxcl2,* no major upregulation of chemokines was moreover observed in pre-metastatic compared to unchallenged lungs indicating that neutrophil accumulation in tumor-bearing animals may be due to different mechanisms other than upregulation of these chemoattractant molecules.

In a second set of factors, which have been described to function as neutrophil recruiters, some more conclusive data could be obtained. In agreement with the analysis of the first set, gene expression was quantified by qRT-PCR on tumor bulk and EO771.LMB cells as well as unchallenged and pre-metastatic lungs. In contrast to *Il-1α*, *Spp1* (Osteopontin) and *Lcn2* (Lipocalin-2), no expression of *Il-1β, Tnfα* and *Csf3* (G-CSF) could be observed in tumor cells alone, indicating that these factors are purely derived from the tumor microenvironment (Figure 4-19 A-C, G-I). Although significant differences in expression were observed for *Csf3* and *Spp1*, no consistent JUNB-dependence could be noticed, excluding these factors as potential key regulators (Figure 4-19 G+H). For *Il-1α, Il-1β, Tnfα* and *Lcn2,* an increase in expression could be detected upon loss of *Junb* by 2.3, 2.9, 1.6 and 7.7-fold, respectively (Figure 4-19 A-C; I). This was particularly consistent for *Il-1β* and *Tnfα.*

Interestingly, expression of these factors was also affected in pre-metastatic lungs. In particular, *Il-1β* was clearly upregulated 4-fold in pre-metastatic KO lungs, whereas this increase was much milder in unchallenged lungs (Figure 4-19 E). The expression pattern of *Il-1β* therefore corresponds well with the previously observed neutrophil infiltration. Enhanced expression in pre-metastatic lungs was also detected for *Tnfα* and *Lcn2,* albeit not as consistently (Figure 4-19 F+L). For *Il-1α, Csf3* and *Spp1* no regulation of gene expression in a JUNB-dependent manner was detected (Figure 4-19 D, J+K). In the case of *Il-1α,* expression was even diminished in pre-metastatic compared to unchallenged lungs.

In conclusion, *Il-1β* and *Tnfα* display an expression pattern, which is dependent on JUNB and correlates very well with the numbers of neutrophils, both in EO771.LMB primary tumors as well as in pre-metastatic lungs. The fact that *Il-1β* and *Tnfα* could hardly be detected in EO771.LMB breast cancer cells, further supports the assumption that these factors are derived from the stroma. In addition, also classical neutrophil attracting chemokines, such as *Cxcl1, Cxcl2* and *Cxcl5* showed enhanced expression, which was, however, only observed in primary tumors but not in lungs.

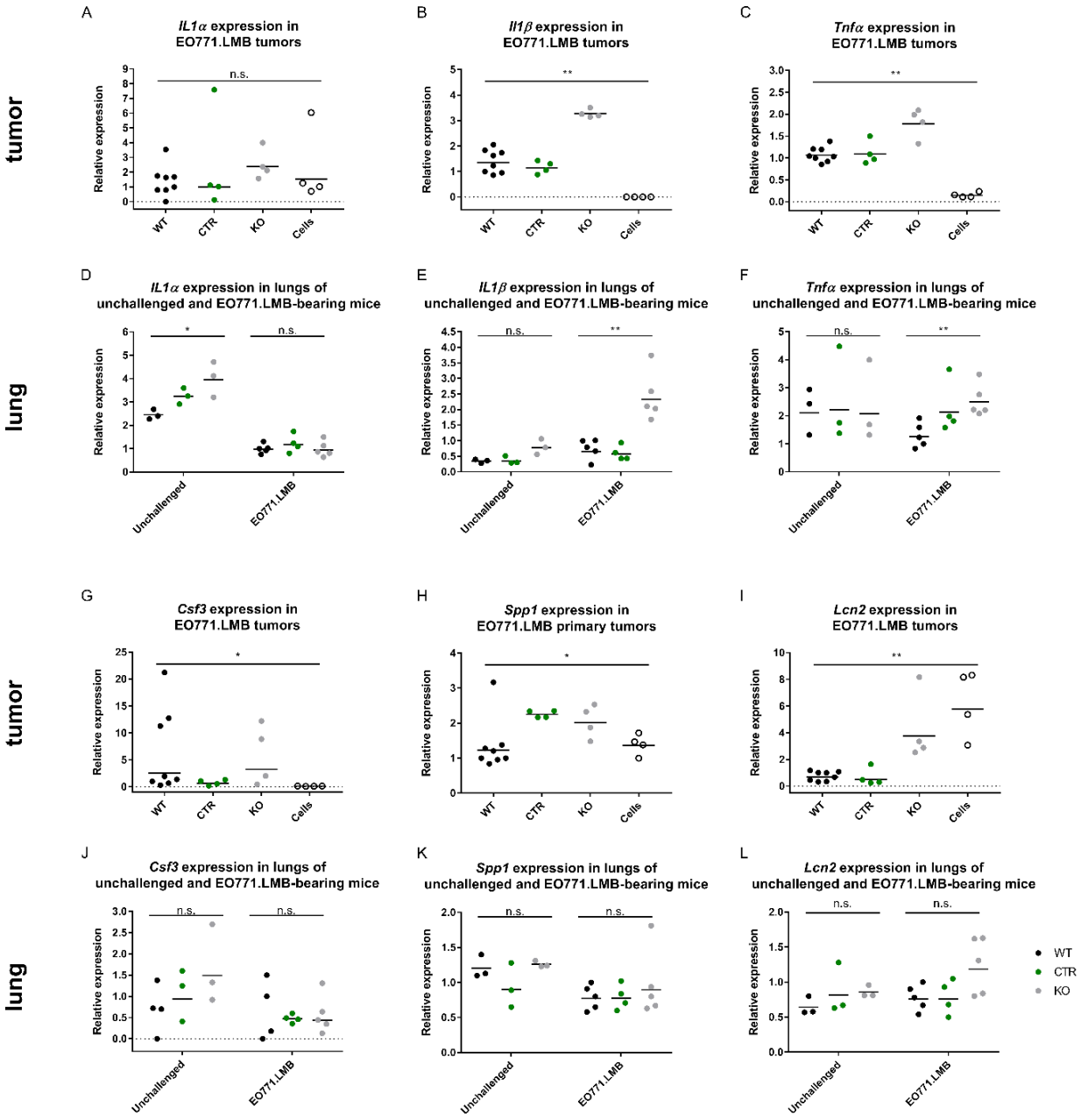

Figure 4-19: Stromal *Junb* ablation influences the expression of neutrophil-attracting factors.

Expression was quantified by qRT-PCT in the tumor bulk isolated from mice with stromal *Junb* deletion or respective controls, as well as in EO771.LMB cells in vitro: *Il-1α (A), Il-1β* (B), *TNFα* (C), *Csf3* (G), *Spp1* (H) and *Lcn2* (I). In parallel, these factors were also investigated in lungs isolated from unchallenged or tumor-bearing mice (D-F, J-L). Data are represented as geometric mean. Significance was assessed by Kruskal-Wallis test with P<0.05 as the limit of significance. *P≤0.05 and **P<0.01.

Taken together, these data provide a first clue that alterations in neutrophil-recruiting factors may indeed play a role in JUNB-dependent neutrophil infiltration and metastasis.

4.4.2. Functional assessment of neutrophils in JUNB-dependent metastasis

After identifying *Il-1β* and *TNFα* as potential key factors regulating neutrophil infiltration in the EO771.LMB primary tumors and pre-metastatic lungs, the cell type serving as their source, still had to be identified. Furthermore, a direct proof was missing, that indeed neutrophils facilitated metastasis to the lungs. Thus, in order to identify, whether JUNB loss in neutrophils was required for the observed metastatic phenotype, two approaches were followed: (I) bone marrow transplantations were performed to determine whether JUNB in the stroma or in cells derived from the hematopoietic system was essential, and (II) neutrophils were depleted pharmacologically using an antibody specifically targeting neutrophils.

4.4.2.1. Identification of cell type: bone marrow transplantations

In the first approach, mice with stromal ablation of *Junb* were subjected to bone marrow transplantations in order to decipher, whether the enhanced metastatic burden was due to JUNB loss in cells derived from the hematopoietic compartment, such as immune cells, or from the stroma, for example endothelial cells or fibroblasts. With this experiment it should further be clarified, whether neutrophil accumulation upon *Junb* KO was due to a neutrophil-intrinsic mechanism or whether secretion of neutrophil-recruiting factors by stromal cells was decisive.

For bone marrow transplantations, WT or *Junb* KO mice were lethally irradiated and subsequently reconstituted with bone marrow isolated either from WT or KO mice. This experimental setup resulted in a total of four groups: WT donor-WT recipient (WT>WT), KO donor-WT recipient (KO>WT), WT donor-KO recipient (WT>KO) and KO donor-KO recipient (KO>KO). In order to be able to differentiate between bone marrow donor and recipient, mice expressing different isoforms of CD45, which can be differentiated by flow cytometric analysis, were used: CD45.1 or CD45.2. *Junb* KO mice are congenic C57BL/6N and consequently express the alloantigen CD45.2. Depending on the experimental group, respective WT mice were chosen being either positive for CD45.1 or CD45.2. As *Junb* KO mice, had not previously been backcrossed to a CD45.1 positive genetic background, donor and recipient could not be differentiated in the KO donor-KO recipient group. As both donor and recipient mice did, however, carry the same stromal deletion for *Junb*, this issue was disregarded. Successful reconstitution of the bone marrow was confirmed by flow cytometric analysis of whole blood using antibodies specifically labelling CD45.1 or CD45.2. After confirmation of successful transplantation, the spontaneous metastasis assay with the EO771.LMB cells was performed immediately after. The complete experimental setup is presented schematically in Figure 4-20.

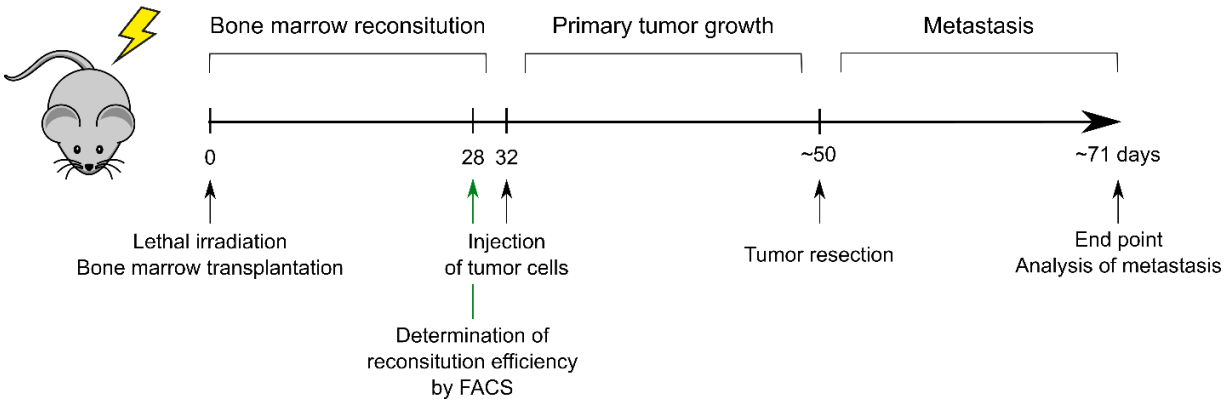

Figure 4-20: Schematic representation of the experimental setup for the bone marrow transplantation experiments.

A spontaneous metastasis assay was performed subsequently to whole body irradiation and bone marrow reconstitution.

The dose for lethal irradiation is of extraordinary importance for a successful bone marrow transplantation. If mice are irradiated sublethally, not all hematopoietic stem cells are eradicated leading to low reconstitution efficiencies. Furthermore, sublethal irradiation poses the risk of transplant rejection. Too high doses on the other side can lead to radiation-induced sickness and mortality [308]. C57BL/6 mice naturally tolerate higher doses of irradiation than other commonly used mouse strains [309, 310]. The *Junb* KO mice used in this metastasis project have, however, never been subjected to irradiation. Due to the smaller size and the generally more fragile appearance, there was considerable doubt whether KO mice could tolerate the same doses as WT C57BL/6 mice. In order to exclude, that mice suffer from irradiation-induced morbidity, they were regularly checked for abnormal behavior and body weight. In the first days after bone marrow transplantation, all mice lost weight (Figure 4-21 A). Weight loss was slightly stronger in KO animals irrespective of whether they had been reconstituted with WT or KO bone marrow but none of the mice exceeded weight loss of 20%. Approximately one week after bone marrow transplantation, mice had recovered and regained their starting body weight. Thereafter, all experimental mice, independent of genotype, put on weight similarly as untreated mice. In conclusion, WT and KO mice tolerated the same dose of irradiation well and no morbidity was observed.

Reconstitution efficiency was determined by flow cytometric analysis of blood four weeks after bone marrow transplantation. Gating on forward (FSC) versus side scatter (SSC) revealed the typical separation of leukocyte subpopulations: granulocytes, monocytes and lymphocytes, indicating that these populations are already re-established after bone marrow transplantation. (Figure 4-21 C). Subsequent to exclusion of cell doublets and dead cells, reconstitution efficiency was determined by gating on CD45.1+ versus CD45.2+ cells (Figure 4-21 D). Analysis of all mice, revealed a high reconstitution efficiency above 80%, which was on average even higher for irradiated KO mice (Figure 4-21 B). Reconstitution efficiency was again measured at the end point of the experiment. Efficiency further increased to above 87% for all groups. Mice which did not show these high efficiencies were excluded from subsequent analyses.

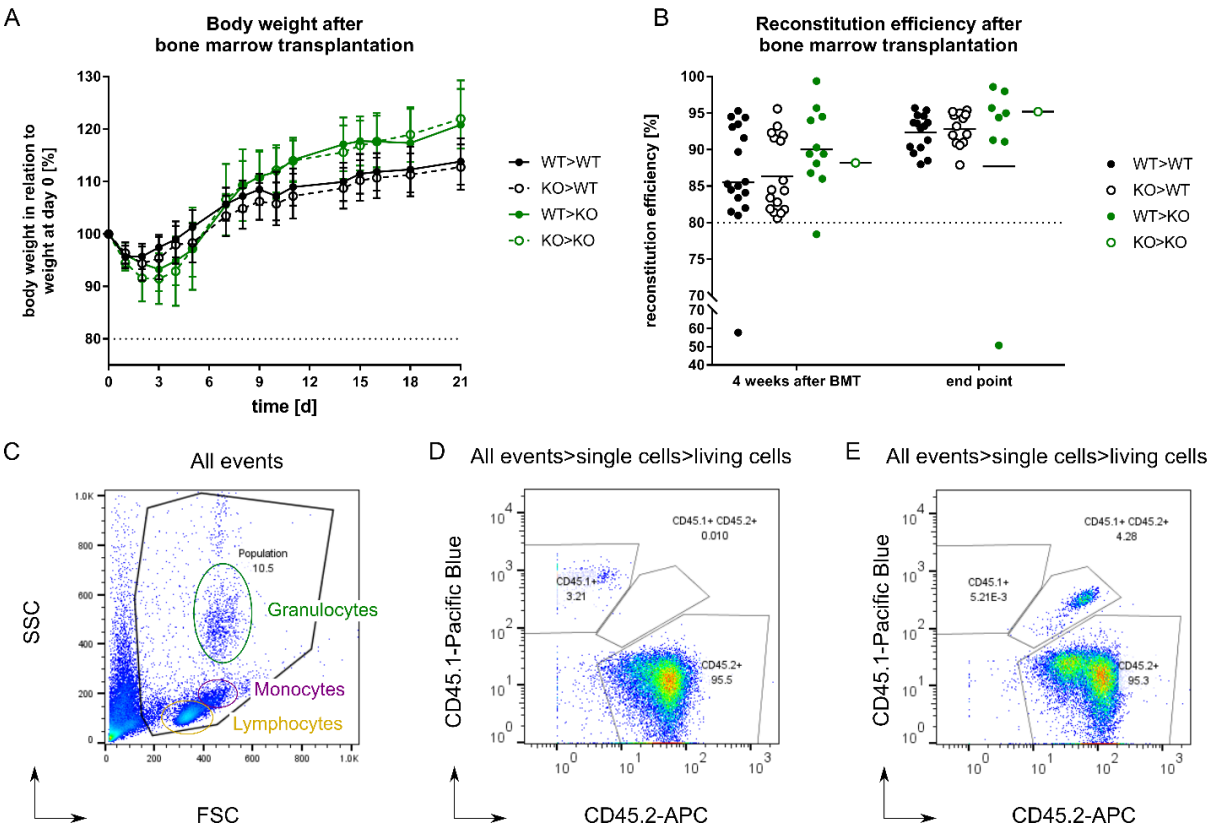

Figure 4-21: Body weight curves and reconstitution efficiency after bone marrow transplantation.

Junb KO mice tolerated lethal doses of irradiation similarly well as WT mice and showed comparable reconstitution efficiencies after bone marrow transplantation. All groups of mice showed an initial weight loss after bone marrow transplantation but quickly recovered thereafter (A). Bone marrow transplantation was efficient as assessed by flow cytometric analysis in all groups after four weeks and was even higher at end point (B). Flow cytometry revealed distinct leukocyte subpopulations by gating of forward (FSC) versus side scatter (SSC): granulocytes (green), monocytes (purple), lymphocytes (yellow) (C). Gating strategy for the assessment of the reconstitution efficiency: CD45.1 versus CD45.2, a representative plot for a KO>WT mouse is shown (D). CD45.1+CD45.2+ double positive cell population in KO>KO mouse (E).

Surprisingly though, for some KO mice or WT mice reconstituted with KO bone marrow, a CD45.1+ CD45.2+ double positive population could be observed (Figure 4-21 E). In depth investigation on the origin of these KO mice revealed, that originally FVB/N mice had been used for the generation of the *Col1α2*-Cre mice [234]. FVB/N mice typically express the CD45.1 alloantigen. CD45.1 expression, thus, remained despite numerous generations of backcrossing. The advantage of this double positivity was, however, that the reconstitution efficiency could also be analyzed for one KO>KO mouse. Efficiency was thereby at a comparable level as for WT>KO mice (Figure 4-21 B).

After successful establishment of these bone marrow transplantation experiments, the spontaneous metastasis assay was conducted subsequently. The EO771.LMB cell line was used, because the difference in distant metastasis upon stromal *Junb* deletion was only apparent with this cell line. In agreement with previous experiments, EO771.LMB cells were injected orthotopically into the mammary fat pad on day 32 after bone marrow reconstitution.

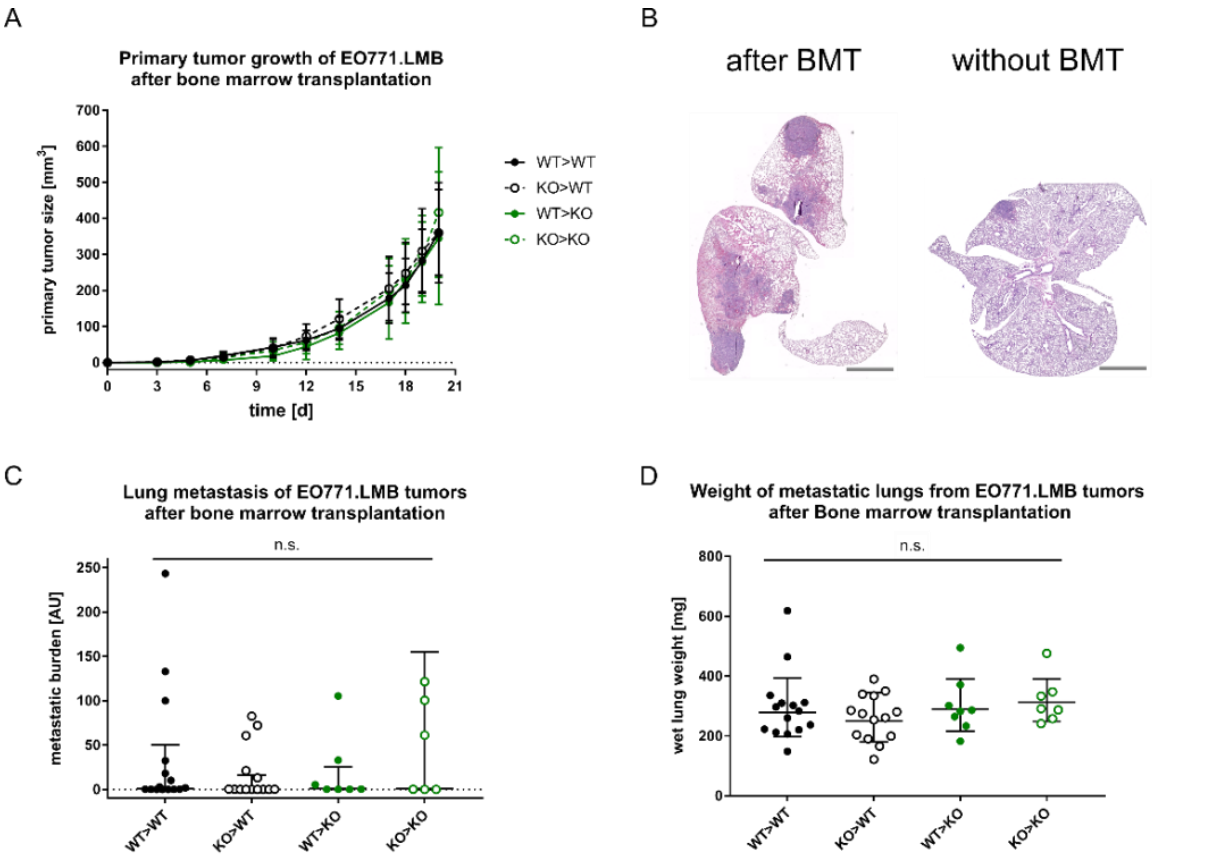

Figure 4-22: Primary tumor growth and distant metastasis is unaffected by JUNB deletion in either the hematopoietic or stromal compartment.

(A) Primary tumor growth of EO771.LMB tumors was similar in all experimental groups. Lung metastasis was generally stronger in mice that had undergone bone marrow transplantations (BMT) in comparison to mice that had not. Representative images of hematoxylin eosin-stained lung sections of a WT>WT mouse (left) and a CTR mouse (right) is shown (B). Lung metastasis was similar in all experimental groups as determined by quantification of the *mCherry* reporter in genomic DNA by qRT-PCR (C) and by measuring the wet lung weight at end point (D). Significance was assessed by Kruskal-Wallis test (C) or One-way ANOVA (D) with $P<0.05$ as the limit of significance. *$P\leq0.05$ and **$P<0.01$.

Primary tumor growth was followed over time and was indistinguishable between the different experimental groups (Figure 4-22 A). In comparison to growth curves without prior bone marrow transplantations, tumor growth was, however, slightly delayed (Figure 4-2 C). A volume of roughly 500 mm^3 was only reached at day 20-23 in contrast to day 17-20 in the initial experiments. After primary tumor removal at 500 mm^3, mice were allowed to recover for 21 days until they were euthanized and lungs were investigated for metastasis. Already upon macroscopic examination, lung metastasis seemed stronger in all experimental groups in comparison to metastatic burden of EO771.LMB tumors in mice which had not undergone bone marrow transplantations (BMT) (Figure 4-22 B). The impression that lung metastasis was also not different between the experimental groups was further confirmed by quantification of the *mCherry* reporter by qRT-PCR on DNA level and by determination of the lung weights at end point (Figure 4-22 C+D). Considering that *Junb* is lost in the same cellular compartments in KO mice without BMT as well as in KO>KO mice after BMT, metastatic load was expected to be similar. Indeed, lung metastasis in KO>KO mice did resemble the pattern observed for KO mice: some animals did not show any nodules, whereas others showed robust metastasis (Figure 4-22 C). Correspondingly, WT>WT mice should behave similar in respect to metastasis

as the WT and CTR group of previous experiments. In contrast to initial experiments, where metastasis was very weak in both control groups, after BMT, WT>WT mice showed very prominent lung metastasis (Figure 4-22 B+C).

Taken together, lung metastasis was generally stronger after BMT than had been observed in initial experiments with EO771.LMB cells. Against expectations, lung metastasis was similar between all experimental groups Therefore, these data do not justify a conclusion as of whether JUNB loss in the hematopoietic or stromal compartment is essential for distant lung metastasis.

Apart from metastasis, this experiment also had the aim to examine, whether enhanced neutrophil recruitment in *Junb* KO mice was due to a neutrophil intrinsic mechanism or whether it was potentially mediated by another stromal cell type. For this purpose, EO771.LMB primary tumors isolated from experimental mice after they had undergone BMT were analyzed for *Ly6g* expression. In contrast to tumors isolated in the previous experiments without BMT, the level of *Ly6g* expression was comparable in all groups (Figure 4-23 A). Moreover, the previously observed strong upregulation of *Ly6g* was not detected in KO mice transplanted with KO bone marrow. On the contrary, expression levels were more similar to WT and CTR mice. This implies that neutrophil infiltration into these tumors was independent from JUNB, irrespective of its cellular source. In order to assess, whether only neutrophil infiltration was compromised or also systemic levels were impacted, circulating neutrophils were investigated. Flow cytometric analysis of whole blood determined a substantially higher number of neutrophils, defined as CD11b+Ly6G+Ly6C^{int}, already present in unchallenged *Junb* KO mice compared to WT (Figure 4-23 B). In mice which had undergone BMT, a significant difference in circulating neutrophils was detected at end point (Figure 4-23 B). Mice with stromal loss of *Junb* showed trice as high levels of neutrophils than mice expressing *Junb* in the stroma. This was irrespective of whether mice had received JUNB WT or KO bone marrow during transplantation. These results were further supported by measuring absolute neutrophil counts in whole blood using the Hemavet 950FS (Drew Scientific, USA). Automated cell counting could not confirm the higher neutrophil count in KO mice under non-challenged basal conditions, but significantly different levels were noted already four weeks after BMT which were further enhanced at end point (Figure 4-23 D). At end point, when metastases had been observed, considerable more neutrophils were detected than at the beginning of the spontaneous metastasis assay (4 weeks after BMT) in all experimental groups. This increase was even more pronounced in mice lacking JUNB in the stroma, being in agreement with the data obtained by flow cytometry.

As this increase in neutrophil count did, however, not completely correspond to enhanced metastatic burden in these animals, I expanded my investigation to other cell types. Monocytes, as assessed by *Ly6c* expression, were enhanced in pre-metastatic lungs and EO771.LMB primary tumors derived from JUNB KO animals (Figure 4-12 G+H). Furthermore, monocytes have repeatedly been associated with extravasation and metastatic seeding [311-313]. Quantification of circulating monocyte levels, classified as CD11b+Ly6G-Ly6C^{hi}, by flow cytometry, revealed a considerable higher number in non-tumor bearing KO mice than in WT (Figure 4-23 C). At metastatic end point, monocyte levels were increased on average by 60% in mice with stromal loss of *Junb*, which was not as strongly as neutrophil levels. No significant difference between the different experimental groups was observed. These findings were supported by absolute cell counting. Although more monocytes were detected at end point compared to basal levels or after BMT, absolute monocyte counts were independent of JUNB expression (Figure 4-23 E).

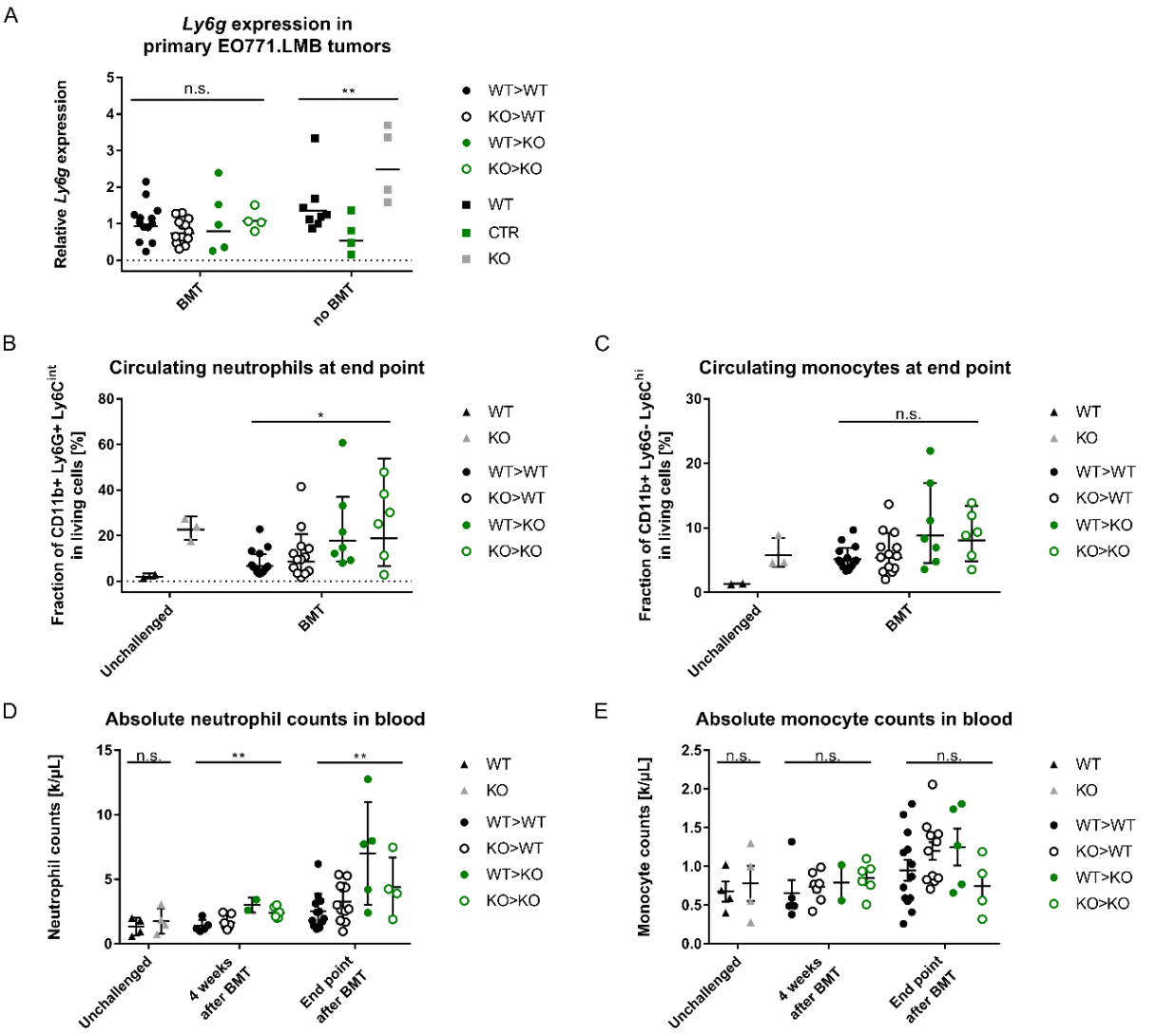

Figure 4-23: Neutrophil levels in mice that had undergone bone marrow transplantations.

Neutrophil levels were quantified by expression analysis for *Ly6g* in EO771.LMB primary tumors isolated from different experimental groups (A). Levels of circulating CD11b+Ly6G+Ly6C^{int} neutrophils were altered depending on JUNB expression as assessed by flow cytometry (B), which was supported by automated cell counting (D). Circulating CD11b+Ly6G-Ly6c^{hi} monocytes were unaffected by JUNB loss in either cellular compartment as determined by flow cytometry (C) and absolute cell counting (E). Significance was assessed by Kruskal-Wallis test (A, B+C) or One-way ANOVA (D+E) with $P<0.05$ as the limit of significance. Significance was tested by unpaired t-test for unchallenged mice (D+E). *$P\leq0.05$, **$P<0.01$.

In conclusion, these data indicate, that in particular circulating neutrophils and not monocytes are increased in mice with stromal *Junb* deletion. This argues for an indirect mechanism whereby neutrophil recruitment is mediated by another stromal cell type rather than a neutrophil intrinsic mechanism. Yet, these enhanced levels of circulating neutrophils did not translate into an increased infiltration into primary EO771.LMB tumors potentially pointing towards an adverse effect induced by whole body irradiation. This is further substantiated by the strikingly enhanced lung metastasis in mice which had undergone BMT in contrast to mice which had not been irradiated.

4.4.2.2. Pharmacological neutrophil depletion

In the second approach, neutrophils were depleted pharmacologically in order to determine whether neutrophil accumulation is functionally linked to the enhanced metastatic burden in KO animals.

For this purpose, a protocol was followed as essentially described by Coffelt et al. [91]. Neutrophils were depleted during the initial phase of the spontaneous metastasis assay with the EO771.LMB cell line, which is schematically represented in the figure below (Figure 4-24).

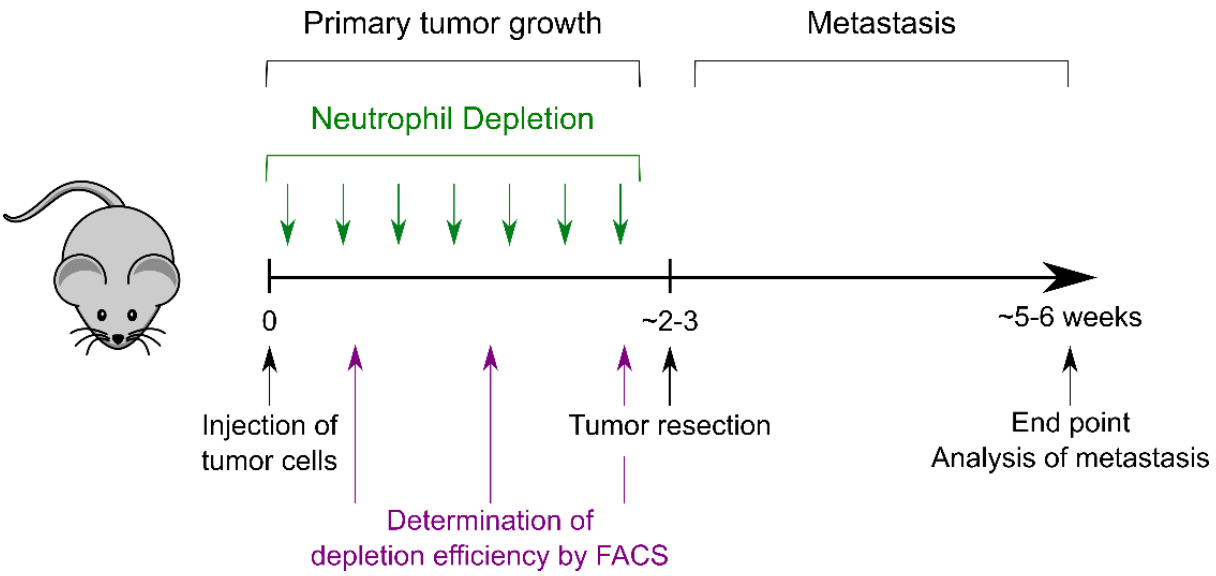

Figure 4-24: Schematic representation of the experimental setup for the neutrophil depletion experiments.

Neutrophils were depleted pharmacologically by repeated injections of anti-Ly6G antibody 1A8 during the initial phase of the spontaneous metastasis assay.

Neutrophil depletion was achieved by repeated i.p. injections of the neutrophil-specific antibody anti-Ly6G (clone 1A8). The control group received the respective isotype control anti-trinitrophenol (clone 2A3) at the same time intervals, injection volumes and dose. Depletion was initiated at day 2 after tumor cell injection when the primary tumor was already palpable. Subsequently, antibody treatments were repeated every 2-3 days for a total of seven injections until the primary tumor had reached a volume of 500 mm^3. Then, the primary tumor was excised and mice were sacrificed for the analysis of distant metastasis 21 days after. In order to determine the efficiency of the neutrophil depletion, circulating neutrophil levels were assessed in whole blood. For this reason, blood was drawn from the tail vein once a week starting the day after the first antibody injection. Whole blood was analyzed by multi-color flow cytometry. In parallel, automatic cell counting was performed in order to determine absolute neutrophil counts and to confirm data obtained by flow cytometry.

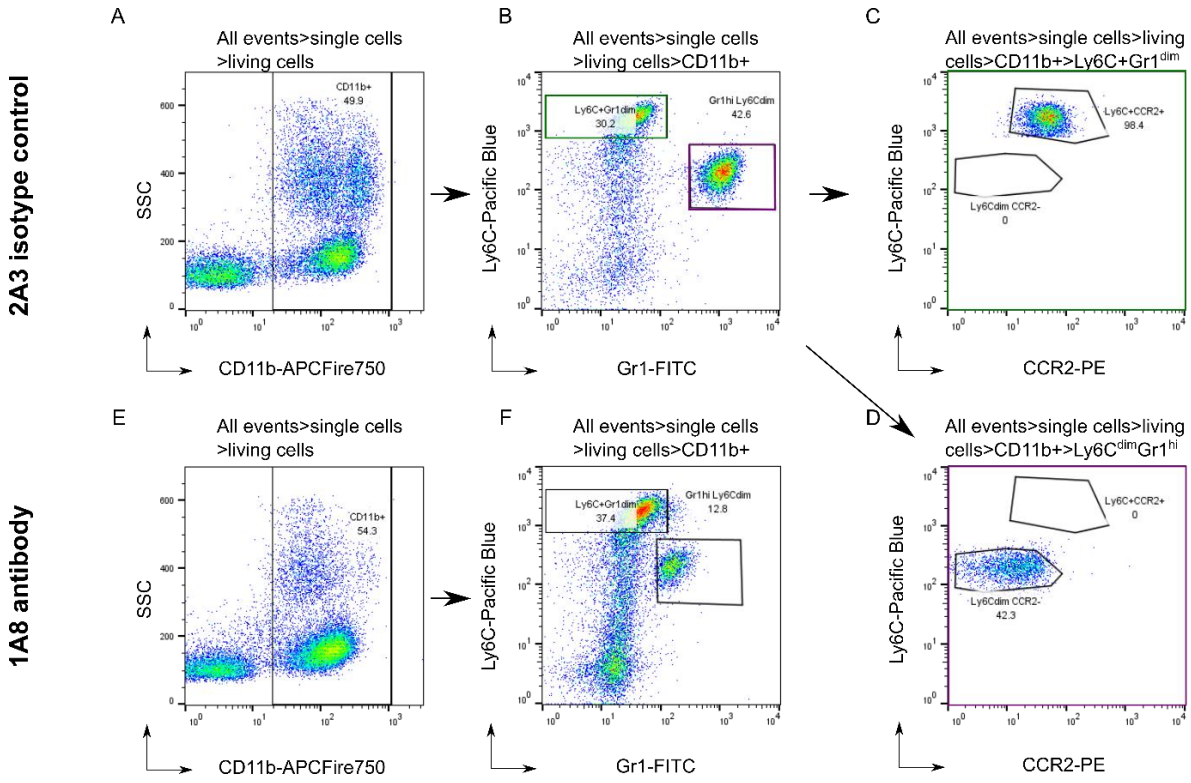

Figure 4-25: Gating strategy for flow cytometric analysis accurately identified myeloid cells, monocytes and neutrophils in whole blood.

Whole blood is subjected to erythrocyte lysis and subsequently stained with a multi-color panel, in order to identify all CD11b+ myeloid cells (A, E) and Gr1^{hi}Ly6C^{dim} neutrophils and Ly6C+Gr1^{dim} monocytes (B, F), as shown for a representative example of mice treated with 2A3 isotype control. Correct gating on monocytes was confirmed by positive staining for CCR2 (C). Neutrophils were CCR2- (D). Upon treatment with depleting antibody anti Ly6G (1A8) no difference was observed in total CD11b+ myeloid cells (E) and Ly6C+Gr1^{dim} monocytes but Gr1^{hi}Ly6C^{dim} neutrophils were shifted left (F).

For flow cytometric analysis, all myeloid cells were identified by CD11b staining after erythrocyte lysis and exclusion of doublets and dead cells (Figure 4-25 A). For identification of monocytes and neutrophils, a different strategy was applied than for the analysis of the bone marrow experiments. As anti-Ly6G 1A8 was used for depletion *in vivo*, the same antibody clone could not be used for analysis *ex vivo* due to potential false-negative results [314]. Analysis was therefore performed with anti-Gr1 (clone RB6-8C5), which recognizes both Ly6C and Ly6G. In order to differentiate between monocytes and neutrophils, a co-staining with Ly6C was, thus, required. Gating on CD11b+ myeloid cells revealed two distinct populations: Gr1^{hi}Ly6C^{dim} neutrophils and Ly6C+Gr1^{dim} monocytes (Figure 4-25 B). Accurate identification was subsequently confirmed by analysis of CCR2 expression. Thereby, monocytes stained positive for CCR2, whereas neutrophils were negative for CCR2, verifying the applied gating strategy (Figure 4-25 C+D). When blood was isolated from mice injected with isotype control (2A3), neutrophils stained highly positive for Gr1 (Figure 4-25 B). Upon treatment with depleting antibody 1A8, a left shift of the neutrophil population was observed (Figure 4-25 F). As binding of antibody 1A8 has, however, also been reported to interfere with RB6-8C5 binding, this implies that neutrophils indeed bound anti-Ly6G 1A8. In order to account for this shift, the neutrophil gate was adjusted for mice treated with anti-Ly6G.

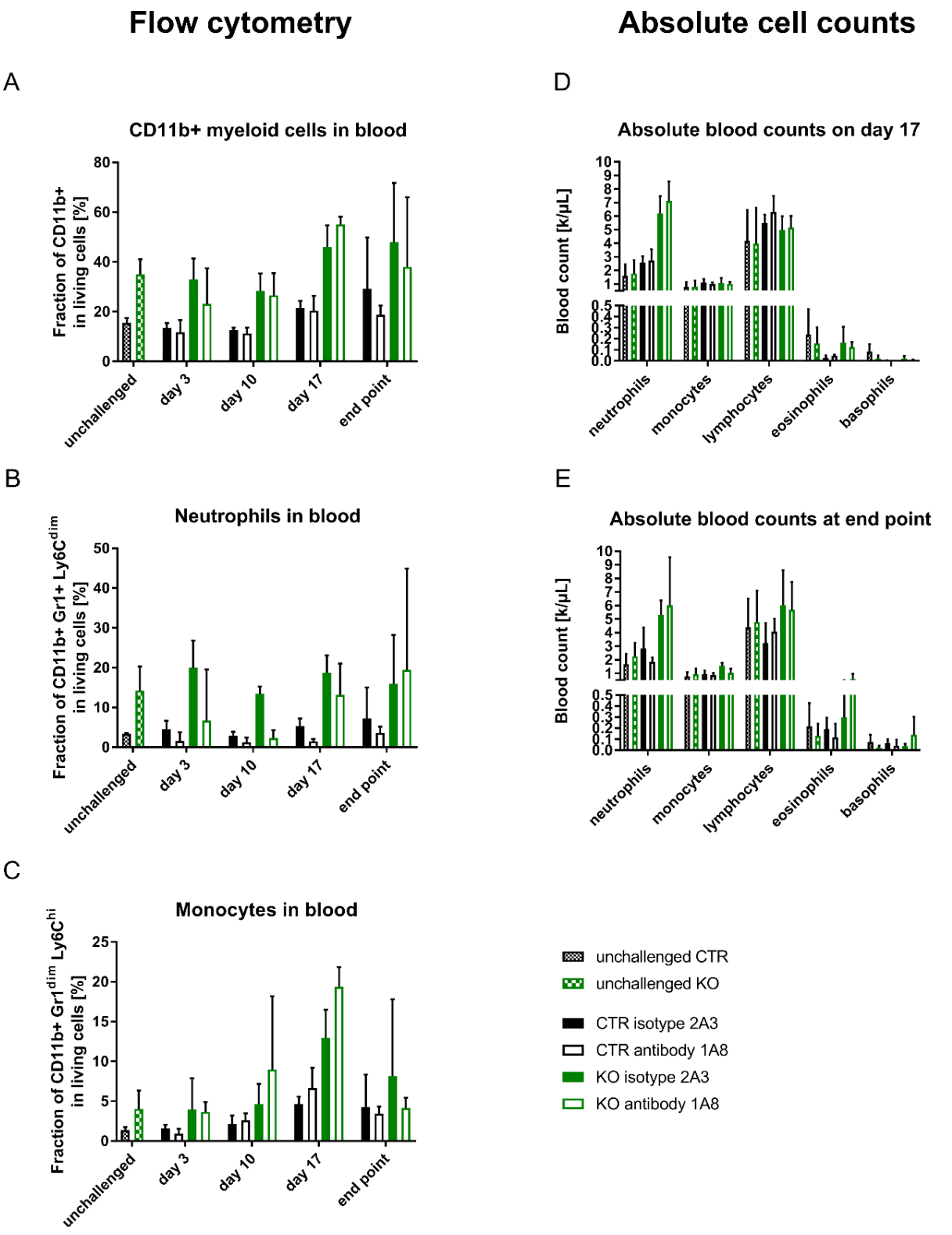

Figure 4-26: Quantification of immune cell populations after treatment with neutrophil depleting antibody 1A8 or respective isotype control.

Levels of CD11b+ myeloid cells were not affected by 1A8 treatment (A). Neutrophils were specifically depleted at day 10 after tumor cell injection but no differences were observed thereafter (B). Monocytes were not directly targeted by anti-Ly6G but levels were increased after treatment both in CTR and KO mice (C). Absolute cell counting confirmed that circulating neutrophil levels are higher in KO mice than in CTRs but no difference was observed upon neutrophil depletion both at day 17 and at end point in any of the investigated cell types (D+E). For quantification of flow cytometry at least 30000 events were analyzed.

In order to determine, whether the neutrophil population was not only shifted but also reduced in numbers, flow cytometric data were analyzed in more detail. Quantification revealed, that already unchallenged mice with stromal *Junb* deletion did have more than 2-fold higher numbers of circulating CD11b+ myeloid cells, which increased even more during tumor progression (Figure 4-26 A). Despite KO mice having higher levels, no difference was observed upon neutrophil depletion, neither in KO nor in CTR mice. By gating specifically on the neutrophil population, 4-fold more neutrophils were observed in KO compared to CTR, when mice were unchallenged (Figure 4-26 B). This difference furthermore persisted with progressing disease. In addition, flow cytometric analysis revealed a striking paucity of neutrophils in mice that had received anti-Ly6G antibody injections. On day 10 after tumor injection, neutrophils were depleted by 80%, whereas on day 17 depletion was already not as efficient anymore reaching only 25%. Eventually, levels were indistinguishable again at end point. Despite efficient neutrophil depletion on day 10, no reduction of circulating monocyte levels was determined indicating that anti-Ly6G indeed specifically targets neutrophils (Figure 4-26 C). On the contrary, monocyte levels were even increased by almost 50% upon neutrophil depletion both in CTR and KO mice, potentially revealing a compensatory effect.

Due to the aforementioned binding competition between antibody clones 1A8 and RB6-5C8, neutrophil depletion efficiency was not only assessed by flow cytometry but also by automated absolute cell counting. Absolute cell counts on day 17 showed that neutrophils were specifically enhanced 2.4-fold in *Junb* KO animals compared to CTR but no difference was observed between mice injected with depleting antibody versus isotype control (Figure 4-26 D). Concomitantly, no changes were apparent in any other cell population, such as monocytes, lymphocytes, eosinophils and basophils, confirming the specificity of anti-Ly6G antibody. At end point, blood counts resembled the levels on day 17. Neutrophil levels were still almost 2-fold higher upon JUNB KO but no change was observed upon treatment with anti-Ly6G (Figure 4-26 E).

Taken together, these data show, that anti-Ly6G antibody indeed specifically targets neutrophils and also stays bound as indicated by the reduction of mean fluorescence intensity for Gr1 observed by flow cytometry. Absolute cell counting did reveal, though, that these neutrophils are still present in the circulation irrespective of whether anti-Ly6G has bound or not. In conclusion, treatment with neutrophil depleting antibody 1A8 does not actually deplete neutrophils but may interfere with recruitment out of the circulation into the tissues.

Hence, in order to assure that neutrophils are indeed absent in the tissue, their presence after anti-Ly6G treatment was evaluated by gene expression analysis and immunofluorescent staining in EO771.LMB primary tumor and pre-metastatic lungs. For this purpose, mice were treated with anti-Ly6G antibody or isotype control as previously indicated (Figure 4-24). In order to enable the assessment of primary tumors and lungs immediately after antibody treatment, mice were sacrificed at the time point of primary tumor resection when the tumor had reached a volume of approximately 500 mm^3. Subsequent examination of primary tumors and pre-metastatic lungs by gene expression analysis reproduced data obtained in earlier experiments. A significant increase of *Ptprc, Itgam* and *Ly6g* expression was revealed in KO mice compared to CTR (Figure 4-27 A-F). Further resembling previous data, the difference in *Ly6g* levels between KO and CTR were more striking in pre-metastatic lungs (almost 5-fold) than in primary tumors, where expression was enhanced by 1.8-fold (Figure 4-27 E+F). Considering the inefficient neutrophil depletion in the circulation, it was moreover not surprising, that neutrophils were not impaired from entering neither EO771.LMB primary tumors nor pre-metastatic lungs upon anti-Ly6G treatment (Figure 4-27 E-G). Despite

repeated injections of neutrophil-specific antibody 1A8, neutrophils were still present at similar levels as in control-injected mice as determined by *Ly6g* gene expression and immunohistochemical staining for LY6B.2. Taken together, neutrophils were not efficiently ablated neither in the circulation nor in examined peripheral tissues despite continuous treatment with anti-Ly6G antibody 1A8.

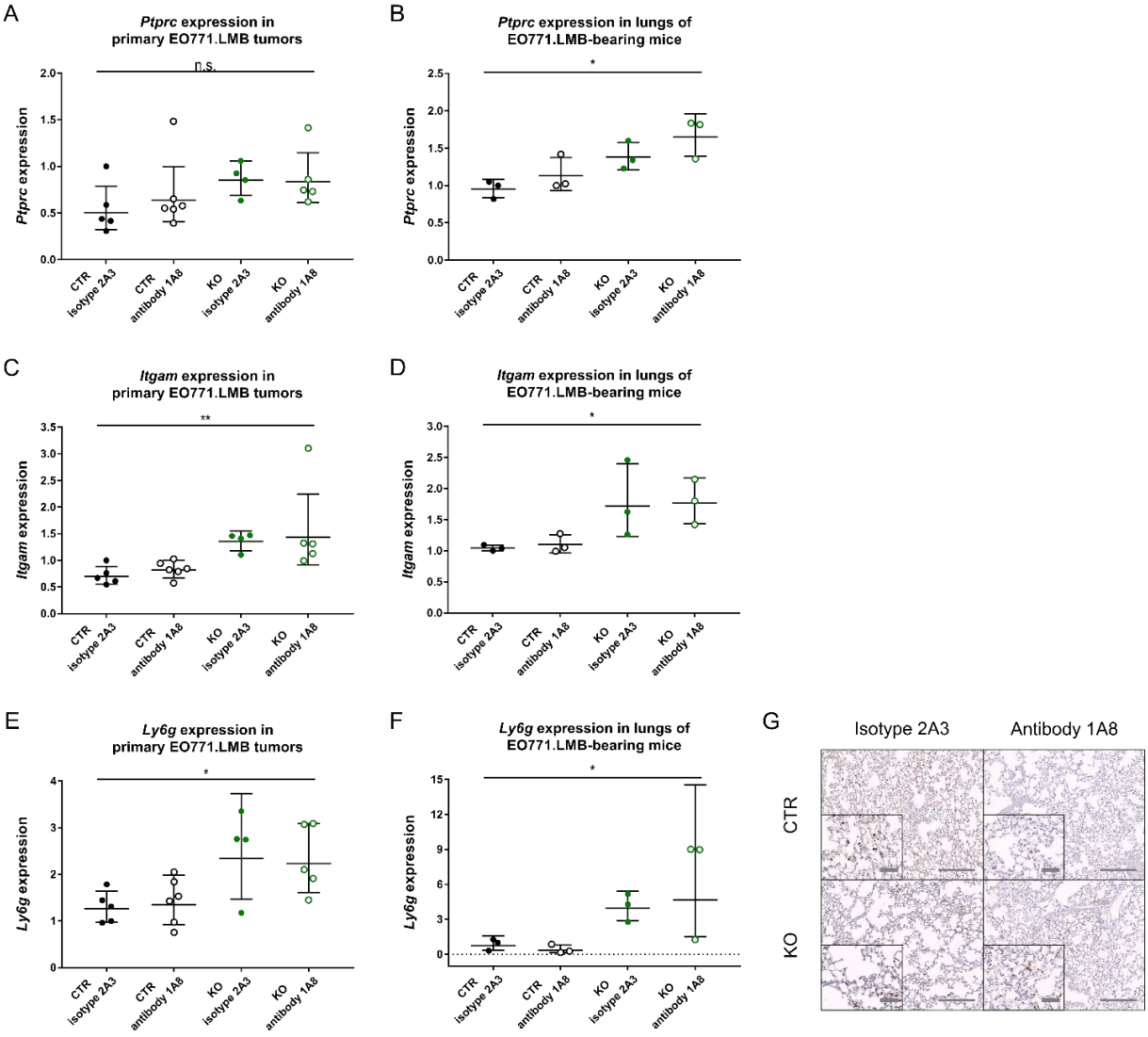

Figure 4-27: Treatment with neutrophil-specific antibody anti-Ly6G 1A8 does not impair neutrophil recruitment.

Gene expression analysis revealed an increase in *Ptprc* (A), *Itgam* (C) and *Ly6g* (E) expression in primary EO771.LMB tumors and pre-metastatic lungs (B, D, F) derived from KO mice compared to CTRs. No reduction in neutrophil infiltration was apparent upon anti-Ly6G treatment as assessed by gene expression analysis for *Ly6g* in EO771.LMB primary tumors (E) and pre-metastatic lungs (F) as well as by immunohistochemical staining for LY6B.2 in pre-metastatic lungs. Representative images are displayed in (G) with scale bar 200 µm, scale bar of inset 50 µm. Data are represented as geometric mean±geometric SD. Significance was assessed by Kruskal-Wallis test with P≤0.05 as the limit of significance. *P≤0.05 and **P<0.01.

In line with previous findings, primary tumor growth was not affected neither by stromal loss of *Junb* nor by treatment with anti-Ly6G antibody (Figure 4-28 A). Antibody injections did also not alter the kinetics of primary tumor growth, as sizes of approximately 500 mm^3 were reached also between days 17-20, just alike the initial experiments (Figure 4-2 C). Reproducing the original phenotype, lung metastatic burden as determined by quantification of the *mCherry* sequence in genomic DNA by qRT-PCR was enhanced in *Junb* KO mice compared to the CTR (Figure 4-28 B). Surprisingly, lung metastasis was unchanged upon injection of anti-LY6G, both in CTR and KO mice (Figure 4-28 B+C).

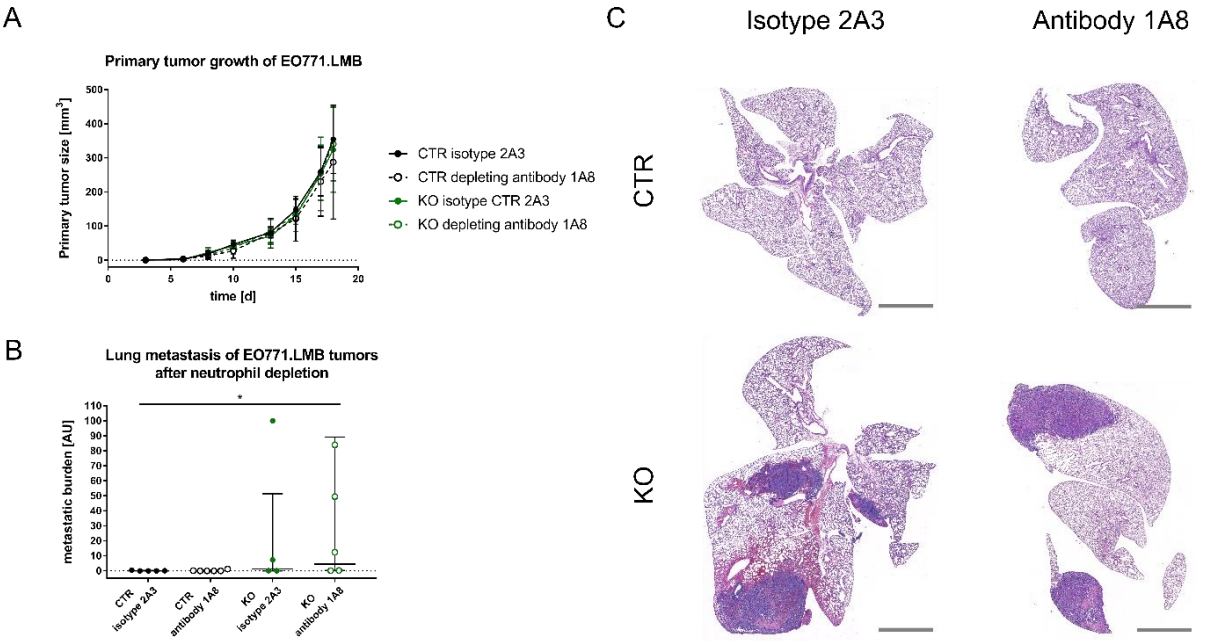

Figure 4-28: Primary tumor growth and lung metastasis of EO771.LMB tumors were not affected by anti-Ly6G treatment.

Primary tumor growth was not altered neither by JUNB loss nor by neutrophil depletion with anti-Ly6G antibody injection (A). Metastatic burden in the lungs as assessed by quantification of the *mCherry* reporter in genomic DNA by qRT-PCR was enhanced upon stromal *Junb* deletion but not different between mice which had received treatment with anti-Ly6G or isotype control (B). Representative pictures of metastasis lungs stained with hematoxylin and eosin (C). Scale bar 2000 µm. Data are represented as geometric mean±geometric SD. Significance was assessed by Kruskal-Wallis test with $P<0.05$ as limit of significance. *$P \leq 0.05$. n=4-6.

In conclusion, pharmacological neutrophil depletion by injection with anti-Ly6G antibody was evidently insufficient, so that neutrophil accumulation in primary tumors and pre-conditioned lungs induced by JUNB loss could not be impeded. Consequently, neutrophil accumulation could functionally not be linked to the enhanced metastatic burden in *Junb* KO mice.

5 DISCUSSION

5. DISCUSSION

Multiple studies have revealed that JUNB can function as an oncogene, albeit initially it has been described as a tumor suppressor. Data on the association of JUNB with invasion and metastasis are limited and largely conflicting so far. In the only functional study, loss of JUNB in head and neck squamous cell carcinoma cell lines was shown to impede distant metastasis in an experimental assay in nude mice [226]. Yet, this study had multiple limitations, such as the artificial introduction of high numbers of CTCs into the circulation and the use of a xenotransplantation model. Xenotransplantations completely neglect the complex interplay between tumor cells and the syngeneic microenvironment, including the immune system.

As JUNB had furthermore been reported to be an essential transcriptional regulator in various cell types of the tumor microenvironment, the goal of this study was to clarify functionally, whether and in which way stromal-derived JUNB influences metastasis. For this purpose, JUNB was ablated genetically in the stroma of mice and distant metastasis was evaluated using different spontaneous metastasis models, thereby enabling the evaluation of all steps of the metastatic cascade.

In this dissertation, I clearly show for the first time, that JUNB indeed influences metastasis. Distant metastasis to the lungs was significantly increased upon stromal deletion of *Junb* compared to *Junb*$^{+/+}$ control mice in the EO771.LMB breast cancer model. This JUNB-dependent metastatic phenotype was, however, not observed in the LL/2-Luc model. In the B16F10 model, no clear conclusion could be drawn due to the inefficiency of spontaneous metastasis. In order to determine the step in the metastatic cascade influenced by JUNB loss, an experimental metastasis assay using EO771.LMB cells was conducted. No significant difference in metastatic burden in the lungs could be determined in *Junb* KO mice compared to CTR animals indicating that JUNB loss does not promote tumor cell extravasation and metastatic colonization. Subsequent analyses of major components of the microenvironment revealed no alterations in vessel as well as fibroblast density and vascular permeability but identified a prominent accumulation of neutrophils in EO771.LMB primary tumors and even more strikingly in pre-metastatic lungs derived from *Junb* KO mice. Concomitantly, neutrophil recruiting factors, such as *Il-1β*, *Tnfα, Cxcl1, Cxcl2* and *Cxcl5* were upregulated in EO771.LMB primary tumors and pre-metastatic lungs upon stromal deletion of *Junb*. In order to determine whether JUNB loss in neutrophils is required for the increase in metastasis, two complementary approaches were followed: (I) mice were subjected to bone marrow transplantations and (II) neutrophils were depleted pharmacologically. Bone marrow transplantation experiments showed no difference in distant metastasis but revealed elevated levels of circulating neutrophils in mice with stromal *Junb* KO irrespective of whether they had been transplanted with WT or KO bone marrow. These findings imply that neutrophil recruitment is mediated by another stromal cell type rather than a neutrophil intrinsic mechanism. In order to directly link neutrophil infiltration to increased distant metastasis, neutrophils were depleted pharmacologically using the neutrophil-specific antibody anti-LY6G 1A8. Despite initially highly efficient depletion of circulating neutrophils, neutrophil recruitment to the pre-metastatic lungs was indifferent upon injection of anti-LY6G compared to the respective isotype control. Similarly, distant metastasis was unaffected by treatment with anti-LY6G. Yet, the neutrophil depletion experiment does confirm the original data and clearly shows that loss of stromal JUNB promotes distant metastasis to the lungs.

5.1. B16F10 cells do metastasize very inefficiently in the spontaneous metastasis model

In contrast to my expectations, metastasis was extremely inefficient in the B16F10 melanoma model after primary tumor resection, so that the role of JUNB in metastasis could not be assessed in this model.

Although the B16F10 cell line is predominantly used to study metastasis in the experimental metastasis assay after tail vein injection [251-253], also spontaneous metastasis has been reported [254-257]. In these spontaneous metastasis assays, the primary tumor had, however, been allowed to either reach large sizes or it had been implanted at anatomical locations restraining its size. Due to these space limitations, for example in the ear [256, 315, 316] or tail [257], tumor cells are forced to leave the primary tumor thereby facilitating metastasis to the lymph nodes and distant organs, such as lung. With increasing size, tumors furthermore start to grow invasively, thus, increasing the likelihood to seed metastases. Following a similar experimental setup as in this project, Zang et al. observed distant metastases after subcutaneous injection of B16F10 and primary tumor resection [317]. A further detailed assessment did, however, reveal, that lung metastasis was only observed in mutant *Shb* +/- mice (Src homology domain containing protein B) but not in the respective wildtype controls. Furthermore, primary tumors had been allowed to reach sizes beyond 700 mm^3, likely explaining the appearance of macroscopic lesions in the author's investigation [317].

Apart from experimental differences also the way of tumor transplantation may have affected metastatic dissemination. B16F10 melanoma cells had been implanted subcutaneously into the flanks of mice, whereas EO771.LMB cells had been injected orthotopically into the mammary fat pad. The importance of the local stroma has already been highlighted in earlier studies. Wilmanns et al. demonstrated that colon cancer grown at different anatomic sites, ectopically or orthotopically, responded differentially to chemotherapeutic agents [318]. Similar findings in small-cell lung carcinoma [319] and fibrosarcoma [320] confirmed the necessity of orthotopic models. Apart from therapeutic response, the microenvironment also influences metastatic efficiency. In several investigations, orthotopic implantation has been demonstrated to promote invasion and metastasis as compared to ectopic tumor growth [321-324]. In a different approach, co-transplantation of tumor spheroids with orthotopic stromal cells at an ectopic location, was shown to facilitate tumor growth and angiogenesis as compared to implantation of tumor cells alone or co-implantation with stromal cells derived from other organs [325]. As highlighted in these studies, the absence of the orthotopic stroma may therefore provide a legitimate explanation for why B16F10 cells did not yield efficient metastasis.

The orthotopic stroma also comprises blood endothelial and lymphatic vessels. The presence of these vessels further dictates metastatic patterns and efficiency. The close proximity of tumor cells to pre-existing vessels in the skin may therefore be another explanation for why B16F10 has been reported to metastasize to sentinel lymph nodes and lung when injected intradermally in contrast to subcutaneous implantation [326]. In contrast to prominent blood vasculature, in the present work B16F10 primary tumors have failed to efficiently recruit lymphatic vessels as determined by the rare presence of LYVE-1+ lymphatic vessels in immunofluorescent staining of tumor sections. Despite tumor-induced pre-conditioning of sentinel lymph nodes, no lymph node metastases were detected in the B16F10 model. Melanoma has, however, been shown to primarily metastasize via the lymphatic system and

lymph node metastasis furthermore serves as an important prognostic factor [118, 327, 328]. It can, thus, be speculated that lymphangiogenesis was not sufficiently enough induced in B16F10 melanoma in this study in order to establish an extensive connection of the primary tumor with pre-existing lymphatics from the skin. The absence of these lymphatic vessels may consequently have prevented the tumor cells from spreading locally to sentinel lymph nodes and distantly to the lung.

5.2. Metastasis in the Lewis lung carcinoma model was JUNB-independent

In contrast to the B16F10 model, LL/2-Luc cells led to overt metastasis in both control and stromal *Junb* knockout mice in a nearly identical time frame. In distinction from the EO771.LMB model, no JUNB-dependent metastatic phenotype could, however, be observed.

The function of JUNB as an oncogene or as a tumor suppressor has been shown to depend on tumor stage but predominantly on the cancer entity. Consequently, also the role of JUNB may be more decisive in breast cancer metastasis than in metastasis of lung cancer as both may rely on different intrinsic molecular mechanisms. For example, LL/2-Luc cells showed marked primary tumor invasion into the peritoneal wall, a feature which was hardly observed for the EO771.LMB cells. Besides being intrinsically more aggressive and invasive, LL/2-Luc cells also exhibit a different route of dissemination compared to EO771.LMB. In principle, cancers can metastasize via two routes: either via the lymphatic or the blood vascular system. Recently, it has, however, also been shown that cancer cells derived from metastatic lymph nodes can spread further and seed in the lung [326]. Solid tumors, such as breast cancer, melanoma and lung cancer, are predominantly found to metastasize via the lymphatic route in patients [116, 118, 329, 330]. In line with the human data, several reports detected lymph node metastases in the EO771 (the parental cell line which EO771.LMB was derived from) [331] and LL/2-Luc model [267]. I could furthermore verify, that also EO771.LMB cells do metastasize to lymph nodes (data not shown). Yet, in contrast to the clinical situation and previous mouse experiments, in my hands LL/2-Luc primary tumors predominantly metastasized to the lung via the hematogenous route, as indicated by the rare occurrence of lymph node metastasis in the spontaneous metastasis assay. These differences may partially be due to the already mentioned different injection sites. Nevertheless, EO771.LMB and LL/2-Luc exhibit different preferences in respect to hematogenous and lymphatic dissemination, which may have been another contributing factor to JUNB-dependent metastasis in the EO771.LMB but not in the LL/2-Luc model.

Apart from these intrinsic differences, there are also some obvious discrepancies in the applied experimental design between the EO771.LMB and the LL/2-Luc model. As already described above, ectopically and orthotopically implanted tumors differ in their response towards therapy and metastatic efficiency, but also alterations in gene expression have been observed [332]. Not surprisingly, the two human glioma cell lines U251 and U87 exhibited vastly different gene expression profiles when grown *in vitro* in comparison to *in vivo,* but major changes were also observed when implanted subcutaneously into the hind leg instead of intracerebrally [333]. This may indicate that the orthotopic environment is essential for JUNB-dependent metastatic dissemination.

5.3. JUNB promotes distant metastasis in the EO771.LMB breast cancer model

In this dissertation, a spontaneous metastasis assay with EO771.LMB breast cancer cells was successfully established. Orthotopic injections into the mammary fat pad enabled the accurate mimicking of the adequate tumor microenvironment. Primary tumor resections led to the reproducible appearance of distant metastases in the lungs in a relatively short time and without the need to grow primary tumors to large sizes. Labelling of the tumor cells with an mCherry reporter furthermore aided quantification of distant metastasis in a dual approach: one part of the lung was used for quantification of the reporter in genomic DNA by qRT-PCR and the second part was utilized for immunohistochemical staining for mCherry. With this assay, the functional contribution of stromal JUNB to distant metastasis was assessed.

In line with previous reports, tumor growth of EO771.LMB primary tumors was not affected by *Junb* deletion [232]. Strikingly, stromal loss of *Junb* did, however, increase the capacity of these cells to metastasize spontaneously to the lungs. This was apparent already by macroscopic examination but further validated following quantification by qRT-PCR and immunohistochemistry. In order to decipher at which step of the metastatic cascade *Junb* loss was required, an experimental metastasis assay was performed. Yet, lung colonization after tail vein injection of the tumor cells did not reveal a significant difference in lung metastatic burden. In fact, metastasis seemed to be even slightly impaired upon *Junb* deletion. These findings imply, that JUNB does not promote metastasis by facilitating extravasation but is more likely to enhance the initial steps of the metastatic cascade, such as tumor cell intravasation. As the detection of CTCs in this model was, however, unsuccessful, the effect of *Junb* loss on intravasation could not be answered directly. Other than promoting intravasation, loss of *Junb* may also have influenced the formation of a pre-metastatic niche. Consequently, no metastasis-boosting effect would have been observed in the absence of a primary tumor. In order to determine whether ablation of *Junb* may have facilitated intravasation or promoted the establishment of a pre-metastatic niche, EO771.LMB primary tumor and pre-metastatic lungs were investigated for cellular changes as will be discussed in the following section.

5.4. JUNB does not influence metastatic spread due to vascular defects

The advantage of being able to study the whole metastatic cascade in the spontaneous metastasis assay is also a major obstacle in the quest for the underlying molecular mechanism. In addition, deletion of *Junb* using *Col1α2*-driven expression of Cre recombinase results in ablation of *Junb* in a plethora of mesenchymal-derived cells, such as endothelial cells, smooth muscle cells and fibroblasts, but also in a variety of cells derived from the hematopoietic compartment, such as immune cells [234]. Thus, multiple cellular compartments which have been attributed essential contributions to metastatic spread are affected by JUNB loss and could potentially cause the observed phenotype. For this reason, these major cellular compartments were investigated for JUNB-dependent alterations.

The vascular system is especially important for metastatic spread as it provides the major entry points and conduits for disseminated tumor cells to reach distant organs but it also mediates tumor cell adherence as an essential step of extravasation. Moreover, the vascular system is of extreme importance for the sustained supply of nutrients and oxygen not only to the primary

tumor but also to the metastatic site. In addition, successful metastatic colonization has been shown to depend on nearby vessels. Sprouting tip cells provide necessary signals, e.g. secretion of TGFβ and periostin, enabling dormant cells to escape dormancy, proliferate and grow out [334].

Over the past years, JUNB has been established as an essential transcriptional regulator controlling vascular development and homeostasis. This was already determined early on by the finding that global *Junb* KO resulted in embryonic lethality due to defects in placentation and neovascularization [181]. *Junb* KO embryos failed to establish sufficient connections with the maternal circulatory system consequently leading to growth retardation and mortality. In subsequent studies, JUNB was furthermore found to be important for hypoxia- [189] and hypoglycemia-induced [335] *Vegf* induction, vascular morphogenesis [228] and tumor angiogenesis [189]. In vascular smooth muscle cells, JUNB evidently influences motility and contractility via its target *Myl9* [229]. Therefore, I initially hypothesized that the prominent lung metastasis could be the result of vascular defects. For this reason, blood vascular density was assessed by immunofluorescent staining for the pan-endothelial marker CD31 on paraffin-embedded tissue of EO771.LMB primary tumors. Contrary to my expectations, no difference could be determined upon JUNB loss.

Besides hematogenous spread, lymphatic vessels provide an alternative route of dissemination for metastatic cells. For breast cancer, lymphatic metastasis is furthermore described to be the predominant route [329]. This is evidenced by frequent lymph node involvement in patients concerned [330, 336, 337], a finding I could also reproduce *in vivo* in mice using the EO771.LMB model. Junb has been implicated in lymphatic development in zebrafish [227]. Ablation of *junb* genetically using the CRISPR/Cas9 (Clustered Regularly Interspaced Short Palindromic Repeats) system or transiently by morpholino-mediated knockdown led to a failure of the formation of the parachordal lymphangioblast, the precursor of the thoracic duct, the major lymphatic vessel in zebrafish [227, 245]. Yet, evaluation of lymphatic vascular density in EO771.LMB primary tumors, did not reveal any JUNB-dependent changes.

As primary tumor growth was unaffected by loss of JUNB, though, I reasoned that the vasculature of tumor-preconditioned organs may rather be affected than that of the primary tumor itself. Vascular changes by tumor-derived factors in lymph nodes and lungs have been associated with disease progression and overall survival [268, 269, 338]. As differences in size between tumor-draining and non-draining lymph nodes could already readily be detected macroscopically and were more pronounced in the B16F10 than in the EO771.LMB model, I decided to study B16F10-pre-conditioned lymph nodes in more detail. Despite the apparent enlargement of tumor-draining lymph nodes compared to non-draining counterparts, histologic assessment of lymph node vasculature did not reveal any JUNB-dependent defects. Considering that the B16F10 model did only metastasize very inefficiently and no lymph node metastases were apparent macroscopically, these findings may not be surprising. Nevertheless, in addition to a generally increased blood vascular and lymphatic vascular density, lymph node pre-conditioning frequently manifests as morphological changes of high endothelial venules [68] and enlargement of lymph node sinuses [268, 339, 340]. Although no gross differences were detected upon JUNB loss, these features were not examined in detail. Consequently, JUNB-dependent changes in lymph node pre-conditioning cannot completely be excluded.

As no major differences were obvious in the lymph nodes, the following investigations were focused on the lungs as the future metastatic sites. Apart from the mere presence of blood and lymphatic vessels as entry points for disseminated tumor cells, the functionality of these vessels is key for metastatic spread [341-344]. JUNB may be involved in the regulation of vascular permeability via its direct target *Myl9* [229]. JUNB-deficient vascular smooth muscle cells, fibroblasts [229] and endothelial cells [228] showed decreased motility and cytoskeletal remodeling, an essential prerequisite for vascular permeability [345, 346]. Since the stromal compartment in the different tumor models being used in this dissertation is identical with regard to JUNB presence and absence, respectively, I assessed blood vascular permeability in the LL/2-Luc model. In this model sufficient metastasis was also seen in control mice, thus, allowing for comparative analysis. Extravasated FITC-dextran was readily detectable in primary LL/2-Luc tumors by fluorescent microscopy of tumor sections co-stained for the endothelial marker CD31. No enhanced permeability in *Junb* KO mice was, however, determined upon quantification by fluorescence measurement.

Overall, no differences in blood endothelial or lymphatic density as well as permeability could be detected which could account for the observed increase in distant metastasis upon *Junb* loss. These findings are in line with a previous report from our lab demonstrating that loss of stromal JUNB does not affect primary tumor growth and angiogenesis in the B16 melanoma and LL/2-Luc model [232]. Neither microvascular density nor relative blood volume nor maturation status of the tumor vasculature were altered upon deletion of stromal *Junb* [232].

As the functionality of the vasculature was only examined in the LL/2-Luc model which did not show the JUNB-dependent metastatic phenotype, though, model-specific differences cannot be excluded. Due to the robustness of LL/2-Luc metastasis, subtle increases in permeability or disturbances of endothelial junctions may have been masked. In addition to vascular permeability, tumor cell extravasation was not promoted in the experimental metastasis assay with EO771.LMB cells further arguing against defects in vascular integrity and endothelial junctions upon *Junb* deletion. Nevertheless, tumor cell extravasation was determined in the absence of a primary tumor, whereas permeability was assessed in tumor-bearing animals. Consequently, tumor-induced changes cannot be ruled out. Moreover, endothelial cells lacking JUNB may also express different sets or varying levels of adhesion molecules, which could have contributed to the enhanced tumor cell adhesion and facilitated colonization. In primary human keratinocytes, loss of JUNB resulted in the upregulation of Intercellular Adhesion Molecule 1 (ICAM-1) as well as N-Cadherin and downregulation of Integrin alpha 2 [347]. In comparison to WT littermates, ICAM-1-deficient mice have been shown to be more susceptible to liver metastasis from colon carcinoma [348] but have also been reported to be protected from lymphoma metastasis [349]. Despite these contrary findings, the importance of ICAM-1 in metastatic spread is evident. N-Cadherin facilitated binding of invasive breast cancer cells to stromal cells [350] and Integrin alpha 2 suppressed breast cancer metastasis [351]. JUNB was furthermore suggested to regulate the expression of vascular adhesion molecule 1 (VCAM-1) [352]. VCAM-1 is essential for leukocyte diapedesis and has been implicated in metastasis in a multitude of studies [338, 353-355]. ICAM-1 and VCAM-1 are of particular interest as they are upregulated upon pro-inflammatory stimuli such as TNFα [356] and IL-1β [357] which were found upregulated in EO771.LMB primary tumors and pre-metastatic lungs isolated from *Junb* KO mice in the present work. ICAM-1 [355, 358] and VCAM-1 [359] furthermore mediated adhesion and infiltration into the lungs of neutrophils and other immune cells in several experimental mouse models. These potential changes in adhesion would have remained undetected when determining the functionality of the vessels with FITC-dextran. It may therefore be speculated that an enhanced expression of adhesion molecules induced by

pro-inflammatory signals in *Junb* KO mice may have facilitated neutrophil infiltration and distant metastasis.

5.5. JUNB does not impact fibroblast density

In addition to blood and lymphatic endothelial cells, fibroblasts make up the majority of the tumor stroma. In the tumor, fibroblasts are often present in an activated state, as so-called cancer-associated fibroblasts (CAFs), rendering them more prone to support tumor growth and metastatic spread. They not only provide an essential structural stability by secretion of ECM molecules, such as collagens (type I, III, IV and V) [272, 360, 361], fibrillin [272], fibronectin [272, 361] and laminin [361] but have also been shown to influence tumor cell behavior by secretion of growth factors and chemokines [361, 362]. More recently, fibroblasts have been demonstrated to actively drag cancer cells by heterophilic N-Cadherin E-cadherin interactions, thus, stimulating tumor invasion and spread [363]. Especially in breast cancer, the presence of CAFs has been correlated with disease progression [364] and response to therapy [365]. As JUNB has been implicated in fibroblast proliferation and transformation [196], fibroblast abundance was quantified in EO771.LMB primary tumors.

Fibroblast research is hindered by the lack of specific markers. Typically, fibroblasts are characterized by expression for vimentin, FSP1 as well as FAP, and αSMA for activated fibroblasts [362]. Investigation of these markers by qRT-PCR or immunohistochemistry did, however, reveal, that vimentin and FSP1 are abundantly expressed by EO771.LMB cells excluding their use in this study. Expression of *Fap* was not affected by *Junb* loss. In order to validate this finding on protein level and to assess fibroblast morphology and distribution, an immunohistological staining for fibroblast markers was performed. Immunohistochemistry for FAP did not result in an adequate staining pattern, whereas immunofluorescence for αSMA did only show positive staining around large vessels arguing that these cells are rather vascular smooth muscle cells than fibroblasts. In the search of alternative fibroblast markers, podoplanin was recently used to identify fibroblasts in B16 melanoma [274], human breast cancer biopsies [275] and synovial tissue [276]. Immunohistochemistry for podoplanin did not result in JUNB-dependent differences, neither in abundance, distribution nor morphology. In recent years, it has, however, become increasingly evident, that fibroblasts are not a homogeneous population but are rather composed of several distinct subpopulations. These subpopulations have been identified and also characterized according to their marker expression [272, 276, 366-368] and have been shown to elicit a differential response towards chemo- and immunotherapy [365, 369, 370], or influence tumor cell proliferation and stemness [369, 371]. Podoplanin-expressing CAFs have been reported to inhibit tumor cell invasion [372], whereas CAFs identified by αSMA and *FAP* enhanced migration and tumor formation [373]. Consequently, it is possible that fibroblasts identified by *Fap* expression or immunohistochemistry for podoplanin in this study represent only one or two fibroblast subtypes, which are not affected by *Junb* deletion.

Several groups have established that normal fibroblasts and CAFs differ dramatically in their transcriptome and proteome [374-377]. Strikingly, fibroblasts also exhibit differential gene expression profiles when isolated from the skin of various anatomical sites [272]. Here, the abundance of fibroblasts was only investigated in EO771.LMB primary tumors. Yet, it is conceivable that lung fibroblasts may be affected differently by stromal JUNB loss. As podoplanin is, however, abundantly expressed by type 1 alveolar cells, another fibroblast

marker would have been needed for analysis [378]. Apart from type 1 alveolar cells, podoplanin is also prominently expressed by other cell types present in the tumor microenvironment. Podoplanin is commonly used as a marker for lymphatic endothelial cells [379] but has also been described to be expressed by different populations of macrophages [380, 381] and in basal keratinocytes during wound healing [382]. Although structures clearly identifiable as lymphatic vessels were omitted from analysis, it cannot be excluded that other PDPN+ cell types were included and may consequently have skewed the quantification. Concludingly, in order to assure the unambiguous identification of fibroblasts and fibroblast subtypes, several markers would have needed to be assessed, preferably in combination.

In addition to phenotypic differences in terms of marker expression, fibroblasts, similarly to (lymphatic) endothelial cells or immune cells discussed later on, can also present with an altered secretome. Multiple fibroblast-secreted factors, such as lipocalin 2 [230], granulocyte-macrophage colony-stimulating factor (GM-CSF) [187, 246], keratinocyte growth factor [187, 246], TNFα [383] and Interferon-γ [161] are in fact regulated by JUNB. Nevertheless, expression of fibroblast-secreted factors has not been assessed comprehensively in this study. A plethora of cytokines, which are partially also secreted by fibroblasts, will, however, be discussed in a later section. Besides growth factors and cytokines, fibroblasts are particularly known for their production of ECM molecules. Upon activation, for example in a cancer setting, fibroblasts secrete higher amounts of ECM components, but also the composition is vastly abnormal [361]. In contrast to normal tissue, CAFs secrete higher amounts of collagens, proteoglycans, hyaluronic acid, chrondroitin sulfate and fibronectin, which are partially also structurally altered [384, 385]. These ECM molecules can aid cancer progression by forming “tracks” for cancer cells but also by functioning as binding sites for adhesion molecules present on the surface of disseminated cancer cells [386, 387]. JUNB has been implicated in the regulation of fibronectin, collagen type VII alpha 1 [388] and collagen type I alpha 2 upon stimulation with TGFβ [389]. Although no gross differences were determined by trichrome staining, it cannot be fully ruled out, that *Junb* KO fibroblasts may specifically have contributed to the metastatic phenotype via a fibroblast-derived factor or ECM.

5.6. Stromal JUNB KO promotes immune cell infiltration into primary EO771.LMB tumors and pre-metastatic lungs

The immune system is essential for the surveillance and elimination of extrinsic danger signals, such as pathogens, but also intrinsic threats, for example tissue damage. In addition, the immune system plays a pivotal role in the development and progression of cancer. In the initial steps, neoplastic transformed cells are recognized by various cells of the adaptive and innate immune system and subsequently eliminated. Some tumor cells are able to escape from this immunosurveillance, though, enabling outgrowth and tumor dissemination [390]. Immunoevasion is mediated by tumor cells decreasing their immunogenicity, e.g. by downregulation of MHC molecules, or by active modulation of the immune cells by factors derived from tumor cells or the microenvironment [391, 392]. JUNB has been attributed important functions in several immune cell types involved in immunosurveillance and immune evasion, which are illustrated in the table below (Table 5-1).

Table 5-1: Functions of JUNB in immune cells

Cell type	JUNB-mediated response	Reference
T_H2 (T helper cell)	Promotes T_H2 differentiation, induces *Il-4,* represses *Intfg*	[190, 191, 393]
T_H17	Activation of T_H17-lineage specifying genes upon inflammation, repression of regulators for other CD4+ T cell subsets (T_H1, T_H2, Treg), induced *Il-23*	[394-397]
Effector Tregs	Homeostasis, induced Treg effector genes	[398]
Dendritic cells	Induction of pro-inflammatory cytokines *Tnfα, Il-6*, and *Il-12* upon LPS treatment	[247]
Macrophages	Macrophage activation Macrophage recruitment in psoriasis	[233] [160]
Myeloid cells	Myeloid differentiation Mediates monopoiesis	[231, 399] [400]
NK cells	JUNB mediated NK cell killing by regulation of RAE-1ε expression on target cells	[401]
Neutrophils	Regulation of iNOS expression Neutrophil recruitment in psoriasis	[402] [160]

Due to the involvement of JUNB in overwhelmingly many different immune cell types, which may contribute to JUNB-dependent metastasis, immune cell infiltration was first assessed using the pan-immune cell marker CD45. A significant increase in immune cell infiltration was detected upon stromal loss of *Junb* in EO771.LMB primary tumors but more strikingly in pre-metastatic lungs. Upon closer examination of distinct immune cell types, it became clear, that in particular CD11b+ myeloid cells which were expressing *Ly6g* and LY6B.2 had accumulated in the pre-metastatic lungs as determined by gene expression analysis and immunohistochemistry. Due to specific marker expression, morphology, size and spatial distribution, these cells could clearly be identified as neutrophils [291, 403]. This conclusion was further supported by the significant upregulation of *S100a8* and *S100a9* in KO lungs. S100A8/A9 are abundantly expressed in the cytosol of neutrophils and are frequently used as neutrophil markers [96, 404, 405]. Other assessed myeloid cell types, such as monocytes, macrophages and NK cells, did not show this prominent upregulation of specific markers in pre-metastatic lungs isolated from *Junb* KO animals, consequently arguing against these cell types being responsible for the observed enhanced myeloid cell infiltration. Upon examination of cells of the adaptive immune response, no apparent changes were detected in infiltration of CD3+ T cells, Tregs and cytotoxic T cells into pre-metastatic lungs. Yet, EO771.LMB primary tumors from KO animals showed a lower abundance of CD3+ T cells, which was not the result of diminished levels of Tregs or cytotoxic T cells. In conclusion, immune cell infiltration upon JUNB loss was predominantly altered in pre-metastatic lungs but not as strongly affected in primary tumors. Remarkably, especially cells of the myeloid lineage, in particular neutrophils, were found to be accumulated in mice with stromal deletion of *Junb*.

Strikingly, these differences in neutrophil infiltration detected in the EO771.LMB model were also obvious in the B16F10 and LL/2-Luc model. Neutrophil recruitment to the pre-metastatic lungs was significantly enhanced upon stromal *Junb* deletion in all three models. The extent

of upregulation was, however, remarkably different. Whereas neutrophil accumulation was comparable between the B16F10 and EO771.LMB model, it was tremendously boosted in the LL/2-Luc model. In LL/2-Luc tumor-bearing WT and CTR mice, neutrophil infiltration into lungs already reached similar levels as in lungs from KO mice pre-conditioned with EO771.LMB tumors. Neutrophil levels in LL/2-Luc tumor-bearing KO mice exceeded levels reached in the EO771.LMB model by far. Similar findings in infiltration had already been reported by Dawson and colleagues [406]. The authors found a higher number of bone marrow derived cells accumulating in Lewis lung primary tumors and metastatic lungs compared to B16F10, did, however, not further define the identity of these cells. Assuming that neutrophils in the pre-metastatic lung promote metastasis, as frequently reported [91, 96, 407], the high metastatic burden in the LL/2-Luc model may be explained by the immense numbers of detected neutrophils. Neutrophils may have been present in such high numbers already in WT and CTR mice that additional accumulation upon *Junb* loss did not result in a further boost of metastasis formation. Supporting this hypothesis, Granot et al. found prominent accumulation of neutrophils in the circulation and in lungs pre-conditioned by the highly metastatic 4T1 breast cancer cell line but virtually no elevation when mice were injected with the weakly-metastatic 66cl4 cells [92, 408].

Although the dual approach of quantifying immune cell populations by gene expression analysis and immunohistochemistry, identified prominent neutrophil accumulation in pre-metastatic lungs, this approach clearly has limitations. Most obviously, the analyses were based on the expression of individual markers, supposedly exclusively expressed by the respective cell type. For example, the transcription factor FOXP3 is widely used to specifically label Tregs [292, 293]. Research over the past years has, however, revealed the expression of FOXP3 in additional cell types, such as CD8+ regulatory T cells [409, 410], invariant NK T cells [410, 411] and mammary epithelium [410, 412]. FOXP3 expression in myeloid cells remains controversial [410]. Similarly, in agreement with its common use, F4/80 was utilized in this project to identify macrophages. Recent evidence does indicate its expression by Langerhans cells and eosinophils, though [281]. Furthermore, the expression of CD11b, which is widely regarded as a myeloid cell marker, by memory B cells is often neglected [413]. Despite its commercial name, anti-neutrophil antibody 7/4, which I used to assess neutrophil infiltration, does in fact not only label neutrophils. Contrarily, the 7/4 antibody reacts with the LY6B.2 antigen and evidently also marks newly generated inflammatory monocytes, a subset of activated macrophages as well as some progenitor cells [291]. These examples illustrate the requirement for combinatorial strategies. The study would have benefited from elaborate analysis by flow cytometry, allowing the use of simultaneous assessment of multiple markers and aiding the unambiguous identification of cell populations. Nevertheless, in this project, various immune cell types were assessed using either multiple different markers or combinations thereof. This is exemplified by the dual labeling of CD3 and CD8 in order to accurately distinguish cytotoxic T cells. The identification of neutrophils is based on even more complementary approaches: although the overexpression of *Ly6g* already indicated neutrophil accumulation, this was confirmed by corresponding expression patterns of *S100a8/a9*, positive staining for LY6B.2 and fitting morphological features.

Surprisingly, specific markers of all investigated myeloid cell populations showed significantly elevated expression in EO771.LMB primary tumors from KO mice on RNA level. This did, however, only translate into enhanced infiltration on protein level in the case of neutrophils. For all other subpopulations, no difference was visible. Similarly, in the examination of the cells of the adaptive immune system, inconsistencies were detected in gene expression analysis, but were not as obvious upon immunohistological assessment. Consequently, these

discrepancies may be the result of the higher detection sensitivity of gene expression analysis compared to immunohistochemistry. Cells expressing the respective marker at low levels may simply not have been detected by immunohistochemistry. Moreover, all expression analyses were performed on only four tumors, whereas a higher number of samples was used for quantification of immunohistochemistry. Furthermore, distinct immune subsets express CD45 at varying levels, so that an increase in *Ptprc* expression may have reflected the altered immune cell composition in EO771.LMB primary tumors [414].

Only recently, it has been shown that deletion of *Junb* in FOXP3+ Tregs leads to a reduction of Treg numbers [398]. Interestingly, this effect was observed in the colon, but not in lung, liver, skin or spleen. Therefore, it may be speculated, that JUNB regulates immune cell infiltration differently in various tissues. This may explain why JUNB-dependent accumulation of neutrophils is more robust in pre-metastatic lungs compared to primary tumors.

Furthermore, as indicated in Table 5-1, JUNB has less frequently been indicated in regulating immune cell accumulation, but is more commonly described to mediate immune cell activation or differentiation. It is, thus, conceivable, that although apart from neutrophils no alterations in cell abundance were visible upon *Junb* loss, these immune cells may still exhibit phenotypic differences. This is of particular interest considering neutrophils and their interplay with other cells of the immune system. Neutrophils have been reported to enable CD8+ T cell migration to inflamed tissue upon influenza infection [415] and are able to efficiently cross-present antigens to T cells [416]. Yet, also in cancer, neutrophils influence cytotoxic T cells by impacting T cell migration, activation, proliferation and cytokine-release [91, 417, 418]. In particular, neutrophils can suppress T cell-mediated immunity via increased expression of PD-L1 [419] or inducible nitric oxide synthetase (iNOS) [420]. Due to these immunosuppressive functions of neutrophils, they are also often regarded as myeloid-derived suppressor cells (MDSC). MDCS are generally defined as cells of myeloid origin, which are present in an immature state and able to suppress T cell activity [421]. In mice, MDSCs comprise a heterogeneous population of polymorphonuclear MDSCs (PMN-MDSCs), defined as $CD11b^{+}Ly6G^{+}Ly6C^{low}$, and monocytic (M-MDSCs) MDSCs, which are characterized as $CD11b^{+}Ly6G^{-}Ly6C^{hi}$ [421]. Due to overlapping marker expression and morphology, the distinction of PMN-MDSCs and neutrophils is complicated and is generally based on phenotypic differences: PMN-MDSCs are, in contrast to neutrophils, able to induce immunosuppression [421, 422]. In addition, PMN-MDSCs are less granular than neutrophils but express higher levels of arginase 1 [423], CD11b and CD66b [424]. After density-gradient centrifugation, neutrophils can be differentiated into low density (LDN) and high density neutrophils (HDN). HDN are generally regarded as classical neutrophils, whereas LDN were shown to also possess immunosuppressive functions classifying them as PMN-MDSCs [425]. Because of the mentioned similarities and multiple studies reporting about vastly different functions exerted by neutrophils, it is, however, currently controversial whether neutrophils and PMN-MDSCs are indeed two different rather than one plastic cell population [422, 426]. Since, I did not assess the immunosuppressive functions of the granulocytes accumulated in *Junb* KO mice, I refer to these cells as neutrophils rather than PMN-MDSCs.

5.7. Neutrophil-recruiting factors are expressed in a JUNB-dependent manner

Besides regulating immune cell differentiation and activation, JUNB has also been shown to mediate neutrophil recruitment in psoriasis [160]. In this context, a plethora of pro-inflammatory cytokines, such as *Il-1α, Il-1β, Ccl2, Ccl3, Ccl4, Cxcl2, Tnfα and S100a8/a9,* were shown to be deregulated upon *Junb* deletion in epidermal keratinocytes. In order to clarify, whether neutrophil recruiting factors may also be upregulated upon stromal JUNB loss in this project and may consequently have been the cause of the increased neutrophil infiltration, they were examined by gene expression analysis in EO771.LMB primary tumors and pre-metastatic lungs.

Classical neutrophil chemoattractants regulate neutrophil egress from the bone marrow into the circulation, e.g. CXCL12, or control neutrophil recruitment out of the circulation into peripheral tissues, for example CXCL1, CXCL2 and CXCL5 [296, 303]. Examination of these chemokines, revealed a specific upregulation of these factors in tumors isolated from *Junb* KO mice. *Cxcl1, Cxcl2* and *Cxcl5* were, however, also highly expressed by EO771.LMB tumor cells and no JUNB-dependent expression was determined in pre-metastatic lungs. *Cxcl2* expression furthermore varied a lot between WT and CTR mice. Overall, this implies that tumor cells are the predominant source of these chemokines rather than the microenvironment. The fact that expression was inconsistent, in the case of *Cxcl2*, and that enhanced expression was only obvious in the primary tumor but not in the lungs further implies that these changes may not be due to the absence or presence of JUNB in the stroma. *Cxcl12* was the only chemokine which was not expressed by the tumor cells indicating that it is purely derived from the tumor stroma. Moreover, *Cxcl12* showed consistent upregulation upon *Junb* loss, both in primary tumors and pre-metastatic lungs. Yet, enhanced *Cxcl12* levels mediate neutrophil retention in the bone marrow, which is in stark contrast to the observed neutrophil accumulation in *Junb* KO mice [427]. *Cxcl12* expression has, however, also been reported in capillary endothelial cells, likely contributing to neutrophil margination in the lungs [296]. The lung has frequently been described to contain large pools of marginated neutrophils [428-430]. Nevertheless, no distinction of neutrophils in the lung within the vasculature or outside in the parenchyma was attempted in this project. For this reason, no conclusion can be drawn as of whether in fact the marginated neutrophil pool was specifically enhanced in tumor-bearing KO mice rather than recruitment into the tissue. In addition to the production of CXCL12 by endothelial cells and by CXCL12-abundant reticular cells (CAR) in the bone marrow [431], neutrophils themselves have also been demonstrated to express CXCL12 [415]. The enhanced expression of *Cxcl12* upon loss of JUNB may therefore simply reflect the increased neutrophil numbers. Furthermore, CXCL12 is not only important for maintaining neutrophil homeostasis but has also been shown to attract Tregs [418], MDSCs [418], endothelial progenitors [432] and most strikingly CXCR4+ tumor cells [433, 434]. Although, *Cxcr4* expression by EO771.LMB breast cancer cells has not been verified, CXCL12 may potentially have facilitated metastasis in a more direct manner. More recently, Ahirwar and colleagues demonstrated, that CXCL12 mediates vascular leakiness thereby promoting tumor intravasation and metastasis [432]. This function of CXCL12 can, however, be excluded in this project, as no changes in vascular permeability were determined upon *Junb* loss. Finally, enhanced *Cxcl12* expression upon *Junb* KO may also have been the result of increased JUN activity as mode of compensation, as *Cxcl12* has been shown to be a direct JUN target [246].

In addition to classical neutrophil chemoattractants, several other cytokines and factors have been previously published to act as neutrophil attractants. Mice deficient for CCL2 exhibited reduced bacterial clearance after bacterial infection concomitant with attenuated neutrophil influx [304, 435]. Platelet-derived CCL5 mediated neutrophil recruitment in an experimental model of acute colitis [305]. Osteopontin KO mice showed an impaired intraperitoneal neutrophil recruitment after injection of sodium periodate [306]. Expression of *Il-1α* correlated well with neutrophil infiltration in the initial phase of sterile inflammation [300]. In EO771.LMB primary tumors and pre-metastatic lungs, *Il-1α, Spp1, Ccl2* and *Ccl5* were not found to be consistently altered upon JUNB ablation indicating that these factors do not play a role in JUNB-dependent neutrophil accumulation.

Furthermore, G-CSF is essential for maintaining the balance of neutrophil levels in homeostasis and under stress, both systemic and local [297, 298, 436, 437]. Lipocalin-2 was implicated in neutrophil infiltration by inducing G-CSF and CXCL1 in alveolar macrophages after infection with *M. tuberculosis* [438]. Both, G-CSF and lipocalin-2 have been identified as JUNB targets in fibroblasts during cutaneous wound healing [246]. In the current project, no consistent regulation of *Csf3* and *Lcn-2* by JUNB could be determined. Although alterations of *Csf3* and *Lcn-2* did reach significance in EO771.LMB primary tumors, these changes were very inconsistent for *Csf3* and were not detected in pre-metastatic lungs. In contrast, *Lcn-2-* was strongly upregulated upon JUNB loss in primary tumors, which was also determined in pre-metastatic lungs. Nevertheless, *Lcn-2* expression was highest in EO771.LMB cells, indicating that *Lcn-2* is not predominantly derived from the microenvironment. A contribution of lipocalin-2 to JUNB-dependent neutrophil recruitment can, however, not be excluded completely.

IL-1 has initially been associated with neutrophil recruitment by transcriptionally activating *IL-8* expression (the human orthologue of *Cxcl1, Cxcl2* and *Cxcl5*) [439]. In line with IL-1, also TNFα has been described to induce *IL-8* in human hepatocytes [440]. Further research did moreover support the notion, that both IL-1β [441-443] and TNFα indeed mediate neutrophil recruitment [442, 444]. Assessment of *Il-1β* and *Tnfα* expression in this project did reveal their absence in EO771.LMB cells but also their strong induction in the tumor bulk isolated from *Junb* KO mice. This finding indicates that *Il-1β* and *Tnfα* are specifically induced in cells of the tumor microenvironment upon JUNB deletion. Remarkably, these changes in expression were similar in pre-metastatic lungs: whereas no difference was observed in unchallenged mice, both cytokines were upregulated in pre-metastatic lungs of KO animals. Therefore, the expression patterns of *Tnfα* and even more strikingly *Il-1β*, correlate very well with the observed neutrophil levels. Nevertheless, it has to be mentioned that both TNFα and IL-1β can also be produced by neutrophils themselves, so that, in line with *Cxcl12* mentioned earlier, enhanced expression may only reflect higher neutrophil abundance [445]. TNFα and IL-1β have furthermore been described to induce upregulation of endothelial adhesion molecules in the lung, such as VCAM-1, thus, enabling leukocyte adhesion and diapedesis [446]. As no prominent upregulation of classical neutrophil chemoattractants was determined in pre-metastatic lungs, induction of VCAM-1 by TNFα and IL-1β derived from the tumor microenvironment upon *Junb* deletion may provide another explanation for the elevated neutrophil recruitment.

5.8. Bone marrow transplantations point towards JUNB in the stromal rather than in the hematopoietic compartment being essential for neutrophil recruitment

So far, it had been established in this dissertation, that loss of stromal *Junb* promoted breast cancer metastasis which was accompanied by the accumulation of neutrophils in the pre-metastatic lungs and in primary tumors. Concomitantly, the upregulation of neutrophil-attracting cytokines *Il-1β* and *Tnfα* was observed in these tissues. The cellular source of these cytokines was, however, still unclear. Thus, in order to identify, whether the metastatic phenotype was due to a neutrophil-intrinsic mechanism or regulated by neutrophil recruiting factors expressed by the stroma, bone marrow transplantations were performed.

After lethal irradiation of the mice, bone marrow chimeric mice were successfully generated as indicated by the high reconstitution efficiencies exceeding 87% at end point. In agreement with previous experiments, tumor growth of EO771.LMB primary tumors was unchanged by JUNB loss in either compartment. In slight distinction, primary tumor growth was, however, delayed by approximately 3 days in all experimental groups. Examination of lung metastasis revealed a massively elevated metastatic burden in all experimental groups in comparison to animals which had not undergone bone marrow transplantations. Unexpectedly and in contrast to the initial metastasis experiment, no difference was observed between the experimental groups. As, it has been reported that whole body irradiation renders mice immunosuppressed up to several weeks after irradiation [308, 447, 448], this may potentially have aided metastatic spread in the bone marrow transplantation experiment. After BMT, blood counts typically return to normal within 4-6 weeks but the immune system is generally considered to be fully reconstituted only after approximately 10 weeks [449, 450]. Yet, different immune cell populations do exhibit tremendous differences in recovery times. In several publications, experiments are performed earliest 6-8 weeks after BMT in order to ensure that all immune cell populations have been re-established and have re-gained their respective functions [451-453]. Nevertheless, I implanted tumor cells already 32 days after BMT due to several reasons: (I) neutrophils are the first cell type to recover already 2 weeks after BMT [450] and (II) *Junb* KO mice present with age-related defects. Beyond approximately 20-25 weeks, *Junb* KO mice exhibit reddened skin and itching corresponding to the development of inflammation resembling psoriasis [230]. In order to circumvent these issues, animals could not be allowed to recover for more than 4 weeks considering an age of 8 weeks when irradiated and 5-6 weeks for the spontaneous metastasis assay. Despite general immunosuppression, primary tumor growth was only slightly delayed in these mice indicating that the immune system did not play a decisive role in primary tumor growth. This notion is further supported by the fact, that although an increased infiltration of immune cells had been observed in the initial experiment without BMT, primary tumor growth was indifferent. The delay in primary tumor development may, however, have promoted dissemination of tumor cells due to the prolonged time until primary tumor resection, which may eventually have led to enhanced metastasis independently of JUNB. An alternative explanation is provided by the fact, that irradiation frequently induces fibrosis [454]. Fibrosis has moreover been linked to elevated metastasis in an experimental model of breast cancer [455].

Although the metastatic phenotype upon *Junb* loss could not be reproduced in this setting, mice with deletion of *Junb* in the stromal compartment still showed higher levels of circulating neutrophils. This result points towards an indirect mechanism of neutrophil recruitment mediated by the stroma rather than a neutrophil-intrinsic effect. Nevertheless, higher systemic

neutrophil levels were also already detected by flow cytometry in unchallenged mice, a finding which was not confirmed by absolute cell counting. Due to the fact that flow cytometry relies on the expression of specific markers rather than morphological features, flow cytometry data were regarded as more accurate. Hence, higher neutrophil levels in the circulation and consequently recruitment to the tissue may simply be a result of the expansion of the myeloid compartment in *Junb* KO mice. In earlier studies, ectopic expression of *Junb* in long-term hematopoietic stem cells (LT-HSC) led to a reduction of LT-HSC frequencies, whereas ablation of *Junb* resulted in a myeloproliferative disorder with specific expansion of LT-HSC and GMP [209]. Remarkably, this myeloproliferative disorder was only observed when *Junb* was absent from LT-HSC but not in later steps of myelopoiesis [209]. In the present experiment, elevated systemic neutrophil levels were, however, only observed in mice with stromal *Junb* KO but not in mice with *Junb* deletion in the hematopoietic compartment, i.e. in mice which had been reconstituted with KO bone marrow. Furthermore, neutrophil levels were particularly enhanced upon tumor growth and also infiltration into the tissue was only increased in the presence of a primary tumor but not in unchallenged animals. Taken together, this implies that neutrophil numbers are specifically upregulated in tumor-bearing mice with stromal deletion of *Junb* and is not caused by defected myelopoiesis.

Despite these elevated neutrophil levels in the circulation, no increased recruitment into primary EO771.LMB tumors was visible, though. This indicates that stromal cell types or signals derived from these cells were absent after BMT. For example, tissue-resident macrophages, prominent producers of IL-1β, require approximately 10 weeks after BMT to recover [450]. Thus, it can be speculated, that the absence of these cells may have prevented neutrophil accumulation in the tissue of KO mice thereby abolishing JUNB-dependent metastasis. As JUNB has, however, been shown to differentially control *Il-1β* in different cell types [233, 456], this regulation has to be investigated in more detail in this setting. Moreover, it is possible, that neutrophil infiltration into the primary tumors is irrelevant for metastasis. As neutrophil infiltration into pre-metastatic lungs after BMT was not assessed, this theory cannot be confirmed. Furthermore, whole body irradiation has been reported to induce IL-1β production, which could consequently have facilitated neutrophil recruitment [457]. Yet, neutrophil infiltration into the primary tumors was alleviated after BMT compared to mice which had not undergone irradiation, making this explanation less likely.

5.9. Pharmacological neutrophil depletion is very inefficient

After the bone marrow transplantation experiments had pointed towards a role of stromal JUNB in neutrophil recruitment, neutrophil accumulation and metastasis had still not been linked functionally. Research over the recent years has frequently associated neutrophils with metastasis and several reports pointed towards a function of neutrophils in preparing the pre-metastatic niche [458-461]. In this context, neutrophils have, however, been shown to both stimulate and impair metastatic spread. In agreement with findings in this dissertation, Granot et al. demonstrated neutrophil accumulation in pre-conditioned lungs by 4T1 and MMTV-PyMT tumors [92]. Yet, the authors found these neutrophils to inhibit metastatic seeding in the lung. Other reports confirmed neutrophil accumulation in the pre-metastatic lungs in experimental breast cancer models, but revealed metastasis-promoting effects of neutrophils. Coffelt and colleagues identified neutrophils to stimulate metastasis via suppression of CD8+ T cells [91], whereas Wculek and Malanchi demonstrated that neutrophil-derived leukotrienes promoted

the selection of tumor subpopulations with high tumorigenic potential [96]. Recently, another study revealed that neutrophils in the pre-metastatic niche facilitate colonization by actively capturing tumor cells by forming neutrophil extracellular traps (NET) [407]. NETosis was thereby stimulated by tumor-derived factors, such as IL-8, G-CSF, CXCL1, or CXCL2.

In order to investigate, whether neutrophils indeed facilitated metastasis in this project, neutrophils were ablated pharmacologically using the neutrophil-specific antibody anti-LY6G 1A8. In order to assess the efficiency of neutrophil depletion, neutrophil levels were analyzed in whole blood. Due to the fact that the antibody anti-LY6G 1A8 was already used for *in vivo* injection, flow cytometry analysis was performed using anti-GR1 to exclude false negative results. Anti-GR1 RB6-8C5 and anti-LY6G 1A8 do, however, both recognize an epitope on LY6G and have been reported to compete with each other [314], likely explaining the observed left shift in GR1 mean fluorescence intensity. Administration of anti-LY6G led to a reduction of circulating neutrophil levels in *Junb* KO mice by day 10 after tumor cell inoculation as assessed by flow cytometry. Antibody injection had no effect on other immune cell populations confirming its specificity. Flow cytometric analysis of KO mice showed, that depletion efficiency was, however, already markedly reduced on day 17 and completely abolished at end point, which was confirmed by automated cell counting. These results indicate that anti-LY6G specifically targeted neutrophils and also efficiently bound to LY6G up to day 10. Beyond day 10, binding efficiency decreased potentially owing to the vast abundance of neutrophils in KO animals. Interestingly, Granot and colleagues reported similar findings. The authors reported effective depletion in Balb/c mice until day 14 after tumor cell implantation, but no significant difference thereafter [92]. To date, the mechanism of action for anti-Ly6G antibody 1A8 has not been resolved conclusively. Several researchers have pointed out, that the efficiency of neutrophil depletion using antibody 1A8 varies tremendously depending on the examined tissue [314, 462, 463]. Hence, in order to assure that neutrophils are indeed absent in the tissue, gene expression analysis and immunohistochemistry for LY6B.2 was performed. My results clearly confirmed the upregulation of markers of immune cell infiltration in EO771.LMB primary tumors and pre-metastatic lungs derived from KO animals, but results also proved that anti-LY6G treatment had no effect on neutrophil recruitment into the tissues. Taken together, antibody treatment was not sufficient to efficiently ablate neutrophils in tumor-bearing KO mice. This failure may either be the result of the tremendous numbers of neutrophils in the circulation of KO animals or may actually be a biological effect. As pointed out by Moses and colleagues, treatment with anti-LY6G led to cells being more resistant towards apoptosis and enhanced extramedullary granulopoiesis [463]. Very recently, Faget and colleagues demonstrated ineffectiveness of anti-LY6G in C57BL/6J mice in contrast to other investigated mice strains [464]. The authors explained this finding by the elevation of self-renewal of neutrophils in the circulation as indicated by increased abundance of immature neutrophils and the absence of mature neutrophils in the bone marrow.

Considering the low depletion efficiency, it was, thus, not surprising, that anti-LY6G treatment did not result in a reduction of metastasis as originally expected. Yet, this experiment clearly confirmed the higher metastatic load in the lungs of mice with a stromal deletion of *Junb.*

5.10. Conclusion, future perspectives and clinical relevance

Herein, for the first time, I present direct functional evidence, that stromal JUNB indeed promotes metastatic spread in a murine model of breast cancer. As tumor cell extravasation

was not facilitated in the absence of a primary tumor, it is likely to assume that JUNB influences the initial steps of the metastatic cascade, such as intravasation. Considering, however, that no major defects in the vasculature of the primary tumor were observed and changes in immune cell infiltration, in particular of neutrophils, were much more pronounced in the pre-metastatic lungs, JUNB is more likely to promote distant metastasis by facilitating the establishment of a pre-metastatic niche. Bone marrow transplantation experiments further supported the notion that the accumulation of neutrophils in the pre-metastatic lungs is mediated by loss of JUNB in stromal cells rather than in the hematopoietic compartment. These findings argue for an indirect mechanism rather than a neutrophil-intrinsic effect, which is further supported by JUNB-dependent regulation of several neutrophil recruiting factors, in particular *Il-1β*. Yet, injection of LY6G-specific antibody did not result in an efficient pharmacological ablation of neutrophils, so that direct functional proof to support this hypothesis is still missing. Nevertheless, the neutrophil depletion experiment clearly confirmed the original data, that loss of *Junb* in the stroma facilitates distant metastasis to the lungs.

The results of this dissertation clearly point towards JUNB controlling metastasis via regulation of neutrophil recruitment into the pre-metastatic niche. Due to the inefficient pharmacological neutrophil depletion, neutrophils should be ablated genetically in order to directly proof this hypothesis. Recently, a new mouse model was generated which allows the specific ablation of neutrophils upon injection of diphtheria toxin [465]. Mice expressing Cre recombinase under the control of the *Mrp8* promoter were crossed with ROSA-iDTR^{KI} mice which carry the Cre-inducible simian diphtheria toxin receptor [466]. The necessity to generate mice which are additionally deleted for *Junb* in the stroma on this background, does, however, require an elaborate breeding scheme. Less technical challenging albeit less specific is the pharmacological depletion of neutrophils with anti-GR1. Although GR1 also targets monocytes and MDSCs, this depletion strategy has just very recently proven to be more effective than anti-LY6G [464].

Bone marrow transplantation experiments further indicated that loss of JUNB in the stromal compartment and not in the hematopoietic compartment is required for neutrophil accumulation in pre-metastatic lungs. In order to directly proof this notion and establish the link to metastasis, the spontaneous metastasis assay should be performed in mice with cell type-specific *Junb* ablation. In order to exclude a neutrophil-intrinsic mechanism, *Junb* can be deleted specifically in neutrophils using *Mrp8*-Cre mentioned above [231] or utilizing a *Lyz2*-driven Cre to ablate *Junb* in the myeloid lineage [467-469]. Due to the fact, that neutrophil accumulation was increased upon stromal deletion of *Junb* in this project and ablation in fibroblasts led to an induction of *Il-1β*, it may be speculated that in fact JUNB in fibroblasts is decisive for the metastatic phenotype [456]. For this purpose, metastasis can be studied in the spontaneous assay using Cre recombinase driven by a *Sm22* promoter. This promoter has been described to be specific for myofibroblasts but has also been shown to be active in myeloid cells, thus, reducing its utility for this study [470]. More specifically, loss of JUNB in fibroblasts can be achieved using a *Col1α2*-CreER(T) line [471] which is currently established.

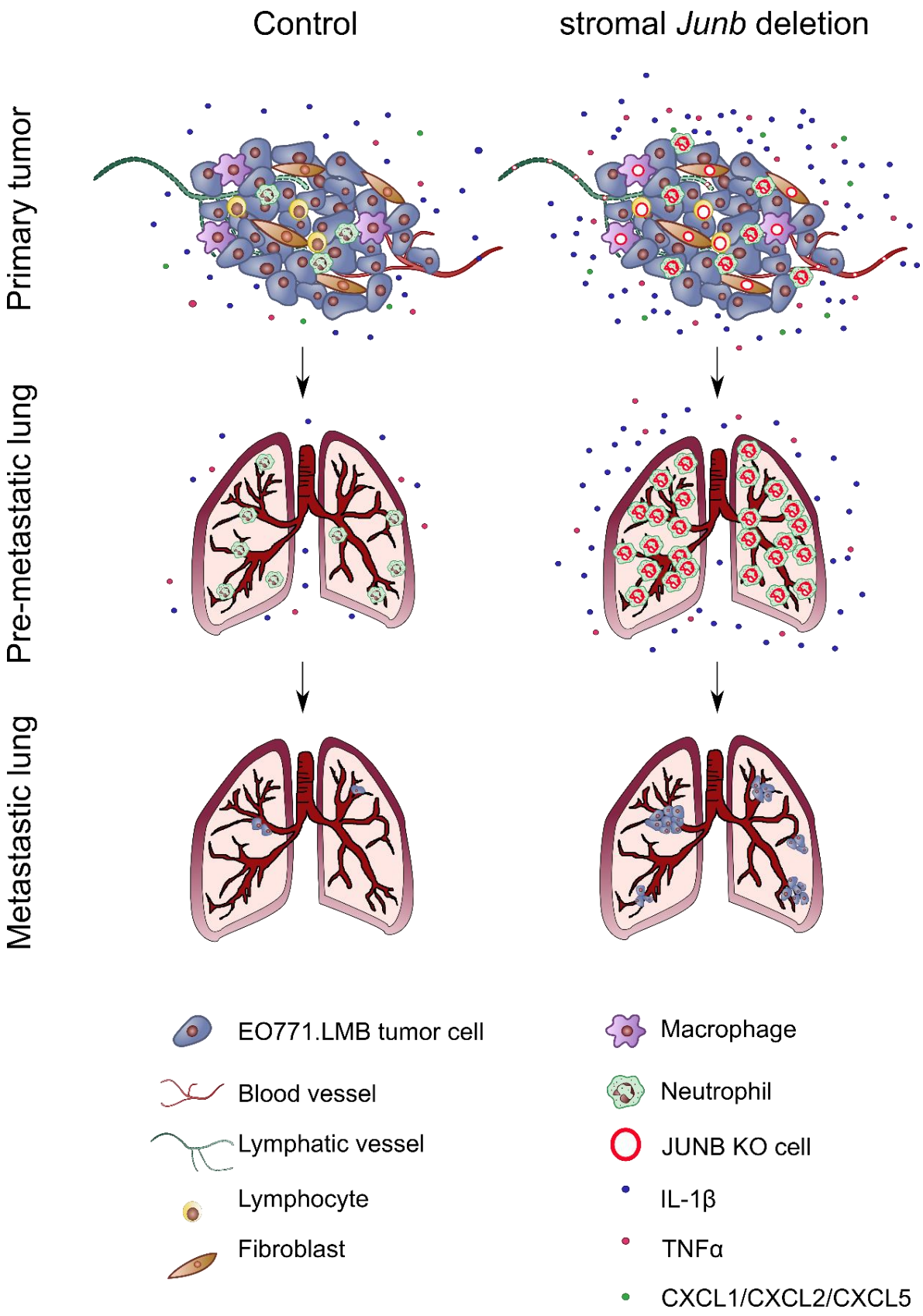

Figure 5-1: Graphical summary of the results of this work.

EO771.LMB primary tumors and the cells of the tumor microenvironment secrete neutrophil-recruiting factors which attract neutrophils to pre-metastatic lungs, which in turn mediate lung metastasis. Upon loss of JUNB in the stroma, higher levels of neutrophil-recruiting factors are released, which potentiate neutrophil accumulation to the pre-metastatic lungs consequently facilitating distant metastasis.

In order to directly assess, whether JUNB enhances metastatic seeding by preparing a pre-metastatic niche, it would be feasible to combine the spontaneous and experimental metastasis assay. Metastasis should be analyzed after tail vein injection in tumor-bearing mice. To investigate, whether specifically extravasation and seeding are facilitated, these experiments should be analyzed at early time points after intravenous injection or in an *ex vivo* pulmonary metastasis assay [472].

The results obtained in this thesis have direct implications in the treatment of breast cancer. Due to the frequent overexpression of AP-1 in breast cancer specimens and its association with tumor progression and invasion, several strategies to inhibit AP-1 activity have been developed [150-155]. On the basis of the findings in this dissertation, it can, however, be speculated that targeting of AP-1/JUNB may in fact even be detrimental to the patient by increasing the risk for the development of distant metastasis. Any potential therapy based on decreasing AP-1/JUNB activity would have to be carefully designed to exclusively target tumor cells but leave cells of the microenvironment unaffected.

6 REFERENCES

6. REFERENCES

1. Cancer Research UK. *Worldwide Cancer Statistics*. 2018 [cited 2018 13 Dec]; Available from: https://www.cancerresearchuk.org/health-professional/cancer-statistics/worldwide-cancer.
2. World Health Organization. *Cancer Key facts*. 2018 [cited 2018 13 Dec]; Available from: https://www.who.int/news-room/fact-sheets/detail/cancer.
3. Celià-Terrassa, T. and Y. Kang, *Distinctive properties of metastasis-initiating cells.* Genes & Development, 2016. **30**(8): p. 892-908.
4. Giampieri, S., et al., *Localized and reversible TGFbeta signalling switches breast cancer cells from cohesive to single cell motility.* Nature Cell Biology, 2009. **11**(11): p. 1287-96.
5. Friedl, P. and D. Gilmour, *Collective cell migration in morphogenesis, regeneration and cancer.* Nat Rev Mol Cell Biol, 2009. **10**(7): p. 445-57.
6. Sahai, E. and C.J. Marshall, *Differing modes of tumour cell invasion have distinct requirements for Rho/ROCK signalling and extracellular proteolysis.* Nature Cell Biology, 2003. **5**(8): p. 711-9.
7. Lu, P., V.M. Weaver, and Z. Werb, *The extracellular matrix: A dynamic niche in cancer progression.* Journal of Cell Biology, 2012. **196**(4): p. 395-406.
8. Sternlicht, M.D., et al., *The stromal proteinase MMP3/stromelysin-1 promotes mammary carcinogenesis.* Cell, 1999. **98**(2): p. 137-46.
9. Lee, K.H. and J.-R. Kim, *Regulation of HGF-mediated cell proliferation and invasion through NF-kappaB, JunB, and MMP-9 cascades in stomach cancer cells.* Clin Exp Metastasis, 2012. **29**(3): p. 263-72.
10. Provenzano, P.P., et al., *Collagen reorganization at the tumor-stromal interface facilitates local invasion.* BMC Medicine, 2006. **4**(1): p. 38.
11. Wyckoff, J.B., J.E. Segall, and J.S. Condeelis, *The Collection of the Motile Population of Cells from a Living Tumor.* Cancer Research, 2000. **60**(19): p. 5401-5404.
12. Wyckoff, J., et al., *A Paracrine Loop between Tumor Cells and Macrophages Is Required for Tumor Cell Migration in Mammary Tumors.* Cancer Research, 2004. **64**(19): p. 7022-7029.
13. *Chapter 3, The Lymphatic Vasculature*, in *Capillary Fluid Exchange: Regulation, Functions, and Pathology.*, J. Scallan, V.H. Huxley, and R.J. Korthuis, Editors. 2010, Morgan & Claypool Life Sciences: San Rafael (CA).
14. Wiley, H.E., et al., *Expression of CC chemokine receptor-7 and regional lymph node metastasis of B16 murine melanoma.* Journal of the National Cancer Institute, 2001. **93**(21): p. 1638-43.
15. Shields, J.D., et al., *Chemokine-mediated migration of melanoma cells towards lymphatics – a mechanism contributing to metastasis.* Oncogene, 2006. **26**: p. 2997.
16. Aceto, N., et al., *En Route to Metastasis: Circulating Tumor Cell Clusters and Epithelial-to-Mesenchymal Transition.* Trends in Cancer, 2015. **1**(1): p. 44-52.
17. Rejniak, K., *Investigating dynamical deformations of tumor cells in circulation: predictions from a theoretical model.* Frontiers in Oncology, 2012. **2**(111).
18. Kim, Y.-N., et al., *Anoikis Resistance: An Essential Prerequisite for Tumor Metastasis.* International Journal of Cell Biology, 2012. **2012**.

19. Mani, S.A., et al., *The Epithelial-Mesenchymal Transition Generates Cells with Properties of Stem Cells.* Cell, 2008. **133**(4): p. 704-715.

20. Duda, D.G., et al., *Malignant cells facilitate lung metastasis by bringing their own soil.* Proceedings of the National Academy of Sciences of the United States of America. 2010. **107**(50): p. 21677-21682.

21. Yu, M., et al., *RNA sequencing of pancreatic circulating tumour cells implicates WNT signalling in metastasis.* Nature, 2012. **487**: p. 510.

22. Aceto, N., et al., *Circulating tumor cell clusters are oligoclonal precursors of breast cancer metastasis.* Cell, 2014. **158**(5): p. 1110-1122.

23. Au, S.H., et al., *Clusters of circulating tumor cells traverse capillary-sized vessels.* Proceedings of the National Academy of Sciences of the United States of America, 2016. **113**(18): p. 4947-4952.

24. Hong, Y., F. Fang, and Q. Zhang, *Circulating tumor cell clusters: What we know and what we expect (Review).* International journal of oncology, 2016. **49**(6): p. 2206-2216.

25. Nieswandt, B., et al., *Lysis of Tumor Cells by Natural Killer Cells in Mice Is Impeded by Platelets.* Cancer Research, 1999. **59**(6): p. 1295-1300.

26. Watson, N.F.S., et al., *Expression of the stress-related MHC class I chain-related protein MICA is an indicator of good prognosis in colorectal cancer patients.* International Journal of Cancer, 2006. **118**(6): p. 1445-1452.

27. Wu, M.-S., et al., *Cytokeratin 8-MHC class I interactions: A potential novel immune escape phenotype by a lymph node metastatic carcinoma cell line.* Biochemical and Biophysical Research Communications, 2013. **441**(3): p. 618-623.

28. Mazel, M., et al., *Frequent expression of PD-L1 on circulating breast cancer cells.* Molecular Oncology, 2015. **9**(9): p. 1773-1782.

29. Yue, C., et al., *Dynamic change of PD-L1 expression on circulating tumor cells in advanced solid tumor patients undergoing PD-1 blockade therapy.* Oncoimmunology, 2018. **7**(7): p. e1438111-e1438111.

30. Baccelli, I., et al., *Identification of a population of blood circulating tumor cells from breast cancer patients that initiates metastasis in a xenograft assay.* Nature Biotechnology, 2013. **31**: p. 539.

31. Steinert, G., et al., *Immune Escape and Survival Mechanisms in Circulating Tumor Cells of Colorectal Cancer.* Cancer Research, 2014. **74**(6): p. 1694-1704.

32. Azevedo, A.S., et al., *Metastasis of circulating tumor cells: favorable soil or suitable biomechanics, or both?* Cell adhesion & migration, 2015. **9**(5): p. 345-356.

33. Miles, F.L., et al., *Stepping out of the flow: capillary extravasation in cancer metastasis.* Clinical & Experimental Metastasis, 2008. **25**(4): p. 305-324.

34. Guba, M., et al., *Overexpression of melanoma inhibitory activity (MIA) enhances extravasation and metastasis of A-mel 3 melanoma cells in vivo.* British Journal of Cancer, 2000. **83**: p. 1216.

35. Steinbauer, M., et al., *GFP-transfected tumor cells are useful in examining early metastasis in vivo, but immune reaction precludes long-term tumor development studies in immunocompetent mice.* Clinical & Experimental Metastasis, 2003. **20**(2): p. 135-141.

36. Reymond, N., B.B. d'Água, and A.J. Ridley, *Crossing the endothelial barrier during metastasis.* Nature Reviews: Cancer, 2013. **13**: p. 858.

37. Schlüter, K., et al., *Organ-specific metastatic tumor cell adhesion and extravasation of colon carcinoma cells with different metastatic potential.* American Journal of Pathology, 2006. **169**(3): p. 1064-1073.

38. Scherbarth, S. and F.W. Orr, *Intravital Videomicroscopic Evidence for Regulation of Metastasis by the Hepatic Microvasculature: Effects of Interleukin-1α on Metastasis and the Location of B16F1 Melanoma Cell Arrest.* Cancer Research, 1997. **57**(18): p. 4105-4110.

39. Haq, M., et al., *Rat Prostate Adenocarcinoma Cells Disseminate to Bone and Adhere Preferentially to Bone Marrow-derived Endothelial Cells.* Cancer Research, 1992. **52**(17): p. 4613-4619.

40. Scott, L.J., et al., *Interactions of human prostatic epithelial cells with bone marrow endothelium: binding and invasion.* British journal of cancer, 2001. **84**(10): p. 1417-1423.

41. Giavazzi, R., et al., *Rolling and adhesion of human tumor cells on vascular endothelium under physiological flow conditions.* Journal of Clinical Investigation, 1993. **92**(6): p. 3038-3044.

42. Laferriere, J., F. Houle, and J. Huot, *Adhesion of HT-29 colon carcinoma cells to endothelial cells requires sequential events involving E-selectin and integrin beta4.* Clinical & Experimental Metastasis, 2004. **21**(3): p. 257-64.

43. Tözeren, A., et al., *E-selectin-mediated dynamic interactions of breast-and colon-cancer cells with endothelial-cell monolayers.* International Journal of Cancer, 1995. **60**(3): p. 426-431.

44. Napier, S.L., et al., *Selectin ligand expression regulates the initial vascular interactions of colon carcinoma cells: the roles of CD44v and alternative sialofucosylated selectin ligands.* Journal of biological chemistry, 2007. **282**(6): p. 3433-41.

45. Mattila, P., M.-L. Majuri, and R. Renkonen, *VLA-4 integrin on sarcoma cell lines recognizes endothelial VCAM-1. Differential regulation of the VLA-4 avidity on various sarcoma cell lines.* International Journal of Cancer, 1992. **52**(6): p. 918-923.

46. Taichman, D.B., et al., *Tumor cell surface alpha 4 beta 1 integrin mediates adhesion to vascular endothelium: demonstration of an interaction with the N-terminal domains of INCAM-110/VCAM-1.* Cell regulation, 1991. **2**(5): p. 347-355.

47. Klemke, M., et al., *High affinity interaction of integrin α4β1 (VLA-4) and vascular cell adhesion molecule 1 (VCAM-1) enhances migration of human melanoma cells across activated endothelial cell layers.* Journal of Cellular Physiology, 2007. **212**(2): p. 368-374.

48. Bauer, K., C. Mierke, and J. Behrens, *Expression profiling reveals genes associated with transendothelial migration of tumor cells: A functional role for αvβ3 integrin.* International Journal of Cancer, 2007. **121**(9): p. 1910-1918.

49. Fujisaki, T., et al., *CD44 Stimulation Induces Integrin-mediated Adhesion of Colon Cancer Cell Lines to Endothelial Cells by Up-Regulation of Integrins and c-Met and Activation of Integrins.* Cancer Research, 1999. **59**(17): p. 4427-4434.

50. Luzzi, K.J., et al., *Multistep Nature of Metastatic Inefficiency: Dormancy of Solitary Cells after Successful Extravasation and Limited Survival of Early Micrometastases.* American Journal of Pathology, 1998. **153**(3): p. 865-873.

51. Gomis, R.R. and S. Gawrzak, *Tumor cell dormancy.* Molecular Oncology, 2017. **11**(1): p. 62-78.

52. Shibue, T., et al., *The Outgrowth of Micrometastases Is Enabled by the Formation of Filopodium-like Protrusions.* Cancer Discovery, 2012. **2**(8): p. 706-721.

53. Paget, S., *The distribution of secondary growths in cancer of the breast.* Lancet, 1889. **133**(3421): p. 571-573.

54. Virchow, R., *Die Cellularpathologie in ihrer Begründung auf physiologische und pathologische Gewebelehre*. Vol. 1. 1858: August Hirschwald.

55. Ewing, J., *Neoplastic Diseases: A Treatise on Tumours.* 2 ed. 1922, Philadelphia and London: W. B. Saunders company. 1127.

56. Van Marck, V.L. and M.E. Bracke, *Epithelial-Mesenchymal Transitions in Human Cancer*. Madame Curie Bioscience Database. 2000-2013, Austin: Landes Bioscience.

57. Seyfried, T.N. and L.C. Huysentruyt, *On the origin of cancer metastasis.* Critical reviews in oncogenesis, 2013. **18**(1-2): p. 43-73.

58. Reiter, J.G., et al., *Minimal functional driver gene heterogeneity among untreated metastases.* Science, 2018. **361**(6406): p. 1033-1037.

59. Venza, M., et al., *DNA methylation-induced E-cadherin silencing is correlated with the clinicopathological features of melanoma.* Oncology Reports, 2016. **35**(4): p. 2451-60.

60. Jensen, K., et al., *Dynamic changes in E-cadherin gene promoter methylation during metastatic progression in papillary thyroid cancer.* Experimental and Therapeutic Medicine, 2010. **1**(3): p. 457-462.

61. Lawrence, M.S., et al., *Mutational heterogeneity in cancer and the search for new cancer-associated genes.* Nature, 2013. **499**(7457): p. 214-218.

62. Tas, F., *Metastatic Behavior in Melanoma: Timing, Pattern, Survival, and Influencing Factors* Journal of Oncology, 2012. **2012**: p. 9.

63. Reinhard, H., et al., *Rhabdoid tumors in children: prognostic factors in 70 patients diagnosed in Germany.* Journal of Clinical Oncology, 2008. **19**(3): p. 819-23.

64. Zeltzer, P.M., et al., *Metastasis Stage, Adjuvant Treatment, and Residual Tumor Are Prognostic Factors for Medulloblastoma in Children: Conclusions From the Children's Cancer Group 921 Randomized Phase III Study.* Journal of Clinical Oncology, 1999. **17**(3): p. 832-832.

65. Herman, J.G., et al., *Inactivation of CDKN2/p16/MTS1 Gene Is Frequently Associated with Abberant DNA Methylation in All Common Human Cancers.* Cancer Research, 1995.

66. Hanada, M., et al., *bcl-2 gene hypomethylation and high-level expression in B-cell chronic lymphocytic leukemia.* Blood, 1993. **82**(6): p. 1820-1828.

67. Watt, P.M., R. Kumar, and U.R. Kees, *Promoter demethylation accompanies reactivation of the HOX11 proto-oncogene in leukemia.* Genes, Chromosomes and Cancer, 2000. **29**(4): p. 371-377.

68. Sleeman, J.P., *The lymph node pre-metastatic niche.* Journal of Molecular Medicine (Berlin, Germany), 2015.

69. Kaplan, R.N., et al., *VEGFR1-positive haematopoietic bone marrow progenitors initiate the pre-metastatic niche.* Nature, 2005. **438**: p. 820.

70. Peinado, H., et al., *Pre-metastatic niches: organ-specific homes for metastases.* Nature Reviews: Cancer, 2017. **17**: p. 302.

71. Chin, A.R. and S.E. Wang, *Cancer Tills the Premetastatic Field: Mechanistic Basis and Clinical Implications.* Clinical Cancer Research, 2016. **22**(15): p. 3725-3733.

72. Huang, Y., et al., *Pulmonary Vascular Destabilization in the Premetastatic Phase Facilitates Lung Metastasis.* Cancer Research, 2009. **69**(19): p. 7529-7537.

73. Kienast, Y., et al., *Ang-2-VEGF-A CrossMab, a novel bispecific human IgG1 antibody blocking VEGF-A and Ang-2 functions simultaneously, mediates potent anti-tumor, anti-angiogenic, and anti-metastatic efficacy.* Clinical Cancer Research, 2013: p. clincanres.0081.2013.

74. El Rayes, T., et al., *Regulation of Tumor Progression and Metastasis by Bone-Marrow Derived Microenvironments*. Biomarkers of the Tumor Microenvironment. 2017: Springer International Publishing.

75. Grzelak, C.A., A.R. Lim, and C.M. Ghajar, *More Than a Barrier: How the Endothelium Instructs Metastasis*. Biomarkers of the Tumor Microenvironment, ed. L.A. Akslen and R.S. Watnick. Vol. 3. 2017: Springer International Publishing. 25-53.

76. Skobe, M., et al., *Induction of tumor lymphangiogenesis by VEGF-C promotes breast cancer metastasis.* Nature Medicine, 2001. **7**: p. 192.

77. Kajiya, K., et al., *Hepatocyte growth factor promotes lymphatic vessel formation and function.* EMBO Journal, 2005. **24**(16): p. 2885-2895.

78. Hirakawa, S., et al., *VEGF-C–induced lymphangiogenesis in sentinel lymph nodes promotes tumor metastasis to distant sites.* Blood, 2007. **109**(3): p. 1010-1017.

79. Quagliata, L., et al., *Inhibition of VEGFR-3 activation in tumor-draining lymph nodes suppresses the outgrowth of lymph node metastases in the MT-450 syngeneic rat breast cancer model.* Clinical & Experimental Metastasis, 2014. **31**(3): p. 351-365.

80. Karaman, S. and M. Detmar, *Mechanisms of lymphatic metastasis.* Journal of Clinical Investigation, 2014. **124**(3): p. 922-928.

81. Harrell, M.I., B.M. Iritani, and A. Ruddell, *Tumor-Induced Sentinel Lymph Node Lymphangiogenesis and Increased Lymph Flow Precede Melanoma Metastasis.* American Journal of Pathology, 2007. **170**(2): p. 774-786.

82. Erler, J.T., et al., *Lysyl oxidase is essential for hypoxia-induced metastasis.* Nature, 2006. **440**: p. 1222.

83. Høye, A.M. and J.T. Erler, *Structural ECM components in the premetastatic and metastatic niche.* American Journal of Physiology: Cell Physiology, 2016. **310**(11): p. C955-C967.

84. Aguado, B.A., et al., *Extracellular matrix mediators of metastatic cell colonization characterized using scaffold mimics of the pre-metastatic niche.* Acta Biomaterialia, 2016. **33**: p. 13-24.

85. Liu, Y. and X. Cao, *Characteristics and Significance of the Pre-metastatic Niche.* Cancer Cell, 2016. **30**(5): p. 668-681.

86. Fong, M.Y., et al., *Breast-cancer-secreted miR-122 reprograms glucose metabolism in premetastatic niche to promote metastasis.* Nature Cell Biology, 2015. **17**: p. 183.

87. Hiratsuka, S., et al., *MMP9 induction by vascular endothelial growth factor receptor-1 is involved in lung-specific metastasis.* Cancer Cell, 2002. **2**(4): p. 289-300.

88. Costa-Silva, B., et al., *Pancreatic cancer exosomes initiate pre-metastatic niche formation in the liver.* Nature Cell Biology, 2015. **17**: p. 816.

89. Hiratsuka, S., et al., *The S100A8–serum amyloid A3–TLR4 paracrine cascade establishes a pre-metastatic phase.* Nature Cell Biology, 2008. **10**: p. 1349.

90. Seubert, B., et al., *Tissue inhibitor of metalloproteinases (TIMP)-1 creates a premetastatic niche in the liver through SDF-1/CXCR4-dependent neutrophil recruitment in mice.* Hepatology, 2015. **61**(1): p. 238-248.

91. Coffelt, S.B., et al., *IL-17-producing γδ T cells and neutrophils conspire to promote breast cancer metastasis.* Nature, 2015. **522**: p. 345.

92. Granot, Z., et al., *Tumor Entrained Neutrophils Inhibit Seeding in the Premetastatic Lung.* Cancer Cell, 2011. **20**(3): p. 300-314.

93. Hiratsuka, S., et al., *Tumour-mediated upregulation of chemoattractants and recruitment of myeloid cells predetermines lung metastasis.* Nature Cell Biology, 2006. **8**: p. 1369.

94. Kowanetz, M., et al., *Granulocyte-colony stimulating factor promotes lung metastasis through mobilization of Ly6G+Ly6C+ granulocytes.* Proceedings of the National Academy of Sciences of the United States of America, 2010. **107**(50): p. 21248-21255.

95. Wu, C.-F., et al., *The lack of type I interferon induces neutrophil-mediated pre-metastatic niche formation in the mouse lung.* International Journal of Cancer, 2015. **137**.

96. Wculek, S.K. and I. Malanchi, *Neutrophils support lung colonization of metastasis-initiating breast cancer cells.* Nature, 2015. **528**(7582): p. 413-417.

97. Fremder, E., et al., *Tumor-derived microparticles induce bone marrow-derived cell mobilization and tumor homing: A process regulated by osteopontin.* International Journal of Cancer, 2014. **135**(2): p. 270-281.

98. Kang, Y., et al., *A multigenic program mediating breast cancer metastasis to bone.* Cancer Cell, 2003. **3**(6): p. 537-549.

99. Müller, A., et al., *Involvement of chemokine receptors in breast cancer metastasis.* Nature, 2001. **410**: p. 50.

100. Yan, H.H., et al., *Gr-1+CD11b+ Myeloid Cells Tip the Balance of Immune Protection to Tumor Promotion in the Premetastatic Lung.* Cancer Research, 2010. **70**(15): p. 6139-6149.

101. Carter, R.Z., et al., *Tumour but not stromal expression of β3 integrin is essential, and is required early, for spontaneous dissemination of bone-metastatic breast cancer.* Journal of Pathology, 2015. **235**(5): p. 760-772.

102. Budczies, J., et al., *The landscape of metastatic progression patterns across major human cancers.* Oncotarget, 2014. **6**(1): p. 570-583.

103. Kakhki, V.R.D., et al., *Pattern and distribution of bone metastases in common malignant tumors.* Nuclear Medicine Review. Central & Eastern Europe, 2013. **16**(2): p. 66-69.

104. Weiss, L., *Comments on hematogenous metastatic patterns in humans as revealed by autopsy.* Clinical & Experimental Metastasis, 1992. **10**(3): p. 191-9.

105. Urosevic, J., et al., *Colon cancer cells colonize the lung from established liver metastases through p38 MAPK signalling and PTHLH.* Nature Cell Biology, 2014. **16**: p. 685.

106. Obenauf, A.C. and J. Massagué, *Surviving at a distance: organ specific metastasis.* Trends in Cancer, 2015. **1**(1): p. 76-91.

107. Aird, W.C., *Phenotypic Heterogeneity of the Endothelium.* Circulation Research, 2007. **100**(2): p. 158-173.

108. Pauli, B.U. and C.L. Lee, *Organ preference of metastasis. The role of organ-specifically modulated endothelial cells.* Laboratory Investigation, 1988. **58**(4): p. 379-87.

109. Huang, R. and E.K. Rofstad, *Integrins as therapeutic targets in the organ-specific metastasis of human malignant melanoma.* Journal of Experimental & Clinical Cancer Research, 2018. **37**(1): p. 92.

110. Brodt, P., et al., *Liver endothelial E-selectin mediates carcinoma cell adhesion and promotes liver metastasis.* International Journal of Cancer, 1997. **71**(4): p. 612-619.

111. Hiratsuka, S., et al., *Endothelial focal adhesion kinase mediates cancer cell homing to discrete regions of the lungs via E-selectin up-regulation.* Proceedings of the National Academy of Sciences of the United States of America, 2011. **108**(9): p. 3725-30.

112. Lafouresse, F., et al., *L-selectin controls trafficking of chronic lymphocytic leukemia cells in lymph node high endothelial venules in vivo.* Blood, 2015. **126**(11): p. 1336-1345.

113. Benedicto, A., I. Romayor, and B. Arteta, *Role of liver ICAM-1 in metastasis.* Oncology letters, 2017. **14**(4): p. 3883-3892.

114. Hoshino, A., et al., *Tumour exosome integrins determine organotropic metastasis.* Nature, 2015. **527**: p. 329.

115. Follain, G., et al., *Hemodynamic Forces Tune the Arrest, Adhesion, and Extravasation of Circulating Tumor Cells.* Developmental Cell, 2018. **45**(1): p. 33-52.e12.

116. Popper, H.H., *Progression and metastasis of lung cancer.* Cancer metastasis reviews, 2016. **35**(1): p. 75-91.

117. Yates, L.R., et al., *Genomic Evolution of Breast Cancer Metastasis and Relapse.* Cancer Cell, 2017. **32**(2): p. 169-184.e7.

118. Zbytek, B., et al., *Current concepts of metastasis in melanoma.* Expert review of dermatology, 2008. **3**(5): p. 569-585.

119. Sinn, H.-P. and H. Kreipe, *A Brief Overview of the WHO Classification of Breast Tumors, 4th Edition, Focusing on Issues and Updates from the 3rd Edition.* Breast Care, 2013. **8**(2): p. 149-154.

120. Harris, L.N., et al., *Use of Biomarkers to Guide Decisions on Adjuvant Systemic Therapy for Women With Early-Stage Invasive Breast Cancer: American Society of Clinical Oncology Clinical Practice Guideline.* Journal of Clinical Oncology, 2016. **34**(10): p. 1134-1150.

121. Hortobagyi, G.N., S.B. Edge, and A. Giuliano, *New and Important Changes in the TNM Staging System for Breast Cancer*. American Society of Clinical Oncology Educational Book 38. Vol. 38. 2018. 457-467.

122. Sørlie, T., et al., *Gene expression patterns of breast carcinomas distinguish tumor subclasses with clinical implications.* Proceedings of the National Academy of Sciences of the United States of America, 2001. **98**(19): p. 10869-10874.

123. Dai, X., et al., *Breast cancer intrinsic subtype classification, clinical use and future trends.* American journal of cancer research, 2015. **5**(10): p. 2929-2943.

124. Fan, C., et al., *Concordance among Gene-Expression–Based Predictors for Breast Cancer.* New England Journal of Medicine, 2006. **355**(6): p. 560-569.

125. Hu, Z., et al., *The molecular portraits of breast tumors are conserved across microarray platforms.* BMC Genomics, 2006. **7**(1): p. 96.

126. Parker, J.S., et al., *Supervised Risk Predictor of Breast Cancer Based on Intrinsic Subtypes.* Journal of Clinical Oncology, 2009. **27**(8): p. 1160-1167.

127. Cheang, M.C.U., et al., *Ki67 Index, HER2 Status, and Prognosis of Patients With Luminal B Breast Cancer.* Journal of the National Cancer Institute, 2009. **101**(10): p. 736-750.

128. Wu, Q., et al., *Breast cancer subtypes predict the preferential site of distant metastases: a SEER based study.* Oncotarget, 2017. **8**(17): p. 27990-27996.

129. Perou, C.M., et al., *Molecular portraits of human breast tumours.* Nature, 2000. **406**: p. 747.

130. Sotiriou, C., et al., *Breast cancer classification and prognosis based on gene expression profiles from a population-based study.* Proceedings of the National Academy of Sciences of the United States of America, 2003. **100**(18): p. 10393-10398.

131. Kennecke, H., et al., *Metastatic Behavior of Breast Cancer Subtypes.* Journal of Clinical Oncology, 2010. **28**(20): p. 3271-3277.

132. Chen, W., et al., *Organotropism: new insights into molecular mechanisms of breast cancer metastasis.* npj Precision Oncology, 2018. **2**(1): p. 4.

133. Arpino, G., et al., *Infiltrating lobular carcinoma of the breast: tumor characteristics and clinical outcome.* Breast Cancer Research, 2004. **6**(3): p. R149-R156.

134. Siegel, R.L., K.D. Miller, and A. Jemal, *Cancer statistics, 2018.* CA: A Cancer Journal for Clinicians, 2018. **68**(1): p. 7-30.

135. Redig, A.J. and S.S. McAllister, *Breast cancer as a systemic disease: a view of metastasis.* Journal of Internal Medicine, 2013. **274**(2): p. 113-126.

136. Chan, C.W.H., et al., *Novel Strategies on Personalized Medicine for Breast Cancer Treatment: An Update.* International journal of molecular sciences, 2017. **18**(11): p. 2423.

137. Cancer Research UK. *Treatment options*. 2017 [cited 2019 12 Jan]; Available from: https://www.cancerresearchuk.org/about-cancer/breast-cancer/treatment/treatment-decisions

138. Fallahpour, S., et al., *Breast cancer survival by molecular subtype: a population-based analysis of cancer registry data.* CMAJ Open, 2017. **5**(3): p. E734-E739.

139. Nagini, S., *Breast Cancer: Current Molecular Therapeutic Targets and New Players.* Anti-Cancer Agents in Medicinal Chemistry, 2017. **17**(2): p. 152-163.

140. Tong, C.W.S., et al., *Recent Advances in the Treatment of Breast Cancer.* Frontiers in Oncology, 2018. **8**(227).

141. Johnston, S.R.D., et al., *Fulvestrant plus anastrozole or placebo versus exemestane alone after progression on non-steroidal aromatase inhibitors in postmenopausal patients with hormone-receptor-positive locally advanced or metastatic breast cancer (SoFEA): a composite, multicentre, phase 3 randomised trial.* Lancet Oncology, 2013. **14**(10): p. 989-998.

142. Berrada, N., S. Delaloge, and F. André, *Treatment of triple-negative metastatic breast cancer: toward individualized targeted treatments or chemosensitization?* Annals of Oncology, 2010. **21**(suppl_7): p. vii30-vii35.

143. Robson, M., et al., *Olaparib for Metastatic Breast Cancer in Patients with a Germline BRCA Mutation.* New England Journal of Medicine, 2017. **377**(6): p. 523-533.

144. Brahmer, J., et al., *Nivolumab versus Docetaxel in Advanced Squamous-Cell Non–Small-Cell Lung Cancer.* New England Journal of Medicine, 2015. **373**(2): p. 123-135.

145. Motzer, R.J., et al., *Nivolumab versus Everolimus in Advanced Renal-Cell Carcinoma.* New England Journal of Medicine, 2015. **373**(19): p. 1803-1813.

146. Ferris, R.L., et al., *Nivolumab for Recurrent Squamous-Cell Carcinoma of the Head and Neck.* New England Journal of Medicine, 2016. **375**(19): p. 1856-1867.

147. Rittmeyer, A., et al., *Atezolizumab versus docetaxel in patients with previously treated non-small-cell lung cancer (OAK): a phase 3, open-label, multicentre randomised controlled trial.* Lancet, 2017. **389**(10066): p. 255-265.

148. Adams, S., et al., *Phase 2 study of pembrolizumab (pembro) monotherapy for previously treated metastatic triple-negative breast cancer (mTNBC): KEYNOTE-086 cohort A.* Journal of Clinical Oncology, 2017. **35**(15_suppl): p. 1008-1008.

149. McCubrey, J.A., et al., *Targeting signal transduction pathways to eliminate chemotherapeutic drug resistance and cancer stem cells.* Advances in enzyme regulation, 2010. **50**(1): p. 285-307.

150. Shen, Q., P.H.J.J.o.M.G.B. Brown, and Neoplasia, *Novel Agents for the Prevention of Breast Cancer: Targeting Transcription Factors and Signal Transduction Pathways.* Journal of Mammary Gland Biology and Neoplasia, 2003. **8**(1): p. 45-73.

151. Ludes-Meyers, J.H., et al., *AP-1 blockade inhibits the growth of normal and malignant breast cells.* Oncogene, 2001. **20**: p. 2771.

152. Liu, Y., et al., *AP-1 blockade in breast cancer cells causes cell cycle arrest by suppressing G1 cyclin expression and reducing cyclin-dependent kinase activity.* Oncogene, 2004. **23**: p. 8238.

153. Liu, Y., et al., *Inhibition of AP-1 transcription factor causes blockade of multiple signal transduction pathways and inhibits breast cancer growth.* Oncogene, 2002. **21**: p. 7680.

154. Leaner, V.D., H. Donninger, and M.J. Birrer, *Transcription Factors as Targets for Cancer Therapy: AP-1 a Potential Therapeutic Target.* Current Cancer Therapy Reviews, 2007. **3**(1): p. 1-6.

155. Ye, N., et al., *Small Molecule Inhibitors Targeting Activator Protein 1 (AP-1).* Journal of Medicinal Chemistry, 2014. **57**(16): p. 6930-6948.

156. Hess, J., P. Angel, and M. Schorpp-Kistner, *AP-1 subunits: quarrel and harmony among siblings.* Journal of cell science, 2004. **117**(Pt 25): p. 5965-73.

157. Shaulian, E., *AP-1: The Jun proteins: Oncogenes or tumor suppressors in disguise?* Cell Signal, 2010. **22**(6): p. 894-9.

158. Shaulian, E. and K. Michael, *AP-1 in cell proliferation and survival.* Oncogene, 2001. **20**(19): p. 2390-2400.

159. Andrecht, S., et al., *Cell cycle promoting activity of JunB through cyclin A activation.* Journal of biological chemistry, 2002. **277**(39): p. 35961-8.

160. Zenz, R., et al., *Psoriasis-like skin disease and arthritis caused by inducible epidermal deletion of Jun proteins.* Nature, 2005. **437**(7057): p. 369-75.

161. Thomsen, M.K., et al., *JUNB/AP-1 controls IFN-gamma during inflammatory liver disease.* Journal of Clinical investigation, 2013. **123**(12): p. 5258-68.

162. Chinenov, Y. and T.K. Kerppola, *Close encounters of many kinds: Fos-Jun interactions that mediate transcription regulatory specificity.* Oncogene, 2001. **20**: p. 2438.

163. McBride, K. and M. Nemer, *The C-Terminal Domain of c-fos Is Required for Activation of an AP-1 Site Specific for jun-fos Heterodimers.* Molecular and Cellular Biology, 1998. **18**(9): p. 5073-5081.

164. Ramirez-Carrozzi, V. and T. Kerppola, *Asymmetric Recognition of Nonconsensus AP-1 Sites by Fos-Jun and Jun-Jun Influences Transcriptional Cooperativity with NFAT1.* Molecular and Cellular Biology, 2003. **23**(5): p. 1737-1749.

165. Angel, P. and J. Hess, *The Multi-Gene Family of Transcription Factor AP-1*. 2 ed. Handbook of Cell Signaling. Vol. 1. 2010: Elsevier Inc. 3048.

166. Glover, J.N.M. and S.C. Harrison, *Crystal structure of the heterodimeric bZIP transcription factor c-Fos–c-Jun bound to DNA.* Nature, 1995. **373**(6511): p. 257-261.

167. Ryder, K. and D. Nathans, *Induction of protooncogene c-jun by serum growth factors.* Proceedings of the National Academy of Sciences of the United States of America, 1988. **85**(22): p. 8464-8467.

168. Lamph, W.W., et al., *Induction of proto-oncogene JUN/AP-1 by serum and TPA.* Nature, 1988. **334**(6183): p. 629-631.

169. Kyriakis, J.M., *Activation of the AP-1 Transcription Factor by Inflammatory Cytokines of the TNF Family.* Gene Expression, 1999. **7**(4-5): p. 217-231.

170. Woodgett, J.R., J. Avruch, and J.M. Kyriakis, *Regulation of nuclear transcription factors by stress signals.* Clinical and Experimental Pharmacology and Physiology, 1995. **22**(4): p. 281-283.

171. Swenson, W.G., B.R.K. Wuertz, and F.G. Ondrey, *Tobacco carcinogen mediated up-regulation of AP-1 dependent pro-angiogenic cytokines in head and neck carcinogenesis.* Molecular Carcinogenesis, 2011. **50**(9): p. 668-679.

172. Angel, P., et al., *The jun proto-oncogene is positively autoregulated by its product, Jun/AP-1.* Cell, 1988. **55**(5): p. 875-885.

173. Angel, P., et al., *Phorbol ester-inducible genes contain a common cis element recognized by a TPA-modulated trans-acting factor.* Cell, 1987. **49**(6): p. 729-739.

174. Kamei, Y., et al., *A CBP Integrator Complex Mediates Transcriptional Activation and AP-1 Inhibition by Nuclear Receptors.* Cell, 1996. **85**(3): p. 403-414.

175. Horvai, A.E., et al., *Nuclear integration of JAK/STAT and Ras/AP-1 signaling by CBP and p300.* Proceedings of the National Academy of Sciences of the United States of America, 1997. **94**(4): p. 1074-1079.

176. Liberati, N.T., et al., *Smads bind directly to the Jun family of AP-1 transcription factors.* Proceedings of the National Academy of Sciences of the United States of America, 1999. **96**(9): p. 4844-4849.

177. Chen, L., et al., *Structure of the DNA-binding domains from NFAT, Fos and Jun bound specifically to DNA.* Nature, 1998. **392**: p. 42.

178. Bassuk, A.G. and J.M. Leiden, *A direct physical association between ETS and AP-1 transcription factors in normal human T cells.* Immunity, 1995. **3**(2): p. 223-237.

179. Hilberg, F., et al., *c-Jun is essential for normal mouse development and hepatogenesis.* Nature, 1993. **365**(6442): p. 179-181.

180. Johnson, R.S., et al., *A null mutation at the c-jun locus causes embryonic lethality and retarded cell growth in culture.* Genes & Development, 1993. **7**(7b): p. 1309-1317.

181. Schorpp-Kistner, M., et al., *JunB is essential for mammalian placentation.* EMBO Journal, 1999. **18**(4): p. 934-48.

182. Schreiber, M., et al., *Placental vascularisation requires the AP-1 component fra1.* Development, 2000. **127**(22): p. 4937-4948.

183. Karreth, F., et al., *The AP1 transcription factor Fra2 is required for efficient cartilage development.* Development, 2004. **131**(22): p. 5717-5725.

184. Passegué, E., et al., *JunB can substitute for Jun in mouse development and cell proliferation.* Nature Genetics, 2002. **30**: p. 158.

185. Eferl, R., et al., *Functions of c-Jun in liver and heart development.* Journal of cell biology, 1999. **145**(5): p. 1049-1061.

186. Zenz, R., et al., *c-Jun regulates eyelid closure and skin tumor development through EGFR signaling.* Developmental Cell, 2003. **4**(6): p. 879-89.

187. Szabowski, A., et al., *c-Jun and JunB Antagonistically Control Cytokine-Regulated Mesenchymal & Epidermal Interaction in Skin.* Cell, 2000. **103**(5): p. 745-755.

188. Stepniak, E., et al., *c-Jun/AP-1 controls liver regeneration by repressing p53/p21 and p38 MAPK activity.* Genes & Development, 2006. **20**(16): p. 2306-2314.

189. Schmidt, D., et al., *Critical role for NF-kappaB-induced JunB in VEGF regulation and tumor angiogenesis.* EMBO Journal, 2007. **26**(3): p. 710-9.

190. Li, B., et al., *Regulation of IL-4 expression by the transcription factor JunB during T helper cell differentiation.* EMBO Journal, 1999. **18**(2): p. 420-432.

191. Hartenstein, B., et al., *Th2 cell-specific cytokine expression and allergen-induced airway inflammation depend on JunB.* EMBO Journal, 2002. **21**(23): p. 6321-9.

192. Wagner, E.F., *Functions of AP1 (Fos/Jun) in bone development.* Annals of the rheumatic diseases, 2002. **61 Suppl 2**(Suppl 2): p. ii40-ii42.

193. Velazquez, F.N., et al., *Brain development is impaired in c-fos -/- mice.* Oncotarget, 2015. **6**(19): p. 16883-16901.

194. Bakiri, L., et al., *Cell cycle-dependent variations in c-Jun and JunB phosphorylation: a role in the control of cyclin D1 expression.* EMBO Journal, 2000. **19**(9): p. 2056-2068.

195. Sunters, A., et al., *Accelerated Cell Cycle Progression in Osteoblasts Overexpressing the c-fos Proto-oncogene: Induction of Cyclin A and Enhanced CDK2 Activity.* Journal of Biological Chemistry, 2004. **279**(11): p. 9882-9891.

196. Passegué, E. and E.F. Wagner, *JunB suppresses cell proliferation by transcriptional activation of p16INK4a expression.* EMBO Journal, 2000. **19**(12): p. 2969-79.

197. Maki, Y., et al., *Avian sarcoma virus 17 carries the jun oncogene.* Proceedings of the National Academy of Sciences of the United States of America, 1987. **84**(9): p. 2848-2852.

198. van Straaten, F., et al., *Complete nucleotide sequence of a human c-onc gene: deduced amino acid sequence of the human c-fos protein.* Proceedings of the National Academy of Sciences of the United States of America, 1983. **80**(11): p. 3183-3187.

199. Tom Curran, A., et al., *Viral and cellular fos proteins: A comparative analysis.* Cell, 1984. **36**(2): p. 259-268.

200. Dusty Miller, A., T. Curran, and I.M. Verma, *c-fos protein can induce cellular transformation: A novel mechanism of activation of a cellular oncogene.* Cell, 1984. **36**(1): p. 51-60.

201. Rüther, U., et al., *Deregulated c-fos expression interferes with normal bone development in transgenic mice.* Nature, 1987. **325**(6103): p. 412-6.

202. Schütte, J., J.D. Minna, and M.J. Birrer, *Deregulated expression of human c-jun transforms primary rat embryo cells in cooperation with an activated c-Ha-ras gene and transforms rat-1a cells as a single gene.* Proceedings of the National Academy of Sciences of the United States of America, 1989. **86**(7): p. 2257-61.

203. Saez, E., et al., *c-fos is required for malignant progression of skin tumors.* Cell, 1995. **82**(5): p. 721-732.

204. Young, M.R., et al., *Transgenic mice demonstrate AP-1 (activator protein-1) transactivation is required for tumor promotion.* Proceedings of the National Academy of Sciences of the United States of America, 1999. **96**(17): p. 9827-32.

205. Eferl, R., et al., *Liver Tumor Development: c-Jun Antagonizes the Proapoptotic Activity of p53.* Cell, 2003. **112**(2): p. 181-192.

206. Schütte, J., et al., *jun-B inhibits and c-fos stimulates the transforming and trans-activating activities of c-jun.* Cell, 1989. **59**(6): p. 987-97.

207. Steidl, U., et al., *Essential role of Jun family transcription factors in PU.1 knockdown-induced leukemic stem cells.* Nature Genetics, 2006. **38**(11): p. 1269-77.

208. Yang, M.Y., et al., *JunB gene expression is inactivated by methylation in chronic myeloid leukemia.* Blood, 2003. **101**(8): p. 3205-11.

209. Passegue, E., et al., *Chronic myeloid leukemia with increased granulocyte progenitors in mice lacking junB expression in the myeloid lineage.* Cell, 2001. **104**(1): p. 21-32.

210. Kharman-Biz, A., et al., *Expression of activator protein-1 (AP-1) family members in breast cancer.* BMC Cancer, 2013. **13**: p. 441.

211. Langer, S., et al., *Jun and Fos family protein expression in human breast cancer: correlation of protein expression and clinicopathological parameters.* European journal of gynaecological oncology, 2006. **27**(4): p. 345-52.

212. Konishi, N., et al., *Function of JunB in Transient Amplifying Cell Senescence and Progression of Human Prostate Cancer.* Clinical Cancer Research, 2008. **14**(14): p. 4408-4416.

213. Thomsen, M.K., et al., *Loss of JUNB/AP-1 promotes invasive prostate cancer.* Cell death and differentiation, 2015. **22**(4): p. 574-82.

214. Schorpp, M., et al., *The human ubiquitin C promoter directs high ubiquitous expression of transgenes in mice.* Nucleic acids research, 1996. **24**(9): p. 1787-1788.

215. Mathas, S., et al., *Aberrantly expressed c-Jun and JunB are a hallmark of Hodgkin lymphoma cells, stimulate proliferation and synergize with NF-κB.* EMBO Journal, 2002. **21**(15): p. 4104-4113.

216. Mao, X., et al., *Amplification and overexpression of JUNB is associated with primary cutaneous T-cell lymphomas.* Blood, 2003. **101**(4): p. 1513-1519.

217. Rassidakis, G.Z., et al., *JunB expression is a common feature of CD30+ lymphomas and lymphomatoid papulosis.* Modern pathology, 2005. **18**(10): p. 1365-1370.

218. Wang, H., M. Birkenbach, and J. Hart, *Expression of Jun family members in human colorectal adenocarcinoma.* Carcinogenesis, 2000. **21**(7): p. 1313-7.

219. Neyns, B., et al., *Expression of the jun family of genes in human ovarian cancer and normal ovarian surface epithelium.* Oncogene, 1996. **12**(6): p. 1247-57.

220. Kanno, T., et al., *JunB promotes cell invasion and angiogenesis in VHL-defective renal cell carcinoma.* Oncogene, 2012. **31**(25): p. 3098-110.

221. Bossy-Wetzel, E., R. Bravo, and D. Hanahan, *Transcription factors junB and c-jun are selectively up-regulated and functionally implicated in fibrosarcoma development.* Genes & Development, 1992. **6**(12a): p. 2340-2351.

222. Johannessen, C.M., et al., *A melanocyte lineage program confers resistance to MAP kinase pathway inhibition.* Nature, 2013. **504**: p. 138.

223. Sundqvist, A., et al., *Specific interactions between Smad proteins and AP-1 components determine TGFbeta-induced breast cancer cell invasion.* Oncogene, 2013. **32**(31): p. 3606-15.

224. Pang, M.F., et al., *TGF-beta1-induced EMT promotes targeted migration of breast cancer cells through the lymphatic system by the activation of CCR7/CCL21-mediated chemotaxis.* Oncogene, 2015.

225. Gong, C., et al., *Abnormally expressed JunB transactivated by IL-6/STAT3 signaling promotes uveal melanoma aggressiveness via epithelial–mesenchymal transition.* Bioscience Reports, 2018. **38**(4): p. BSR20180532.

226. Hyakusoku, H., et al., *JunB promotes cell invasion, migration and distant metastasis of head and neck squamous cell carcinoma.* Journal of Experimental & Clinical Cancer Research, 2016. **35**(1): p. 6.

227. Kiesow, K., et al., *Junb controls lymphatic vascular development in zebrafish via miR-182.* Scientific Reports, 2015. **5**: p. 15007.

228. Licht, A.H., et al., *JunB is required for endothelial cell morphogenesis by regulating core-binding factor beta.* Journal of Cell Biology, 2006. **175**(6): p. 981-91.

229. Licht, A.H., et al., *Junb regulates arterial contraction capacity, cellular contractility, and motility via its target Myl9 in mice.* Journal of Clinical Investigation, 2010. **120**(7): p. 2307-18.

230. Florin, L., et al., *Delayed Wound Healing and Epidermal Hyperproliferation in Mice Lacking JunB in the Skin.* Journal of Investigative Dermatology, 2006. **126**(4): p. 902-911.

231. Passegué, E., E.F. Wagner, and I.L. Weissman, *JunB Deficiency Leads to a Myeloproliferative Disorder Arising from Hematopoietic Stem Cells.* Cell, 2004. **119**(3): p. 431-443.

232. Braun, J., et al., *Loss of stromal JUNB does not affect tumor growth and angiogenesis.* International Journal of Cancer, 2014. **134**(6): p. 1511-6.

233. Fontana, M.F., et al., *JUNB is a Key Transcriptional Modulator of Macrophage Activation.* The Journal of Immunology, 2015. **194**(1): p. 177-186.

234. Florin, L., et al., *Cre recombinase-mediated gene targeting of mesenchymal cells.* Genesis, 2004. **38**(3): p. 139-144.

235. Schwenk, F., U. Baron, and K. Rajewsky, *A cre-transgenic mouse strain for the ubiquitous deletion of loxP-flanked gene segments including deletion in germ cells.* Nucleic acids research, 1995. **23**(24): p. 5080-5081.

236. Shaul, M.E., et al., *Tumor-associated neutrophils display a distinct N1 profile following TGFβ modulation: A transcriptomics analysis of pro- vs. antitumor TANs.* Oncoimmunology, 2016. **5**(11): p. e1232221.

237. Jiang, H.-M., et al., *Role for Granulocyte Colony Stimulating Factor in Angiotensin II–Induced Neutrophil Recruitment and Cardiac Fibrosis in Mice.* American Journal of Hypertension, 2013. **26**(10): p. 1224-1233.

238. Fridlender, Z.G., et al., *Polarization of Tumor-Associated Neutrophil Phenotype by TGF-β: "N1" versus "N2" TAN.* Cancer Cell, 2009. **16**(3): p. 183-194.

239. Yu, P.F., et al., *TNFα-activated mesenchymal stromal cells promote breast cancer metastasis by recruiting CXCR2+ neutrophils.* Oncogene, 2016. **36**: p. 482.

240. Tomita, K., et al., *CXCL10-Mediates Macrophage, but not Other Innate Immune Cells-Associated Inflammation in Murine Nonalcoholic Steatohepatitis.* Scientific Reports, 2016. **6**: p. 28786.

241. Denaës, T., et al., *The Cannabinoid Receptor 2 Protects Against Alcoholic Liver Disease Via a Macrophage Autophagy-Dependent Pathway.* Scientific reports, 2016. **6**: p. 28806-28806.

242. Johnstone, C.N., et al., *Functional and molecular characterisation of EO771.LMB tumours, a new C57BL/6-mouse-derived model of spontaneously metastatic mammary cancer.* Disease Models & Mechanisms, 2015. **8**(3): p. 237-251.

243. Takase, H.M., et al., *FGF7 is a functional niche signal required for stimulation of adult liver progenitor cells that support liver regeneration.* Genes & development, 2013. **27**(2): p. 169-181.

244. Fusella, F., et al., *The IKK/NF-κB signaling pathway requires Morgana to drive breast cancer metastasis.* Nature Communications, 2017. **8**(1): p. 1636.

245. Gutierrez Miranda, L., *JUNB regulatory functions in lymphangiogenesis: from mESCs to zebrafish*, in *Faculty of Biosciences*. 2018, Heidelberg University: Heidelberg.

246. Florin, L., et al., *Identification of novel AP-1 target genes in fibroblasts regulated during cutaneous wound healing.* Oncogene, 2004. **23**: p. 7005.

247. Gomard, T., et al., *An NF-κB–Dependent Role for JunB in the Induction of Proinflammatory Cytokines in LPS-Activated Bone Marrow–Derived Dendritic Cells.* PLoS One, 2010. **5**(3): p. e9585.

248. Francia, G., et al., *Mouse models of advanced spontaneous metastasis for experimental therapeutics.* Nature Reviews: Cancer, 2011. **11**: p. 135.

249. Brodie, S.G., et al., *Multiple genetic changes are associated with mammary tumorigenesis in Brca1 conditional knockout mice.* Oncogene, 2001. **20**: p. 7514.

250. Gómez-Cuadrado, L., et al., *Mouse models of metastasis: progress and prospects.* Disease models & mechanisms, 2017. **10**(9): p. 1061-1074.

251. van Deventer, H.W., et al., *Transfection of Macrophage Inflammatory Protein 1α into B16 F10 Melanoma Cells Inhibits Growth of Pulmonary Metastases But Not Subcutaneous Tumors.* The Journal of Immunology, 2002. **169**(3): p. 1634-1639.

252. Burghoff, S., et al., *Growth and metastasis of B16-F10 melanoma cells is not critically dependent on host CD73 expression in mice.* BMC Cancer, 2014. **14**(1): p. 898.

253. Winkelmann, C.T., et al., *Microimaging Characterization of a B16-F10 Melanoma Metastasis Mouse Model.* Molecular Imaging, 2006. **5**(2): p. 7290.2006.00011.

254. Giavazzi, R., et al., *Metastasizing capacity of tumour cells from spontaneous metastases of transplanted murine tumours.* British journal of cancer, 1980. **42**(3): p. 462-472.

255. Duong, T., et al., *Genetic Ablation of SOX18 Function Suppresses Tumor Lymphangiogenesis and Metastasis of Melanoma in Mice.* Cancer Research, 2012. **72**(12).

256. Bobek, V., et al., *A Clinically Relevant, Syngeneic Model of Spontaneous, Highly Metastatic B16 Mouse Melanoma.* Anticancer Research, 2010. **30**(12): p. 4799-4803.

257. Eberting, C.L.D., et al., *Histologic Progression of B16 F10 Metastatic Melanoma in C57BL/6 Mice Over a Six Week Time Period: Distant Metastases before Local Growth.* Journal of Dermatology, 2004. **31**(4): p. 299-304.

258. Rashidi, B., et al., *A highly metastatic Lewis lung carcinoma orthotopic green fluorescent protein model.* Clinical & Experimental metastasis, 2000. **18**(1): p. 57-60.

259. Yan, L. and L.C. DeMars, *Effects of dietary fat on spontaneous metastasis of Lewis lung carcinoma in mice.* Clinical & Experimental Metastasis, 2010. **27**(8): p. 581-590.

260. Lin, T.-J., et al., *Rapamycin Promotes Mouse 4T1 Tumor Metastasis that Can Be Reversed by a Dendritic Cell-Based Vaccine.* PLoS one, 2015. **10**(10): p. e0138335.

261. Smith, M.C.P., et al., *CXCR4 Regulates Growth of Both Primary and Metastatic Breast Cancer.* Cancer research, 2004. **64**(23): p. 8604-8612.

262. Bailey-Downs, L.C., et al., *Development and Characterization of a Preclinical Model of Breast Cancer Lung Micrometastatic to Macrometastatic Progression.* PLoS one, 2014. **9**(5): p. e98624.

263. Yan, L. and L.C. DeMars, *Effects of a High-Fat Diet on Spontaneous Metastasis of Lewis Lung Carcinoma in Plasminogen Activator Inhibitor-1 Deficient and Wild-Type Mice.* PloS One, 2014. **9**(10): p. e110869.

264. Leibovici, J., et al., *Combined Treatment of Lewis Lung Carcinoma by Tumor Excision and Levan.* Oncology, 1981. **38**(1): p. 31-34.

265. La Porta, S., et al., *Endothelial Tie1-mediated angiogenesis and vascular abnormalization promote tumor progression and metastasis.* Journal of Clinical Investigation, 2018. **128**(2): p. 834-845.

266. Viski, C., et al., *Endosialin-Expressing Pericytes Promote Metastatic Dissemination.* Cancer research, 2016. **76**(18): p. 5313-5325.

267. Bugge, T.H., et al., *Growth and Dissemination of Lewis Lung Carcinoma in Plasminogen-Deficient Mice.* Blood, 1997. **90**(11): p. 4522-4531.

268. Qian, C.-N., et al., *Preparing the "Soil": The Primary Tumor Induces Vasculature Reorganization in the Sentinel Lymph Node before the Arrival of Metastatic Cancer Cells.* Cancer Research, 2006. **66**(21): p. 10365-10376.

269. Lee, S.Y., et al., *Changes in specialized blood vessels in lymph nodes and their role in cancer metastasis.* Journal of translational medicine, 2012. **10**(2016).

270. Lee, M., et al., *Transcriptional programs of lymphoid tissue capillary and high endothelium reveal control mechanisms for lymphocyte homing.* Nature Immunology, 2014. **15**: p. 982.

271. Kahounová, Z., et al., *The fibroblast surface markers FAP, anti-fibroblast, and FSP are expressed by cells of epithelial origin and may be altered during epithelial-to-mesenchymal transition.* Cytometry, 2018. **93**(9): p. 941-951.

272. Chang, H.Y., et al., *Diversity, topographic differentiation, and positional memory in human fibroblasts.* Proceedings of the National Academy of Sciences of the United States of America, 2002. **99**(20): p. 12877-12882.

273. da Silva, A.C., et al., *Role of Alpha-Smooth Muscle Actin and Fibroblast Activation Protein Alpha in Ovarian Neoplasms.* Gynecologic and Obstetric Investigation, 2018. **83**(4): p. 381-387.

274. Lakins, M.A., et al., *Cancer-associated fibroblasts induce antigen-specific deletion of CD8+T Cells to protect tumour cells.* Nature Communications, 2018. **9**(1): p. 948.

275. Niemiec, J., et al., *Podoplanin-positive Cancer-associated Stromal Fibroblasts in Primary Tumor and Synchronous Lymph Node Metastases of HER2-overexpressing Breast Carcinomas.* Anticancer Research, 2018. **38**(4): p. 1957-1965.

276. Mizoguchi, F., et al., *Functionally distinct disease-associated fibroblast subsets in rheumatoid arthritis.* Nature Communications, 2018. **9**(1): p. 789.

277. Schmid, M.C., et al., *Integrin CD11b activation drives anti-tumor innate immunity.* Nature Communications, 2018. **9**(1): p. 5379.

278. Nowarski, R., et al., *Innate Immune Cells in Inflammation and Cancer.* Cancer immunology research, 2013. **1**(2): p. 77-84.

279. Noy, R. and Jeffrey W. Pollard, *Tumor-Associated Macrophages: From Mechanisms to Therapy.* Immunity, 2014. **41**(1): p. 49-61.

280. Italiani, P. and D. Boraschi, *Development and Functional Differentiation of Tissue-Resident Versus Monocyte-Derived Macrophages in Inflammatory Reactions*, in *Macrophages: Origin, Functions and Biointervention*, M. Kloc, Editor. 2017, Springer International Publishing: Cham. p. 23-43.

281. dos Anjos Cassado, A., *F4/80 as a Major Macrophage Marker: The Case of the Peritoneum and Spleen*, in *Macrophages: Origin, Functions and Biointervention*, M. Kloc, Editor. 2017, Springer International Publishing: Cham. p. 161-179.

282. Suzuki, Y., et al., *Utility of Macrophage-activated Marker CD163 for Diagnosis and Prognosis in Pulmonary Tuberculosis.* Annals of the American Thoracic Society, 2017. **14**(1): p. 57-64.

283. Herrera, M., et al., *Cancer-associated fibroblast and M2 macrophage markers together predict outcome in colorectal cancer patients.* Cancer Science, 2013. **104**(4): p. 437-444.

284. Barros, M.H.M., et al., *Macrophage Polarisation: an Immunohistochemical Approach for Identifying M1 and M2 Macrophages.* PLoS one, 2013. **8**(11): p. e80908.

285. Wu, J. and L.L. Lanier, *Natural Killer Cells and Cancer.* Advances in Cancer Research, 2003. **90**: p. 127-156.

286. Merzoug, L.B., et al., *Conditional ablation of NKp46+ cells using a novel Ncr1greenCre mouse strain: NK cells are essential for protection against pulmonary B16 metastases.* European Journal of Immunology, 2014. **44**(11): p. 3380-3391.

287. Levi, I., et al., *Characterization of tumor infiltrating natural killer cell subset.* Oncotarget, 2015. **6**(15): p. 13835-13843.

288. Vgenopoulou, S., et al., *Immunohistochemical evaluation of immune response in invasive ductal breast cancer of not-otherwise-specified type.* The Breast, 2003. **12**(3): p. 172-178.

289. Bio-Rad Laboratories. Cell Frequency Flow cytometry. 2017 [cited 2019 08 Feb]; Available from: https://www.bio-rad-antibodies.com/flow-cytometry-cell-frequency.html.

290. Galani, I.E. and E. Andreakos, *Neutrophils in viral infections: Current concepts and caveats.* Journal of Leukocyte Biology, 2015. **98**(4): p. 557-564.

291. Rosas, M., et al., *The myeloid 7/4-antigen defines recently generated inflammatory macrophages and is synonymous with Ly-6B.* Journal of Leukocyte Biology, 2010. **88**(1): p. 169-180.

292. Fontenot, J.D., M.A. Gavin, and A.Y. Rudensky, *Foxp3 programs the development and function of CD4+CD25+ regulatory T cells.* Nature Immunology, 2003. **4**: p. 330.

293. Hori, S., T. Nomura, and S. Sakaguchi, *Control of Regulatory T Cell Development by the Transcription Factor Foxp3.* Science, 2003. **299**(5609): p. 1057-1061.

294. Summers, C., et al., *Neutrophil kinetics in health and disease.* Trends in immunology, 2010. **31**(8): p. 318-324.

295. Renkawitz, J. and M. Sixt, *A Radical Break: Restraining Neutrophil Migration.* Developmental Cell, 2016. **38**(5): p. 448-450.

296. Devi, S., et al., *Neutrophil mobilization via plerixafor-mediated CXCR4 inhibition arises from lung demargination and blockade of neutrophil homing to the bone marrow.* Journal of Experimental Medicine, 2013. **210**(11): p. 2321-2336.

297. Petit, I., et al., *G-CSF induces stem cell mobilization by decreasing bone marrow SDF-1 and up-regulating CXCR4.* Nature Immunology, 2002. **3**: p. 687.

298. Semerad, C.L., et al., *G-CSF potently inhibits osteoblast activity and CXCL12 mRNA expression in the bone marrow.* Blood, 2005. **106**(9): p. 3020-3027.

299. Lee, P.Y., et al., *IL-1α Modulates Neutrophil Recruitment in Chronic Inflammation Induced by Hydrocarbon Oil.* The Journal of Immunology, 2011. **186**(3): p. 1747-1754.

300. Rider, P., et al., *IL-1α and IL-1β Recruit Different Myeloid Cells and Promote Different Stages of Sterile Inflammation.* The Journal of Immunology, 2011. **202**(5): p. 1102048.

301. Miller, L.S., et al., *Inflammasome-Mediated Production of IL-1β Is Required for Neutrophil Recruitment against Staphylococcus aureus In Vivo.* The Journal of Immunology, 2007. **179**(10): p. 6933-6942.

302. Biondo, C., et al., *The Interleukin-1β/CXCL1/2/Neutrophil Axis Mediates Host Protection against Group B Streptococcal Infection.* Infection and Immunity, 2014. **82**(11): p. 4508-4517.

303. Kolaczkowska, E. and P. Kubes, *Neutrophil recruitment and function in health and inflammation.* Nature Reviews: Immunology, 2013. **13**(3): p. 159.

304. Balamayooran, G., et al., *Monocyte Chemoattractant Protein 1 Regulates Pulmonary Host Defense via Neutrophil Recruitment duringEscherichia coli Infection.* Infection and Immunity, 2011. **79**(7): p. 2567-2577.

305. Yu, C., et al., *Platelet-Derived CCL5 Regulates CXC Chemokine Formation and Neutrophil Recruitment in Acute Experimental Colitis.* Journal of Cellular Physiology, 2016. **231**(2): p. 370-376.

306. Koh, A., et al., *Role of osteopontin in neutrophil function.* Immunology, 2007. **122**(4): p. 466-475.

307. Moschen, A.R., et al., *Lipocalin-2: A Master Mediator of Intestinal and Metabolic Inflammation.* Trends in Endocrinology & Metabolism, 2017. **28**(5): p. 388-397.

308. Duran-Struuck, R. and R.C. Dysko, *Principles of bone marrow transplantation (BMT): providing optimal veterinary and husbandry care to irradiated mice in BMT studies.* Journal of the American Association for Laboratory Animal Science: JAALAS, 2009. **48**(1): p. 11-22.

309. Hanson, W.R., et al., *Comparison of Intestine and Bone Marrow Radiosensitivity of the BALB/c and the C57BL/6 Mouse Strains and Their B6CF1 Offspring.* Radiation Research, 1987. **110**(3): p. 340-352.

310. Dubé, P. *Considerations for Rodent Irradiation*. 2017 [cited 2019 28 Jan]; Available from: https://www.taconic.com/taconic-insights/oncology-immuno-oncology/rodent-irradiation-considerations.html.

311. Butler, K.L., E. Clancy-Thompson, and D.W. Mullins, *CXCR3(+) monocytes/macrophages are required for establishment of pulmonary metastases.* Scientific reports, 2017. **7**: p. 45593-45593.

312. Kitamura, T., et al., *Monocytes Differentiate to Immune Suppressive Precursors of Metastasis-Associated Macrophages in Mouse Models of Metastatic Breast Cancer.* Frontiers in Immunology, 2018. **8**(2004).

313. Qian, B.-Z., et al., *CCL2 recruits inflammatory monocytes to facilitate breast-tumour metastasis.* Nature, 2011. **475**: p. 222.

314. Ma, C. and T.F. Greten, *Editorial: "Invisible" MDSC in tumor-bearing individuals after antibody depletion: fact or fiction?* Journal of Leukocyte Biology, 2016. **99**(6): p. 794-794.

315. Potez, M., et al., *Characterization of a B16-F10 melanoma model locally implanted into the ear pinnae of C57BL/6 mice.* PloS one, 2018. **13**(11): p. e0206693-e0206693.

316. Li, X., et al., *VEGFR2 pY949 signalling regulates adherens junction integrity and metastatic spread.* Nature Communications, 2016. **7**: p. 11017.

317. Zang, G., et al., *Vascular dysfunction and increased metastasis of B16F10 melanomas in Shb deficient mice as compared with their wild type counterparts.* BMC Cancer, 2015. **15**(1): p. 234.

318. Wilmanns, C., et al., *Orthotopic and ectopic organ environments differentially influence the sensitivity of murine colon carcinoma cells to doxorubicin and 5-fluorouracil.* International Journal of Cancer, 1992. **52**(1): p. 98-104.

319. Kuo, T.H., et al., *Site-specific chemosensitivity of human small-cell lung carcinoma growing orthotopically compared to subcutaneously in SCID mice: the importance of orthotopic models to obtain relevant drug evaluation data.* Anticancer research, 1993. **13**(3): p. 627-30.

320. Fidler, I.J., et al., *Modulation of tumor cell response to chemotherapy by the organ environment.* Cancer Metastasis Rev, 1994. **13**(2): p. 209-22.

321. Fidler, I.J., *Models for Spontaneous Metastasis.* Cancer Research, 2006. **66**(19): p. 9787-9787.

322. Kubota, T., *Metastatic models of human cancer xenografted in the nude mouse: The importance of orthotopic transplantation.* Journal of cellular biochemistry, 1994. **56**(1): p. 4-8.

323. Togo, S., et al., *Host Organ Specifically Determines Cancer Progression.* Cancer Research, 1995. **55**(3): p. 681-684.

324. Boehle, A.S., et al., *An improved orthotopic xenotransplant procedure for human lung cancer in SCID bg mice.* The Annals of Thoracic Surgery, 2000. **69**(4): p. 1010-1015.

325. Borgstrom, P., et al., *Co-implanting orthotopic tissue creates stroma microenvironment enhancing growth and angiogenesis of multiple tumors [version 2; referees: 2 approved].* F1000 Research, 2013. **2**(129).

326. Pereira, E.R., et al., *Lymph node metastases can invade local blood vessels, exit the node, and colonize distant organs in mice.* Science, 2018. **359**(6382): p. 1403-1407.

327. Bartlett, E.K., et al., *Identification of Patients with Intermediate Thickness Melanoma at Low Risk for Sentinel Lymph Node Positivity.* Annals of surgical oncology, 2016. **23**(1): p. 250-256.

328. Weide, B., et al., *Melanoma Patients with Unknown Primary Site or Nodal Recurrence after Initial Diagnosis Have a Favourable Survival Compared to Those with Synchronous Lymph Node Metastasis and Primary Tumour.* PLoS one, 2013. **8**(6): p. e66953.

329. Ran, S., et al., *Lymphangiogenesis and lymphatic metastasis in breast cancer.* Pathophysiology, 2010. **17**(4): p. 229-251.

330. Rahman, M. and S. Mohammed, *Breast cancer metastasis and the lymphatic system.* Oncology letters, 2015. **10**(3): p. 1233-1239.

331. Bassukas, I.D. and B. Maurer-Schultze, *Growth of metastases of the mouse adenocarcinoma EO 771: an allometric relationship between growth of the primary tumors and their metastases.* Clin Exp Metastasis, 1990. **8**(4): p. 329-43.

332. Singh, R.K., R. Tsan, and R. Radinsky, *Influence of the host microenvironment on the clonal selection of human colon carcinoma cells during primary tumor growth and metastasis.* Clinical & experimental metastasis, 1997. **15**(2): p. 140-50.

333. Camphausen, K., et al., *Influence of in vivo growth on human glioma cell line gene expression: Convergent profiles under orthotopic conditions.* Proceedings of the National Academy of Sciences of the United States of America, 2005. **102**(23): p. 8287-8292.

334. Ghajar, C.M., et al., *The perivascular niche regulates breast tumour dormancy.* Nature Cell Biology, 2013. **15**(7): p. 807-817.

335. Textor, B., et al., *c-Jun and JunB are essential for hypoglycemia-mediated VEGF induction.* Annals of the New York Academy of Sciences, 2006. **1091**: p. 310-8.

336. Blackburn, H.L., et al., *Breast Cancer Metastasis to the Axillary Lymph Nodes: Are Changes to the Lymph Node "Soil" Localized or Systemic?* Breast Cancer (Auckl), 2017. **11**: p. 1178223417691246-1178223417691246.

337. Rose, B.S., et al., *Effect of lymph node metastasis size on breast cancer-specific and overall survival in women with node-positive breast cancer.* Breast cancer research and treatment, 2015. **152**(1): p. 209-216.

338. Tichet, M., et al., *Tumour-derived SPARC drives vascular permeability and extravasation through endothelial VCAM1 signalling to promote metastasis.* Nature Communications, 2015. **6**: p. 6993.

339. Hirakawa, S., et al., *VEGF-A induces tumor and sentinel lymph node lymphangiogenesis and promotes lymphatic metastasis.* Journal of Experimental Medicine, 2005. **201**(7): p. 1089-1099.

340. Ogawa, F., et al., *Prostanoid induces premetastatic niche in regional lymph nodes.* Journal of Clinical Investigation, 2014. **124**(11): p. 4882-4894.

341. Criscuoli, M.L., M. Nguyen, and B.P. Eliceiri, *Tumor metastasis but not tumor growth is dependent on Src-mediated vascular permeability.* Blood, 2005. **105**(4): p. 1508-1514.

342. Galaup, A., et al., *Angiopoietin-like 4 prevents metastasis through inhibition of vascular permeability and tumor cell motility and invasiveness.* Proceedings of the National Academy of Sciences of the United States of America

2006. **103**(49): p. 18721-18726.

343. Roblek, M., et al., *CCL2 is a vascular permeability factor inducing CCR2-dependent endothelial retraction during lung metastasis.* Molecular Cancer Research, 2018: p. molcanres.0530.2018.

344. García-Román, J. and A. Zentella-Dehesa, *Vascular permeability changes involved in tumor metastasis.* Cancer Letters, 2013. **335**(2): p. 259-269.

345. Zeng, L., et al., *HMG CoA reductase inhibition modulates VEGF-induced endothelial cell hyperpermeability by preventing RhoA activation and myosin regulatory light chain phosphorylation.* FASEB Journal, 2005. **19**(13): p. 1845-1847.

346. Shehadeh, L.A., et al., *Dynamic Regulation of Vascular Myosin Light Chain (MYL9) with Injury and Aging.* PLoS one, 2011. **6**(10): p. e25855.

347. Zhang, X., et al., *RNA-Seq and ChIP-Seq reveal SQSTM1/p62 as a key mediator of JunB suppression of NF-kappaB-dependent inflammation.* J Invest Dermatol, 2015. **135**(4): p. 1016-24.

348. Yang, M., et al., *ICAM-1 suppresses tumor metastasis by inhibiting macrophage M2 polarization through blockade of efferocytosis.* Cell Death & Disease, 2015. **6**: p. e1780.

349. Aoudjit, F., E.F. Potworowski, and Y. St-Pierre, *Bi-Directional Induction of Matrix Metalloproteinase-9 and Tissue Inhibitor of Matrix Metalloproteinase-1 During T Lymphoma/Endothelial Cell Contact: Implication of ICAM-1.* The Journal of Immunology, 1998. **160**(6): p. 2967-2973.

350. Hazan, R.B., et al., *N-Cadherin Promotes Adhesion Between Invasive Breast Cancer Cells and the Stroma.* Cell Adhesion and Communication, 1997. **4**(6): p. 399-411.

351. Ramirez, N.E., et al., *The α2β1 integrin is a metastasis suppressor in mouse models and human cancer.* Journal of Clinical Investigation, 2011. **121**(1): p. 226-237.

352. Berry, J., et al., *JunB as a potential mediator of PTHrP actions: new gene targets Ephrin B1 and VCAM-1.* Oral Diseases, 2008. **14**(8): p. 713-726.

353. Kong, D.-H., et al., *Emerging Roles of Vascular Cell Adhesion Molecule-1 (VCAM-1) in Immunological Disorders and Cancer.* International journal of molecular sciences, 2018. **19**(4): p. 1057.

354. Schlesinger, M. and G. Bendas, *Vascular cell adhesion molecule-1 (VCAM-1)—An increasing insight into its role in tumorigenicity and metastasis.* International Journal of Cancer, 2015. **136**(11): p. 2504-2514.

355. Wieland, E., et al., *Endothelial Notch1 Activity Facilitates Metastasis.* Cancer Cell, 2017. **31**(3): p. 355-367.

356. Lee, C.-W., et al., *Transcriptional regulation of VCAM-1 expression by tumor necrosis factor-α in human tracheal smooth muscle cells: Involvement of MAPKs, NF-κB, p300, and histone acetylation.* Journal of cellular physiology, 2006. **207**(1): p. 174-186.

357. Figenschau, S.L., et al., *ICAM1 expression is induced by proinflammatory cytokines and associated with TLS formation in aggressive breast cancer subtypes.* Scientific Reports, 2018. **8**(1): p. 11720.

358. Yang, L., et al., *ICAM-1 regulates neutrophil adhesion and transcellular migration of TNF-α-activated vascular endothelium under flow.* Blood, 2005. **106**(2): p. 584-592.

359. Cui, A., et al., *VCAM-1-mediated neutrophil infiltration exacerbates ambient fine particle-induced lung injury.* Toxicology Letters, 2019. **302**: p. 60-74.

360. Rodemann, H.P. and G.A. Muller, *Characterization of human renal fibroblasts in health and disease: II. In vitro growth, differentiation, and collagen synthesis of fibroblasts from kidneys with interstitial fibrosis.* American Journal of Kidney Diseases, 1991. **17**(6): p. 684-6.

361. Kalluri, R. and M. Zeisberg, *Fibroblasts in cancer.* Nature Reviews: Cancer, 2006. **6**: p. 392.

362. Augsten, M., *Cancer-Associated Fibroblasts as Another Polarized Cell Type of the Tumor Microenvironment.* Frontiers in Oncology, 2014. **4**(62).

363. Labernadie, A., et al., *A mechanically active heterotypic E-cadherin/N-cadherin adhesion enables fibroblasts to drive cancer cell invasion.* Nature Cell Biology, 2017. **19**: p. 224.

364. Toullec, A., et al., *Oxidative stress promotes myofibroblast differentiation and tumour spreading.* EMBO Molecular Medicine, 2010. **2**(6): p. 211-230.

365. Brechbuhl, H.M., et al., *Fibroblast Subtypes Regulate Responsiveness of Luminal Breast Cancer to Estrogen.* Clinical Cancer Research, 2017. **23**(7): p. 1710-1721.

366. Sugimoto, H., et al., *Identification of fibroblast heterogeneity in the tumor microenvironment.* Cancer Biology & Therapy, 2006. **5**(12): p. 1640-6.

367. Bartoschek, M., et al., *Spatially and functionally distinct subclasses of breast cancer-associated fibroblasts revealed by single cell RNA sequencing.* Nature Communications, 2018. **9**(1): p. 5150.

368. Xie, T., et al., *Single-Cell Deconvolution of Fibroblast Heterogeneity in Mouse Pulmonary Fibrosis.* Cell Reports, 2018. **22**(13): p. 3625-3640.

369. Su, S., et al., *CD10+GPR77+ Cancer-Associated Fibroblasts Promote Cancer Formation and Chemoresistance by Sustaining Cancer Stemness.* Cell, 2018. **172**(4): p. 841-856.e16.

370. Costa, A., et al., *Fibroblast Heterogeneity and Immunosuppressive Environment in Human Breast Cancer.* Cancer Cell, 2018. **33**(3): p. 463-479.e10.

371. Patel, A.K., et al., *A subtype of cancer-associated fibroblasts with lower expression of alpha-smooth muscle actin suppresses stemness through BMP4 in oral carcinoma.* Oncogenesis, 2018. **7**(10): p. 78.

372. Yamanashi, T., et al., *Podoplanin Expression Identified in Stromal Fibroblasts as a Favorable Prognostic Marker in Patients with Colorectal Carcinoma.* Oncology, 2009. **77**(1): p. 53-62.

373. Wang, L., et al., *Cancer-associated fibroblasts enhance metastatic potential of lung cancer cells through IL-6/STAT3 signaling pathway.* Oncotarget, 2017. **8**(44).

374. Sadlonova, A., et al., *Identification of molecular distinctions between normal breast-associated fibroblasts and breast cancer-associated fibroblasts.* Cancer microenvironment, 2009. **2**(1): p. 9-21.

375. Berdiel-Acer, M., et al., *Differences between CAFs and their paired NCF from adjacent colonic mucosa reveal functional heterogeneity of CAFs, providing prognostic information.* Molecular oncology, 2014. **8**(7): p. 1290-1305.

376. Herrera, M., et al., *Differential distribution and enrichment of non-coding RNAs in exosomes from normal and Cancer-associated fibroblasts in colorectal cancer.* Molecular Cancer, 2018. **17**(1): p. 114-114.

377. Wang, J. and R. Yamada, *In silico study of medical decision-making for rare diseases: heterogeneity of decision-makers in a population improves overall benefit.* PeerJ, 2018. **6**: p. e5677.

378. Rishi, A.K., et al., *Cloning, Characterization, and Developmental Expression of a Rat Lung Alveolar Type I Cell Gene in Embryonic Endodermal and Neural Derivatives.* Developmental Biology, 1995. **167**(1): p. 294-306.

379. Baluk, P. and D.M. McDonald, *Markers for Microscopic Imaging of Lymphangiogenesis and Angiogenesis.* Annals of the New York Academy of Sciences, 2008. **1131**(1): p. 1-12.

380. Kerrigan, A.M., et al., *Podoplanin-expressing inflammatory macrophages activate murine platelets via CLEC-2.* Journal of thrombosis and haemostasis, 2012. **10**(3): p. 484-486.

381. Hou, T.Z., et al., *A distinct subset of podoplanin (gp38) expressing F4/80+ macrophages mediate phagocytosis and are induced following zymosan peritonitis.* FEBS Letters, 2010. **584**(18): p. 3955-3961.

382. Gandarillas, A., et al., *Induction of PA2.26, a cell-surface antigen expressed by active fibroblasts, in mouse epidermal keratinocytes during carcinogenesis.* Molecular Carcinogenesis, 1997. **20**(1): p. 10-18.

383. Guinea-Viniegra, J., et al., *TNFalpha shedding and epidermal inflammation are controlled by Jun proteins.* Genes & development, 2009. **23**(22): p. 2663-2674.

384. Rønnov-Jessen, L., O.W. Petersen, and M.J. Bissell, *Cellular changes involved in conversion of normal to malignant breast: importance of the stromal reaction.* Physiological reviews, 1996. **76**(1): p. 69-125.

385. Erdogan, B., et al., *Cancer-associated fibroblasts promote directional cancer cell migration by aligning fibronectin.* Journal of Cell Biology, 2017. **216**(11): p. 3799-3816.

386. Gaggioli, C., et al., *Fibroblast-led collective invasion of carcinoma cells with differing roles for RhoGTPases in leading and following cells.* Nature Cell Biology, 2007. **9**: p. 1392.

387. Jinka, R., et al., *Alterations in Cell-Extracellular Matrix Interactions during Progression of Cancers.* International journal of cell biology, 2012. **2012**: p. 219196-219196.

388. Gervasi, M., et al., *JunB contributes to Id2 repression and the epithelial–mesenchymal transition in response to transforming growth factor–β.* Journal of Cell Biology, 2012. **196**(5): p. 589-603.

389. Ponticos, M., et al., *Failed degradation of JunB contributes to overproduction of type I collagen and development of dermal fibrosis in patients with systemic sclerosis.* Arthritis & rheumatology (Hoboken, N.J.), 2015. **67**(1): p. 243-253.

390. Paul, S. and G. Lal, *Development and Function of Natural Killer Cells and Its Importance in Cancer Immunotherapy*. Immunology, ed. M. Hayat. Vol. 1. 2017, London: Academic Print. 286.

391. Garcia-Lora, A., I. Algarra, and F. Garrido, *MHC class I antigens, immune surveillance, and tumor immune escape.* Journal of Cellular Physiology, 2003. **195**(3): p. 346-355.

392. Swann, J.B. and M.J. Smyth, *Immune surveillance of tumors.* Journal of Clinical Investigation, 2007. **117**(5): p. 1137-1146.

393. Voice, J., et al., *c-Maf and JunB Mediation of Th2 Differentiation Induced by the Type 2 G Protein-Coupled Receptor (VPAC2) for Vasoactive Intestinal Peptide.* The Journal of Immunology, 2004. **172**(12): p. 7289-7296.

394. Carr, T.M., et al., *JunB promotes Th17 cell identity and restrains alternative CD4+ T-cell programs during inflammation.* Nature Communications, 2017. **8**(1): p. 301.

395. Moon, Y.-M., et al., *The Fos-Related Antigen 1–JUNB/Activator Protein 1 Transcription Complex, a Downstream Target of Signal Transducer and Activator of Transcription 3, Induces T Helper 17 Differentiation and Promotes Experimental Autoimmune Arthritis.* Frontiers in Immunology, 2017. **8**(1793).

396. Yamazaki, S., et al., *The AP-1 transcription factor JunB is required for Th17 cell differentiation.* Scientific Reports, 2017. **7**(1): p. 17402.

397. Hasan, Z., et al., *JunB is essential for IL-23-dependent pathogenicity of Th17 cells.* Nature Communications, 2017. **8**: p. 15628.

398. Koizumi, S.-i., et al., *JunB regulates homeostasis and suppressive functions of effector regulatory T cells.* Nature Communications, 2018. **9**(1): p. 5344.

399. Lord, K.A., et al., *Proto-oncogenes of the fos/jun family of transcription factors are positive regulators of myeloid differentiation.* Molecular and Cellular Biology, 1993. **13**(2): p. 841-851.

400. Liu, H., et al., *Reciprocal effects of C/EBPα and PKCδ on JunB expression and monocytic differentiation depend upon the C/EBPα basic region.* Blood, 2003. **101**(10): p. 3885-3892.

401. Nausch, N., et al., *Cutting Edge: The AP-1 Subunit JunB Determines NK Cell-Mediated Target Cell Killing by Regulation of the NKG2D-Ligand RAE-1ε.* The Journal of Immunology, 2006. **176**(1): p. 7-11.

402. Ratajczak-Wrona, W., et al., *Role of AP-1 family proteins in regulation of inducible nitric oxide synthase (iNOS) in human neutrophils.* Journal of Immunotoxicology, 2013. **10**(1): p. 32-39.

403. Lee, P.Y., et al., *Ly6 family proteins in neutrophil biology.* Journal of Leukocyte Biology, 2013. **94**(4): p. 585-594.

404. Yoshioka, Y., et al., *Neutrophils and the S100A9 protein critically regulate granuloma formation.* Blood Advances, 2016. **1**(3): p. 184-192.

405. Srikrishna, G., *S100A8 and S100A9: new insights into their roles in malignancy.* Journal of innate immunity, 2011. **4**(1): p. 31-40.

406. Dawson, M.R., et al., *VEGFR1-activity-independent metastasis formation.* Nature, 2009. **461**(7262): p. E4-E5.

407. Lee, W., et al., *Neutrophils facilitate ovarian cancer premetastatic niche formation in the omentum.* Journal of Experimental Medicine, 2018. **2016**(1): p. jem.20181170.

408. Eckhardt, B.L., et al., *Genomic Analysis of a Spontaneous Model of Breast Cancer Metastasis to Bone Reveals a Role for the Extracellular Matrix.* Molecular Cancer Research, 2005. **3**(1): p. 1-13.

409. Bisikirska, B., et al., *TCR stimulation with modified anti-CD3 mAb expands CD8+ T cell population and induces CD8+CD25+ Tregs.* Journal of Clinical Investigation, 2005. **115**(10): p. 2904-2913.

410. Devaud, C., P.K. Darcy, and M.H.J.C.I. Kershaw, Immunotherapy, *Foxp3 expression in T regulatory cells and other cell lineages.* Cancer Immunology, Immunotherapy, 2014. **63**(9): p. 869-876.

411. Monteiro, M., et al., *Identification of Regulatory Foxp3+ Invariant NKT Cells Induced by TGF-β.* The Journal of Immunology, 2010. **185**(4): p. 2157-2163.

412. Zuo, T., et al., *FOXP3 is a novel transcriptional repressor for the breast cancer oncogene SKP2.* Journal of Clinical Investigation, 2007. **117**(12): p. 3765-3773.

413. Kawai, K., et al., *CD11b-mediated migratory property of peripheral blood B cells.* Journal of Allergy and Clinical Immunology, 2005. **116**(1): p. 192-197.

414. Hendrickx, A. and X. Bossuyt, *Quantification of the leukocyte common antigen (CD45) in mature B-cell malignancies.* Cytometry, 2001. **46**(6): p. 336-9.

415. Lim, K., et al., *Neutrophil trails guide influenza-specific CD8+ T cells in the airways.* Science, 2015. **349**(6252): p. aaa4352.

416. Beauvillain, C., et al., *Neutrophils efficiently cross-prime naive T cells in vivo.* Blood, 2007. **110**(8): p. 2965-2973.

417. Governa, V., et al., *The Interplay Between Neutrophils and CD8+ T Cells Improves Survival in Human Colorectal Cancer.* Clinical Cancer Research, 2017. **23**(14): p. 3847-3858.

418. van der Woude, L.L., et al., *Migrating into the Tumor: a Roadmap for T Cells.* Trends in Cancer, 2017. **3**(11): p. 797-808.

419. Wang, T.-t., et al., *Tumour-activated neutrophils in gastric cancer foster immune suppression and disease progression through GM-CSF-PD-L1 pathway.* Gut, 2017. **66**(11): p. 1900-1911.

420. Hu, X., et al., *Programming of the Development of Tumor-Promoting Neutrophils by Mesenchymal Stromal Cells.* Cellular Physiology and Biochemistry, 2014. **33**(6): p. 1802-1814.

421. Gabrilovich, D.I., *Myeloid-Derived Suppressor Cells.* Cancer immunology research, 2017. **5**(1): p. 3-8.

422. Aarts, C.E.M. and T.W. Kuijpers, *Neutrophils as myeloid-derived suppressor cells.* European Journal of Clinical Investigation, 2018. **48**(S2): p. e12989.

423. Rodriguez, P.C., et al., *Arginase I–Producing Myeloid-Derived Suppressor Cells in Renal Cell Carcinoma Are a Subpopulation of Activated Granulocytes.* Cancer Research, 2009. **69**(4): p. 1553-1560.

424. Youn, J.-I., et al., *Characterization of the nature of granulocytic myeloid-derived suppressor cells in tumor-bearing mice.* Journal of Leukocyte Biology, 2012. **91**(1): p. 167-181.

425. Brandau, S. and D. Hartl, *Lost in neutrophil heterogeneity? CD10!* Blood, 2017. **129**(10): p. 1240-1241.

426. Bronte, V., et al., *Recommendations for myeloid-derived suppressor cell nomenclature and characterization standards.* Nature Communications, 2016. **7**: p. 12150.

427. Eash, K.J., et al., *CXCR2 and CXCR4 antagonistically regulate neutrophil trafficking from murine bone marrow.* Journal of Clinical Investigation, 2010. **120**(7): p. 2423-2431.

428. Kreisel, D., et al., *In vivo two-photon imaging reveals monocyte-dependent neutrophil extravasation during pulmonary inflammation.* Proceedings of the National Academy of Sciences of the United States of America, 2010. **107**(42): p. 18073-18078.

429. Lien, D.C., et al., *Physiological neutrophil sequestration in the lung: visual evidence for localization in capillaries.* Journal of applied physiology, 1987. **62**(3): p. 1236-1243.

430. Doyle, N.A., et al., *Neutrophil margination, sequestration, and emigration in the lungs of L-selectin-deficient mice.* Journal of Clinical Investigation, 1997. **99**(3): p. 526-533.

431. Sugiyama, T., et al., *Maintenance of the Hematopoietic Stem Cell Pool by CXCL12-CXCR4 Chemokine Signaling in Bone Marrow Stromal Cell Niches.* Immunity, 2006. **25**(6): p. 977-988.

432. Ahirwar, D.K., et al., *Fibroblast-derived CXCL12 promotes breast cancer metastasis by facilitating tumor cell intravasation.* Oncogene, 2018. **37**(32): p. 4428-4442.

433. Tommelein, J., et al., *Cancer-Associated Fibroblasts Connect Metastasis-Promoting Communication in Colorectal Cancer.* Frontiers in Oncology, 2015. **5**(63).

434. Domanska, U.M., et al., *A review on CXCR4/CXCL12 axis in oncology: No place to hide.* European Journal of Cancer, 2013. **49**(1): p. 219-230.

435. Balamayooran, G., et al., *Intrapulmonary G-CSF Rescues Neutrophil Recruitment to the Lung and Neutrophil Release to Blood in Gram-Negative Bacterial Infection in MCP-1 -/-Mice.* The Journal of Immunology, 2012. **189**(12): p. 1200585.

436. Knudsen, E., et al., *G-CSF enhances the proliferation and mobilization, but not the maturation rate, of murine myeloid cells.* European Journal of Haematology, 2011. **87**(4): p. 302-311.

437. Gregory, A.D., et al., *Regulation of systemic and local neutrophil responses by G-CSF during pulmonary Pseudomonas aeruginosa infection.* Blood, 2007. **109**(8): p. 3235-3243.

438. Guglani, L., et al., *Lipocalin 2 Regulates Inflammation during Pulmonary Mycobacterial Infections.* PLoS one, 2012. **7**(11): p. e50052.

439. Sica, A., et al., *IL-1 transcriptionally activates the neutrophil chemotactic factor/IL-8 gene in endothelial cells.* Immunology, 1990. **69**(4): p. 548-553.

440. Osawa, Y., et al., *Tumor Necrosis Factor Alpha-Induced Interleukin-8 Production via NF-κB and Phosphatidylinositol 3-Kinase/Akt Pathways Inhibits Cell Apoptosis in Human Hepatocytes.* Infection and Immunity, 2002. **70**(11): p. 6294-6301.

441. Miller, L.S., et al., *Inflammasome-Mediated Production of IL-1β Is Required for Neutrophil Recruitment against Staphylococcus aureus In Vivo.* The Journal of immunology, 2007. **179**(10): p. 6933-6942.

442. Hattar, K., et al., *Cell Density Regulates Neutrophil IL-8 Synthesis: Role of IL-1 Receptor Antagonist and Soluble TNF Receptors.* The Journal of Immunology, 2001. **166**(10): p. 6287-6293.

443. Prince, L.R., et al., *The role of interleukin-1beta in direct and toll-like receptor 4-mediated neutrophil activation and survival.* American Journal of Pathology, 2004. **165**(5): p. 1819-1826.

444. Lukacs, N.W., et al., *TNF-alpha mediates recruitment of neutrophils and eosinophils during airway inflammation.* The Journal of Immunology, 1995. **154**(10): p. 5411-5417.

445. Tecchio, C. and M.A. Cassatella, *Neutrophil-derived chemokines on the road to immunity.* Seminars in Immunology, 2016. **28**(2): p. 119-128.

446. McHale, J.F., et al., *TNF-α and IL-1 Sequentially Induce Endothelial ICAM-1 and VCAM-1 Expression in MRL/lpr Lupus-Prone Mice.* The Journal of Immunology, 1999. **163**(7): p. 3993-4000.

447. Gibson, B.W., et al., *Comparison of Cesium-137 and X-ray Irradiators by Using Bone Marrow Transplant Reconstitution in C57BL/6J Mice.* Comparative medicine, 2015. **65**(3): p. 165-172.

448. McFarland, H.I., et al., *Regulatory T Cells in γ Irradiation-Induced Immune Suppression.* PLoS one, 2012. **7**(6): p. e39092.

449. de Winther, M.P.J. and P. Heeringa, *Bone Marrow Transplantations to Study Gene Function in Hematopoietic Cells*, in *Transgenic Mouse Methods and Protocols*, M.H. Hofker and J. van Deursen, Editors. 2011, Humana Press: Totowa, NJ. p. 309-320.

450. Aparicio-Vergara, M., et al., *Bone marrow transplantation in mice as a tool for studying the role of hematopoietic cells in metabolic and cardiovascular diseases.* Atherosclerosis, 2010. **213**(2): p. 335-344.

451. Dawson, M.R., et al., *VEGFR1 Activity Modulates Myeloid Cell Infiltration in Growing Lung Metastases but Is Not Required for Spontaneous Metastasis Formation.* PLoS one, 2009. **4**(9): p. e6525.

452. Hara, T., et al., *Mint3 in bone marrow-derived cells promotes lung metastasis in breast cancer model mice.* Biochemical and Biophysical Research Communications, 2017. **490**(3): p. 688-692.

453. Machein, M.R. and K.H. Plate, *Bone Marrow Chimera Experiments to Determine the Contribution of Hematopoietic Stem Cells to Cerebral Angiogenesis*, in *Cerebral Angiogenesis: Methods and Protocols*, R. Milner, Editor. 2014, Springer New York: New York, NY. p. 275-288.

454. Straub, J.M., et al., *Radiation-induced fibrosis: mechanisms and implications for therapy.* Journal of Cancer Research and Clinical Oncology, 2015. **141**(11): p. 1985-1994.

455. Cox, T.R., et al., *LOX-mediated collagen crosslinking is responsible for fibrosis-enhanced metastasis.* Cancer Research, 2013. **73**(6): p. canres.2233.2012.

456. Schorpp-Kistner, M., *IL1 in fibroblasts*. 2019: unpublished.

457. Bigildeev, A.E., et al., *Interleukin-1 beta is an irradiation-induced stromal growth factor.* Cytokine, 2013. **64**(1): p. 131-137.

458. Liu, Y., et al., *Tumor Exosomal RNAs Promote Lung Pre-metastatic Niche Formation by Activating Alveolar Epithelial TLR3 to Recruit Neutrophils.* Cancer Cell, 2016. **30**(2): p. 243-256.

459. Donati, K., et al., *Neutrophil-Derived Interleukin 16 in Premetastatic Lungs Promotes Breast Tumor Cell Seeding.* Cancer Growth and Metastasis, 2017. **10**: p. 1179064417738513.

460. Park, J., et al., *Cancer cells induce metastasis-supporting neutrophil extracellular DNA traps.* Science translational medicine, 2016. **8**(361): p. 361ra138-361ra138.

461. Liang, W., Q. Li, and N. Ferrara, *Metastatic growth instructed by neutrophil-derived transferrin.* Proceedings of the National Academy of Sciences of the United States of America, 2018. **115**(43): p. 11060-11065.

462. Jaeger, B.N., et al., *Neutrophil depletion impairs natural killer cell maturation, function, and homeostasis.* Journal of Experimental Medicine, 2012. **209**(3): p. 565-580.

463. Moses, K., et al., *Survival of residual neutrophils and accelerated myelopoiesis limit the efficacy of antibody-mediated depletion of Ly-6G+ cells in tumor-bearing mice.* Journal of Leukocyte Biology, 2016. **99**(6): p. 811-823.

464. Faget, J., et al., *Efficient and specific Ly6G+ cell depletion: A change in the current practices toward more relevant functional analyses of neutrophils.* bioRxiv, 2018: p. 498881.

465. Reber, L.L., et al., *Neutrophil myeloperoxidase diminishes the toxic effects and mortality induced by lipopolysaccharide.* Journal of Experimental Medicine, 2017. **214**(5): p. 1249-1258.

466. Buch, T., et al., *A Cre-inducible diphtheria toxin receptor mediates cell lineage ablation after toxin administration.* Nature Methods, 2005. **2**: p. 419.

467. Abram, C.L., et al., *Comparative analysis of the efficiency and specificity of myeloid-Cre deleting strains using ROSA-EYFP reporter mice.* Journal of immunological methods, 2014. **408**: p. 89-100.

468. Clausen, B.E., et al., *Conditional gene targeting in macrophages and granulocytes using LysMcre mice.* Transgenic Research, 1999. **8**(4): p. 265-277.

469. Fontana, M.F., et al., *Myeloid expression of the AP-1 transcription factor JUNB modulates outcomes of type 1 and type 2 parasitic infections.* Parasite immunology, 2015. **37**(9): p. 470-478.

470. Shen, Z., et al., *Smooth muscle protein 22 alpha-Cre is expressed in myeloid cells in mice.* Biochemical and biophysical research communications, 2012. **422**(4): p. 639-642.

471. Zheng, B., et al., *Ligand-Dependent Genetic Recombination in Fibroblasts: A Potentially Powerful Technique for Investigating Gene Function in Fibrosis.* American Journal of Pathology, 2002. **160**(5): p. 1609-1617.

472. Mendoza, A., et al., *Modeling metastasis biology and therapy in real time in the mouse lung.* Journal of Clinical Investigation, 2010. **120**(8): p. 2979-2988.

7 SUPPLEMENT

7. SUPPLEMENT

7.1. Declaration

I hereby declare that except where specific reference is made to the work of others, the contents of this dissertation are original and based on results of my own investigations.

This dissertation has not been submitted for consideration for any other degree or qualification.

Heidelberg, March 2019

Juliane Wutschka

7.2. Acknowledgements

I still cannot believe that I am actually finishing my thesis. But here I am writing the final lines almost to the day 4 years after I received the email that I had gotten the position at DKFZ. It's been an incredible journey since then, with countless ups and downs, frustration and seemingly endless workload. But I also met so many amazing people, shared so many hilarious moments in and outside of the lab and made tons of experiences that I wouldn't want to miss for anything. I am grateful for so many people, who accompanied me through this time.

First of all, I would like to thank **Peter Angel** for accepting me into his lab, for all the scientific discussions and for being my first examiner.

I also would like to thank **Marina Schorpp-Kistner**, for the close supervision and all the support throughout these years. I appreciate that your door was always open and thank you for all the discussions we had and all the input you provided, which guided me through the course of my PhD.

I am grateful to **Jonathan Sleeman** for being a valuable member of my TAC committee and for accepting the responsibility to be my second examiner.

Moreover, I would like to thank **Gudrun Rappold** and **Viktor Umansky** for being examiners in my disputation.

Furthermore, I would like to acknowledge **Andreas Fischer** for being a supportive member of my TAC committee.

During this time, I had the pleasure to work with so many incredible people in the lab. First and foremost, **Betty**, who did not only contribute a second pair of helping hand during the operations as initially planned but eventually turned into a vital support. With you I have not only gained outstandingly competent technical support but also personally with your contagious good mood and positive spirit you always managed to cheer me up and motivated me to keep on going. Without you this thesis would for sure have been extremely much harder and I would not be able to write these lines here now. THANK YOU!

Also a big thank you to the rest of the present and former **JUNB group**. **Laurita**, who introduced me to how to work in Angel's lab. The fishycist's (L)aura is still around and I could swear I hear "Wutskaaaaa" sometimes. **Melanie**, who always allowed me to steal some buffers, never got tired of answering all my stupid questions about waste disposal and mouse breedings and for being so amazing in finding long lost lab utensils. Thank you also to **Thomas**, especially for providing IT support and **Sören** for being such a pleasant travel companion to Lisbon ;-)

Of course I am also thankful for all the remaining people of the **Angel lab**, who created such a positive atmosphere, made it a really fun time and provided all these amazing cakes. Free food Friday will be missed. I particularly would like to mention **Tanja**, for all the moments of moral and immunological support, for all the shared frustration and your ability to always find something positive. **Barbara**, for your cheerful attitude, many helpful comments to my work and for dealing the precious slots at the slide scanner ;) Furthermore I'd like to thank **Alina, Tine, Lena, Sabrina, Doris** (thanks a lot for proofreading although you were sick), **Macrina** and **Te** for providing some positive distraction during lunch and coffee breaks and for being amazing lab mates.

Furthermore I'd like to acknowledge all the people who have contributed to this work in the one or other way. **Damir Krunic** for sharing his ImageJ skills with me, **Manuela Brom** for introducing me to the world of the light microscopy core facility, all the people of the FACS core facility, especially **Bernd** and **Michael**, whom I spent quite some hours with, all the animal care takers, on whose work I heavily relied on, **Tim Holland-Letz** and **Annette Kopp-Schneider** for statistical advice.

Although I admittedly spent a lot of time at work, I am extremely grateful for all the people "outside" who always reminded me that there is so much more than science.

My sparkling and glamorous DKFZ ladies, **Lina, Laura, Meli** and **Sara**, I am so happy to have met you that I cannot put it into words. You led me into the world of girly talk and trash TV. I went through all up and downs with you, all these moments of crazy laughter and deep frustration. PhD wouldn't have been the same without you :-*

All the people from the Wednesday lunches, **Chris, Jan, Oli, Stephan** and **Tamara**. You provided such a welcome distraction from work that I was always looking forward to our "dates".

All my friends from near and far, especially **Christinaaa, Maria** (D) and **Maria** (GR tack så mycket!), **Julia, Steffi** and **Max** for all our (travel) adventures, looong skype calls, postcards, WhatsApps and whatever other way of communication. Although you weren't always here, I knew I could always rely on your support and deep friendship <3

Natürlich danke ich vor allem auch meiner **Familie**, insbesondere **meinen Eltern**. Ohne eure andauernde Unterstützung und Liebe wäre dieser Weg durch Studium und Promotion doppelt so hart und halb so lustig gewesen. Ihr habt immer ein offenes Ohr gehabt, auch wenn ich wieder mal über die gleichen Probleme lamentiert habe. Ihr habt mich immer unterstützt, motiviert und versucht mir bei der Arbeit zu helfen, sei es durch Zeitungsausschnitte oder durch moralische Unterstützung. Dafür danke ich euch von Herzen.

Nakonec bych chtěla zvlášť poděkovat **Leovi** za jeho neutuchající podporu a neuvěřitelnou trpělivost, kterou se mnou měl. I v nejtěžších chvílích jsi mě dokázal povzbudit, vždy jsi mi dodal odvahu a navíc jsi zajišťoval stálý přísun banánů. Moc se těším na všechna naše budoucí (cestovní) dobrodružství. Thank you broučku.